Universitat Politècnica de València

Materials Technological Institute

Synthesis and characterization of new polymer electrolytes to use in fuel cells fed with bio-alcohols

Submitted by:

Soraya C. Sánchez Ballester

Supervised by:

Dr. Amparo Ribes Greus

Dr. Vicente Soria Sanchis

Valencia, July 2017

A la meua mare

Declaration

This is a doctoral thesis submitted to the Universitat Politècnica de València in partial fulfillment of the requirements for the degree of Doctor of Philosophy in Engineering and Industrial Production with International mention.

This work has not been previously submitted for any degree and is believed to be wholly original. The research has been carried out by me in the Universitat Politècnica de València (Spain), National Institute for Materials Science (Japan) and Instituto de Ciencia y Tecnología de Polímeros-CSIC (Spain).

Some of the chapters are presented in the style of journal articles. Even though the experimental works has been carried by me, the other authors have contributed to the discussion of the results and advices.

Soraya C. Sánchez Ballester

Acknowledgements

Arribat aquest moment, voldria agrair a totes aquelles persones que heu fet possible aquesta gran aventura plena d´aprenentatge professional i personal. Sense vosaltres no havera segut possible.

En primer lloc agraïr la tasca dels meus dos guies professionals, la Dr. Amparo Ribes Greus i el Dr. Vicent Soria Sanchis, per la seua confiança en mi per a poder desenvolupar el present treball. Amparo, gràcies per donar-me la oportunitat de fer el doctorat al teu grup d´investigació, el qual més que un grup d´investigació és una gran família. Gràcies per la teua orientació i estímul al llarg d'estos anys de doctorat i convivència. Vicent, gràcies per confiar en mi des del primer moment. Per estar sempre ahí, en les bones i en les no tan bones. Per a tu mai és mal moment, sempre tens temps per a transmitir-me eixa força que desprens. Mil gràcies, perquè aquesta passió que tenim pels polímers ha resultat en una bonica amistat. Com tu dius…Som un gran equip!

I would like to express my gratitude to Dr. Katsuhiko Ariga for giving me the opportunity to work in his Supermolecules research group during my two internships in the National Institute for Material Science in Japan. Very special thanks to Dr. Gaulthier Rydzek for all his wise advices and his enormous help throughout my study. It was a pleasure to work with you; thanks for discover me the science from your amazing point of view.

Al Dr. Julio San Román por darme la oportunidad de poder realizar una parte fundamental de mi trabajo en su grupo de Biopolimeros en el ICTP-CSIC de Madrid. Gracias por tu confianza y disponibilidad, y por transmitirme de esa forma tan positiva que te caracteriza tu pasión por la investigación. A todo el equipo del grupo de Biopolimeros, gracias por hacerme sentir como en casa, però en especial al Dr. Luis Rojo por introducirme en el mundo de las bacterias y descubrir juntos lo "*killers*" que podian llegar a ser mis membranas.

Al Dr. Benito Gimeno i al Dr. Rafael Mata per tota la vostra ajuda en posar a la nostra disposició l´equip d´Espectroscopía Fotoelectrónica de raigs X. Benito, moltíssimes gràcies per la teua ajuda i dedicació amb les classes de física i els circuits elèctrics, tu vares fer de lo difícil algo fàcil.

Agraïr tant als tècnics de laboratori de la Universitat de València (UV) com al Servei de Microscòpia Electrònica de la Universitat Politècnica de València (UPV) per permetre el desenvolupament de part d´aquest treball a les seues instal·lacions. Gràcies també a la Dr. Clara Gómez per les facilitats donades per accedir a algunes de les tècniques instrumentals ubicades a les instal·lacions del ICMUV i del departament de Química Física de la UV.

Marga, moltíssimes gràcies per la teua implicació amb tot el que fas, i per la teua paciència al explicar-me una i mil voltes cada dubte que m´ha sorgit al llarg de la tesi,

Summary

Poly(vinyl alcohol) (PVA)-based membranes have gathered significant interest because of their film forming ability and low cost. These films are usually crosslinked to provide a macromolecular network with high dimensional stability. PVA can be modified by introduction of sulfonic acid groups (sPVA) contributing to increase its proton conductivity (σ_{prot}). In addition, the preparation of hybrid organic-inorganic composite membranes by the addition of graphene oxide (GO) as nano-filler not only reinforces the matrix but also decreases the permeability of solvents. All this has motivated the use of these materials for the preparation of proton exchange membranes (PEMs) for direct methanol fuel cell (DMFC) applications.

Contribution I presents the chemical schemes followed for the bi-sulfonation of the PVA, the synthesis of GO and the preparation of PVA/GO and sPVA/GO composite membranes. In addition, a structural, morphological, thermal, and mechanical characterization of the starting materials and the composite membranes were performed. Finally, in order to evaluate the suitability of the prepared PEMs in fuel cells, the σ_{prot} was evaluated at room temperature. The results showed that the addition of GO (1 wt.%) into the sPVA matrix, 30sPVA/GO membrane, enhance by 89% the σ_{prot} compared to its homologue membrane, 30sPVA, free-standing of GO.

In **Contribution II**, the proton conductive properties of the previously prepared membranes were investigated as a function of the structural (bi-sulfonation) and morphological (crosslinking and addition of GO) modifications. The bi-sulfonated membrane reinforced with GO, 30sPVA/GO, stands out over the rest. The addition of GO improves considerably its σ_{prot} (20.96 mS/cm at 90 °C) and its maximum power density (P_{max}) in the H_2-O_2 fuel cell test (13.9 mW/cm^2 at 25 ℃).

In **Contribution III** was studied the effect of a new variable, the sufonation of the GO (sGO), on the functional properties of the composites PVA/sGO and sPVA/sGO for DMFC applications. In addition, the results were compared to that obtained for the previously described PVA/GO and sPVA/GO composites. The results conclude that, contrary to expectations, the multiple sulfonation of the 30sPVA/sGO composite strongly reduces the σ_{prot} (5.22 mS/cm at 50 °C) compared to its homologue 30sPVA/GO (8.42 mS/cm at 50 °C), despite its higher values of ion exchange capacity (IEC). Finally, the 30PVA/sGO composite (1.85 mW/cm^2) shows a significant improvement of the DMFC performance (50 °C, 4M methanol solution) compared to the 30sPVA/GO composite (1.00 mW/cm^2).

The Layer-by-Layer (LbL) assembly method was used in **Contribution IV** for the preparation of composite membranes assembled via hydrogen bonding interactions. To do this, GO/PVA and GO/sPVA bilayers were deposited on the surface of 15PVA and 15sPVA substrate membranes, respectively. The composites were denoted as

15PVA(GO/PVA)$_n$ and 15sPVA(GO/sPVA)$_n$ where n is the number of deposited bilayers, in our case n ranges between 1 and 3. Finally, the potential of the composite membranes for DMFC applications were evaluated, showing the best performance the 15sPVA(GO/sPVA)$_1$ composite.

Finally, the **Contribution V** was focused on the preparation of composite membranes by LbL Assembly method, but in this case the assembly forces were electrostatic interactions. The GO was dispersed in a poly(allyl amine hydrochloride) solution (GO-PAH) in order to obtain a positively charged solution. The composites were assembled by alternate deposition of GO-PAH and sPVA layers on the surface of 15PVA and 15sPVA substrates, obtaining as a result the composites 15PVA(GO-PAH/sPVA)$_n$ and 15sPVA(GO-PAH/sPVA)$_n$. The best value of σ_{prot} (8.26 mS/cm at 90 °C) was obtained for the 15PVA(GO-PAH/sPVA)$_1$ composite, almost twice that the value obtained for its homologue sulfonated composite 15sPVA(GO-PAH/sPVA)$_1$ (4.96 mS/cm a 90 °C).

Resum

Membranes constituïdes a base d´alcohol polivinílic (PVA) han despertat un gran interès a causa del seu baix cost i el seu fàcil processament per conformar-les en forma de films. Aquests films freqüentment són sotmesos a entrecreuament per disposar d'una xarxa macromolecular amb una elevada estabilitat dimensional. La modificació del PVA per introducció de grups sulfònics (sPVA) canvia l'estructura del polímer contribuint a augmentar la seua conductivitat protònica (σ_{prot}). A més, la preparació de membranes híbrides orgànic-inorgànics (*composites*) mitjançant l´addició d'òxid de grafè (GO) reforça la matriu, alhora que disminueix la seua permeabilitat enfront de dissolvents. Tot això ha motivat l'ús d'aquests materials per a la preparació de membranes d'intercanvi protònic (PEMs) emprades en piles de combustible de metanol (DMFCs).

En la *Contribució I* es presenten els esquemes químics conduents a la bi-sulfonació del PVA, la síntesi del GO i la preparació de les membranes *composite* PVA/GO i sPVA/GO. A més, es va realitzar la caracterització estructural, morfològica, tèrmica i mecànica de cada un dels materials de partida i de les membranes *composite*. Finalment, per tal d'avaluar la seua idoneïtat com a PEMs en piles de combustible, es va mesurar la seua σ_{prot} a temperatura ambient. Els resultats obtinguts van mostrar que l´addició de GO (1 wt.%) com a nano-càrrega en la matriu de sPVA genera un *composite*, 30sPVA/GO, amb una σ_{prot} que supera en un 89% a la de la seua membrana homòloga sense càrrega, 30sPVA.

La *Contribució II* tracta d'explorar les propietats conductores de les membranes *composite* preparades prèviament en funció de la modificació estructural (bi-sulfonació) i morfològica (reticulació i addició de GO). La membrana bi-sulfonada i reforçada amb GO, 30sPVA/GO, destaca sobre la resta. L'addició de GO millora considerablement tant la σ_{prot} (20.96 mS/cm a 90 °C) com la densitat de potència màxima (P_{max}) a la pila de combustible d'hidrogen (13.9 mW/cm^2 a temperatura ambient).

En la *Contribució III* es va estudiar l'efecte d'una nova variable, la sulfonació del GO (sGO), sobre les propietats funcionals dels *composites* PVA/sGO i sPVA/sGO per aplicacions en DMFC. A més, es va dur a terme un estudi comparatiu amb els *composites* PVA/GO i sPVA/GO prèviament descrits. Els resultats van concloure que en contra del que s'esperava, la múltiple sulfonació de la membrana 30sPVA/sGO redueix fortament la seua σ_{prot} (5.22 mS/cm a 50 °C) en comparació amb la seua homòloga 30sPVA/GO (8.42 mS/cm a 50 °C), tot i que mostra valors superiors de capacitat d'intercanvi iònic (IEC). Finalment, el rendiment de la membrana 30PVA/sGO (1.85 mW/cm^2) en una DMFC (50 °C, dissolució de metanol 4M) va mostrar una millora significativa en comparació amb la membrana 30sPVA/GO (1.00 mW/cm^2).

El mètode de *Layer-by-Layer (LBL) assembly* es va emprar en la ***Contribució IV*** per a la preparació de *composites* acoblats mitjançant enllaços per pont d'hidrogen. Amb aquest fi, es va dur a terme la deposició de bicapes de GO/PVA i GO/sPVA sobre els substrats 15PVA i 15sPVA, respectivament. Els *composites* es van codificar com a $15PVA(GO/PVA)_n$ i $15sPVA(GO/sPVA)_n$ on *n* és el nombre de bicapes dipositades, en el nostre cas *n* varia entre 1 i 3. Finalment, es va avaluar el seu potencial per a aplicacions en DMFC, presentant el millor comportament el *composite* $15sPVA(GO/sPVA)_1$.

Finalment, la ***Contribució V*** va dedicada a la fabricació de *composites* mitjançant el mètode de *LBL Assembly*, però en aquest cas acoblats a través d'interaccions electrostàtiques. El GO es va dispersar en una dissolució de hidroclorur de polialilamina (GO-PAH), per tal de dotar-lo de càrrega positiva. L'acoblament es va realitzar per deposició alterna de capes de GO-PAH i sPVA, obtenint-se els *composites* $15PVA(GO-PAH/sPVA)_n$ i $15sPVA(GO-PAH/sPVA)_n$. El millor valor de σ_{prot} (8.26 mS/cm a 90 ºC) es va obtenir per al *composite* $15PVA(GO-PAH/sPVA)_1$, sent gairebé el doble que l'obtingut per al seu homòleg sulfonat $15sPVA(GO-PAH/sPVA)_1$ (4.96 mS/cm a 90 ºC).

Resumen

Membranas constituidas básicamente por alcohol polivinílico (PVA) han despertado un gran interés debido a su bajo coste y su fácil procesado para conformarlas en forma de films. Estos films frecuentemente son sometidos a entrecruzamiento para disponer de una red macromolecular con una elevada estabilidad dimensional. La modificación del PVA por introducción de grupos sulfónicos (sPVA) cambia la estructura del polímero contribuyendo a aumentar su conductividad protónica (σ_{prot}). Además, la preparación de membranas híbridas orgánico-inorgánicas (*composites*) mediante la adición de óxido de grafeno (GO) refuerza la matriz, a la vez que disminuye su permeabilidad frente a disolventes. Todo ello ha motivado el uso de estos materiales para la preparación de membranas de intercambio protónico (PEMs) empleadas en pilas de combustible de metanol (DMFCs).

En la ***Contribución I*** se presentan los esquemas químicos conducentes a la bi-sulfonación del PVA, la síntesis del GO y la preparación de las membranas *composite* PVA/GO y sPVA/GO. Además, se realizó la caracterización estructural, morfológica, térmica y mecánica de cada uno de los materiales de partida y de los *composite*. Finalmente, con el fin de evaluar su idoneidad como PEMs en pilas de combustible, se evaluó su σ_{prot} a temperatura ambiente. Los resultados obtenidos mostraron que la adición de GO (1 wt.%) como nano-carga a la matriz de sPVA genera un *composite*, 30sPVA/GO, cuya σ_{prot} supera en un 89 % a la de su membrana homóloga sin carga, 30sPVA.

La ***Contribución II*** trata de explorar las propiedades conductoras de las membranas preparadas previamente en función de la modificación estructural (bi-sulfonación) y la morfológica (reticulación y adición de GO). La membrana bi-sulfonada y reforzada con GO, 30sPVA/GO, destaca sobre el resto. La adición de GO mejora considerablemente tanto la σ_{prot} (20.96 mS/cm a 90 ºC) como la densidad de potencia máxima (P_{max}) en pila de combustible de hidrógeno (13.9 mW/cm^2 a temperatura ambiente).

En la ***Contribución III*** se estudió el efecto de una nueva variable, la sulfonación del GO (sGO), sobre las propiedades funcionales de los *composites* PVA/sGO y sPVA/sGO en aplicaciones de DMFC. Además, se llevó a cabo un estudio comparativo con los *composite* PVA/GO y sPVA/GO previamente descritos. Los resultados concluyeron que, en contra a lo esperado, la múltiple sulfonación de la membrana 30sPVA/sGO reduce fuertemente su σ_{prot} (5.22 mS/cm a 50 ºC) en comparación con su homóloga 30sPVA/GO (8.42 mS/cm a 50 ºC), aun mostrando valores superiores de capacidad de intercambio iónico (IEC). Finalmente, el rendimiento de la *composite* 30PVA/sGO (1.85 mW/cm^2) en una DMFC (50 ºC, disolución de metanol 4M) mostró una mejora significativa en comparación con la *composite* 30sPVA/GO (1.00 mW/cm^2).

El método de *Layer-by-Layer (LbL) assembly* se empleó en la **Contribución IV** para la preparación de *composites* ensamblados mediante enlaces por puente de hidrógeno. Para ello, se llevó a cabo la deposición de bicapas de GO/PVA y GO/sPVA sobre los substratos 15PVA y 15sPVA, respectivamente. Los *composites* se codificaron como 15PVA(GO/PVA)$_n$ y 15sPVA(GO/sPVA)$_n$ siendo *n* el número de bicapas depositadas, en nuestro caso *n* varía entre 1 y 3. Por último, se evaluó su potencial para aplicaciones en DMFC, presentando el mejor comportamiento el *composite* 15sPVA(GO/sPVA)$_1$.

Finalmente, la **Contribución V** va dedicada a la fabricación de *composites* mediante el método de *LbL Assembly*, pero en este caso a través de interacciones electrostáticas. El GO se dispersó en una disolución de hidrocloruro de polialilamina (GO-PAH), con el fin de dotarlo de carga positiva. El ensamblaje se realizó por deposición alterna de capas de GO-PAH y sPVA, obteniéndose los *composites* 15PVA(GO-PAH/sPVA)$_n$ y 15sPVA(GO-PAH/sPVA)$_n$. El mejor valor de σ_{prot} (8.26 mS/cm a 90 ºC) se obtuvo para el *composite* 15PVA(GO-PAH/sPVA)$_1$, siendo casi el doble que el obtenido para su homólogo sulfonado 15PVA(GO-PAH/sPVA)$_1$ (4.96 mS/cm a 90 ºC).

Abbreviations

AFC	Alkaline Fuel Cell
AFM	Atomic Force Microscopy
ATR	Attenuated Total Reflectance
D_{MeOH}	Methanol diffusion coefficient
DMFC	Direct Methanol Fuel Cell
E_a	Activation Energy
EDX	Energy Dispersive X-ray spectroscopy
EIS	Electrochemical Impedance Spectroscopy
FC	Fuel Cell
FTIR	Fourier Transform Infrared Spectroscopy
GA	Glutaraldehyde
GDL	Gas Diffusion Layer
GO	Graphene Oxide
ICP-OES	Inductively Coupled Plasma-Optical Emission Spectroscopy
IEC	Ion Exchange Capacity
LbL	Layer-by-Layer
MCFC	Molten Carbonate Fuel Cell
MHM	Modified Hummers Method
MU	Methanol Uptake
P_{max}	Maximum Power density
PAFC	Phosphoric Acid Fuel Cell
PAH	Poly(allylAmine) Hydrochloride
PEM	Proton Exchange Membrane
PEMFC	Proton Exchange Membrane Fuel Cell
PFSA	Perfluorosulfonic Acid
PVA	Poly(vinyl alcohol)
σ_{elect}	Electrical conductivity

σ_{prot}	Proton conductivity
SEM	Scanning Electron Microscopy
sGO	Sulfonated Graphene Oxide
SOFC	Solid Oxide Fuel Cell
sPVA	Sulfonated poly(vinyl alcohol)
SSA	Sulfosuccinic acid
SW	Swelling ratio
TEM	Transmission Electron Microscopy
TGA	Thermogravimetric Analysis
WU	Water Uptake
XPS	X-Ray Photoelectron Spectroscopy
XRD	X-Ray Diffraction

Summary PVA-based proton exchange membranes

Number	Acronym	Description	Chapter-Contribution
M1	15PVA	Inter-sulfonated membrane: PVA crosslinked with SSA (15 wt.%)	4-I / II
M2	30PVA	Inter-sulfonated membrane: PVA crosslinked with SSA (30 wt.%)	4-I / II
M3	15sPVA	Inter- and intra- sulfonated membrane: sPVA crosslinked with SSA (15 wt.%)	4-I / II
M4	30sPVA	Inter- and intra- sulfonated membrane: sPVA crosslinked with SSA (30 wt.%)	4-I / II
M5	15PVA/GO	Inter-sulfonated composite: 15PVA reinforced with GO (1 wt.%)	4-I / II / III
M6	30PVA/GO	Inter-sulfonated composite: 30PVA reinforced with GO (1 wt.%)	4-I / II / III
M7	15sPVA/GO	Inter- and intra- sulfonated composite: 15sPVA reinforced with GO (1 wt.%)	4-I / II / III
M8	30sPVA/GO	Inter- and intra- sulfonated composite: 30sPVA reinforced with GO (1 wt.%)	4-I / II / III
M9	15PVA/sGO	Multi-sulfonated composite: 15PVA reinforced with sGO (1 wt.%)	4-III
M10	30PVA/sGO	Multi-sulfonated composite: 30PVA reinforced with sGO (1 wt.%)	4-III
M11	15sPVA/sGO	Multi-sulfonated composite: 15sPVA reinforced with sGO (1 wt.%)	4-III
M12	30sPVA/sGO	Multi-sulfonated composite: 30sPVA reinforced with sGO (1 wt.%)	4-III
M13	15PVA(GO/PVA)$_1$	Hydrogen-bonding LbL composite: 1 bilayer GO/PVA	5-IV
M14	15PVA(GO/PVA)$_3$	Hydrogen-bonding LbL composite: 3 bilayers GO/PVA	5-IV
M15	15sPVA(GO/sPVA)$_1$	Sulfonated Hydrogen-bonding LbL composite: 1 bilayer GO/sPVA	5-IV

M16	15sPVA(GO/sPVA)$_3$	Sulfonated Hydrogen-bonding LbL composite: 3 bilayers GO/sPVA	5-IV
M17	15PVA(GO-PAH/sPVA)$_1$	Electrostatic LbL composite: 1 bilayer GO-PAH/sPVA	5-V
M18	15PVA(GO-PAH/sPVA)$_3$	Electrostatic LbL composite: 3 bilayers GO-PAH/sPVA	5-V
M19	15sPVA(GO-PAH/sPVA)$_1$	Sulfonated Electrostatic LbL composite: 1 bilayer GO-PAH/sPVA	5-V
M20	15sPVA(GO-PAH/sPVA)$_3$	Sulfonated Electrostatic LbL composite: 3 bilayers GO-PAH/sPVA	5-V

Contents

Chapter 1. Motivation and Overview

Chapter 2. Introduction

Chapter 3. Experimental part

Chapter 4. Solution-cast proton exchange composite membranes

Bi-sulfonation of poly(vinyl alcohol)/graphene oxide composite membranes for Proton Exchange Membrane Fuel Cell applications. Part 1: Membrane preparation and characterization

Bi-sulfonation of poly(vinyl alcohol)/graphene oxide composite membranes for Proton Exchange Membrane Fuel Cell applications. Part 2: Functional membrane properties

Chapter 5. Layer-by-Layer assembled proton exchange composite membranes

Layer-by-Layer assembly of poly(vinyl alcohol)/graphene oxide hybrid composite membranes via hydrogen-bonding interactions for direct methanol fuel cells

Layer-by-Layer assembly of poly(vinyl alcohol)/graphene oxide hybrid composite membranes via electrostatic interactions for direct methanol fuel cells

Chapter 6. Conclusions and further work

List of Figures

Chapter 1

Chapter 2

Chapter 3

Chapter 4

Chapter 5

List of Schemes

Chapter 2

Chapter 3

Chapter 4

Chapter 5

List of Tables

Chapter 5

Motivation and Overview

Chapter 1

1.1. Motivation

Fossil fuels, which include solid fuels (coal), liquid hydrocarbon (oil) and gaseous hydrocarbon (natural gas), are the most used energy sources for stationary power generation and transportation; whereas only a small part of the energy comes from renewable sources as shown in Figure 1.1 [1].
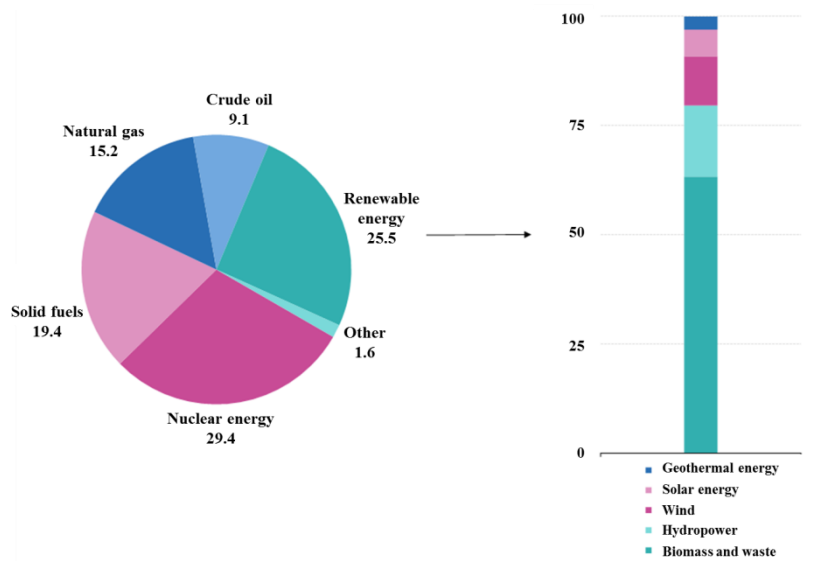
Figure 1.1. Production of primary energy 2014, EU-28 (% of total, based on tonnes of oil equivalent) (Source: Eurostat)

However, there are two main problems associated with the continued use of fossil fuels. The first one is that fossil fuels are an exhaustible energy source. The second one is the increase of greenhouse gas emissions coming from the combustion of fossil fuels along with other pollutants [2], [3]. Unless the energy system changes drastically, the global climate will be affected in the coming 100 years. The greenhouse gases emissions would lead to an increase of the average global temperature of about 4°C. This would cause extreme weather events such as heat waves and heavy rains [4].

It is clear that a change towards more sustainable energy systems with less greenhouse emissions is needed. In this sense, the international community has embraced the agreement COP21, in which 195 countries adopted the first universal legally binding global climate deal. It aims to keep "the increase in the global average temperature to well below 2 °C above pre-industrial levels and to pursue efforts to limit warming to 1.5 °C" [4].

In this context, the carbon-based energy systems should change to alternative energies. Among the different alternatives, solar, wind and tidal energy may make a significant contribution to our needs; however these contributions could be limited and there was not expected to exceed 10 % of the total demand of energy [1], [4].

Therefore, new energy carriers that contribute to the decarbonization of the primary energy are needed. Hydrogen is a versatile and clean energy carrier that can be used either as a direct fuel, or as feedstock in industry to generate energy. It can be produced from renewable electricity (electrolysis process), and from carbon-abated fossil fuels. Moreover, hydrogen produces zero emissions at the point of use, and can be stored and transported at high energy density in both liquid and gaseous form. All of these unique properties make hydrogen a powerful fuel either for direct combustion or for being used in fuel cells to produce electricity. Figure 1.2 shows the hydrogen benefits for both the energy system and end-use applications [3], [4].
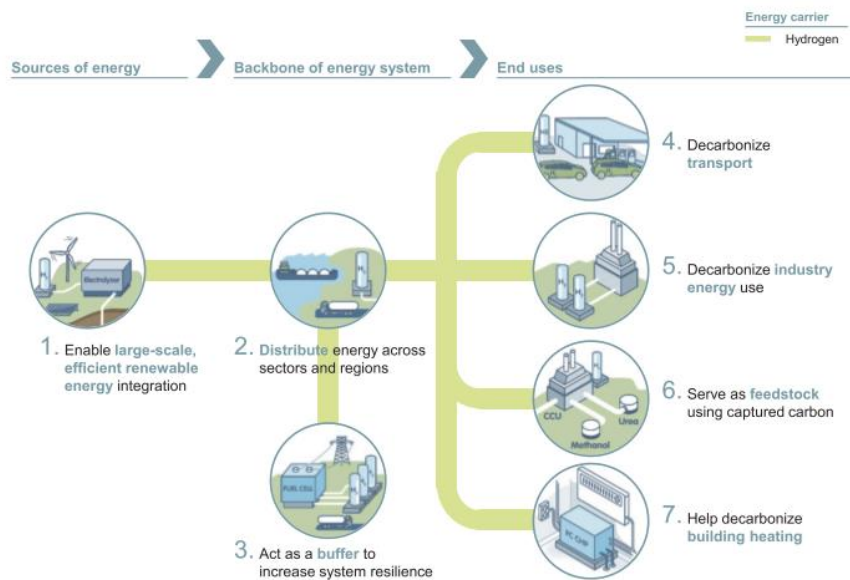
Figure 1.2. Hydrogen roles in decarbonizing major sectors of economy (Source: Hydrogen council [4])

A Fuel Cell (FC) is a device that converts the chemical energy of hydrogen into electricity through an electrochemical reaction, producing water and heat as by-products. Hence, FCs can be considered as a promising power generation systems contributing to the decarbonization [1] [3]. Moreover, the efficiency of FCs to convert chemical energy to electrical energy is higher than that obtained in the conversion of

thermal to mechanical energy in combustion engines, since the latter is limited by the Carnot cycle [5].

However, factors such as fuel cells durability and cost are still one of the major barriers to large-scale commercialization. Among various kinds of fuel cells, polymer electrolyte membrane fuel cells (PEMFC) are easy to be miniaturized and they are also suited as energy sources for automobiles as well as domestic applications and portable devices. One of the most important components in a PEMFC is the polymer electrolyte membrane, also known as proton exchange membrane (PEM), which undergoes degradation during long-term operations. The lifetime required by a commercial fuel cell is over 5000 operating hours for light-weight vehicles and over 40,000 h for stationary power generation with less than a 10% performance decay [6], [7]. Most fuel cells currently exhibit major performance decay after around a thousand hours of operation [8].

The most widely used solid PEMs in fuel cells are perfluorosulfonic acid membranes such as Nafion®. However, they have some drawbacks that must be overcome before their potential use in direct methanol fuel cells (DMFCs). The most significant drawbacks of these membranes are their relatively high cost in the range of US $ 800/m^2, and their limited stability at temperatures substantially above 100°C [9]. Moreover, there is a problem of methanol crossover when used in direct methanol fuel cell. Therefore, there is a need to develop less expensive new materials in order to improve fuel-cell performance.

A literature search on fuel cell membranes since 1990 has revealed thousands of patents and journal publications, which clearly indicated the importance of this subject. Regarding to it, polymer electrolytes membranes based on poly(vinyl alcohol) (PVA) have been recently receiving increasing attention due to their good chemical and mechanical stability, excellent film-forming property, non-toxicity and low cost.

1.2. Aim of the thesis

The aim of this thesis is the design, preparation and characterization of new proton exchange membranes (PEMs) based on inexpensive materials with high proton conductivity and low methanol permeability for their use as electrolytes in Direct Methanol Fuel Cells (DMFCs). For this purpose, hybrid organic-inorganic composite membranes have been prepared by selecting the poly(vinyl alcohol) (PVA) as polymer matrix and the graphene oxide (GO) as inorganic filler. In order to find a simple and effective procedure for the preparation of hybrid organic-inorganic composite membranes two different methods have been evaluated: solution-casting method and Layer-by-Layer (LbL) assembly method. Moreover, the multiple sulfonation of the composite membranes components, as strategy, has been used in order to enhance their proton conductivity. In this sense, the functional properties of the composite membranes have been evaluated by the effect of the intra- and inter-sulfonation of the

polymer matrix accomplished by direct sulfonation of the PVA with propane sultone (sPVA) and the crosslinking reaction using sulfosuccinic acid (SSA), respectively. In addition, a further sulfonation of the inorganic filler (sGO) has been carried out to investigate its ability to improve the proton-conducting domains in the composites. The different properties required in a PEM for DMFC applications such as thermal and mechanical stability, diffusion and proton transport properties, proton conductivity, methanol permeability and H_2-O_2 fuel cell and DMFC tests have been studied. The results have been analyzed and discussed in order to evaluate the potential of the prepared composite membranes as new proton exchange membranes for DMFC.

1.3. Outline of the thesis

The main body of the thesis is made up of six chapters, which are divided as follows:

Chapter 1 summarizes an overview of the thesis, including a brief introduction of the motivation to pursue alternatives energies to fossil fuels, highlighting the importance of fuel cells. The aim and the scope of the thesis are also given in this chapter.

Chapter 2 gives a brief introduction to fuel cells, particularly to Proton Exchange Membrane Fuel Cells (PEMFCs), as well as to the most commonly membranes used as electrolytes in this context. Among the different alternatives, poly(vinyl alcohol) is presented as a promising material, its intrinsic advantages and their current modification studies reported in the literature are also summarized in this chapter. In addition, a short reference to graphene oxide (GO) based PVA composites is included.

Chapter 3 presents the experimental procedure followed for the preparation of the starting materials (sPVA, GO and sPVA), and describes the two methodologies used for the preparation of the hybrid organic-inorganic composite membranes: solution-casting and Layer-by-Layer (LbL) assembly. A short description of the different characterization techniques used in this thesis is also described here.

Chapter 4 deals with the preparation of PVA-based composite membranes by solution-casting method. This chapter is divided into three different parts. In the first part (**Contribution I**) the preparation of sulfonated PVA/GO crosslinked composite membranes is deeply described. The effect of the sulfonation and crosslinking degree of the polymer matrix and the addition of graphene oxide (GO) on the structural (FTIR, XRD), morphological (SEM, TEM), thermal (TGA) and mechanical (tensile test) properties is discussed. Furthermore, proton conductivity measurements of the composite membranes are conducted in order to evaluate their potential as PEMs. The second part (**Contribution II**) is focused on the study of the functional properties of the GO composite membranes previously prepared in part one. In this regard, the membranes are evaluated as a function of the water contact angle, water uptake (WU) and swelling ratio (SW), ion exchange capacity (IEC), proton conductivity (σ_{prot}) and their performance in a H_2-O_2 fuel cell. Finally, the third part (**Contribution III**) introduces the sulfonation of GO (sGO) as a new strategy to improve the proton

conductivity of composite membranes. The structural, thermal, mechanical and proton-conducting properties of the composite membranes are studied in detail. Likewise, the methanol permeability and the performance in a DMFC are also evaluated.

Chapter 5 describes the preparation of composite membranes using Layer-by-Layer (LbL) assembly method, in which GO is deposited on the surface of two different substrates, 15PVA and 15sPVA. According to the intermolecular forces responsible to keep the LbL-assembled structure, two types of composite membranes were prepared: Hydrogen-bonding LbL membranes (**Contribution IV**) and Electrostatic LbL membranes (**Contribution V**). The effect of the sulfonation of the substrate, the number of deposited bilayers and the type of interactions involved for the stabilization of the LbL assembly on the proton-conducting properties was investigated. Moreover, methanol diffusion measurements were conducted as a preliminary assay, in order to explore their feasibility for DMFC applications.

Chapter 6 summarizes the general conclusions and the future work that could be developed from this study.

Figure 1.3 compiles the experimental strategy followed for the preparation of proton exchange membranes.
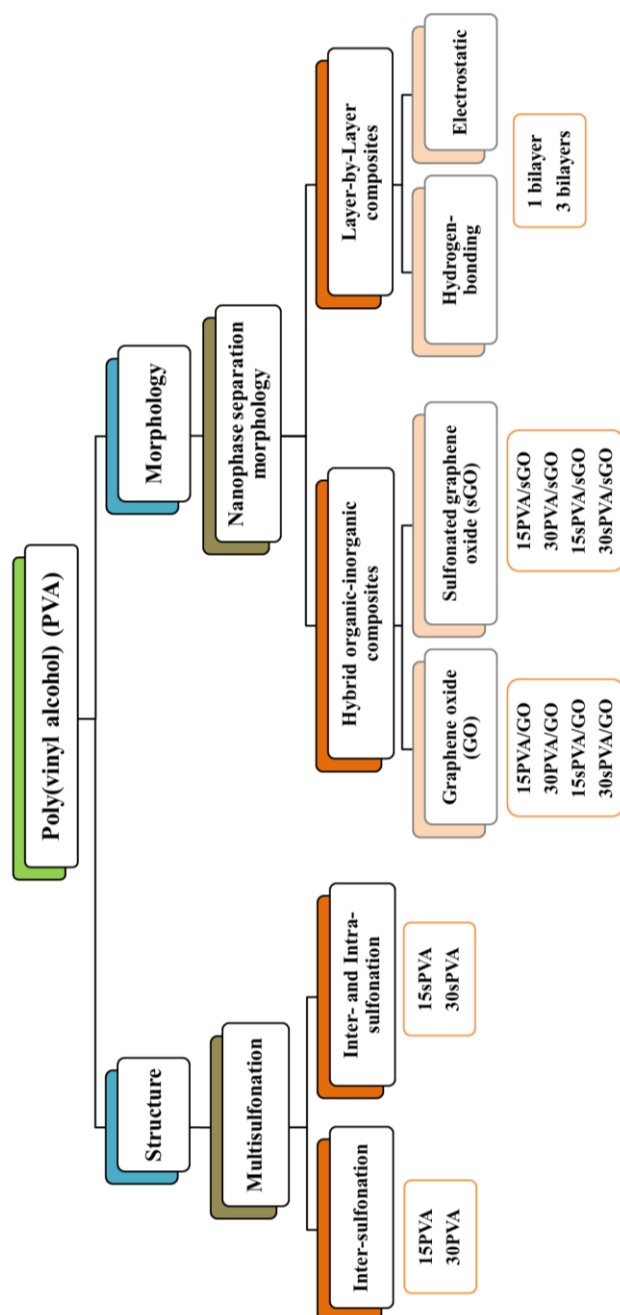
**Figure 1.3. Summary of the strategy followed for the preparation of polymer electrolyte
membranes (PEMs) for Direct Methanol Fuel Cells (DMFCs)**

References

[1] Shripad T. Revankar and P. Majumdar, *Fuel Cells: Principles, Design, and Analysis*. CRC Press, 2016.

[2] Mamadou S. Diallo, Neil A. Fromer, and Myung S. Jhon, *Nanotechnology for Sustainable Development*, Springer, 2014.

[3] F. Barbir, *PEM Fuel Cells: Theory and Practice*, Elsevier, 2013.

[4] Hydrogen Council, "How hydrogen empowers the energy transition," January, 2017.

[5] Matthew M. Mench, *Fuel Cell Engines*, John Wiley & Sons, 2008.

[6] W. Schmittinger and A. Vahidi, "A review of the main parameters influencing long-term performance and durability of PEM fuel cells," J. Power Sources, vol. 180, no. 1, pp. 1–14, 2008.

[7] Y. Wang, K. S. Chen, J. Mishler, S. C. Cho, and X. C. Adroher, "A review of polymer electrolyte membrane fuel cells: Technology, applications, and needs on fundamental research," Appl. Energy, vol. 88, no. 4, pp. 981–1007, 2011.

[8] J. P. Meyers et al., "Scientific Aspects of Polymer Electrolyte Fuel Cell Durability and Degradation . Chemical Scientific Aspects of Polymer Electrolyte Fuel Cell Durability and Degradation," vol. 107, pp. 3904–3951, 2007.

[9] S. Javaid and T. Matsuura, *Polymer Membranes for Fuel Cells*. Springer, 2009.

Introduction

Chapter 2

2.1. Fundamentals of Fuel Cells (FCs)

A fuel cell (FC) is an electrochemical device that converts the chemical energy from a fuel into electricity [1]. The main elements in a fuel cell are the electrodes, anode and cathode, and the electrolyte. The electrolyte is situated between the anode and the cathode preventing their direct contact and allowing ion transport through it from the anode to the cathode. The oxidation reaction of the fuel, usually hydrogen, takes place at the anode, releasing electrons and ions. The electrons pass through an external circuit and the ions migrate through the electrolyte to reach the cathode. At the cathode, the oxygen undergoes a reduction reaction by combining with the incoming ions and electrons, producing water. It is important that the electrolyte material only allows ion transport but not electrons [2]–[5]. A general scheme of a fuel cell is shown in Scheme 2.1.
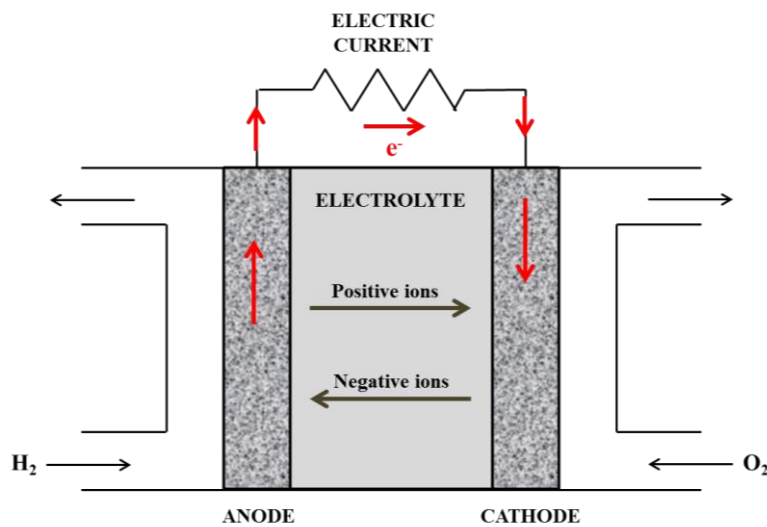
Scheme 2.1. Basic elements in a fuel cell (FC)

A fuel cell have the following characteristics [6]:

- It is an energy converting device
- The energy conversion is via an electrochemical process
- It converts the chemical energy into electricity in only one step
- It does not store the reactants within the reactor

A fuel cell has several characteristics similar to a battery. Both fuel cell and battery consist of two electrodes and an electrolyte, and generate electricity from an electrochemical reaction. In batteries, the reactants involved in the electrochemical reactions are already inside of the device. When the reactants are exhausted, the battery is discharged. There are rechargeable batteries, which means that the battery can be recharged reversing the electrochemical reaction by applying an external electrical source of current. However, a complete charging cycle takes several hours to be completed. Fuel cells, unlike batteries, operate continuously as long as a constant supply of fuel and oxidant is provided. Summing up, the limited lifetime of batteries and the need for an external energy source to recharge them makes batteries an energy storage device. In contrast, fuel cells are energy conversion devices. The absence of charge-discharge cycles in fuel cells enhances the stability of the electrolyte and the other materials of the cell, increasing the device lifetime [1], [6]. The main characteristics of batteries and fuel cells are included in Table 2.1 for comparison.

Table 2.1. Comparison of the main characteristics of batteries and fuel cells [6]

Parameter	Battery	Fuel Cell
Reaction type	Electrochemical	Electrochemical
Efficiency	High	High
Fuel Location	Inside	Outside
Refueling	Electrical charging	Add fuel
Refueling time	Long (hours)	Short (minutes)
Running time per refueling	Short	Long
Reaction noise	No	Low

2.2. Classification of Fuel Cells

The different types of fuel cells can be classified depending on the type of electrolyte, fuel type, temperature of operation and the physical nature of the electrolyte (solid or liquid). According to the type of electrolyte, the most common fuel cells are [5], [7]-[9]:

- Alkaline Fuel Cells (AFC)

- Phosphoric Acid Fuel Cells (PAFC)

- Molten Carbonate Fuel Cells (MCFC)

- Solid Oxide Fuel Cells (SOFC)

- Proton Exchange Membrane Fuel Cells (PEMFC)

Alkaline Fuel Cells (AFCs)

An AFC can use as electrolyte a potassium hydroxide solution (KOH) or a sodium hydroxide solution (NaOH). The mobile ion transported through the electrolyte is the hydroxyl ion (OH^-). At the anode, the hydroxyl ion reacts with the hydrogen releasing electrons (e^-) and water as a product. The electrons move along an external circuit towards the cathode where they react with the oxygen and water to form new hydroxyl ions. The electrochemical half-reactions in an AFC are:

$$\text{Anode: } 2\,OH^- + H_2 \rightarrow 2\,H_2O + 2e^-$$

$$\text{Cathode: } 1/2\,O_2 + H_2O + 2e^- \rightarrow 2\,OH^-$$

AFCs operate in the temperature range from 60 to 120 °C, with an operating efficiency of 60 %. The use of AFCs is restricted since they can only operate with pure hydrogen and oxygen. This measure is needed in order to avoid the contamination of the NaOH or KOH solutions with CO_2, which would decrease dramatically the electrolyte conductivity. AFCs are the most developed fuel cells in terms of history. This technology has being successfully used in space applications since the 1960s, being further developed by NASA for the Apollo space program.

Phosphoric Acid Fuel Cells (PAFCs)

The electrolyte used in PAFCs is a phosphoric acid (H_3PO_4) solution, being the proton (H^+) the mobile ion. At the anode, the hydrogen is oxidized to protons and electrons. The protons are transferred to the cathode across the electrolyte, while the electrons go through an external electric circuit. At the anode, the protons and the electrons react with the oxygen in a reduction reaction forming water. The electrochemical half-reactions in a PAFC are:

$$\text{Anode: } H_2 \rightarrow 2\,H^+ + 2\,e^-$$

$$\text{Cathode: } 1/2\,O_2 + 2\,e^- + 2\,H^+ \rightarrow H_2O$$
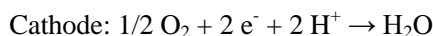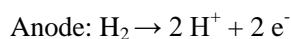
PAFCs are intermediate temperature fuel cells which operate at around 200 ºC, with an operating efficiency of 40%. The PAFC systems are mainly applied for stationary power generation.

Molten Carbonate Fuel Cells (MCFCs)

A molten alkali carbonate such as lithium or potassium carbonate retained in a ceramic matrix is used as electrolyte in MCFCs. The mobile ion in this type of fuel cells is the carbonate ion (CO_3^{-2}). At the anode, the hydrogen is reduced by combination with carbonate ions, releasing electrons to the external electric circuit and producing water and carbon dioxide (CO_2). At the cathode, the oxygen is reduced by reaction with the CO_2 and the incoming electrons, releasing carbonate ions. The electrochemical half-reactions in a MCFC are:

$$\text{Anode: } H_2 + CO_3^{-2} \rightarrow H_2O + CO_2 + 2\,e^-$$

$$\text{Cathode: } 1/2\,O_2 + CO_2 + 2\,e^- \rightarrow CO_3^{-2}$$
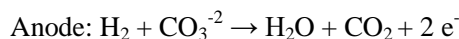
MCFCs are high temperature fuel cells which operate in the range from 600 to 700 °C with an operating efficiency of 65%. At the anode, carbon dioxide is produced as a final product, but it is also consumed at the cathode. Hence, the carbon dioxide produced at the anode can be recovered and recirculated to the cathode contributing to reduce the greenhouse gas emissions. Besides hydrogen, MCFCs can use other types of fuels such as natural gas, biogas and clean coal gas. The main application of MCFCs is in stationary power generation.

Solid Oxide Fuel Cells (SOFCs)

SOFCs use as electrolyte a solid ceramic-based material. The mobile ion in this type of fuel cells is the oxygen ion (O^{-2}). At the cathode, the oxygen takes electrons to form the negatively charged oxygen ion. The oxygen ion is transported across the solid electrolyte towards the anode where it reacts with the hydrogen producing water and releasing electrons. The electrons move to the cathode through an external electric circuit. The electrochemical half-reactions in a SOFC are:

$$\text{Anode: } H_2 + O^{-2} \rightarrow H_2O + 2\,e^-$$

$$\text{Cathode: } 1/2\,O_2 + 2\,e^- \rightarrow O^{-2}$$
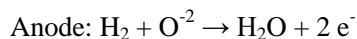
SOFCs are high temperature fuel cells that work in temperature range from 800 ºC to 1000 °C, and their operating efficiency is 65%. They can work with hydrogen or with other fuels such as hydrocarbon including natural gas and clean coal gas. Stationary power generation is among their main applications.

Proton Exchange Membrane Fuel Cells (PEMFC)

The name of proton exchange membrane fuel cells (PEMFCs) comes from the use of polymer membranes as electrolyte being their mobile ion the proton (H^+). This type of fuel cell was first developed by DuPont for the chlor-alkali industry. A basic design of a PEMFC includes the following components [3], [5], [9]–[11]:

- **Electrodes**. There are two electrodes in which the electrochemical reactions take place. The fuel is oxidized at the anode, and the oxidant is reduced at the cathode. The electrodes are coated with a catalyst layer in order to reduce the activation energy of the electrochemical reactions. Electrodes are usually made of porous materials to achieve a high surface area to volume ratio.

- **Electrolyte**. The electrolyte is one of the vital components of a PEMFC; it separates the anode from the cathode avoiding the flow of the reactants from one side to the other of the cell. PEMFCs use a proton exchange membrane (PEM) as electrolyte, which must be permeable to protons while acting as an electronic insulator.

- **Gas diffusion layers (GDL)**: The gas diffusion layers are the components that supply and distribute the fuel and the oxidant to the surface of electrodes. Likewise, GDL remove the exhausted reactants and the reaction products of the electrochemical reactions.

Scheme 2.2 shows a scheme of the basic components in a PEMFC.
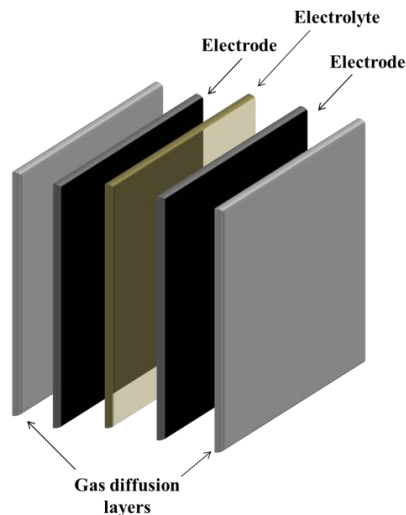
Scheme 2.2. Schematic representation of a PEMFC

In a PEMFC, the supplied fuel (H_2 gas) is transported through the anode electrode, and oxidized at the electrode-membrane interface in the presence of a catalyst layer, releasing electrons and protons. The protons are transported through the electrolyte membrane toward the cathode interface, and the electrons move along the external circuit. At the cathode, the oxygen is reduced at the electrode-membrane interface by combining with the incoming protons and electrons to produce water as final product [3], [5]. A schematic diagram of a PEMFC is shown in Scheme 2.3.
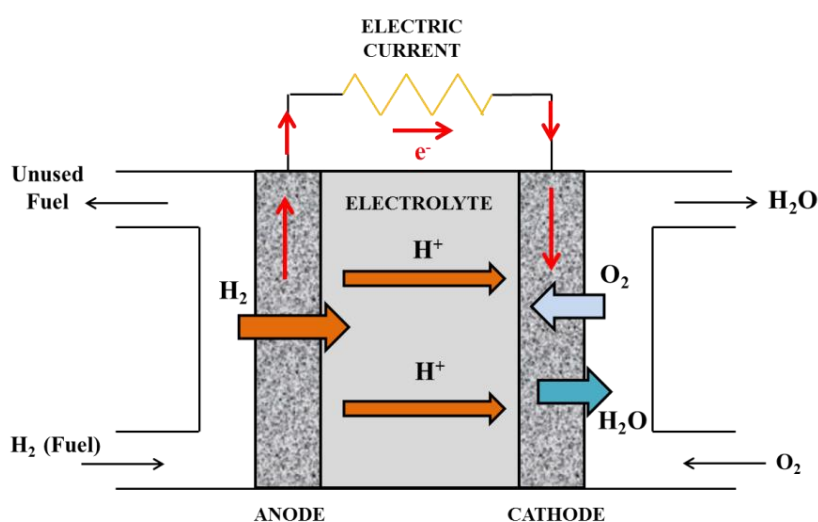
Scheme 2.3. Schematic diagram of a Proton Exchange Membrane Fuel Cell (PEMFC)

The electrochemical half-reactions and the overall reaction that take place in a PEMFC are as follows:

$$\text{Anode: } H_2 \rightarrow 2\,H^+ + 2\,e^-$$

$$\text{Cathode: } 1/2\,O_2 + 2\,H^+ + 2\,e^- \rightarrow H_2O$$

$$\text{Overall reaction: } H_2 + 1/2\,O_2 \rightarrow H_2O$$
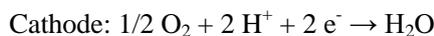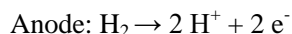
The electrochemical reactions at the anode and the cathode take place at the same time, producing electricity and water. Moreover, the electrolyte must allow only the migration of protons through it, acting as a total insulator to the electrons. Any transfer of electrons through the electrolyte will reduce the pass of electrons along the external electric circuit, causing voltage losses. Likewise, the electrolyte must be impermeable to the fuel; otherwise a reduction of fuel cell performance will be produced [5].

PEMFCs are an attractive type of fuel cells due to their low operating temperature, usually bellow 80 ºC with an efficiency of 60 %. This allows them a start-up much faster than the fuel cells that work at high temperature [4]. Moreover, this kind of fuel cell is compact and lightweight, and it has not corrosive fluid hazards. All these facts make the PEMFCs especially suitable for automotive industry and portable applications [11].

A single PEMFC is only able to produce a certain voltage and current. In order to obtain a higher voltage or current, PEMFCs can be connected in either series or parallel, respectively, forming the so-called stacks [11] as shown in Figure 2.1.
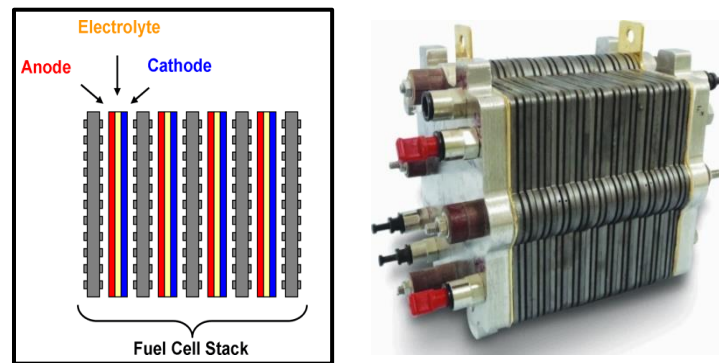
Figure 2.1. Schematic representation of a PEMFC stack [4]

The different types of fuel cells and their most relevant characteristics are summarized in Table 2.2 [9].

Table 2.2. Classification of the different types of fuel cells and their main features

Fuel Cell	Electrolyte	Mobile ion	Operating Temperature (ºC)	Electric efficiency (%)
AFC	KOH / NaOH solution	OH^-	60-120	60
PAFC	H_3PO_4 solution	H^+	160-200	40
MCFC	Lithium or potassium carbonate	CO_3^{-2}	600-700	65
SOFC	Ceramic compound	O^{-2}	800-1000	65
PEMFC	Solid polymer	H^+	20-120	60

2.3.   Direct Methanol Fuel Cells (DMFCs)

PEMFCs are particularly attractive for a wide range of applications because of their high efficiency, compactness, and quick start up. Unfortunately, the use of hydrogen as fuel has several disadvantages. PEMFCs require very pure hydrogen input stream to avoid the poisoning of the catalysts with nitrogen oxides, sulfur oxides or carbon monoxide, which would decrease their performance. Therefore, very strict pretreatment operations are needed before the hydrogen steam enters into the cathode. Moreover, the storage and high flammability problems of hydrogen are not yet completely solved, hence the use of alternatives fuels such as methanol have been investigated [12].

Direct Methanol Fuel Cells (DMFCs), a variation of the PEMFCs, allow the use of methanol (CH_3OH) as a fuel. DMFC gets its name from the use of methanol instead of hydrogen as fuel. Its structure is similar to those PEMFCs, including a proton exchange membrane as electrolyte and two electrodes coated with catalyst layers. Methanol is directly introduced to the fuel cell without reforming processes. Usually, a mixture of methanol and water is supplied to the anode as fuel [5], [4], [13]–[17].

At the anode, the methanol is oxidized to protons, electrons and carbon dioxide. The electrons are transported through an external electric circuit toward the cathode, and the protons migrate through the electrolyte membrane. At the cathode, the protons react with the oxygen and the returning electrons to form water [18]. A schematic diagram of a DMFC is shown in Scheme 2.4.
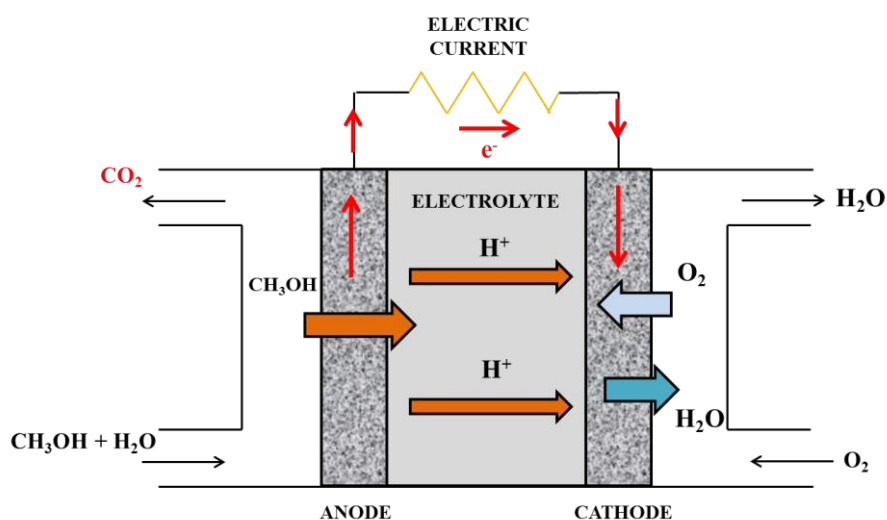
Scheme 2.4. Schematic diagram of a Direct Methanol Fuel Cell (DMFC)

The electrochemical half-reactions taking place in a DMFC are as follows:

$$\text{Anode: } CH_3OH + H_2O \rightarrow CO_2 + 6\,H^+ + 6\,e^-$$

$$\text{Cathode: } 3/2\,O_2 + 6\,H^+ + 6\,e^- \rightarrow 3\,H_2O$$

$$\text{Overall reaction: } CH_3OH + 3/2\,O_2 \rightarrow 2\,H_2O + CO_2$$
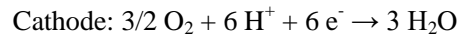
Methanol is liquid in the temperature range from -97 ℃ to 64 ℃ at atmospheric pressure. This allows it to be easily stored and transported as other liquid fuels like gasoline and diesel, making DMFCs suitable for portable technological applications [5]. In addition, methanol can be produced from biomass sources (bio-methanol), balancing the CO_2 formed during fuel cell performance by that consumed in the photosynthesis of plants. Therefore, this process could contribute to diminish the greenhouse effect [13].

However, there are two major technical problems that must be overcome before DMFCs can be successfully used at industrial scale. The first one is the slow methanol oxidation kinetics at the anode. The second one is the diffusion of methanol from the anode to the cathode through the electrolyte, the so-called methanol crossover effect. The operating efficiency of DMFCs is strongly reduced by methanol crossover, since when methanol reaches the cathode it is oxidized, leading to a "mixed potential" and a decreasing of the cell voltage [8], [16], [19].

In order to suppress or mitigate methanol crossover, several approaches have been reported [2], [11], [19]:

- Diluted methanol solutions. The lower the methanol concentration at the anode, the lower the methanol diffusion through the membrane, reducing the methanol crossover.

- Thicker electrolytes clearly reduce the methanol crossover but limit its performance by increasing the fuel cell resistance.

- Developing new proton-conducting membranes less methanol-permeable.

2.4. Proton Exchange Membrane (PEM)

As mentioned above, the proton exchange membrane (PEM) is the main component in a DMFC that allows protons, but not electrons, to go through it. A PEM must meet the following requirements [7], [9]:

- High proton conductivity

- Electrical insulator

- Chemical and electrochemical stability in the fuel cell operating environment (high resistance to oxidation, reduction, and hydrolysis)

- High mechanical and thermal stability under fuel cell operating conditions

- Good dimensional and morphological stability

- Low permeability to fuel and oxidant reactants to maximize the coulombic efficiency

- High durability

- Low cost

The performance of fuel cells depends not only on the performance of the electrochemical reactions, but also on the complex mass and energy transfer processes. To achieve good fuel cell performance, high proton conductivity is essential, especially at high current densities. Therefore, one of the main characteristics to consider in a PEM to evaluate its potential in fuel cell applications is the proton conductivity. The proton transport at a molecular level in hydrated polymer membranes can be understood by two widely recognized models: the Grotthus mechanism and the Vehicular mechanism [17], [20], [21]. Scheme 2.5 shows schematically the differences in proton transport in each model.

- **Grotthus mechanism**. In the Grotthus mechanism, protons hop from one hydrolyzed ionic site ($SO_3^-H_3O^+$) to another through the membrane by the formation and destruction of hydrogen bonds. According to this mechanism, hydrophilic ionic clusters are swollen by absorbing water and consequently form an interconnected network for proton transfer.

- **Vehicular mechanism**. This mechanism involves the movement of hydrated proton aggregates. The hydrated protons carry one or more molecules of water ($H^+(H_2O)_x$) through the membrane and are transferred with them as a result of electro-osmotic drag. The major condition for proton transport through the Vehicular mechanism is the

existence of free volume within the polymer matrix, which allows the passage of hydrated protons through the membrane.
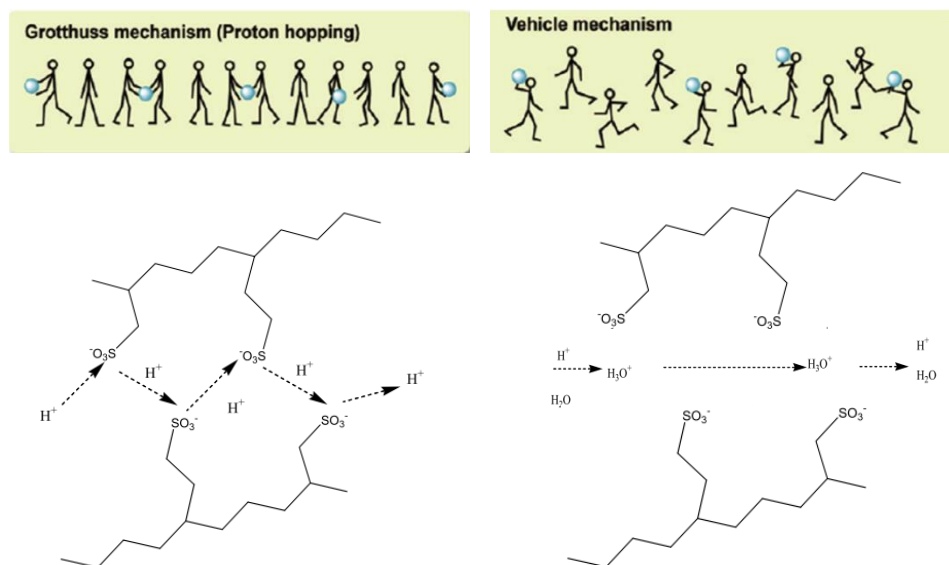
Scheme 2.5. Schematic representation of the Grotthus and Vehicular mechanisms [10], [20]

In this regard, two main types of water can be found in the membranes, free water and linked water. The former is referred to the non-associated water with the polymer matrix that can be readily removed from the membrane and is responsible for the Vehicular transport. The latter is the water associated to the polymer matrix, which remains in the structure of the polymer and is related to the Grotthus transport mechanism.

Therefore, proton conductivity in PEMs is directly related to the hydration of membranes, thus membranes must be designed to reach a certain degree of hydration. The absorbed water helps protons to go through the membrane. Thereby higher water uptake generally improves the proton conductivity. However, an excess of absorbed water can lead to undesired effects such as low dimensional stability and a drastic reduction of the mechanical properties, which reduce the membrane performance. Moreover, high water content can promote methanol crossover. Therefore, an optimal water uptake is needed in PEMs.

2.4.1. Proton Exchange Membranes for DMFCs

Fluorinated polymers

The most common electrolytes used in DMFCs are those based on perfluorosulfonic acid (PFSA) polymers which contain proton conducting groups attached via side chains. PFSA membranes have excellent proton conductivity and high chemical and mechanical stability [9], [22]. Nafion®, a type of PFSA membrane, was first developed and studied at the end of 1960s for its use as separator in the chlor-alkali industry. Nafion® is a free-radical initiated copolymer of a perfluorinated vinyl ether sulfonyl fluoride comonomer with tetrafluoroethylene (TFE) [22], [23]. The sulfonic acid groups ($-SO_3H$) situated in the side chains of the Nafion® give its proton exchange capability. Figure 2.2 shows the chemical structure of Nafion®, where x, y and z can be varied to produce materials with different equivalent weights.
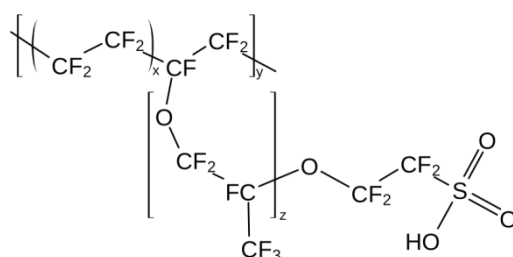
Figure 2.2. Chemical structure of Nafion®

Nafion® exhibits high thermal and mechanical properties, and an excellent oxidative stability under fuel cell operating conditions. Moreover, when Nafion® is fully hydrated shows high proton conductivity (0.1 S/cm) [7], [13]. Therefore, the structure of Nafion® has been extensively studied as a function of its water content, showing that the hydrated membrane contains two different phases; an ionic phase related to the hydrated sulfonic acid groups, and a non-ionic phase associated to the perfluorinated matrix. Several models have been proposed for the prediction of the ionic transport properties of Nafion®. The cluster network model proposed by Gierke [24] predicts that its structure is an inverted micelle in which the ion exchange sites are separated from the fluorocarbon backbone forming clusters with a diameter of approximately 4 mm. The clusters are equally distributed within a continuous fluorocarbon lattice and are interconnected by short narrow channels with a diameter of about 1mm [20], [25]. Figure 2.3 shows the cluster network model proposed by Gierke.
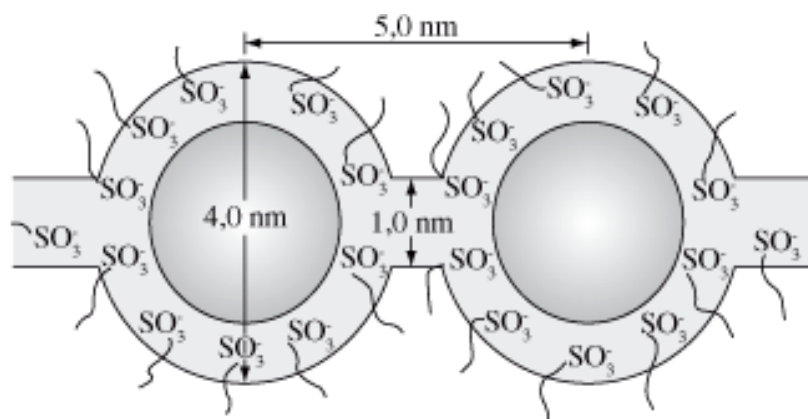
Figure 2.3. Cluster network model proposed by Gierke [20]

Proton transport takes place through these channels and is directly related to the relative humidity (RH) and/or the water content of the membrane. Nafion® shows excellent proton conductivity (between 0.09 and 0.12 S/cm at 80 ºC with a RH 34-100 %). Thus, with increasing the water content, the clusters grow and become interconnected creating percolation paths for the proton conduction. However, lower water content leads to a decrease of the proton current through membrane due to the hydrophilic domains may not be sufficiently connected, showing that proton conductivity and diffusivity depend on the volume fraction of the hydrophilic phase, following the percolation model [26]-[29].

Despite the favorable characteristics of Nafion®, it has high methanol crossover along with a deficiency of proton conductivity when the membrane is not fully hydrated. As methanol is highly soluble in water, the transport of water through the membrane is commonly associated to the methanol permeation [8], [30]. The permeated methanol reaches the cathode where is reduced instead of the oxygen, reducing the cell voltage; this effect is called mixed potential. Therefore, a reduction of water uptake could be considered as an option to reduce methanol crossover. Nevertheless, this would also decrease the proton conductivity. Considering these drawbacks, several alternatives to the PFSA membranes have been studied in order to reduce the methanol crossover and to preserve high proton conductivity for DMFC applications [9], [14], [31].

Non-fluorinated hydrocarbon polymers

Hydrocarbon polymers provide some interesting advantages over PFSA membranes. They are commercially available and their cost is lower than that of Nafion®. Moreover, their structure is easy to modify by grafting polar groups as side chains. Non-fluorinated hydrocarbon polymers can be classified in aliphatic or aromatic

polymers. The aromatic ones contain in their structure benzene rings either in the polymer backbone or the side chain. The aromatic rings offer the possibility to modify the structure by electrophilic and nucleophilic substitution reactions [32]. The aromatic hydrocarbon membranes are the non-fluorinated membranes most commonly used for fuel cell applications, some examples are listed below.

- Sulfonated poly(ether ether ketone) (sPEEK) [33]-[37]

- Sulfonated poly(ether ketone) (sPEK) [38]

- Sulfonated poly(ether sulfone) (sPES) [39]-[41]

- Sulfonated poly(benzimidazole) (sPBI) [42]-[44]

- Sulfonated polyimide (sPI) [45]-[47]

Acid-base complexes

Acid-base complexes are considered as another alternative to PFSA membranes since they have the ability to maintain high proton conductivity at high temperature without dehydration effects. In general, the acid-base complexes used for proton exchange membranes involve the addition of an acid component into an alkaline polymer matrix in order to promote proton conductivity [30], [32]. The phosphoric acid-doped poly(benzimidazole) (PBI/H_3PO_4) membrane is one of the most successful complex used for high temperature fuel cells [48]. The conductivity of (PBI/H_3PO_4) membrane does not depend on hydration degree in contrast to Nafion® but it is strongly sensitive to the doping level of complex with the acid component. In general, the proton conductivity of the acid-base complexes is susceptible to the doping level and the temperature.

Additionally, acid-base polymer blends have been extensively studied to develop alternative membranes with good fuel cell performance and low cost [32]. The acid-base interactions between the polymers of the blend through electrostatic forces and hydrogen bonding interactions control the swelling of the membrane without decreasing its flexibility. Therefore, these membranes have low water uptake, reduced methanol crossover, high proton conductivity, good thermal stability, and high mechanical flexibility and strength. Some examples of acid-base polymer blends are:

- sPSU (sulfonated polysulfone) with PBI [49]

- sPEEK with polyehtyleneimine (PEI) [50], [51]

- sPSU with PEI [52], [53]

- sPEEK with PBI [54]-[56]

In recent years, poly(vinyl alcohol) (PVA) has received increasing attention for DMFC applications due to its good mechanical and chemical stability. PVA has also been extensively used for the pervaporation of alcohol/water mixtures because of its high methanol selectivity; this high chemical selectivity of water over methanol suggests that the use of PVA as electrolyte in DMFC may increase the proton/methanol selectivity.

2.5. Poly(vinyl alcohol) (PVA)

Poly(vinyl alcohol) was prepared by Herman and Haehnel in 1924 by the hydrolysis of polyvinyl acetate in ethanol with potassium hydroxide. PVA has a relatively simple chemical structure with a pendant hydroxyl group. The monomer, vinyl alcohol, does not exist in a stable form. Therefore, PVA is synthesized from the hydrolysis of acetate groups by ester interchange with methanol in the presence of anhydrous sodium methylate or aqueous sodium hydroxide [14], [57]. PVA may have different degrees of hydrolysis as a result of the partial replacement of acetate groups by hydroxyl groups [58]. Figure 2.4 shows the chemical structure of the fully and partially hydrolyzed PVA.
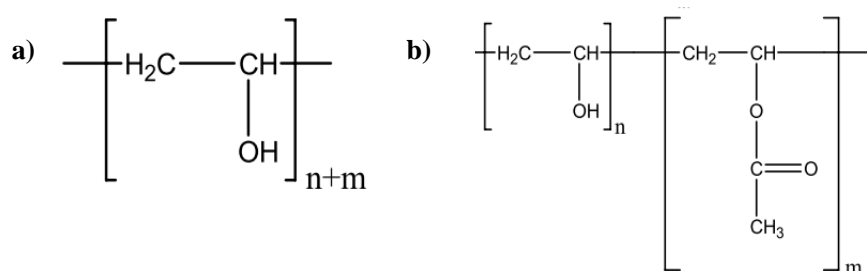
Figure 2.4. Chemical structure of PVA a) fully hydrolyzed and b) partially hydrolyzed [57]

PVA is an odorless, tasteless, non-toxic, translucent and white and/or cream colored granular powder [14]. Moreover, PVA is an excellent insulator, reaching conductivity values of 10^{-10} S/cm. It is also a water-soluble polymer being considered biocompatible and biodegradable. Crosslinking is needed to provide chemical stability to PVA in hydrophilic environments due to its high water solubility.

PVA membranes have been extensively used as alcohol dehydrating agents due to its high water/alcohol selectivity. This makes PVA very useful as electrolyte membrane in DMFC since it can effectively reduce the drawback of methanol crossover [14]. However, pure PVA does not have any protonic conductivity. Hence, PVA requires to be modified in order to promote proton conductivity, improve its mechanical strength,

and reduce its high water solubility. To this purpose, the following modifications are considered:

Direct modification of PVA

Pure PVA can be directly modified with suitable sulfonating agents such as concentrated sulfuric acid, sulfoacetic acid, chlorosulfonic acid or propane sultone in order to promote proton conductivity by attachment of sulfonic acid groups ($-SO_3H$) as side chain groups to the polymer backbone [59], [60].

Modification by copolymerization

Graft copolymerization is one of the most important methods to modify PVA. In order to improve the proton conductivity, mechanical properties and to reduce the water solubility of the PVA-based membranes, hydrophilic and hydrophobic monomers can be chemically grafted to the PVA by irradiation or chemical activation.

Modification by crosslinking

The crosslinking method can be used to obtain three dimensional networks in PVA membrane structure in order to improve its dimensional stability as well as its thermal and mechanical properties [32]. However, an excessive crosslinking degree increases the brittleness of the membrane reducing its mechanical properties. Therefore, a compromise between the crosslinking degree and the mechanical behaviour of membranes is needed. Additionally, proton-conducting groups such as sulfonic acid groups can be introduced into PVA structure by crosslinking reactions using sulfonated crosslinking agents [32]. The different methods commonly used to crosslink PVA are:

- *Crosslinking by irradiation:* crosslinking reactions can be carried out through electron beams or γ-radiation. When PVA is irradiated, H• and OH• radicals arise from water molecules and react with PVA resulting in polymer radicals. These polymer radicals may interact between them by disproportion, and combination through inter- and/or intra- molecular crosslinking, giving a 3D polymer network.

- *Chemical crosslinking:* A variety of chemical crosslinking agents such as sulfosuccinic acid (SSA), poly(acrylic acid) (PAA) and glutaraldehyde (GA) have been employed to form PVA network membranes. When an aldehyde (GA) is used as a crosslinking agent in acidic conditions, the hydroxyl groups of the PVA react with the aldehyde via acetal bond formation. While when carboxylic acid agents are used (SSA, PAA), an esterification reaction occurs between the alcohol groups of PVA and the carboxylic acid groups of the crosslinking agent.

Modification by blending

Polymer blend technology may represent a versatile approach to improve the properties of the PVA-based membranes. The miscibility of two polymers can be effectively improved by favoring specific interactions between their chains, such as hydrogen bonding, ion-dipole and ionic interactions, which can act as an efficient crosslinking agent of the blend, modifying its mechanical and swelling properties [61]. Acid and basic polymer blends, known as acid-base polymers, are commonly used as PEMs. The hydrogen bonding bridges and electrostatic interactions between acid and base polymers contribute notably to control the swelling of the membrane without a decrease in flexibility [61], [62]. Therefore, membranes with high mechanical and thermal properties, low water uptake, reduced methanol crossover and high electrochemical performance can be obtained by polymer blending [61]. PVA-based polymer blends have been prepared with a widely variety of sulfonated polymers like sPEEK, Nafion, poly(styrene sulfonic acid) (PSSA) and poly(2-acrylamido-2-methylpropane sulfonic acid (PAMPS) [63]–[65].

Composites with PVA

One of the most attractive alternatives to improve the performance of PVA membranes in fuel cell applications is the preparation of composite membranes. A polymer composite is defined as a multiphase system consisted of an organic polymer matrix reinforced with a filler [66], [67]. The simplest method for the preparation of polymer composites is the blending method in which the filler is directly mixed with the polymer matrix. The mixing can be done by melt blending or solution blending [9]. The incorporation of filler into a polymer matrix strongly influences the original characteristics of the polymer, due to the strong interfacial interactions between the filler and the polymer matrix. The final properties of the polymer composites depend on the type (inorganic or organic), size and shape of filler that is incorporated, and the filler concentration and interactions with the polymer matrix [68]. The combination of inorganic fillers into organic polymer membranes improves the mechanical properties, the water uptake and the proton conductivity of the composite membrane whereas also suppresses methanol crossover by increasing the transport pathway tortuousness [32].

2.5.1. PVA-based composite membranes with graphene oxide (GO)

Graphene oxide (GO) is an amphiphilic material with a two-dimensional laminated structure which contains oxygen functional groups in its structure such as epoxy and hydroxyl groups on the basal plane, and carboxylic acid groups along the sheet edge according to the Lerf and Klinowski model [69], [70], as shown in Figure 2.5.
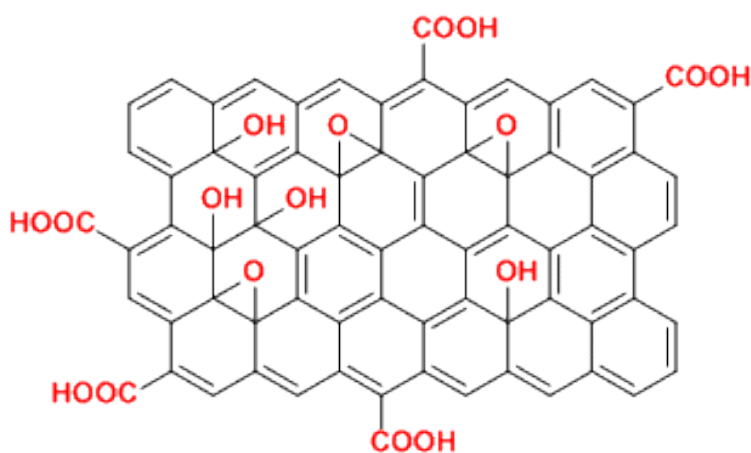
Figure 2.5. Chemical structure of graphene oxide (GO) proposed by Lerf and Klinowski

GO is one of the most attractive inorganic nano-filler to prepare PVA-based composite membranes since is easy to disperse in polar polymers due to the oxygen functional groups contained in its structure. Moreover, its unique structure with high surface area, high mechanical strength, and electric insulating properties promote the formation of proton transport channels through the membrane, while simultaneously acting as a methanol barrier reducing the drawback of crossover [9], [71].

In order to increase the proton conductivity of composite PEMs, the reactive oxygen functional groups of GO including epoxy, hydroxyl and carboxylic acid groups can be chemically modified [72]. Sulfonation is one of the most popular alternatives that are used for GO modification. The introduction of sulfonic acid groups (-SO_3H) in the structure improves the interfacial adhesion between the polymer and the filler and enhances the proton conductivity compared to those composite membranes prepared with GO. Direct sulfonation of GO by covalent attachment of sulfonic acid-containing aryl radicals has been extensively reported, resulting in a significantly improved proton conductivity at low levels of hydration [59], [73]–[78]. Figure 2.6 shows the chemical structure of sulfonated graphene oxide (sGO) obtained by modification with aryl radicals. Therefore, the modification of GO by direct sulfonation seems an attractive

strategy to enhance the mechanical and proton-conducting properties of composite membranes for fuel cell applications.
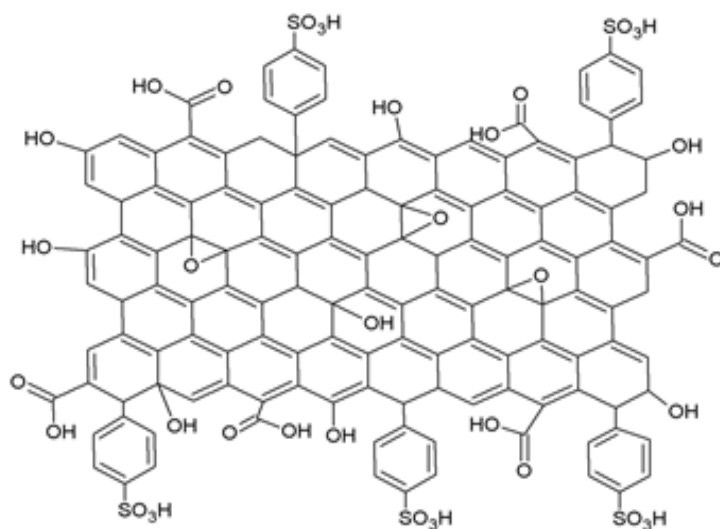
Figure 2.6. Chemical structure of the sulfonated graphene oxide (sGO) obtained by modification with aryl radicals

References

[1] F. Barbir, *PEM Fuel Cells: Theory and Practice*, Elsevier, 2013.

[2] Matthew M. Mench, *Fuel Cell Engines*, John Wiley & Sons, 2008.

[3] L. J. M. J. Blomen, and M. N. Mugerwa, *Fuel Cell Systems*, Springer Science & Business Media, 1993.

[4] EG&G Technical Services, Inc., *Fuel Cell Handbook*, Seventh Edition, 2004.

[5] Shripad T. Revankar, and P. Majumdar, *Fuel Cells: Principles, Design, and Analysis*. CRC Press, 2016.

[6] Z. Qi, *Proton Exchange Membrane Fuel Cells*. CRC Press, 2013.

[7] S. Zaidi and T. Matsuura, *Polymer Membranes for Fuel Cells*. Springer, 2009.

[8] H. Wang, C. Song, X.-Z. R. Yuan, and J. Zhang, *Electrochemical Impedance Spectroscopy in PEM Fuel Cells: Fundamentals and Applications*, Springer, 2010.

[9] K. Pourzare, Y. Mansourpanah, and S. Farhadi, "Advanced nanocomposite membranes for fuel cell applications : A comprehensive review," Biofuel Res. J., vol. 12, pp. 496–513, 2016.

[10] A. M. Felipe, "Preparation and characterisation of new materials for electrolytes used in Direct Methanol Fuel Cells," PhD thesis, Universitat Politècnica de València, 2009.

[11] J. Larminie, and A. Dicks, *Fuel Cell Systems Explained*, Second Edition, Wiley, 2001.

[12] C. Spiegel, *Designing and Building Fuel Cells*. Mc Graw Hill, 2007.

[13] H. Pu, *Polymers for PEM Fuel Cells*. Wiley, 2014.

[14] J. Maiti, N. Kakati, S. H. Lee, S. H. Jee, B. Viswanathan, and Y. S. Yoon, "Where do poly(vinyl alcohol) based membranes stand in relation to Nafion® for direct methanol fuel cell applications?," J. Power Sources, vol. 216, pp. 48–66, 2012.

[15] C. Hartnig and C. Roth, *Polymer Electrolyte Membrane and Direct Methanol Fuel Cell Technology: Fundamentals and Performance of Low Temperature Fuel Cells*. Woodhead Publishing Limited, 2012.

[16] Horacio R. Corti, Ernesto R. Gonzalez, *Direct Alcohol Fuel Cells*, Springer Science & Business Media, 2014.

[17] D. Stolten and B. Emonts, *Fuel Cell Science and Engineering*. Wiley-VCH, 2012.

[18] Andrei A. Kulikovsky, *Analytical modelling of fuel cells*, Elsevier, 2010.

[19] Vladimir S. Bagotsky, *Fuel cells Problems and Solutions*. John Wiley & Sons, 2009.

[20] J. Zhang, H. Zhang, J. Wu, and J. Zhang, *PEM Fuel Cell Testing and Diagnosis*. Elsevier, 2013.

[21] S. Banerjee, *Handbook of specialty fluorinated polymers*. Elsevier, 2015.

[22] W. Grot, *Fluorinated Ionomers*. Second Edition, Elsevier, 2011.

[23] P. K. Shen, C. Y. Wang, S. P. Jiang, X. Sun, and J. Zhang, *Electrochemical Energy: Advanced Materials and Technologies*. CRC Press, 2016.

[24] T. D. Gierke, G. E. Munn, and F. C. Wilson, "The morphology in nafion perfluorinated membrane products, as determined by wide- and small-angle x-ray studies," J. Polym. Sci. Polym. Phys. Ed., vol. 19, no. 11, pp. 1687–1704, Nov. 1981.

[25] M. Leclerc, and R. Gauvin, *Functional Materials: For Energy, Sustainable Development and Biomedical Sciences*. De Gruyter, 2014.

[26] Y. A. Elabd, E. Napadensky, J. M. Sloan, D. M. Crawford, and C. W. Walker, "Triblock copolymer ionomer membranes: Part I. Methanol and proton transport," J. Memb. Sci., vol. 217, no. 1–2, pp. 227–242, 2003.

[27] W. Y. Hsu, J. R. Barkley, and P. Meakin, "Ion percolation and insulator-to-conductor transition in Nafion perfluorosulfonic acid membranes," Macromolecules, vol. 13, no. 1, pp. 198–200, 1980.

[28] A. A. Gronowski, M. Jiang, H. L. Yeager, G. Wu, and A. Eisenberg, "Structure and properties of hydrocarbon ionomer membranes. 1.: Poly(methyl methacrylate-co-methacrylic acid)," J. Memb. Sci., vol. 82, no. 1, pp. 83–97, 1993.

[29] D. Stauffer, and A. Aharony, "Introduction to Percolation Theory," Computer, vol. 1, no. 4. p. 192, 1994.

[30] N. Awanga, A.F. Ismaila, J. Jaafara, T. Matsuuraa, H. Junoha, M. H. D. Othmana, and M. A. Rahmana, "Functionalization of polymeric materials as a high performance membrane for direct methanol fuel cell: A review," React. Funct. Polym., vol. 86, pp. 248–258, 2014.

[31] B. Viswanathan and M. Helen, "Is Nafion®, the only Choice?," Bull. Catal. India, vol. 6, no. January, pp. 50–66, 2007.

[32] S. J. Peighambardoust, S. Rowshanzamir, and M. Amjadi, "Review of the proton exchange membranes for fuel cell applications," Int. J. Hydrogen Energy, vol. 35, no. 17, pp. 9349–9384, 2010.

[33] A. Iulianelli and A. Basile, "Sulfonated PEEK-based polymers in PEMFC and DMFC applications: A review," Int. J. Hydrogen Energy, vol. 37, no. 20, pp. 15241–15255, 2012.

[34] M. I. Ahmad, A. Nafees, and S. O. Dbr, "Development of Novel Composite SPEEK Membrane for Direct Methanol Fuel Cell," Proc. Int. Symp. EcoTopia Sci., vol. 7, pp. 65–69, 2007.

[35] N. Nishad Fathima, R. Aravindhan, D. Lawrence, U. Yugandhar, T. S. R. Moorthy, and B. Unni Nair, "SPEEK polymeric membranes for fuel cell application and their characterization: A review," J. Sci. Ind. Res. (India)., vol. 66, no. 3, pp. 209–219, 2007.

[36] T. Yang, S. X. Zhang, Y. Gao, F. Cheng, J. Tang, and W. Liu, "Multilayer Membranes Based on Sulfonated Poly(ether ether ketone) and Poly(vinyl alcohol) for Direct Methanol Membrane Fuel Cells," Open Fuel Cells J., vol. 1, no. January 2009, pp. 4–8, 2008.

[37] C. de Bonis et al., "Enhancement of proton mobility and mitigation of methanol crossover in sPEEK fuel cells by an organically modified titania nanofiller," J. Solid State Electrochem., vol. 20, no. 6, pp. 1585–1598, 2016.

[38] R. S. Malik, S. N. Tripathi, D. Gupta, and V. Choudhary, "Novel anhydrous composite membranes based on sulfonated poly (ether ketone) and aprotic ionic liquids for high temperature polymer electrolyte membranes for fuel cell applications," Int. J. Hydrogen Energy, vol. 39, no. 24, pp. 12826–12834, 2014.

[39] A. Muthumeenal, S. S. Pethaiah, and A. Nagendran, "Investigation of SPES as PEM for hydrogen production through electrochemical reforming of aqueous methanol," Renew. Energy, vol. 91, pp. 75–82, 2016.

[40] C. Zhang, X. Zhuang, X. Li, W. Wang, B. Cheng, W. Kang, Z. Cai, and M. Li, "Chitin nanowhisker-supported sulfonated poly(ether sulfone) proton exchange for fuel cell applications," Carbohydr. Polym., vol. 140, pp. 195–201, 2016.

[41] R. Zeng, S. Xiao, L. Chen, and Y. Chen, "Sulfonated poly(ether sulfone ether ketone ketone)/sulfonated poly(ether sulfone) blend membranes with reduced methanol permeability," High Perform. Polym., vol. 24, no. 3, pp. 153–160, 2012.

[42] H. Bai and W. S. W. Ho, "New sulfonated polybenzimidazole (SPBI) copolymer-based proton-exchange membranes for fuel cells," J. Taiwan Inst. Chem. Eng., vol. 40, no. 3, pp. 260–267, 2009.

[43] S. Lai, J. Park, S. Cho, M. Tsai, H. Lim, and K. Chen, "Mechanical property enhancement of ultra-thin PBI membrane by electron beam irradiation for PEM fuel cell," Int. J. Hydrogen Energy, vol. 41, no. 22, pp. 9556–9562, 2016.

[44] M. Moradi, A. Moheb, M. Javanbakht, and K. Hooshyari, "Experimental study and modeling of proton conductivity of phosphoric acid doped PBI-Fe$_2$TiO$_5$ nanocomposite membranes for using in high temperature proton exchange membrane fuel cell (HT-PEMFC)," Int. J. Hydrogen Energy, vol. 41, no. 4, pp. 2896–2910, 2016.

[45] Q. Yuan, P. Liu, and G. Baker, "Sulfonated polyimide and PVDF based blend proton exchange membranes for fuel cell applications," J. Mater. Chem. A, vol. 3, no. 7, pp. 3847–3853, 2015.

[46] M. Sakamoto, S. Nohara, K. Miyatake, M. Uchida, M. Watanabe, and H. Uchida, "Effects of Incorporation of SiO$_2$ Nanoparticles into Sulfonated Polyimide Electrolyte Membranes on Fuel Cell Performance under Low Humidity Conditions," Electrochim. Acta, vol. 137, pp. 213–218, 2014.

[47] H. Pan, S. Chen, Y. Zhang, M. Jin, Z. Chang, and H. Pu, "Preparation and properties of the cross-linked sulfonated polyimide containing benzimidazole as electrolyte membranes in fuel cells," J. Memb. Sci., vol. 476, pp. 87–94, 2015.

[48] Q. Li, J. O. Jensen, R. F. Savinell, and N. J. Bjerrum, "High temperature proton exchange membranes based on polybenzimidazoles for fuel cells," Prog. Polym. Sci., vol. 34, no. 5, pp. 449–477, 2009.

[49] D. Xing, and J. Kerres "Improved performance of sulfonated polyarylene ethers for proton exchange membrane fuel cells," Polym. Adv. Technol., vol. 17, no. April, pp. 591–597, 2006.

[50] S. Liu, L. Wang, Y. Ding, B. Liu, X. Han, and Y. Song, "Novel sulfonated poly (ether ether keton)/polyetherimide acid-base blend membranes for vanadium redox flow battery applications," Electrochim. Acta, vol. 130, no. August 2015, pp. 90–96, 2014.

[51] S. Swier, M. T. Shaw, and R. A. Weiss, "Morphology control of sulfonated poly(ether ketone ketone) poly(ether imide) blends and their use in proton-exchange membranes," J. Memb. Sci., vol. 270, no. 1–2, pp. 22–31, 2006.

[52] J. A. Kerres, "Blended and cross-linked ionomer membranes for application in membrane fuel cells," Fuel Cells, vol. 5, no. 2, pp. 230–247, 2005.

[53] J. Kerres, A. Ullrich, F. Meier, and T. Häring, "Synthesis and characterization of novel acid–base polymer blends for application in membrane fuel cells," Solid State Ionics, vol. 125, no. 1, pp. 243–249, 1999.

[54] M. Song, X. Lu, Z. Li, G. Liu, X. Yin, and Y. Wang, "Compatible ionic crosslinking composite membranes based on SPEEK and PBI for high temperature proton exchange membranes," Int. J. Hydrogen Energy, vol. 41, no. 28, pp. 12069–12081, 2016.

[55] H. Zhang, X. Li, C. Zhao, T. Fu, Y. Shi, and H. Na, "Composite membranes based on highly sulfonated PEEK and PBI: Morphology characteristics and performance," J. Memb. Sci., vol. 308, no. 1, pp. 66–74, 2008.

[56] S. Pasupathi, S. Ji, B. Jan Bladergroen, and V. Linkov, "High DMFC performance output using modified acid–base polymer blend," Int. J. Hydrogen Energy, vol. 33, no. 12, pp. 3132–3136, 2008.

[57] S. Patachia, A. J. M. Valente, A. Papanceaa and Victor M. M. Lobo, *Poly (Vinyl Alcohol) (PVA)-Based Polymer Membranes*. Nova Science Publishes, Inc., 2009.

[58] N. Sammes, A. Smirnova, and O. Vasylyev, *Fuel Cell Technologies: State And Perspectives*, Springer, 2005.

[59] H. Beydaghi, M. Javanbakht, and E. Kowsari, "Synthesis and Characterization of Poly(vinyl alcohol)/Sulfonated Graphene Oxide Nanocomposite Membranes for Use in Proton Exchange Membrane Fuel Cells (PEMFCs)," Ind. Eng. Chem. Res., vol. 53, no. 43, pp. 16621–16632, 2014.

[60] S. Yun, H. Im, Y. Heo, and J. Kim, "Crosslinked sulfonated poly(vinyl alcohol)/sulfonated multi-walled carbon nanotubes nanocomposite membranes for direct methanol fuel cells," J. Memb. Sci., vol. 380, no. 1–2, pp. 208–215, 2011.

[61] A.-C. Dupuis, "Proton exchange membranes for fuel cells operated at medium temperatures: Materials and experimental techniques," Prog. Mater. Sci., vol. 56, no. 3, pp. 289–327, Mar. 2011.

[62] H. Ahmad, S. K. Kamarudin, U. A. Hasran, and W. R. W. Daud, "Overview of hybrid membranes for direct-methanol fuel-cell applications," Int. J. Hydrogen Energy, vol. 35, no. 5, pp. 2160–2175, Mar. 2010.

[63] H.-L. Lin, and S.-H. Wang, "Nafion/poly(vinyl alcohol) nano-fiber composite and Nafion/poly(vinyl alcohol) blend membranes for direct methanol fuel cells," J. Memb. Sci., vol. 452, pp. 253–262, Feb. 2014.

[64] S. Mollá, and V. Compañ, "Polymer blends of SPEEK for DMFC application at intermediate temperatures," Int. J. Hydrogen Energy, vol. 39, no. 10, pp. 5121–5136, Mar. 2014.

[65] M. Erkartal et al., "Anhydrous proton conducting poly(vinyl alcohol) (PVA)/ poly(2-acrylamido-2-methylpropane sulfonic acid) (PAMPS)/1,2,4-triazole composite membrane," Int. J. Hydrogen Energy, vol. 41, no. 26, pp. 11321–11330, Jul. 2016.

[66] A. M. Herring, "Inorganic–Polymer Composite Membranes for Proton Exchange Membrane Fuel Cells," J. Macromol. Sci. Part C, vol. 46, no. 3, pp. 245–296, Sep. 2006.

[67] R.-M. Wang, S.-R. Zheng, and Y.-P. Zheng, "Introduction to polymer matrix composites," Polym. matrix Compos. Technol., pp. 1–548, 2011.

[68] S. Kango, S. Kalia, A. Celli, J. Njuguna, Y. Habibi, and R. Kumar, "Surface modification of inorganic nanoparticles for development of organic–inorganic nanocomposites-A review," Prog. Polym. Sci., vol. 38, no. 8, pp. 1232–1261, Aug. 2013.

[69] H. He, J. Klinowski, M. Forster, and A. Lerf, "A new structural model for graphite oxide," Chem. Phys. Lett., vol. 287, no. 1–2, pp. 53–56, Apr. 1998.

[70] A. Lerf, H. He, T. Riedl, M. Forster, and J. Klinowski, "^{13}C and ^{1}H MAS NMR studies of graphite oxide and its chemically modified derivatives," Solid State Ionics, vol. 101–103, pp. 857–862, Nov. 1997.

[71] Z. U. Khan, A. Kausar, and H. Ullah, "A Review on Composite Papers of Graphene Oxide, Carbon Nanotube, Polymer/GO, and Polymer/CNT: Processing Strategies, Properties, and Relevance," Polym. Plast. Technol. Eng., vol. 55, no. 6, pp. 559–581, 2016.

[72] D. R. Dreyer, S. Park, C. W. Bielawski, and R. S. Ruoff, "The chemistry of graphene oxide," Chem. Soc. Rev., vol. 39, no. 1, pp. 228–240, 2010.

[73] H. Beydaghi, M. Javanbakht, and E. Kowsari, "Preparation and physic-chemical performance study of proton exchange membranes based on phenyl sulfonated graphene oxide nanosheets decorated with iron titanate nanoparticles," Polymer (Guildf)., vol. 87, pp. 26–37, 2016.

[74] S. Neelakandan, Noel Jacob K., P. Kanagaraj, R. M. Sabarathinam, A. Muthumeenal, and A. Nagendran, "Effect of sulfonated graphene oxide on the performance enhancement of acid-base composite membranes for direct methanol fuel cells," RSC Adv., vol. 6, no. 57, pp. 51599–51608, 2016.

[75] H. C. Chien, L. D. Tsai, C. P. Huang, C. Y. Kang, J. N. Lin, and F. C. Chang, "Sulfonated graphene oxide/Nafion composite membranes for high-performance direct methanol fuel cells," Int. J. Hydrogen Energy, vol. 38, no. 31, pp. 13792–13801, 2013.

[76] A. K. Sahu, K. Ketpang, S. Shanmugam, O. Kwon, S. Lee, and H. Kim, "Sulfonated Graphene-Nafion Composite Membranes for Polymer Electrolyte Fuel Cells Operating under Reduced Relative Humidity," J. Phys. Chem. C, vol. 120, no. 29, pp. 15855–15866, 2016.

[77] R. Kumar, M. Mamlouk, and K. Scott, "Sulfonated polyether ether ketone – sulfonated graphene oxide composite membranes for polymer electrolyte fuel cells," RSC Adv., vol. 4, no. 2, p. 617, 2014.

[78] Ravikumar and K. Scott, "Freestanding sulfonated graphene oxide paper: a new polymer electrolyte for polymer electrolyte fuel cells," Chem. Commun., vol. 48, no. 45, pp. 1–11, 2012.

Experimental part

Chapter 3

3.1. Synthesis of starting materials

Commercial poly(vinyl alcohol) (PVA), (molecular weight 130000 g/mol , degree of hydrolysis > 99%) supplied by Sigma-Aldrich, was chosen as a polymer matrix for the preparation of proton exchange membranes for DMFCs applications. PVA is an odorless, non-toxic and water-soluble polymer with high selectivity to methanol, good membrane-forming ability and low cost [1]. However, PVA itself does not have any negative charged ions, thus further modification of PVA is needed in order to promote proton conduction through it. Direct sulfonation of the PVA matrix using propane sultone as sulfonating agent was followed as a procedure to improve the proton-conducting properties of PVA.

In addition, graphene oxide (GO) was selected as inorganic filler to prepare PVA-based hybrid organic-inorganic composite membranes. GO was synthesized by oxidation of graphite powder using the Modified Hummers Method (MHM). Further modification of GO was carried out by sulfonation, via free radical addition of the aryl diazonium salt of the sulfanilic acid, in order to study the effect of the multiple sulfonation (polymer matrix and inorganic filler) on the proton conductivity properties of the hybrid composite membranes.

The methodology followed for the synthesis of sulfonated poly(vinyl alcohol) (sPVA), graphene oxide (GO) and sulfonated graphene oxide (sGO) is described below. Scheme 3.1 shows schematically a diagram with the different modifications performed on the starting materials.
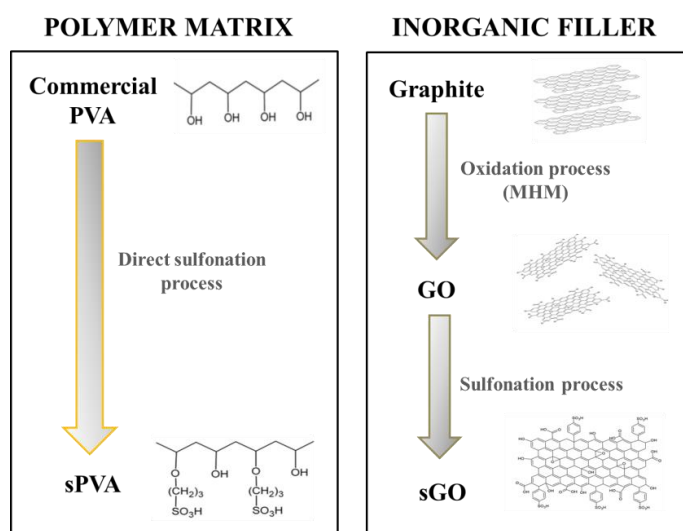
Scheme 3.1. Schematic diagram of the different modifications performed on the starting materials

3.1.1. Chemicals

Poly(vinyl alcohol) (PVA, molecular weight 130000 g/mol degree of hydrolysis, min. 99%), sodium hydride (NaH, dry 95 %), 1,3-propane sultone (97 %), graphite powder (particle size < 20 μm), sodium nitrate ($NaNO_3$, ≥ 99.0 %), sulfanilic acid (99 %), sodium nitrite ($NaNO_2$, 99.5 %), sulfosuccinic acid (SSA, 70 wt.% solution in water), poly(allylamine) hydrochloride (PAH, molecular weight 15000 g/mol) and glutaraldehyde (GA, 25 wt.% solution in water) were purchased from Sigma-Aldrich. Ethanol absolute (EtOH), hydrochloric acid (HCl, 37%), concentrated sulfuric acid (H_2SO_4, 95%), potassium permanganate ($KMnO_4$, extra pure) and hydrogen peroxide (H_2O_2, 30% w/w) were purchased from Scharlab.

3.1.2. Synthesis of sulfonated poly(vinyl alcohol) (sPVA)

Sulfonated poly(vinyl alcohol) (sPVA) was obtained by direct sulfonation of commercial PVA using propane sultone as sulfonating agent [2], [3]. The functionalization reaction was carried out through the following two steps:

1) Sodium sulfonated salt preparation

10 g of commercial PVA were suspended in 250 mL of EtOH. Then, 4,8 g of NaH were slowly added to the suspension under constant mechanical stirring at room temperature. Finally, 5 g of 1,3-propane sultone were added dropwise and the mixture was stirred at 80 ºC for 24 hours. Scheme 3.2 shows a scheme of the procedure followed in this first step.
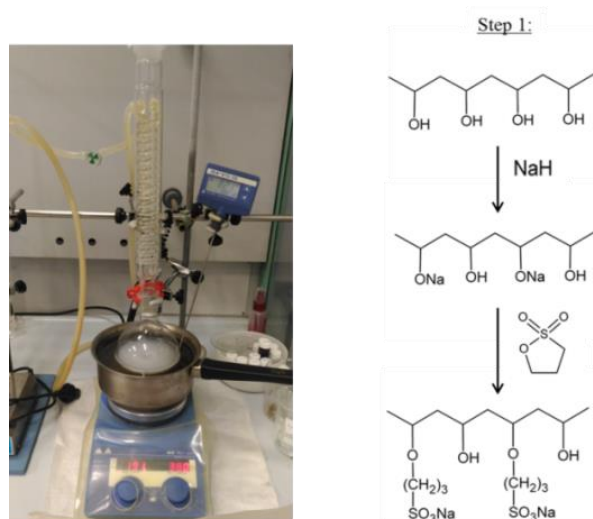
Scheme 3.2. First step of the direct sulfonation process of PVA

2) Protonation process

In a second step, the sodium sulfonated salt was transformed to the protonated form by immersion in HCl solution for 12 hours. The obtained sPVA powder was filtered, washed with EtOH and finally dried for 4 hours in a vacuum oven at 50 ℃. Scheme 3.3 shows a scheme of the protonation step of sPVA.
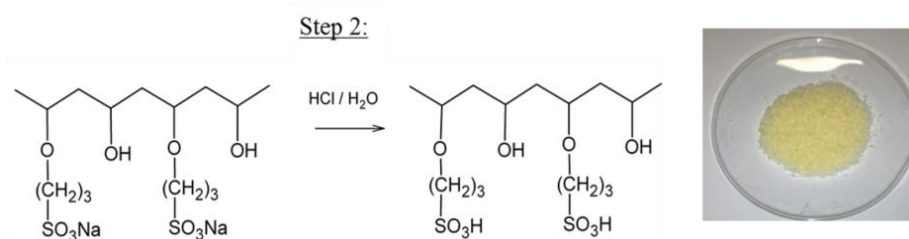
Scheme 3.3. Second step of the direct sulfonation process of PVA

3.1.3. Synthesis of graphene oxide (GO)

Graphene oxide (GO) was obtained from the oxidation of graphite powder using the Modified Hummers Method (MHM) [4], [5], as shown in Scheme 3.4. The steps followed for the preparation of GO are described as follows.

1) 1 g of $NaNO_3$ was added to a suspension of 2 g of graphite in 46 mL of H_2SO_4 under constant stirring, keeping the mixture in an ice bath.

2) After 5 minutes, 6 g of $KMnO_4$ were added gradually to the above solution while keeping the temperature below 20 ℃ to prevent overheating. The ice bath was then removed and the mixture was stirred at 35 ℃ for 30 minutes.

3) The resulting solution was diluted by adding 92 mL of distilled water dropwise under constant stirring. The solution was stirred 1 hour at 35 ℃, and then the temperature was raised to 98 ℃ followed by the addition of 280 mL of distilled water under vigorous stirring.

4) After 30 minutes, the suspension was filtered and treated with 30 mL of 30% H_2O_2 solution.

5) The resulting product was washed several times with HCl and EtOH until the washings reached pH 7. Finally, the GO powder was suspended in distilled water (2 mg/mL) and sonicated for 3 hours, filtered and dried in a vacuum oven for 12 hours.
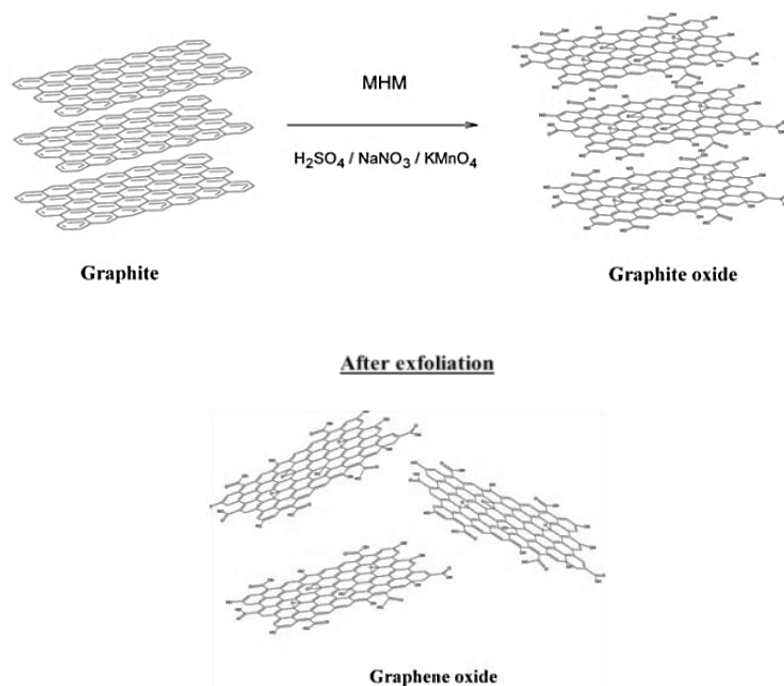
Scheme 3.4. Schematic diagram of the synthesis of GO by Modified Hummers Method (MHM)

3.1.4. Synthesis of sulfonated graphene oxide (sGO)

Sulfonated graphene oxide (sGO) was synthesized from GO via free radical addition using the aryl diazonium salt of sulfanilic acid as adduct (Scheme 3.5) according to this three-step process:

1) 50 mg of GO were added to 8 mL 0.06 M sulfanilic acid solution at 70 °C.

2) Under continuous stirring, 2 mL of 6×10^{-3} M sodium nitrite solution were added dropwise and the mixture was held at 70 °C for 12 hours. The sulfanilic acid diazonium salt obtained *in situ* from the reaction of sulfanilic acid with sodium nitrite was become in aryl radical by transfer of a delocalized electron from GO. The aryl radical then reacts rapidly with the carbon atoms in the GO layers to form new covalent bonds, changing the hybridization from sp^2 to sp^3 [6].

3) The product was washed several times with distilled water and centrifuged until pH 7. Finally, the obtained sGO was filtered and dried in a vacuum oven for 12 hours.
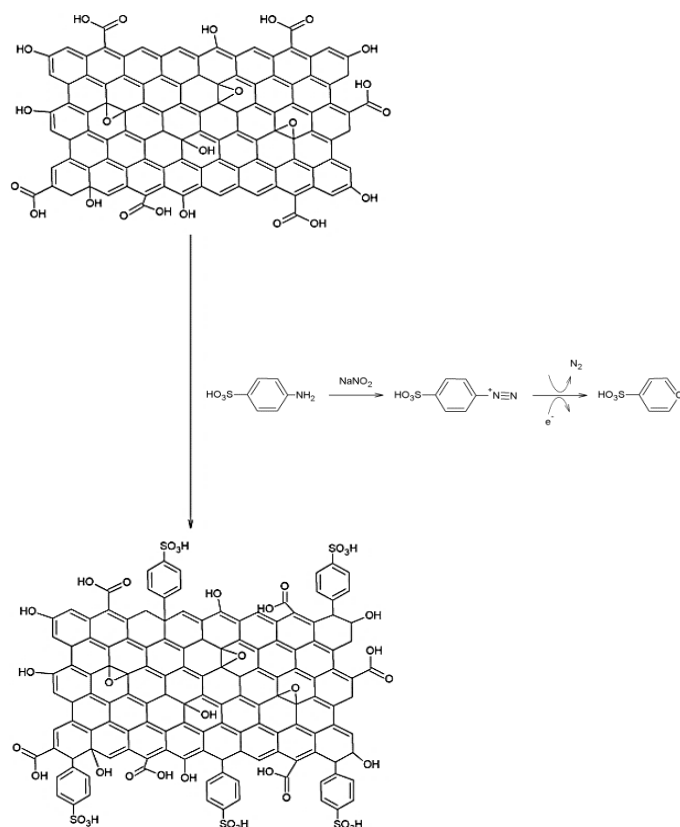
Scheme 3.5. Schematic diagram of the sulfonation process of GO

3.2. Preparation of free-standing GO membranes

PVA-based free-standing GO membranes were prepared by solution-casting method according to the following steps:

1) Preparation of polymer solutions

5 wt.% aqueous solutions of PVA and sPVA were prepared by dissolving the polymer in water and refluxing at 90 ℃ for 6 hours under constant stirring. Then, the solutions were mixed with sulfosuccinic acid (SSA) at two different concentrations, 15 and 30 wt.% respect to polymer, and vigorously stirred at room temperature for 24 hours. The homogeneous solutions were poured onto a Teflon plate and the cast membranes were

allowed to dry at room temperature. Scheme 3.6 illustrates the casting process followed for the preparation of the free-standing GO membranes.
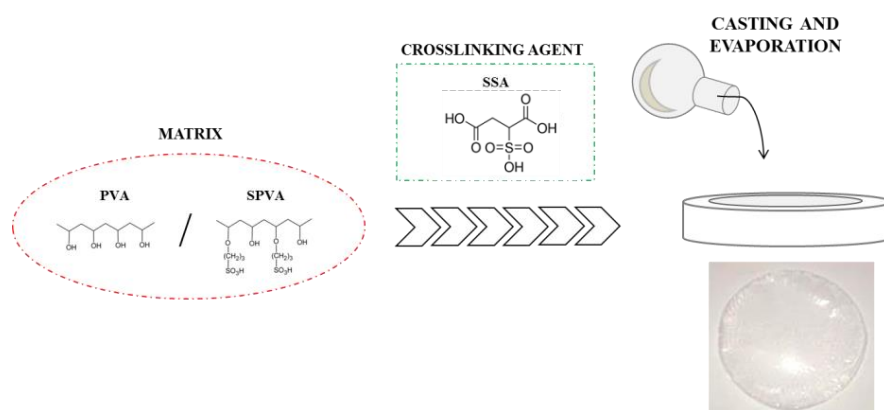
Scheme 3.6. Schematic diagram of the casting process followed for preparation of the free-standing GO membranes

2) Thermal crosslinking process

Finally, the dried membranes were peeled off the Teflon plates and crosslinked at 110 ºC for 2 hours. Scheme 3.7 shows the change of colour that the membranes underwent after crosslinking process. The membranes were identified as *X*PVA, *X*sPVA where *X* indicates the weight percentage of crosslinking agent (SSA).
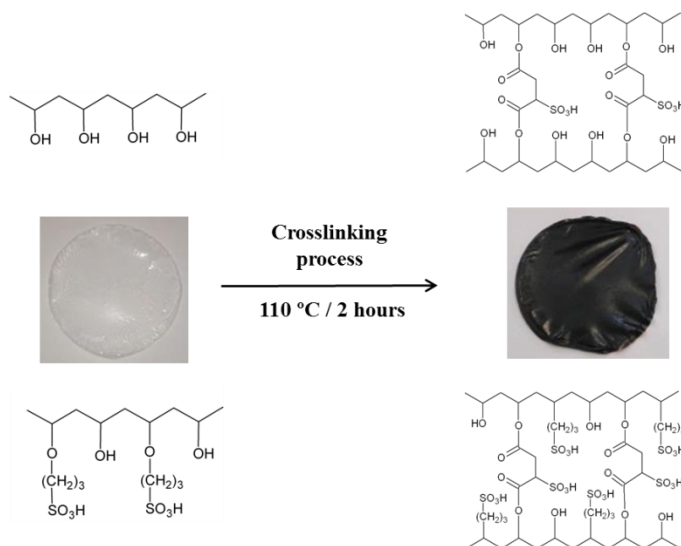
Scheme 3.7. Membrane color change after crosslinking process

3.3. Preparation of hybrid organic-inorganic composite membranes

Two different methods were selected to prepare hybrid organic-inorganic composite membranes:

- Solution-casting method
- Layer-by-Layer assembly method

The steps followed in each method for the preparation of composites are described below.

3.3.1. Solution-casting method

The solvent-cast composites were prepared from two different polymer matrices, PVA and sPVA, using as inorganic nano-filler GO and sGO.

1) *Preparation of polymer/nano-filler solutions*

5 wt.% aqueous solutions of PVA and sPVA were prepared by dissolving the polymer in water and refluxing the solutions at 90 ºC for 6 hours under constant stirring. A 1 wt.% solution of the nano-filler in distilled water was successively sonicated to obtain a homogeneous solution, and was then added to the polymer solutions previously prepared. Finally, the solutions were mixed with SSA at two different concentrations, 15 and 30 wt.% respect to polymer, and vigorously stirred at room temperature for 24 hours. After that, the homogeneous solutions were poured onto a Teflon plate and the cast membranes were allowed to dry at room temperature. Scheme 3.8 shows a schematic diagram of the casting process followed for the preparation of the hybrid organic-inorganic composites.
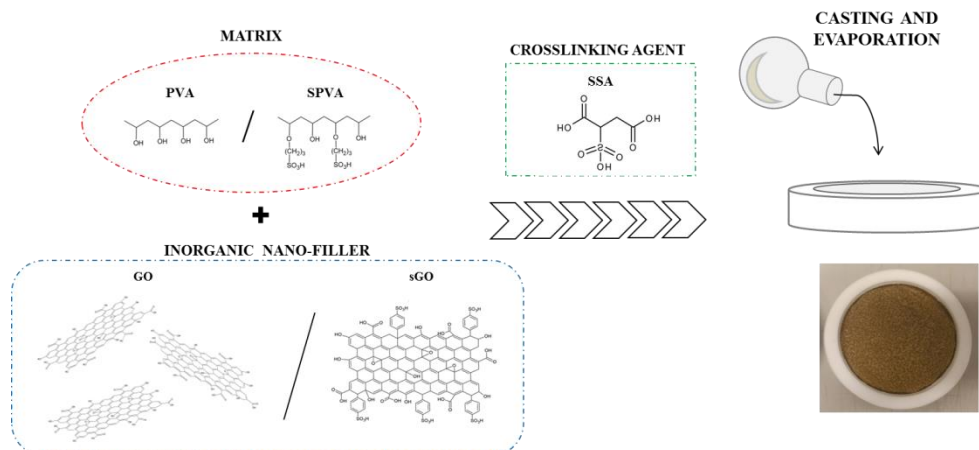
Scheme 3.8. Schematic diagram of the casting process followed to prepare the hybrid organic-inorganic composites

2) Thermal crosslinking process

Finally, the dried composite membranes were peeled off the Teflon plates and then were crosslinked at 110 ºC for 2 hours. Scheme 3.9 shows the change of colour that the composites undergo after crosslinking process. The membranes were identified as *X*PVA/GO, *X*sPVA/GO, *X*PVA/sGO and *X*sPVA/sGO, where *X* denotes the weight percentage of crosslinking agent (SSA).
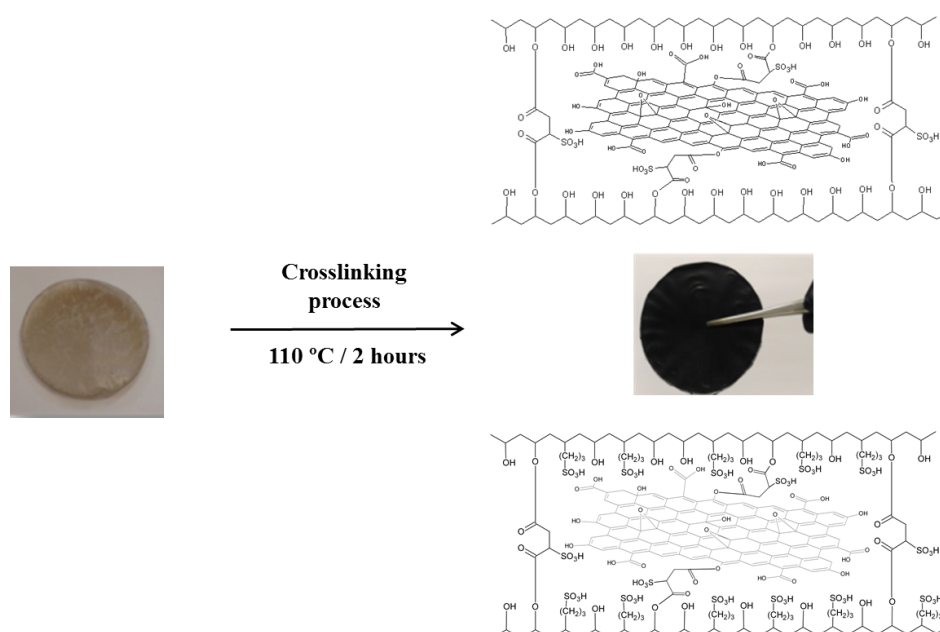
Scheme 3.9. Composite color change after crosslinking process

3.3.2. Layer-by-Layer (LbL) assembly method

The Layer-by-Layer (LbL) assembled composite membranes were prepared through the following steps:

1) Preparation of substrate membranes by solution-casting method

Two types of crosslinked membranes, 15PVA and 15sPVA, were prepared by solution-casting method to use as substrates in the LbL assembly process. 5 wt.% aqueous solutions of PVA and sPVA were prepared by dissolving the polymer in water and refluxing at 90 ºC for 6 hours under continuous stirring. Then, the solutions were mixed with SSA at 15 wt.% and vigorously stirred at room temperature for 24 hours. The homogeneous solutions were poured onto a Teflon plate and the cast membranes

were allowed to dry at room temperature. As the last step, the dried membranes were crosslinked at 110 ℃ for 2 hours.

2) *Layer-by-Layer (LbL) assembly process*

According to the forces responsible to keep the LbL assembled structure, two different types of composite membranes were prepared: Hydrogen-bonding and Electrostatic LbL composite membranes. The methodology followed for the preparation of each type of composite membranes is described below.

Hydrogen-bonding LbL assembled composite membranes

The hydrogen-bonding LbL composite membranes were prepared by alternate deposition of GO layers and polymer (PVA or sPVA) layers onto the surface of 15PVA and 15sPVA substrates, keeping the LbL assembled structure through hydrogen-bonding interactions.

a) *Preparation of the Layer-by-Layer solutions*

The polymer solutions were prepared by dissolving PVA and sPVA (1wt.%) in water and refluxing at 90 ℃ for 6 hours. The GO dispersion in water with a concentration of 1 mg/mL was prepared under sonication for 30 minutes. The pH of the polymer solution and the GO dispersion was adjusted to 3.5. This pH was selected to promote the protonated form of the carboxylic acid groups (-COOH, $pK_a = 4.3$) of GO, in order to assemble the composite membranes via hydrogen bonding interactions [7].

b) *Layer-by-Layer assembly cycle*

The GO/polymer bilayers were deposited onto the surface of the substrates according to the following procedure:

i) Dipping the substrate membrane into the GO dispersion for 30 minutes

ii) Rinsing with Mili-Q water for 5 minutes to remove the weakly bonded molecules

iii) Dipping the substrate membrane into the polymer solution (PVA or sPVA) for 30 minutes

iv) Rinsing with Mili-Q water for 5 minutes to remove the weakly bonded molecules

This procedure corresponds to a single deposition cycle. The process was repeated to increase the number of GO/polymer bilayers on the substrates surface up to three

bilayers. Scheme 3.10 shows schematically the procedure followed in hydrogen-bonding LbL assembly process. The hydrogen-bonding LbL composites were denoted as $15PVA(GO/PVA)_n$ and $15sPVA(GO/sPVA)_n$, where *n* refers to the number of the deposited bilayers.
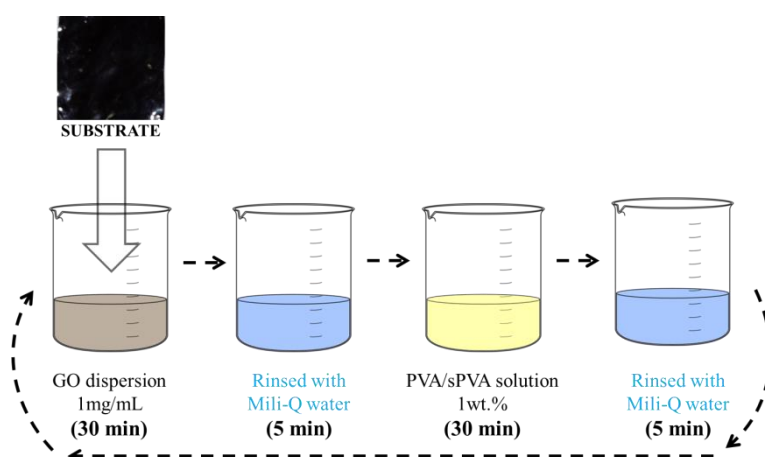
Scheme 3.10. Schematic diagram of the procedure followed in hydrogen-bonding LbL assembly process

Electrostatic LbL assembled composite membranes

The electrostatic LbL composite membranes were prepared by alternate deposition of positively charged GO-poly(allylamine hydrochloride) (PAH) layers and negatively charged sPVA layers on the surface of 15PVA and 15sPVA substrates, keeping the LbL assembled structure through electrostatic interactions.

a) *Preparation of Layer-by-Layer solutions*

sPVA aqueous solution was prepared by dissolving 1 wt.% of polymer in water and refluxing at 90 ºC for 6 hours. The GO-PAH solution was prepared dispersing the GO (1mg/mL) under sonication for 30 minutes in a previously prepared 1 wt.% PAH solution. The pH of GO-PAH and sPVA solutions was adjusted to 5.5 in order to promote the interaction between the carboxylic acid groups of GO in deprotonated form ($-COO^-$, $pK_a = 4.3$) and the amine groups of PAH in protonated form ($-NH_3^+$, $pK_a = 8.5$) during the LbL assembly process via electrostatic interactions with sPVA ($-SO_3^-$, $pK_a = 1$).

b) Layer-by-Layer assembly cycle

The GO-PAH/sPVA bilayers were deposited on the surface of the substrates according to the following procedure:

i) Dipping the substrate membrane into GO-PAH solution for 10 minutes

ii) Rinsing with Mili-Q water for 5 minutes to remove the weakly bonded molecules

iii) Dipping the substrate membrane into sPVA solution for 10 minutes

iv) Rinsing with Mili-Q water for 5 minutes to remove the weakly bonded molecules

This procedure corresponds to a single deposition cycle. The process was repeated to increase the number of GO-PAH/sPVA bilayers on the substrate surface up to three bilayers. Scheme 3.11 shows schematically the procedure followed in electrostatic LbL assembly process. The electrostatic LbL composites were denoted as 15PVA(GO-PAH/sPVA)$_n$ and 15sPVA(GO-PAH/sPVA)$_n$, where n refers the number of the deposited bilayers.
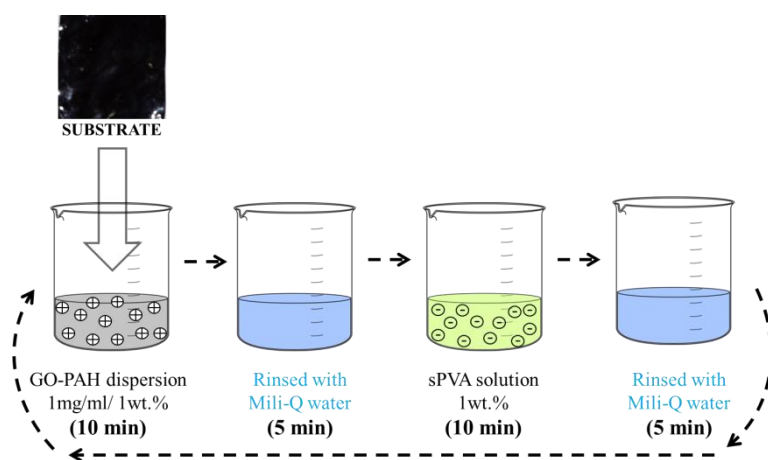
Scheme 3.11. Schematic diagram of the procedure followed in electrostatic LbL assembly process

3) Crosslinking process

Finally, the LbL assembled composites were crosslinked by immersing into 3% solution of glutaraldehyde (GA) for 30 minutes at room temperature in order to fix the deposited bilayers.

3.4. Characterization techniques

Zeta potential

Zeta potential is one of the most effective methods used to measure the surface charge of a particle as well as to quantify the stability of colloidal suspensions.

In most cases, when a solid surface is in contact with an aqueous solution, an electrical charge emerges in the interphase. This charge directly affects to the nearby ions creating a non-uniform charge distribution around the interface known as the electric double layer (EDL) [8], as shown in Figure 3.1.
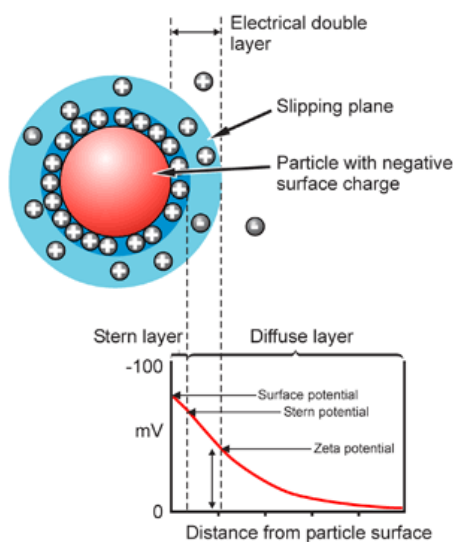
Figure 3.1. Schematic representation of the electrical double layer (EDL) [9]

Stern proposed a model that divides the EDL into two layers: an inner compact layer (Stern layer) and an outer diffuse layer. The counter-ions in the Stern layer are almost immobilized due to its strong interaction with the surface by electrostatic interactions. However, the ions situated further from the Stern layer experience a weaker electrostatic attraction and form the mobile diffuse layer. The boundary separating these two regions is defined as the slipping plane. In the diffuse layer, the electrostatic and thermal forces competing creating a nonzero concentration of ions, that is maximum at the surface and decreases gradually with distance until it reaches equilibrium [9].

The EDL layer neutralizes the surface charge, creating an electro-kinetic potential distribution between the interface and the solution. As can be seen from Figure 3.1, the electrical potential through the Stern layer varies almost linearly, and then decreases

gradually in the diffuse layer until it reaches zero far away from the surface. The electrical potential at the shear plane is known as zeta potential (ξ) [9].

When an electric field is applied tangentially to the EDL, the mobile ions in the diffuse layer begin to migrate towards the appropriate electrode. This ion drag brings the surrounding liquid to move, generating an electroosmotic flow. The movement also generates an electric current. Since the applied electric field is tangential to the surface, the resulting ion migration does not affect the charge density in the EDL [9]. The velocity at the wall is zero and reaches a uniform velocity in the bulk, being the direction and velocity of the motion a function of particle charge, the suspending medium, and the electric field strength [8]. The velocity at the edge of the EDL is given by the classic Helmholtz–Smoluchowski equation:

$$U_{HS} = -\frac{\varepsilon_0\,\varepsilon_r\,\xi\,E_x}{\eta}$$

where E_x is the tangential electric field and ξ is the zeta potential. Usually the group of terms, $\varepsilon_0\varepsilon_r\xi/\eta$, are combined together into a proportionality constant called the electroosmotic mobility (μ_{eo}) of the solid–liquid interface. Thus it is possible to determine the zeta potential by measuring the fluid velocity or volume flow rate under electroosmotic flow [8].

The zeta potential measurements of the solutions used for the preparation of the electrostatic layer-by-layer assembled composites were performed at National Institute for Materials Science in Tsukuba (Japan) using a *Zetasizer Nano ZS (Malvern)* equipment shown in Figure 3.2.

Figure 3.2. *Zetasizer Nano ZS* (**Malvern**) **equipment and its** *Zetasizer nanocell*

Fourier Transform Infrared Spectroscopy (FTIR)

Fourier Transform Infrared Spectroscopy (FTIR) is a useful tool for molecular structural studies, identification, and quantitative analysis in polymeric materials.

FTIR is a technique based on the vibrations of the atoms of a molecule. An infrared spectrum is commonly obtained by passing infrared radiation through a sample and determining what fraction of the incident radiation is absorbed at a particular energy. The energy at which any peak absorbs corresponds to the vibration frequency of each functional group of the sample [10]-[12].

When a molecule shows infrared absorption, the vibration or rotation within the molecule must cause a net change in its electric dipole moment. This is the selection rule for infrared spectroscopy. Therefore, the interaction between the infrared radiation and the molecules may be understood in terms of changes in molecular dipoles [13].

Vibrations can involve either a change in bond length (*stretching*) or bond angle (*bending*). Some bonds can stretch in-phase (*symmetric* stretching) or out-of-phase (*asymmetric* stretching) [10]. Bending vibrations also contribute to infrared spectra. The different types of vibrations are summarized in Figure 3.3.
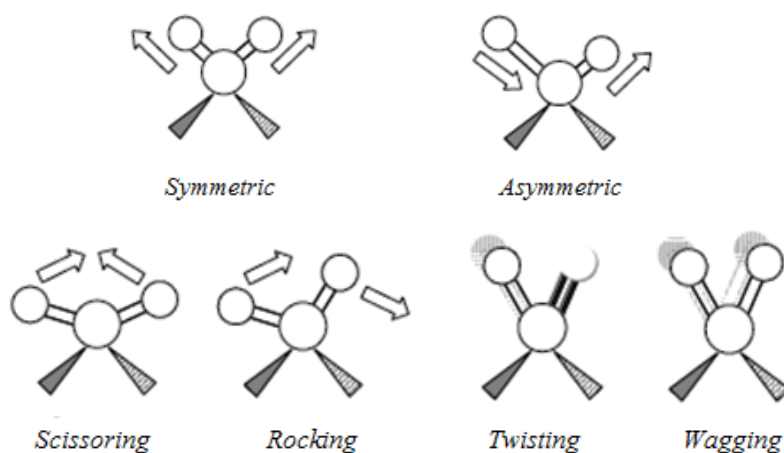
Figure 3.3. Stretching (above) and bending (bellow) vibrations of molecules

The infrared spectrum of a sample is collected by going a beam of infrared light through the sample. The resulting signal is called interferogram and it gives information about the infrared energy that the sample was absorbed. The interferogram signal can not be analyzed directly. Therefore, the interferogram is transformed to frequency domain by the Fourier transform method to obtain the FTIR spectrum [13],

as shown in Figure 3.4. A FTIR spectrum is a plot of the absorbance (or transmittance %) as a function of the frequency, in units of wavenumbers cm^{-1}.
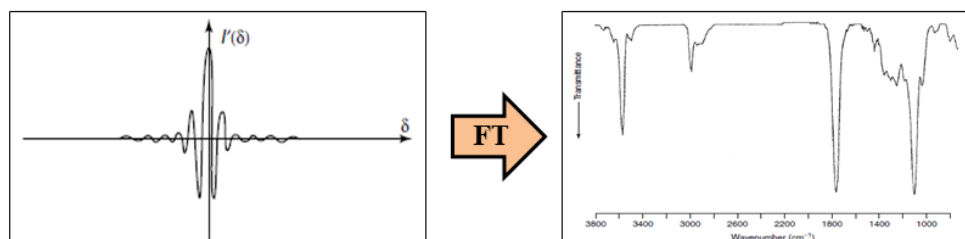
Figure 3.4. Interferogram conversion to the frequency domain

The FTIR analysis was performed at Universitat Politècnica de València (UPV) and Universitat de València (UV) using a *Thermo Nicolet 5700 FT-IR* spectrometer shown in Figure 3.5. The FT-IR spectra were collected in the range of 4000-400 cm^{-1} using the Attenuated Total Reflectance (ATR) mode at a resolution of 4 cm^{-1}. In order to obtain accurate results, 64 scans were performed at three different locations of the sample and the average was calculated. Backgrounds spectra were collected before each series of experiments in order to eliminate any interference from the environment.

Figure 3.5. *Thermo Nicolet 5700 FT-IR* spectrometer

Raman spectroscopy

Raman spectroscopy provides information about molecular vibrations that can be used for sample identification and quantitation. The technique is a form of vibrational spectroscopy much like FTIR spectroscopy; however the physical method of observing the vibrations is different. In Raman spectroscopy is measured the light scattering while the infrared spectroscopy is based on absorption of photons [14].

In Raman spectroscopy, the sample is irradiated by a monochromatic light source, usually a laser, and the scattered light is detected. When light is scattered from a molecule, two types of scattering can be distinguished. The majority of the scattered light has exactly the same frequency as the incident light; this elastic scattering is known as *Rayleigh scattering*. However, the scattering of a small fraction of light is shifted to different frequencies from the frequency of the incident light. This difference leads to an inelastic scatter called *Raman shift* [15], [16]. A Raman spectrum is a plot of the intensity of this *Raman shift* as a function of its frequency difference from the incident radiation, usually in units of wavenumbers cm^{-1}.

Raman analysis was performed at Universitat de València (UV) using a *Horiba XploRA-One* Raman microscope shown in Figure 3.6. The measurements were undergone in the interval of 200-3500 cm^{-1} using a 532 nm laser as a Raman excitation source.

Figure 3.6. *Horiba XploRA-One* **Raman microscope**

Inductively Coupled Plasma-Optical Emission Spectroscopy (ICP-OES)

ICP-OES is one of the most powerful and popular analytical techniques for the determination of trace elements in a sample [17]. The technique is based on the spontaneous emission of photons from atoms and ions that have been excited in a RF discharge. Liquid and gas samples may be injected directly into the instrument, while solid samples require extraction or acid digestion so that the analytes will be present in a solution. The sample is conducted by a peristaltic pump to a nebulizer. The produced aerosol is directed to the core of the inductively coupled argon plasma, where temperatures of approximately 10000 K are attained. At such high temperatures, the aerosol is quickly vaporized, and the analyte species are atomized, ionized and thermally excited. The excited species return to the lowest energy position by emission of a photon with the wavelength characteristic of the element from which it was originated. The intensity of this emission is indicative of the concentration of the element within the sample [17], [18].

The determination of the sulfur content in sulfonated poly(vinyl alcohol) (sPVA) was performed by ICP-OES technique. The analysis was performed in the Institute of Polymer Science and Technology (ICTP-CSIC) of Madrid using a sequential inductively coupled plasma spectrometer (ICP) *Perkin-Elmer Optima 4300 DV ICP-OES* equipped with a spray Scott-type nebulization chamber. The selected spectral line was 180.669 nm and peak area was used for signal acquisition. A picture of the ICP-OES analyzer is shown in Figure 3.7.

Figure 3.7. *Perkin-Elmer Optima 4300 DV ICP-OES* **equipped with a spray** *Scott-type* **nebulization chamber**

X-Ray Photoelectron Spectroscopy (XPS)

X-Ray Photoelectron Spectroscopy (XPS) is a useful technique to study the chemical modification of materials due to its extreme surface sensitivity and its ability to study solids with a minimum of sample preparation [19].

The XPS technique involves the measurement of binding energies of electrons in molecules or lattices. The most commonly used X-ray sources are $MgK_{\alpha1,2}$ and $AlK_{\alpha1,2}$ with photons energies of 1253.7 and 1486.6 eV, respectively. With knowledge of the photon energy and the kinetic energy of the photo-emitted electron, XPS provides a method for the determination of the binding energies of, in principle, all electrons from the core to the valence levels in polymers [20].

A typical XPS spectrum plots the number of electrons detected versus the binding energy of the electrons detected. Therefore, XPS spectra quantify in terms of peak intensities and peak positions. The peak intensities measure how much of a material is at the surface, while the peak positions indicate the elemental and chemical composition.

The XPS analysis was performed in the European Space Agency (ESA) at Universitat de València (UV) using a multi-analysis system SCALAB 210 shown in Figure 3.8. A monochromatic Mg excitation line at 1253.6 eV was applied.

Figure 3.8. *XPS SCALAB 210* **multi-analysis system**

X-ray Diffraction (XRD)

X-ray diffraction (XRD) is a non-destructive analytical technique for identification and quantitative determination of long-range order in various crystalline compounds. X-rays are electromagnetic radiation generated when an electron beam accelerated through a high voltage field hits a metal which acts as an anode [21]. The wavelength (λ) of X-rays is characteristic of the target anode material used and is given by

$$\lambda = \frac{E}{hc}$$

where, *h* is the Planck's constant, *c* is the velocity of light and *E* is the energy of the photon.

The wavelength of X-ray is comparable to the size of atoms; therefore it can be effectively used to measure the structural arrangement of atoms in materials. X-rays interact with electrons in atoms. When X-rays collide with electrons, some of the rays are deflected away from the incident beam direction. If the wavelengths of these scattered X-rays remain unchanged, the process is called an elastic scattering (Thompson Scattering). These are the X-rays measured in diffraction experiments, since carry information about the electron distribution in materials [22].

The X-rays diffracted from different atoms can interfere with each other. If the atoms are arranged in a periodic structure, as in the case of crystals, the peaks in the interference pattern will correspond to the distribution of atoms. The peaks in an X-ray diffraction pattern are directly related to the atomic distances by Bragg's law [23],

$$n\lambda = 2d\,\sin\theta$$

where, λ is the wavelength of X-ray, *d* is the inter-planar distance, θ is the scattering angle and *n* an integer representing the order of the diffraction peak, as shown in Figure 3.9.
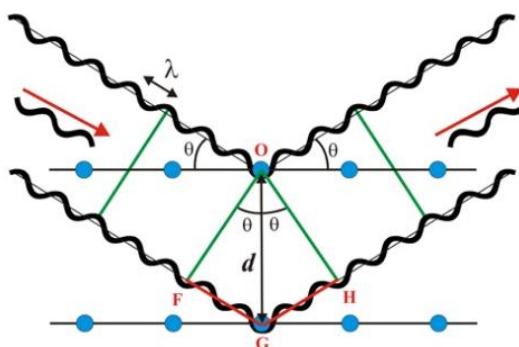
Figure 3.9. Scheme for Bragg's law

The peak position, intensity, and shape provide important information about the long range order in the sample.

The X-Ray diffraction experiments were performed in the Institute of Polymer Science and Technology (ICTP-CSIC) of Madrid using a *D8 Advance A25 Bruker* diffractometer shown in Figure 3.10. The measurements were conducted using a Copper K_α ($\lambda K_\alpha = 0.15418$ nm) radiation and a power setting of 40 kV and 40 mA. The data were collected from 5 to 75° with a scanning step of 0.01 ° and a scan rate of a 0.02 °/s.
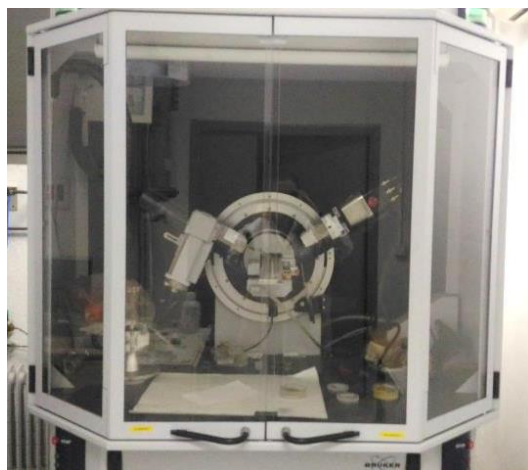
Figure 3.10. *D8 Advance A25 Bruker* **diffractometer**

Thermogravimetric analysis (TGA)

Thermogravimetric analysis (TGA) is a technique used to study the thermal stability of materials. TGA measures the mass changes of the sample as a function of temperature (dynamic mode) or time (isothermal mode) in a controlled atmosphere. The experiments can be carried out in either inert (argon or nitrogen) or oxidant (air or oxygen) atmosphere [24], [25].

The results of TGA are displayed in a thermogravimetric curve (TG curve), called thermogram. TG curve is a sigmoidal curve with one or more stages, depending on the chemical nature of the components and the sample composition. Thermogravimetric results are also commonly displayed as a differential curve or DTG curve obtained from the first derivate of the TG curve. The drops with maximum slope in TG curves correspond to the peaks in DTG curves, Figure 3.11.
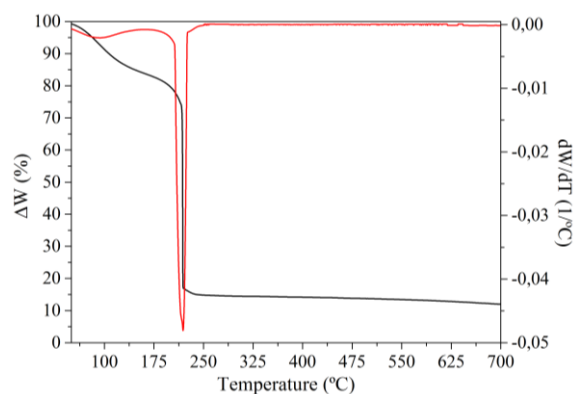
Figure 3.11. Typically TG curve and its corresponding DTG curve

The thermogravimetric analysis was performed in the Institute of Polymer Science and Technology (ICTP-CSIC) of Madrid and at Universitat Politècnica de València (UPV) using a *TA Instruments TGA Q-500* analyzer and a *Mettler-Toledo TGA/SDTA 851e modulus*, respectively. The experiments were conducted under nitrogen atmosphere with a constant heating rate of 10 ºC/min in the range of 25 to 800 ºC. A picture of the both TGA analyzers used to analyze the starting materials and the membranes is shown in Figure 3.12.

Figure 3.12. *TA Instruments TGA Q-500 analyzer* and *Mettler-Toledo TGA/SDTA 851^e modulus* analyzer

Scanning Electron Microscopy (SEM)

The scanning electron microscopy (SEM) is a technique extensively used to the examination and analysis of the morphology and the composition of a sample.

A SEM produces images of a sample by scanning it with a focused beam of electrons [26]. SEM works under high vacuum in order to avoid the obstruction of the electron beam through the microscope by small particles, such as gas molecules or air, which could deflect the electrons, varying the obtained results. The sample is hit by a beam of electrons generated typically from a tungsten filament or a field emission gun. As a result, the sample emits X-rays and three different types of electrons: primary backscattered electrons, secondary electrons and Auger electrons. The primary backscattered electrons and the secondary electrons are used to generate the images. The backscattered electrons are high-energy electrons, the images obtain from them show different brightness depending on the atomic number of the components of the sample. Hence, the image obtained from backscattered electrons is an atomic number map of the specimen surface. On the other hand, the secondary electrons are low energy electrons. These electrons give information about the topography of the sample surface, providing good edge details. In order to increase the secondary electrons emission, heavy metals such as gold or platinum are commonly used to coat the samples [27]-[29].

Additionally, the X-ray emitted can be used to obtain a localized chemical analysis of the sample. The number and energy of the X-rays emitted from the sample can be measured by an Energy Dispersive Spectrometer (EDX). Since the energy emitted by the X-ray is characteristic of each element of the sample, EDX gives information about the elemental composition of the sample [30].

The SEM analysis of the starting materials and the composites was performed in the Institute of Polymer Science and Technology (ICTP-CSIC) of Madrid and at Universitat Politècnica de València (UPV) using a *Hitachi SU8000* Field Emission-Scanning Electron Microscope (FE-SEM) and a *JEOL JSM-6300* scanning electron microscope, respectively. The analysis was carried out with an acceleration voltage of 20 kV. Figure 3.13 shows the pictures of the both equipment SEM used for the morphological analysis.

Figure 3.13. *Hitachi SU8000 FE-SEM* (up) and *JEOL JSM-6300* SEM (down)

Transmission Electron Microscopy (TEM)

The transmission electron microscope is a very powerful tool for material science in which a beam of electrons is transmitted through an ultra-thin sample and the interactions between the electrons and the atoms can be used to obtain structural and chemical composition information from the strong electron-atom interactions.

TEM operates on the same basic principles as the light microscope, but it uses electrons instead of light. Rather than glass lenses focusing the light in the light microscope, the TEM uses electromagnetic lenses to focus the electrons into a very thin beam. Since electrons are very small and easily deflected by gas molecules, it is necessary to use the electron beam in a vacuum environment. The electron beam, generated from a tungsten filament, is passed through a thin-section of sample. The transmitted electrons through the sample are focused on a fluorescence screen or a charge-coupled device (CCD) camera, which gives the image of the section of the

studied sample with different darkness according to its thickness [31]. A schematic diagram of the TEM system is shown in Figure 3.14.
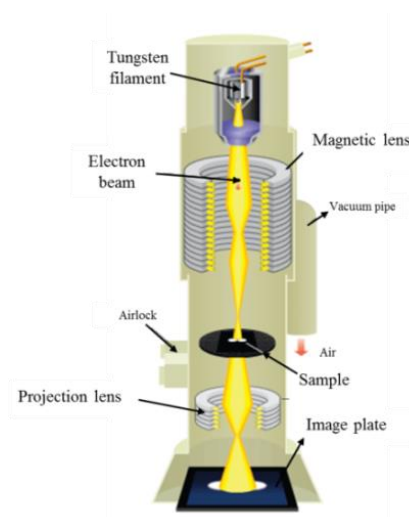
Figure 3.14. Schematic diagram of a TEM system

The TEM analysis of the composites were performed at Universitat de València (UV) using a *JEOL JEM-1010* transmission electron microscope operating at an accelerating voltage of 100 kV. The ultrathin sections were cut with an ultra-microtome *Leica EM UC6*. Figure 3.15 shows the pictures of the both equipment used for the morphological study.

Figure 3.15. *JEOL JEM-1010* transmission electron microscope (left) and ultra-microtome *Leica EM UC6* (right)

Atomic Force Microscopy (AFM)

Atomic Force Microscopy (AFM) is a technique used to characterize surfaces at extremely high resolution. The AFM consist of a cantilever with a sharp tip that is used to scan the specimen surface. The atomic force between the sample and the tip is measured using a laser and a detector to monitor the motion of the cantilever [32]. Figure 3.16 shows the basic components of an AFM. The operating mode can be varied depending on the application: contact mode, non-contact mode and tapping mode.
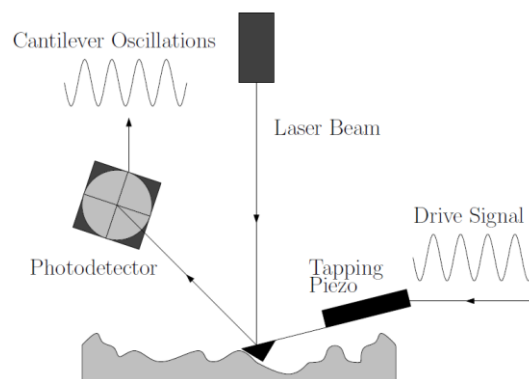
Figure 3.16. Basic components of an AFM

In tapping mode, the cantilever assembly is oscillated near its resonance frequency using a piezoelectric crystal situated in the holder. As tip approaches the surface of the sample, the tip makes contact with the surface for a short time in each oscillation cycle. The interaction between the tip and the sample modify the amplitude, resonance frequency and phase angle of the cantilever. These modifications are used to identify and measure the surface features. A schematic diagram of the tapping mode is shown in Figure 3.17.
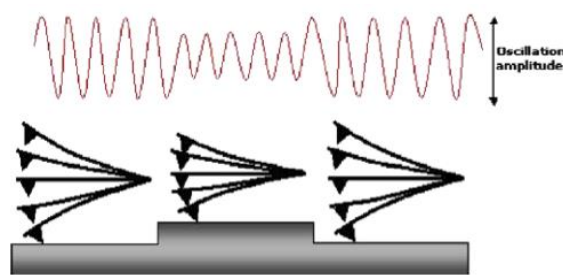
Figure 3.17. Schematic diagram of tapping mode AFM analysis

The AFM measurements were conducted at Institute of Polymer Science and Technology (ICTP-CSIC) of Madrid using a *Multimode Nanoscope IVa, Digital Instrument/ Veeco* operating in tapping mode at room temperature under ambient conditions. Figure 3.18 shows a picture of the AFM equipment used for the analysis.
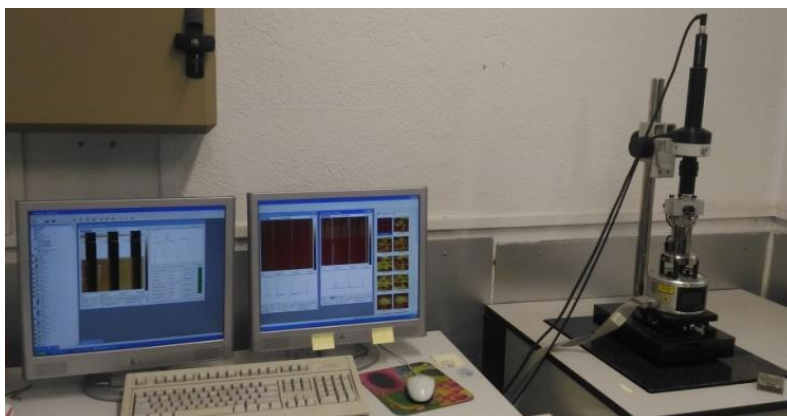
Figure 3.18. *Multimode Nanoscope IVa* **AFM equipment**

Tensile test

A tensile test is a static measurement that consists of applying a controlled load to a specimen while its developed deformation (strain) is measured. The sample is clamped between two fixtures called grips, and it is subjected to a controlled tensile load until fracture. Tensile test specimens are normally shaped like dog-bone, in which the center portion of the specimen is smaller in cross-section than the two ends [33].

The typical curve obtained from tensile test is the load-elongation curve which is converted into stress-strain curve. Several mechanical properties of a material can be obtained from the stress-strain curve, as shown in Figure 3.19. These properties include elastic modulus, elongation, elastic limit, yield strength, ultimate tensile strength, ductility, resilience, and toughness.
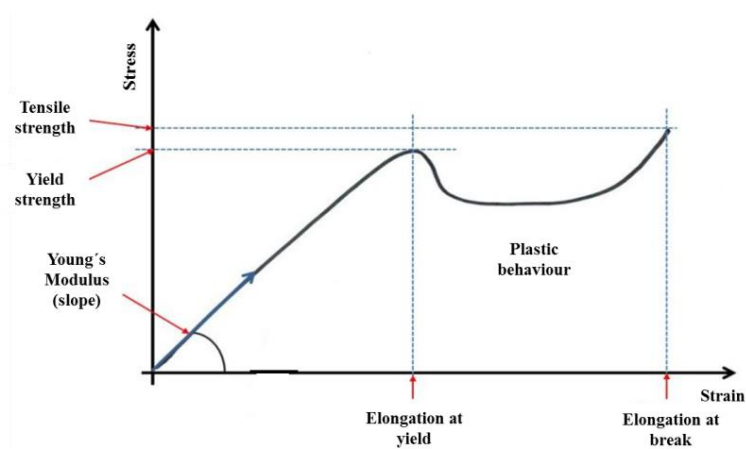
Figure 3.19. Typical stress-strain curve of a polymer

The mechanical properties of the composites prepared by solution-casting method were studied from the stress-strain curves. The measurements were carried out in the Institute of Polymer Science and Technology (ICTP-CSIC) of Madrid using a *MTS QTest 1/L Elite* Dynamometer that is shown in Figure 3.20. The membranes were cut into tensile specimens dog-bone shaped with the gauge length and width of 15 mm x 5 mm, respectively. Tests were conducted with a 100 N load cell under a strain rate of 5 mm/min at room temperature.

Figure 3.20. *MTS QTest 1/L Elite* **Dynamometer (left), and fracture of the specimen after tensile test (right)**

Microhardness measurement

Hardness is the property of a material that allows it to withstand a plastic deformation, usually by penetration. The standard test method used to analyze the hardness of composite membranes is the Vickers Hardness test, in which the depth or area of an indentation made by an indenter of a specific shape, applied with a defined force and during a specific time is measured [34]-[36].

The Vickers hardness test method consists of indenting the test material with a diamond indenter, in the form of a right pyramid with a square base and an angle of 136 degrees between opposite faces subjected to a load between 1 to 100 kgf. The full load is normally applied for 10 to 15 seconds. The two diagonals of the indentation left on the surface of the material after removal of the load are measured using a microscope [37]-[40]. The area of the sloping surface of the indentation is calculated. The Vickers hardness is obtained by dividing the kgf load (P) by the square area (d) of indentation according to the equation shown in Figure 3.21.

$$HV = \frac{2\, P \sin \frac{136°}{2}}{d^2}$$
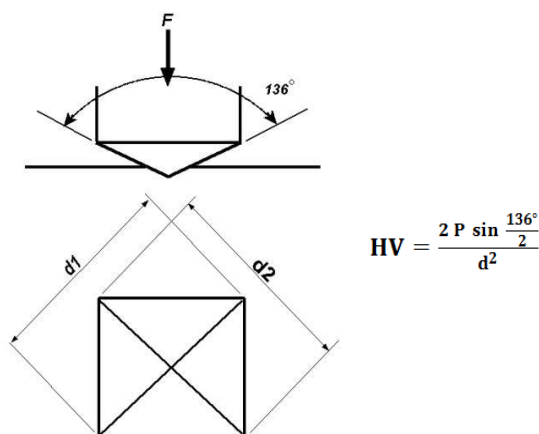
Figure 3.21. Schematic description of Vickers hardness test method

The Vickers microhardness measurements were carried out in the Institute of Polymer Science and Technology (ICTP-CSIC) of Madrid using a Vickers indentor equipped with a *Leitz RZD-DO* microhardness tester. A load of 100 g was used, with a loading cycle of 25 s at room temperature. Hardness was measured immediately after indentation. The experimental values were the average of three measurements. Figure 3.22 shows a picture of the Vickers indentor use for the measurements.

Figure 3.22. Vickers indentor equipped with a *Leitz RZD-DO* microhardness tester

Contact angle

The water contact angle is one of the common ways to measure the wettability of a surface. The contact angle (θ) is defined as the angle formed by the intersection of the liquid-solid interface and the liquid-vapor interface [41]. Figure 3.23 shows the geometrically acquisition of contact angle by applying a tangent line from the contact point along the liquid-vapor interface in the droplet profile.
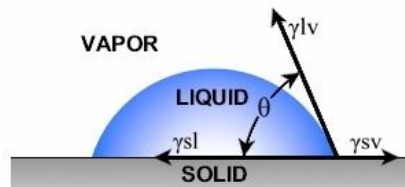
Figure 3.23. Schematic representation of the contact angle (θ) measurement

Low values of contact angle (less than 90º) indicate a strong liquid-solid interaction, and the fluid tends to spread over a large area on the surface wetting well. High values of contact angle (higher than 90º) indicate weak liquid-solid interactions, what means that wetting of the surface is an unfavorable process, so the fluid will minimize its contact with the surface and form a compact liquid droplet; a zero contact angle ($\theta = 0$) indicates complete or perfect wetting [42]. Figure 3.24 shows the different surface wettability measured using contact angle.
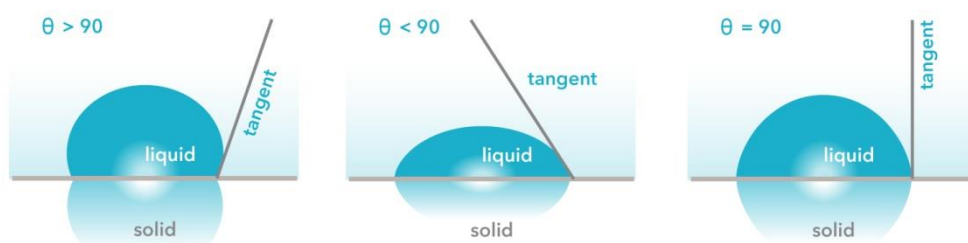
Figure 3.24. Types of surface wettability measured using contact angle (Source: Biolin Scientific)

The wettability measurements of the membranes were performed in the Institute of Polymer Science and Technology (ICTP-CSIC) of Madrid using a *Theta Optical Tensiometer (KSV Instruments, Ltd)* and electrooptics including a CCD camera connected to a computer at room temperature. A drop of distilled water (2 μL) was deposited on the sample surface at five different sites and the average of measured values was taken as a representative value. Figure 3.25 shows a picture of the tensiometer used for the measurements.
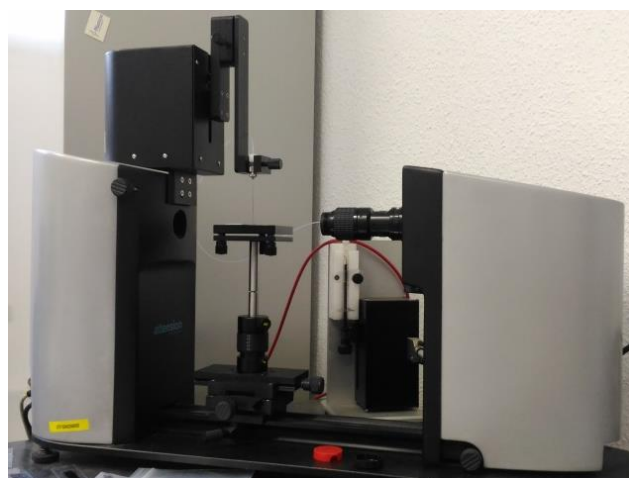
Figure 3.25. *Theta Optical Tensiometer*

Water Uptake (WU) and Swelling ratio (SW)

Water uptake (WU) is a property directly related to the performance of a PEM in DMFC, since it affects both to proton conductivity and methanol crossover. The absorbed water helps to proton transport via two different mechanisms: Grotthus mechanism, in which protons hop from one hydrolyzed site ($H_3O^+SO_3^-$) to another followed by a local molecular rearrangement to allow the next hop; and the Vehicular mechanism, through which the protons diffuse together with the free water molecules by forming the complex H_3O^+ [43]-[45]. Therefore, an optimal water uptake is needed to obtain successful fuel cell performance.

The water uptake measurements were conducted at Universitat Politècnica de València (UPV) by performing swelling tests on the membranes. The samples were cut in a rectangular shape (4×1 cm^2) and dried at 60 ºC under vacuum for 12 hours before analysis. Then, the samples were immersed in tests tubes containing distilled water and kept in isothermal *SELECTA Ultrasonic baths* (T $\pm$ 0.1 ºC) at the required temperature. The absorption of water was measured gravimetrically as a function of time, until no further gain weight was observed. Figure 3.26 shows a picture of the isothermal baths used to measure the water uptake.

Figure 3.26. Isothermal *SELECTA Ultrasonic bath (left)* and a picture of the test tubes with the samples immersed to measure the water uptake (right)

The water uptake, WU %, was calculated as the mass difference between the samples exposed to water (M_{eq}) and the dry sample (M_{dry}). The results were normalized respect to the mass of the dried sample by

$$WU_{eq}(\%) = \frac{M_{eq} - M_{dry}}{M_{dry}} \times 100$$

Moreover, the swelling ratio (SW) of the samples was calculated from the change in length between the fully hydrated at equilibrium and dry samples, L_{eq} and L_{dry}, respectively, as follows

$$SW_{eq}(\%) = \frac{L_{eq} - L_{dry}}{L_{dry}} \times 100$$

Ion Exchange Capacity (IEC)

Ion exchange capacity (IEC) is defined by the number of moles of exchangeable groups, in this case sulfonic acid groups, per unit of mass of dry polymer. Therefore, it is related to the number of available active sites for proton transfer and consequently with the proton conductivity in PEMs [43].

The IEC of the membranes was measured at Universitat Politècnica de Valencia (UPV) by titration method [46]. Dry membranes were weighted and converted to its protonated form by immersing them in a 0.5 M HCl solution for 24 hours. Subsequently, the membranes were washed with distilled water and immersed in a 2M NaCl solution for 24 hours at room temperature to perform the change of protons (H^+) to sodium ions (Na^+). The replaced protons were titrated against a standard 0.1 N (0.0955 ± 0.0009 N) NaOH solution using a phenolphthalein as indicator. The IEC values were obtained by the following equation,

$$IEC(mequiv/g) = \frac{N_{NaOH} \times V_{NaOH}}{W_{dry}}$$

where N_{NaOH} is the normality of the NaOH solution in *mequiv/L*, V_{NaOH} is the volume of the NaOH solution in *liters* (L), and W_{dry} is the weight of the dry membrane in *grams* (g).

Electrochemical Impedance Spectroscopy measurements (EIS)

Impedance measurements were carried out in order to evaluate the proton conductivity and the electrical conductivity of the composites. Electrochemical Impedance Spectroscopy (EIS) is a powerful diagnostic tool that it can be used to characterize limitations and improve the performance of fuel cells. EIS theory is a well-developed branch of AC theory that describes the response of a circuit to an alternating current or voltage as a function of frequency [47].

Both terms impedance and resistance show an opposition to the flow of electrons or current. In DC circuits, only the resistors produce this effect. According to Ohm´s law, the resistance in DC current circuits is defined as,

$$R = \frac{E}{I}$$

where *E* is the voltage measured in *volts* (V), *I* is the current in *amperes* (A)*,* and *R* the resistance in *ohms* (Ω). This relationship measures the electrons opposition to the flow or current through the circuit element that can be applied only to the ideal resistor circuit element.

However, the circuit elements in AC current often exhibit more complex behaviour. Besides the normal resistance, there are two other mechanisms preventing the current flow in an electrical circuit: the voltages induction in the conductor, that it is self-induced by the magnetic fields of current, called inductance (*L*), and the electrostatic charge storage induced by voltage between conductors called capacitance (*C*). The inductance and capacitance are together called the reactance (*X*) [48], [49].

Therefore, the concept of resistance has been extended to the quantity called impedance (*Z*) in the AC circuits. Whereas, the DC signal can be defined as analogous to the AC signal at the frequency tending to zero. The ideal resistance has only magnitude whereas the impedance has both magnitude and phase angle being usually represented in the form of a complex number. The unit of impedance, ohm (Ω), is the same as that of resistance. In the complex plane, the real part of impedance is resistance and the reactance forms the imaginary part of the impedance [48], [49].

The magnitude and the phase angle of the complex impedance can be easily plotted by means of the impedance vector as |Z| and the phase angle as θ, using a phasor diagram. The impedance can be expressed in terms of real and imaginary components by [47]-[49],

$$|Z| = \sqrt{(Z_r^2 + Z_j^2}$$

and the phase angle can be obtained as follows,

$$\theta = \tan^{-1}\left(\frac{Z_j}{Z_r}\right)$$

Nyquist plot and Bode plot are commonly used to represent the impedance measurement. In the Nyquist plot (Figure 3.27a), is plotted the imaginary impedance component (Z") against the real impedance component (Z′) at each excitation frequency. The Nyquist plot shows several advantages over the Bode plot due to the former, makes easy to see the effects of the ohmic resistance (R_Ω) related to the proton conductivity, from the extrapolation of the semicircle towards the left, x axis, to read R_Ω. However, the major limitation of the Nyquist plot is that frequency can not be ascertained by simply looking at the plot. This limitation was overcome in the Bode plot, where both the absolute value of impedance and the phase angle are plotted on the y-axis versus the logarithmic frequency plotted on the x-axis [49]. Since frequency appears in one of the axes, it is easy to understand from the plot how much the impedance depends on the frequency. From the Bode plot, it is also possible to obtain R_Ω. At high frequencies, the ohmic resistance dominates the impedance and the log (R_Ω) can be read from the high frequency horizontal plateau, as can be seen in Figure 3.27b.
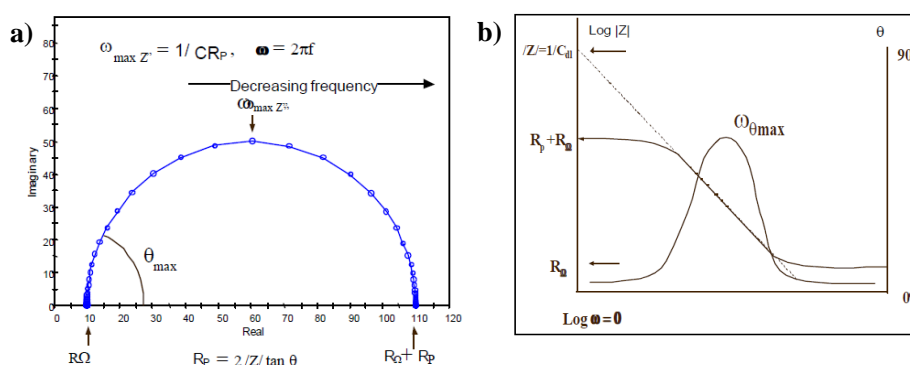
Figure 3.27. Representation of EIS data in a) Nyquist plot, and b) Bode plot

The impedance measurements were conducted at UniversitatPolitècnica de València (UPV) and in the Institute of Polymer Science and Technology (ICTP-CSIC) of Madrid using a *Novocontrol Broadband Dielectric Spectrometer (BDS)*, in the frequency range of 10^{-1} to 10^{7} Hz, connected to an *Alpha-A Frequency Response Analyzer (Novocontrol)*. Figure 3.28 shows a picture of the dielectric spectrometer used for the conductivity analysis.

Figure 3.28. *Novocontrol Broadband Dielectric Spectrometer*

Proton conductivity (σ_{prot}) was measured on a *BDS-1308 (Novocontrol)* liquid parallel plate sample cell, shown in Figure 3.29. The membranes were previously equilibrated with Mili-Q water for 24 hours to ensure fully hydrated state. The measurements were performed at 30, 50, 70 and 90 ºC. The proton conductivity of the membranes was calculated according to

$$\sigma_{prot} = \frac{L}{R\,A}$$

where *L* is the thickness of the conducting membranes in *centimeters* (cm), *A* the area of the electrode in contact with the membrane in cm^2, and *R* the protonic resistance taken from the Bode plot at high frequencies in *ohms* (Ω) [50].

Figure 3.29. *BDS-1308* **liquid parallel plate sample cell used for proton conductivity measurements**

Electrical conductivity was measured at 30 ºC using a *BDS-1200 (Novocontrol)*, parallel plate capacitor cell with two gold-plated electrodes system shown in Figure 3.30. The electrical conductivity was taken at low frequencies, where the measured real part of the conductivity (σ') reaches a plateau which corresponds directly to the DC conductivity (σ_0).

Figure 3.30. *BDS-1200 (Novocontrol)***, parallel plate capacitor cell used for the electrical conductivity measurements**

Methanol diffusion measurements

The methanol barrier properties of the composites were evaluated by means of permeation measurements. In any case, there was not considered as a comprehensive study, but rather as an approximation by using a home-made permeation gravimetric cell, which was allowed us to easily determine several of the methanol permeation parameters through the membrane.

The measurements were performed in the Institute of Polymer Science and Technology (ICTP-CSIC) of Madrid in a gravimetrical Teflon home-made permeation cell. Figure 3.31 shows three different pictures of the permeation cell taken from the front, top and bottom side.

Figure 3.31. Pictures of the home-made gravimetric cell taken from three different views: front, top and bottom side

The Teflon cell is basically a liquid container, which is sealed with the polymer membrane for the permeation measure. The use of Teflon ensures that the liquid does not react with the surface of the cell. The cell consists of two parts. The part that is essentially a liquid container with 12 mm of inside diameter, and another part which is used to seal membrane on the liquid container. The inside diameter of the cell accurately defines the permeation area of the membrane [51].

As a penetrant solvent is placed inside the cell, there is a concentration gradient through the membrane due to the solvent concentration is zero in the other side of the membrane. The solvent molecules that have penetrated through the membrane will be evaporated to the air. The solvent penetration is reflected by the decrease in the overall weight of the cell. The weight decrease as a function of time gives the diffusion coefficients for a given polymer-penetrant system [51].

To perform the diffusion measurements, a protocol similar to the described by B. Harrison et al. [51] and D. De Kee and et al. [52] was followed. The polymer membrane with a known thickness was cut into 15 mm diameter disk. The cell was filled with the penetrant liquid (2M methanol solution), and sealed with the membrane to assay. The two parts were quickly assembled with the membrane clamped to seal the pathway of the solvent. The cell, placed in the position where the liquid is in direct contact with the membrane, was immediately put on an analytical balance inside of a

thermostabilized chamber. The weight loss was recorded as a function of time and the data were used to calculate the methanol diffusion coefficients.

Rogers [53] related the penetrant flux, F(t), to the diffusion coefficient, D, by the following equation,

$$F(t) = -D \left(\frac{\partial c}{\partial x}\right)\Big|_{x=l} = 2c_1 \left(\frac{D}{\pi t}\right)^{1/2} \sum_{m=0}^{\infty} \exp\left[-\frac{(2m+1)^2 l^2}{4Dt}\right]$$

where l is the thickness of the membrane in *centimeters* (cm), c_1 is the penetrant concentration at x = 0, and *D* is a constant diffusion coefficient in cm^2/s.

For small times, only the first term of the series is important and the equation is reduced to,

$$\ln\left(t^{\frac{1}{2}}F\right) = \ln\left[2c_1 \left(\frac{D}{\pi}\right)^{1/2}\right] - \frac{l^2}{4Dt}$$

The plot of the $\ln(t^{1/2} \cdot F)$ versus (1/t) gives a straight line with slope $-l^2/4D$ from which the value of D_{MeOH} can be estimated.

Fuel Cell (FC) tests

H$_2$-O$_2$ fuel cell test

The H$_2$-O$_2$ fuel cell tests were conducted at Universitat Politècnica de València (UPV) using a *H-TEHC PEMFC®-Kit*. Figure 3.32 shows pictures of the assembly of the H$_2$-O$_2$ fuel cell; this includes two Plexiglas blocks containing the gas ports and two 16 cm^2 metal grid electrodes with an elastomer rim with air and gas sealing properties. The membranes were previously equilibrated with Mili-Q water during 24 hours to ensure their fully hydrated state, and were sandwiched between two electrode catalysts sheets (*Fuel Cells Etc, 4 mg/cm^2 platinum black*). The fuel cell worked with the hydrogen and oxygen gases produced from an electrolyser (*Horizon Fuel Cell Technologies*). Fuel cell performance data were acquired with a *Keithley 2400* High Voltage Source Measurement Unit and a *Fluke 73* Multimeter, at 25 ºC and atmospheric pressure.
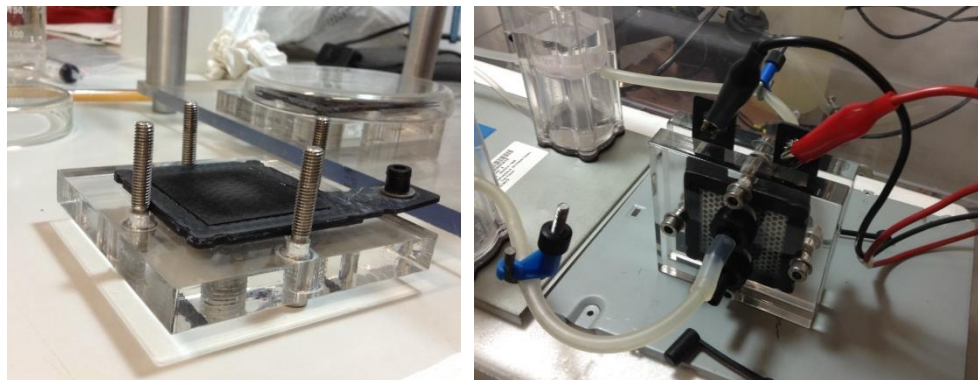
Figure 3.32. Pictures of the *H-TEC PEMFC®-Kit* assembly used to performed the H$_2$-O$_2$ fuel cell test

DMFC

DMFC performance tests of the solvent cast composites were conducted with a single cell at Universidad Politécnica de Madrid (ETS Ingeniería Aeronáutica y del Espacio).

The single DMFC tests were conducted using commercial electrodes, Pt/C (1 mg/cm^2) for the cathode and Pt-Ru/C (3 mg/cm^2) for the anode. The membranes were previously equilibrated with Mili-Q water during 24 hours, and the membrane-electrode assembly was carried out by pressing with the ending plates, without application of any ionomer. The active area of the single cell was approximately 4.3 cm^2. The system was allowed to reach the steady state before recording data points, keeping it at 0.15 V for 15 minutes. The polarization curves of the composite membranes were measured at 50 ºC in the range of methanol concentrations from 1M to 4M, in order to determine the concentration where the power density is maximum. The gas flow rates of the fuel (methanol solution) and oxidant (oxygen) were kept constant at 3 mL/min and 250 mL/min, respectively. All single cell tests were conducted five times, and the results were presented as the average data. Figure 3.33 shows different pictures of the single DMFC used to evaluate the composites performance.

Figure 3.33. Pictures of the single DMFC used to evaluate the performance of the composites

References

[1] S. Patachia, A. J. M. Valente, A. Papanceaa, and Victor M. M. Lobo, *Poly (Vinyl Alcohol) (PVA)-Based Polymer Membranes*. Nova Science Publishes, Inc., 2009.

[2] M. Yoo, M. Kim, Y. Hwang, and J. Kim, "Fabrication of highly selective PVA-g-GO/SPVA membranes via cross-linking method for direct methanol fuel cells," Ionics (Kiel), vol. 20, no. 6, pp. 875–886, 2014.

[3] S. Yun, H. Im, Y. Heo, and J. Kim, "Crosslinked sulfonated poly(vinyl alcohol)/sulfonated multi-walled carbon nanotubes nanocomposite membranes for direct methanol fuel cells," J. Memb. Sci., vol. 380, no. 1–2, pp. 208–215, 2011.

[4] W. S. Hummers and R. E. Offeman, "Preparation of Graphitic Oxide," J. Am. Chem. Soc., vol. 80, no. 6, pp. 1339–1339, 1958.

[5] L. Shahriary and A. A. Athawale, "Graphene Oxide Synthesized by using Modified Hummers Approach," Int. J. Renew. Energy Environ. Eng., vol. 2, no. 1, pp. 58–63, 2014.

[6] H. C. Chien, L. D. Tsai, C. P. Huang, C. Y. Kang, J. N. Lin, and F. C. Chang, "Sulfonated graphene oxide/Nafion composite membranes for high-performance direct methanol fuel cells," Int. J. Hydrogen Energy, vol. 38, no. 31, pp. 13792–13801, 2013.

[7] B. Konkena and S. Vasudevan, "Understanding Aqueous Dispersibility of Graphene Oxide and Reduced Graphene Oxide through pKa Measurements.," J. Phys. Chem. Lett., vol. 3, no. 7, pp. 867–72, Apr. 2012.

[8] B. J. Kirby and E. F. Hasselbrink, "Zeta potential of microfluidic substrates: 1. Theory, experimental techniques, and effects on separations," Electrophoresis, vol. 25, no. 2, pp. 187–202, 2004.

[9] Dongqing Li, *Encyclopedia of Microfluidics and Nanofluidics*, Springer, 2008.

[10] Barbara. H. Stuart, *Infrared Spectroscopy : Fundamentals and Applications*. John Wiley & Sons, 2004.

[11] A. Garton, *Infrared Spectroscopy of Polymer Blends, Composites and Surfaces*. Hanser Gardner Publications, 1992.

[12] Peter R. Griffiths, James A. De Haseth, James D. Winefordner, *Fourier Transform Infrared Spectrometry*, Second Edition, Wiley, 2007.

[13] Mitsuo Tasumi, *Introduction to Experimental Infrared Spectroscopy: Fundamentals and Practical Methods*, Wiley, 2014.

[14] I. R. Lewis and H. Edwards, *Handbook of Raman Spectroscopy: From the Research Laboratory to the Process Line*. CRC Press, 2001.

[15] Richard L. McCreery, *Raman Spectroscopy for Chemical Analysis*. John Wiley & Sons, Inc., 2005.

[16] P. Larkin, *Infrared and Raman Spectroscopy: Principles and Spectral Interpretation*. Elsevier Science, 2011.

[17] Xiandeng Hou, Bradley T. Jones, *Inductively Coupled Plasma–Optical Emission Spectrometry*. John Wiley & Sons, 2008.

[18] A. Helaluddin, R. S. Khalid, M. Alaama, and S. A. Abbas, "Main Analytical Techniques Used for Elemental Analysis in Various Matrices," Trop. J. Pharm. Res., vol. 15, no. 2, p. 427, 2016.

[19] J. V Dawkins, *Developments in Polymer Characterisation*. Springer, 2012.

[20] S. Hofmann, *Auger- and X-Ray Photoelectron Spectroscopy in Materials Science: A User-Oriented Guide*. Springer, 2012.

[21] Jinghua Guo, *X-Rays in Nanoscience: Spectroscopy, Spectromicroscopy, and Scattering Techniques*. Wiley, 2011.

[22] B. Fultz and J. Howe, *Transmission Electron Microscopy and Diffractometry of Materials*, Springer, 2013.

[23] O. H. Seeck and B. Murphy, *X-Ray Diffraction: Modern Experimental Techniques*. CRC Press, 2015.

[24] Edith Turi, *Thermal Characterization of Polymeric Materials*. Elsevier, 2012.

[25] W. M. Groenewoud, *Characterisation of Polymers by Thermal Analysis*. Elsevier, 2001.

[26] F. Liu, J. Wu, K. Chen, and D. Xue, "Morphology study by using scanning electron microscopy," Microsc. Sci. Technol. Appl. Educ., pp. 1781–1792, 2010.

[27] L. Reimer, *Scanning Electron Microscopy: Physics of Image Formation and Microanalysis*. Springer, 2013.

[28] J. Goldstein, D. E. Newbury, D. C. Joy, C. E. Lyman, P. Echlin, E. Lifshin, L. Sawyer, J. R. Michael, *Scanning Electron Microscopy and X-ray Microanalysis*: Third Edition. Springer, 2012.

[29] C. E. Lyman, D. E. Newbury, J. Goldstein, D. B. Williams, A. D. Romig Jr., J. Armstrong, P. Echlin, C. Fiori, D. C. Joy, E. Lifshin, K.-R. Peters, *Scanning Electron Microscopy, X-Ray Microanalysis, and Analytical Electron Microscopy: A Laboratory Workbook*. Springer, 1990.

[30] University of California, "Introduction to Energy Dispersive X-ray Spectrometry (EDS)," pp. 1–12, 2015.

[31] David B. Williams and C. Barry Carter, *Transmission Electron Microscopy: A Textbook for Materials Science*. Springer, 2009.

[32] R. N. Jagtap and A. H. Ambre, "Overview literature on atomic force microscopy (AFM): Basics and its important applications for polymer characterization," Indian J. Eng. Mater. Sci., vol. 13, no. 4, pp. 368–384, 2006.

[33] Joseph R. Davis, *Tensile Testing*, 2nd Edition: ASM International, 2004.

[34] H. F. Mark, *Encyclopedia of polymer science and technology*. John Wiley and Sons, 2007.

[35] H. F. Walker, A. K. ElshennawY, B. C. Gupta, and M. M. S. Vaughn, *The Certified Quality Inspector Handbook*. ASQ Quality Press, 2012.

[36] Warren Blackadder, *MEM30007A Select common engineering materials*. LULU Press, 2014.

[37] F. J. B. Calleja and S. Fakirov, *Microhardness of Polymers*. Cambridge University Press, 2007.

[38] M. M. Yovanovich, "Micro and Macro Hardness Measurements, Correlations, and Contact Models," 44th AIAA Aerospace Sciences Meeting and Exhibit, 9-12 January, pp. 1–28, 2006.

[39] Myer Kutz, T. M. *Handbook of Measurement in Science and Engineering, Volumen 2*. John Wiley & Sons, 2015.

[40] A. S. Wadhwa, Er. H. S. Dhaliwal, *A Textbook of Engineering Material and Metallurgy*. Firewall Media, 2008.

[41] Frederick M. Fowkes, *Contact Angle, Wettability and Adhesion*, no. v. 43. ACS Publications, 1964.

[42] K. L. Mittal, *Advances in Contact Angle, Wettability and Adhesion*, Volume Two. Wiley, 2015.

[43] B. Rieger, A. Künkel, G. W. Coates, R. Reichardt, E. Dinjus, and Thomas A. Zevaco, *Synthetic Biodegradable Polymers*. Springer, 2012.

[44] Kirt A. Page, L. Christopher L. Soles, and James Runt, *Polymers for Energy Storage and Delivery: Polyelectrolytes for Batteries and Fuel Cells*, American Chemical Society, vol. 1096, 2012.

[45] G. A. Ludueña, T. D. Kühne, and D. Sebastiani, "Mixed Grotthuss and vehicle transport mechanism in proton conducting polymers from Ab initio molecular dynamics simulations," Chem. Mater., vol. 23, no. 6, pp. 1424–1429, 2011.

[46] P. K. Tewari, *Nanocomposite Membrane Technology: Fundamentals and Applications*. CRC Press, 2015.

[47] Mark E. Orazem, Bernard Tribollet, *Electrochemical Impedance Spectroscopy*. John Wiley & Sons, 2011

[48] V. Sense, "Electrochemical Impedance Spectroscopy (EIS): A Powerful and Cost- Effective Tool for Fuel Cell Diagnostics," Cell, vol. 35, pp. 1–5, 1990.

[49] N. Sekar and R. P. Ramasamy, "Electrochemical Impedance Spectroscopy for Microbial Fuel Cell Characterization," J. Microb. Biochem. Technol., vol. S6, pp. 1–14, 2013.

[50] X. Qian, N. Gu, Z. Cheng, X. Yang, E. Wang, and S. Dong, "Methods to study the ionic conductivity of polymeric electrolytes using a.c. impedance spectroscopy," J. Solid State Electrochem., vol. 6, no. 1, pp. 8–15, 2001.

[51] C. J. Guo, D. De Kee, B. Harrison, "Diffusion of organic solvents in rubber membranes measured via a new permeation cell," J. App. Poly. Sci. vol. 56, no. 7, pp. 823–829, 2003.

[52] S. Xiao, C. Moresoli, J. Bovenkamp, and D. De Kee, "Sorption and permeation of organic environmental contaminants through PVC geomembranes," J. Appl. Polym. Sci., vol. 63, no. 9, pp. 1189–1197, 1997.

[53] H. Hopfenberg, *Permeability of Plastic Films and Coatings*. Springer, 1976.

Solution-cast proton exchange composite membranes

Chapter 4

4.1. Summary

This chapter is focused in the design, preparation and characterization of PVA-based composite membranes by solution-casting method for use as proton exchange membranes in DMFCs applications.

A new design of membrane morphology with more hydrophilic nanophases, randomly distributed through the membrane was developed in **Contribution I**. To this end, PVA was firstly intra-sulfonated by direct grafting of alkyl-sulfonated chains on the polymer backbone in order to promote proton conductivity. Second, the polymer chains were further inter-sulfonated by crosslinking reaction using sulfosuccinic acid (SSA) as crosslinker agent, which confers dimensional stability and the possibility to accommodate inter-chain sulfonic acid groups responsibly of proton conduction into the matrix. Finally, hybrid organic/inorganic composite membranes were prepared by dispersion of GO into polymer matrix in order to study the effect of a filler addition on the functional properties of the membranes. The structural, morphological, thermal and mechanical characterization of the functionalized PVA membranes were studied and discussed.

The potential of the previously prepared PVA-based membranes was evaluated for fuel cell applications in **Contribution II**. To this end, water contact angle, water uptake (WU) and swelling ratio (SW), ion exchange capacity (IEC), proton conductivity (σ_{prot}) and the H_2-O_2 fuel cell performance were investigated as a function of the intra- and inter-sulfonation of the polymer matrix, and the addition of GO nano-platelets.

Finally, multisulfonated composite membranes prepared by means of the sulfonation of the polymer matrix and the filler (sulfonated graphene oxide, sGO) were investigated in **Contribution III** for DMFC applications. The evaluation of the proton-conducting properties of the multisulfonated composites was done in terms of water contact angle, water and methanol uptake (WU/MU), ion exchange capacity (IEC), proton conductivity (σ_{prot}) and their performance in a H_2-O_2 fuel cell. Furthermore, the methanol permeability and the performance in a DMFC were also assessed.

H^+

-SO₃H groups   -OH groups   GO
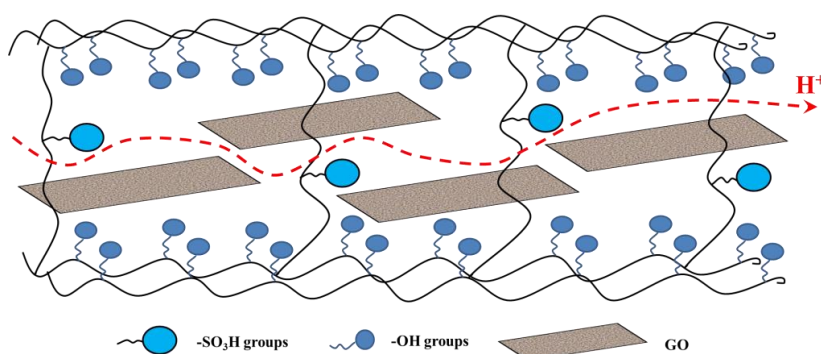
4.2. Contribution I:

Bi-sulfonation of poly(vinyl alcohol)/graphene oxide composite membranes for Proton Exchange Membrane Fuel Cell applications. Part 1: Membrane preparation and characterization

Bi-sulfonation of poly(vinyl alcohol)/graphene oxide composite membranes for Proton Exchange Membrane Fuel Cell applications. Part 1: Membrane preparation and characterization

S. C. Sánchez-Ballester[a], A. Ribes-Greus[a], V. Soria[b], G. Rydzek[c] and K. Ariga[c]

[a]Instituto de Tecnología de Materiales (ITM), Universitat Politècnica de València, Valencia, Spain

[b]ICMUV, Universitat de València, Burjassot, Valencia, Spain

[c]World Premier International (WPI) Research Center for Materials Nanoarchitectonics (MANA), National Institute for Materials Science (NIMS), Tsukuba, Japan.

Abstract

Crosslinked composite membranes based on poly(vinyl alcohol) (PVA) and graphene oxide (GO) were prepared using the solution-casting method for application in fuel cells. The effect of the sulfonation of the polymer matrix as well as the addition of graphene oxide (GO) on the chemical, thermal, mechanical and proton conducting properties of the membranes were studied. The membranes were crosslinked with sulfosuccinic acid (SSA) in order to ensure their dimensional stability and induce proton conductivity by the introduction of sulfonic acid groups. The characteristic properties of the PVA-based membranes were evaluated by Fourier transform infrared (FT-IR), X-ray diffraction (XRD), scanning electron microscopy (SEM), transmission electron microscopy (TEM), thermogravimetric analysis (TGA), tensile test and electrochemical impedance. FTIR spectra evidenced the new ester linkages formed between the polymer matrix and the SSA during the crosslinking reaction. The results of XRD and SEM/TEM corroborate the good dispersion of GO in the polymer matrix. It was found that the addition of GO improves not only the thermal and mechanical stability but also the proton conductivity of the PVA-based membranes Finally, the 30sPVA/GO membrane showed the highest value of proton conductivity, 1.95 mS/cm at 25 ºC, which is an improvement of the 89 % respect its homologue 30sPVA free of filler.

Introduction

Environmental concerns arising from massive fossil energy usage, including the global climate change and the shortage in oil resources, have triggered the search for new sources of energy. Fuel cell (FC) power generation is considered as an attractive alternative due to its high efficiency, reduced dependence on conventional fuel, and low emission of harmful pollutants [1]. A proton exchange membrane fuel cell (PEMFC) is an electrochemical device that directly converts the chemical energy of a fuel into electrical energy [2]. This device consists of two electrodes separated by a proton exchange membrane (PEM). PEM is a crucial part of the fuel cell, allowing facile transport of protons from anode to cathode as well as a barrier to prevent the direct contact of fuel and oxidant. Therefore, PEMs must meet the following characteristics: i) high proton conductivity; ii) low fuel permeability; iii) good thermal and hydrolytic stability; iv) substantial morphological and dimensional stability; v) outstanding mechanical properties, and vi) low cost [3].

Poly(vinyl alcohol) (PVA) is an appealing polymer for PEMs preparation thanks to its chemical stability, good mechanical properties, good film-forming capacity and low cost [4]. However, PVA itself does not possess any negative charged ions, such as carboxylic and sulfonic acid groups, required to proton transport, and swells easily in water. Hence, PVA needs to be modified to promote proton conductivity and improve its water management without destroying its other properties in order to enhance its applicability as a PEM in fuel cell applications.

Three different strategies have been proposed in this study to overcome the weaknesses of PVA [5]. Firstly, the chemical crosslinking of the polymer matrix can remarkably improve the mechanical stability of the PVA-based membranes. The formation of covalent bonds between the polymer chains of PVA restricts its solubility in water. In addition, the use of sulfonated crosslinking agents such as sulfosuccinic acid (SSA) could further improve the proton conductivity of the membranes. The second strategy involves the introduction of negatively charged groups into the PVA structure in order to induce proton conductivity [6]. The attachment of highly proton conductive groups by direct sulfonation (intra-sulfonation process) of the PVA backbone using propane sultone as a sulfonating agent has been proposed as a suitable methodology. Finally, the mechanical stability of PEMs can be increase by preparation of hybrid organic-inorganic composites. In this regard, GO is an attractive material to be used as inorganic nanofiller in PVA-based composite membranes since it is easy to disperse in polar polymers due to the oxygen functional groups (hydroxyl, epoxy and carboxylic acid groups) contained in its structure. Moreover, its unique structure with high surface area, high mechanical strength, and electronic insulation properties favor the formation of proton transport channels through the membrane. Hence, GO can be considered as a good candidate for the preparation of composite PEMs [7].

In this study, novel bi-sulfonated membranes based on poly(vinyl alcohol) were prepared for PEMFC applications. In a first step the PVA matrix was directly sulfonated with propane sultone in order to promote proton conductivity. A further sulfonation was achieved by crosslinking reaction with sulfosuccinic acid (SSA) at two different concentrations (15 and 30 wt.%) to endow dimensional stability and provide additional proton conducting moieties to the membranes. Additionally, composite membranes were prepared by addition of 1 wt.% of GO to the polymer matrix. The effect of the crosslinking degree, the intra-sulfonation of the polymer matrix and the addition of GO nanosheets on the structural, morphological, thermal and mechanical properties was studied. Moreover, the proton conductivity of the membranes was studied in order to evaluate their potential as PEM candidates for fuel cell applications.

Experimental

Chemicals

Graphite powder (particle size < 20 μm), sodium nitrate (NaNO₃, ≥ 99.0%), sodium hydride (NaH, dry 95%), 1,3-propane sultone (97%), poly(vinyl alcohol) (PVA, molecular weight 130000 g/mol degree of hydrolysis, min. 99%) and sulfosuccinic acid (SSA, 70 wt.% solution in water) were purchased from Sigma-Aldrich. Concentrated sulfuric acid (H_2SO_4, 95%), hydrogen peroxide (H_2O_2, 30% w/w), ethanol absolute (EtOH), hydrochloric acid (HCl, 37%), potassium permanganate ($KMnO_4$, extra pure) were purchased from Scharlab.

Synthesis of materials

Synthesis of intra-sulfonated poly(vinyl alcohol) (sPVA)

The synthesis of intra-sulfonated poly(vinyl alcohol) was carried out in two steps as illustrated in Scheme 4.1 [8], [9]. First, 10 g of commercial PVA were dispersed in 250 mL of EtOH. Successively, 4.8 g of NaH were slowly added to the PVA dispersion under constant mechanical stirring at room temperature. Then, 5 g of 1,3-propane sultone were added dropwise and the mixture was stirred at 80 ºC for 24 hours. In a second step, the sodium sulfonated salt was transformed to the protonated form by immersion in a HCl solution for 12 hours. The obtained sPVA powder was filtered, washed with EtOH and finally dried for 4 hours in a vacuum oven at 50 ºC.
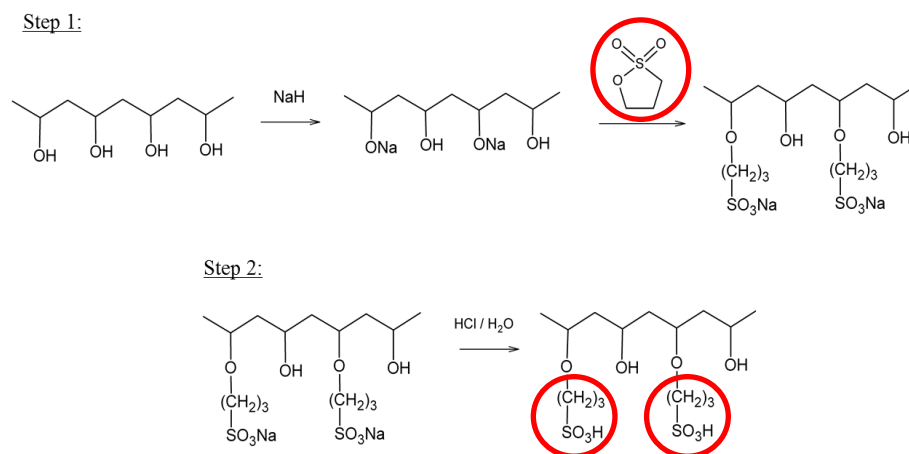
Scheme 4.1. Schematic diagram of intra-sulfonation process of PVA, introducing sulfonic acid groups covalently bonded

Synthesis of graphene oxide (GO)

Graphene oxide was synthesized from graphite powder using the Modified Hummers Method (MHM) [10], [11]. Briefly, 2 g of graphite in 46 mL of concentrated H_2SO_4 were mixed with 1 g of $NaNO_3$ in an ice bath under constant stirring. After 5 minutes, 6 g of $KMnO_4$ were added gradually to the previous solution while keeping the temperature below 20 ℃ to prevent overheating. The ice bath was then removed and the mixture was stirred at 35 ℃ for 30 minutes. The resulting solution was diluted by adding 92 mL of distilled water dropwise under constant stirring. Then, the temperature was increased to 98 ℃ and 280 mL of distilled water were added under vigorous stirring. After 2 hours, the suspension was filtered and treated with 30% H_2O_2 solution. The resulting GO was washed several times with HCl and EtOH until neutralization, followed by filtration. Finally, the powder was suspended in distilled water and sonicated for 3 hours, filtered and dried in a vacuum oven for 12 hours. Scheme 4.2 summarizes the GO preparation process.
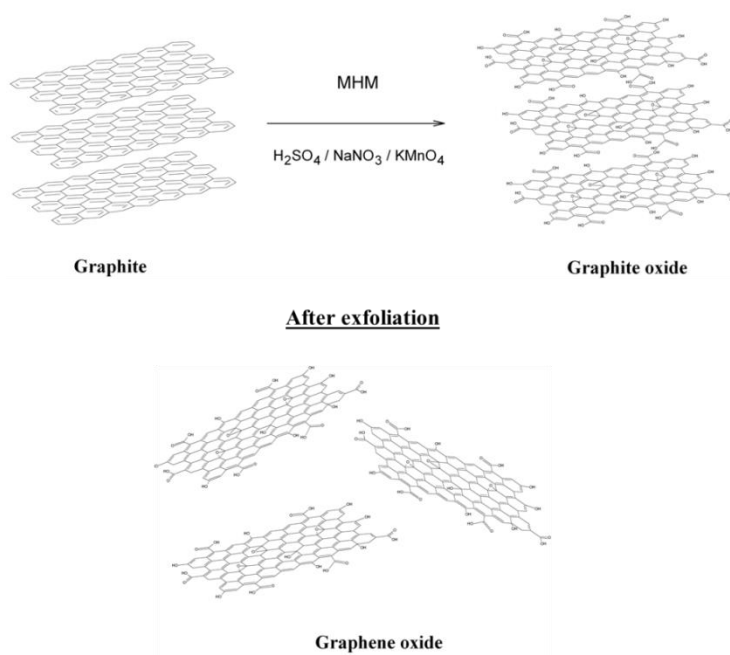
Scheme 4.2. Schematic diagram of GO preparation process

Preparation of crosslinked membranes

Four types of membranes identified as *X*PVA, *Xs*PVA, *X*PVA/GO and *Xs*PVA/GO, where *X* refers to the weigh percentage of SSA and *s* denotes the intra-sulfonation of the PVA chains, were synthesized by solution-casting method. Scheme 4.3 illustrates the three-step methodology followed for the crosslinked membranes preparation. 5 wt.% PVA and sPVA aqueous solutions were prepared by dissolving the polymer in water and refluxing at 90 ºC for 6 hours. To prepare the composite membranes, GO was incorporated to the polymer matrix by solution mixing methodology. A dispersion of GO in distilled water (1 wt.% respect polymer) was sonicated to obtain an homogeneous solution and was then added to the PVA and sPVA solutions previously prepared [12]. Finally, the solutions were mixed with 15 and 30 wt.% of SSA and vigorously stirred at room temperature for 24 hours. The homogeneous solutions were poured onto a Teflon plate and the cast membranes were allowed to dry at room temperature. The dried membranes were peeled off the plates and then crosslinked at 110 ºC for 2 hours. The thickness of the membranes was 116 ± 31 μm. The experimental composition and the nomenclature used for each membrane are shown in Table 4.1.

Table 4.1. Experimental composition and nomenclature of each membrane

Membrane	PVA (wt.%)	sPVA (wt.%)	GO (wt.%)	SSA (wt.%)
15PVA	84.98	–	–	15.02
15sPVA	–	85.00	–	15.00
30PVA	69.91	–	–	30.09
30sPVA	–	69.75	–	30.25
15PVA/GO	83.94	–	1.03	15.03
15sPVA/GO	–	83.93	1.00	15.07
30PVA/GO	68.88	–	1.00	30.12
30sPVA/GO	–	69.10	1.02	29.88
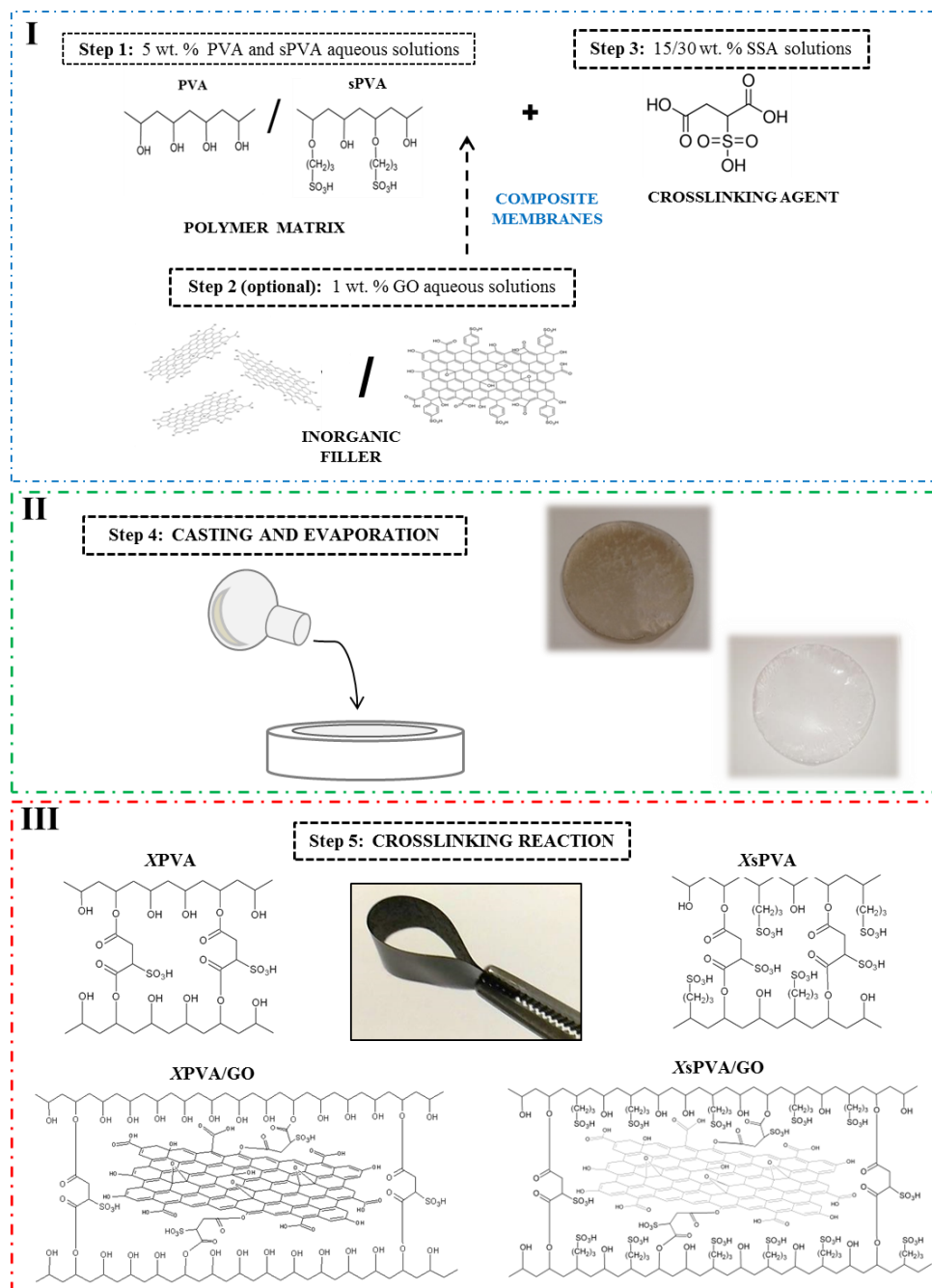
Scheme 4.3. Three-step methodology followed to prepare the crosslinked membranes

Characterization techniques

Fourier Transform Infrared (FTIR) spectra were recorded with a *Thermo Nicolet 5700 FT-IR*. The IR spectra were collected after 64 scans in the 4000-400 cm^{-1} region using the Attenuated Total Reflectance (ATR) mode at a resolution of 4 cm^{-1}. Backgrounds spectra were collected before each series of experiments. All the experiments were performed three times and the average was taken as a representative value.

Raman spectroscopy analysis was carried out using a *Horiba XploRA-One* Raman microscope. Raman excitation source was provided by a 532 nm laser. Spectra were recorded from 200 to 3500 cm^{-1}.

The content of sulfur in sPVA polymer was analyzed by a sequential inductively coupled plasma spectrometer (ICP-OES) *Perkin-Elmer Optima 4300 DV ICP-OES* equipped with a spray Scott-type nebulization chamber. The selected spectral line was 180.669 nm and peak area was used for signal acquisition.

Intercalation and exfoliation of GO into PVA and sPVA matrix were investigated by X-Ray diffraction (XRD) technique using a *D8 Advance A25 Bruker* diffractometer. Copper K$_\alpha$ ($\lambda_{K\alpha}$ = 0.15418 nm) radiation was used with a power setting of 40 kV and 40 mA. Data were collected from 5 to 75° with a scanning step of 0.01 ° and a scan rate of 0.02 °/s.

The XPS spectrum was recorded using a multi-analysis system SCALAB 210 applying a monochromatic Mg excitation line at 1253.6 eV.

The cross-sectional morphology of the membranes was studied in a *Hitachi S-4800* scanning electron microscope with an acceleration voltage of 20 kV. For this purpose, the samples were prepared by immersing the films in liquid nitrogen for 10 minutes before fracture, and next coated with a gold/palladium alloy before analysis.

Transmission Electron Microscopy (TEM) was performed with a *JEOL JEM-1010* microscope operating at an accelerating voltage of 100 kV. GO was dispersed in ethanol under ultrasonication and was dropped onto copper grids before observation. Composite membranes were observed as ultrathin sections prepared with an ultra-microtome *Leica EM UC6* and further transferred to copper grills.

The degradation process and thermal stability of the membranes were investigated by Thermogravimetric Analysis (TGA) on a *TA Instruments TGA Q-500* analyzer. Measurements were carried out under nitrogen atmosphere at 10 ºC/min heating rate covering from 25 to 800 ºC temperature range.

The stress-strain curves of membranes were obtained using a *MTS QTest 1/L Elite* Dynamometer. The membranes were cut into tensile specimens dog-bone shaped with the gauge length and width of 15 mm x 5 mm, respectively. Tests were conducted with a 100 N load cell under a strain rate of 5 mm/min at room temperature. The values were calculated as average over seven specimens of each membrane.

Proton conductivity (σ_{prot}) was measured with a *Novocontrol Broadband Dielectric Spectrometer (BDS)* in the frequency range of 10^{-1} to 10^{7} Hz using an *Alpha-A Frequency Response Analyze)*. A *BDS-1200* parallel-plate capacitor with two gold-plated electrodes system was used as dielectric cell test. The membranes were previously equilibrated with Mili-Q water to ensure fully hydrated state. The measurements were performed at 25 °C. The proton conductivity was calculated according to

$$\sigma_{prot} = \frac{L}{RA}$$

where *L* is the thickness of the conducting membranes in *centimeters* (cm), *A* the area of the electrode in contact with the membrane in cm^2, and *R* the protonic resistance in *ohms* (Ω) taken from the Bode plot at high frequencies [13]

Results and discussion

Intra-Sulfonation of PVA backbone (sPVA)

A visual comparison of the commercial PVA before and after intra-sulfonation process is shown in Figure 4.1. PVA is white as the most polymer platelets, whereas the obtained sPVA changes to a slightly yellow color [14].
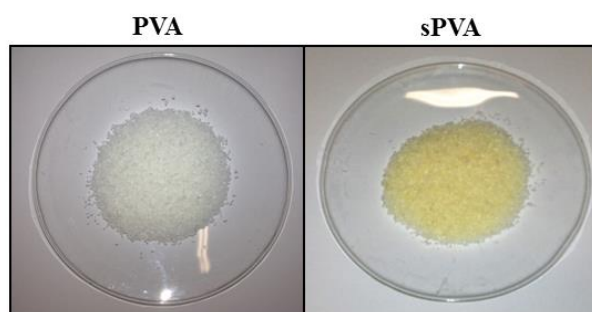
Figure 4.1. Color change observed after intra-sulfonation process of the PVA

Structural characterization

FTIR analysis was performed in order to confirm that the chemical structure of PVA was preserved after the intra-sulfonation, as well as to identify the sulfonic acid groups grafted to PVA backbone. Figure 4.2 compares the FT-IR spectra of PVA and sPVA samples. The broad band observed between 3000 and 3600 cm^{-1} is linked to the stretching vibration of O-H groups involved in the inter- and intramolecular hydrogen bonds [15]–[17]. At 2937 and 2905 cm^{-1} appear the asymmetric and symmetric C-H stretching vibrations of the methylene groups (-CH_2-), respectively. The peak at 1650 cm^{-1} is attributed to the bending vibration of the water molecules associated with the polymeric matrix [15]–[18]. The scissoring and wagging vibration bands of CH_2 are found at 1417 and 1324 cm^{-1}, respectively. It is also possible to identify two bands at 1375 and 1236 cm^{-1} associated to the deformation vibration of the -CH_3 groups, and the stretching vibration of C-O groups from the remaining non-hydrolyzed vinyl acetate groups of PVA, respectively [16], [17]. The band at 1086 cm^{-1} is assigned to C-OH stretching vibration of the alcohol groups. Finally, a new peak at 1045 cm^{-1} is observed in the spectrum of sPVA, corresponding to the stretching vibration of sulfonic acid groups (-SO_3H) [8], [9], [19]. Table 4.2 summarizes the assignment of infrared bands to PVA and sPVA samples.
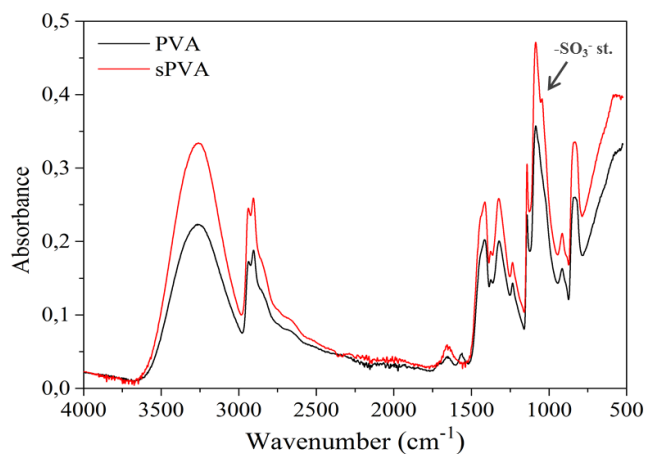
Figure 4.2. Comparison of FT-IR spectra of the PVA and sPVA samples

Table 4.2. Main absorption infrared bands of the PVA and sPVA samples

Wavenumber (cm^{-1})		Assignment
3600-3000	O-H stretching	PVA, sPVA Inter- and intramolecular hydrogen bonding
3000-2840	C-H stretching	PVA, sPVA CH$_2$ asymmetric/symmetric
1660-1640	O-H bending	H$_2$O
1417	C-H bending	PVA, sPVA CH$_2$ scissoring
1375	C-H bending	Acetate CH$_3$ symmetric
1324	C-H bending	PVA, sPVA CH$_2$ wagging
1236	C-O stretching	Acetate
1086	C-OH stretching	PVA, sPVA Secondary alcohol
1045	-SO$_3^-$ stretching	sPVA

The chemical and microstructural modification of the PVA induced by the introduction of –SO₃H groups was studied by XRD, as shown in Figure 4.3. The intensity of the peak at 2θ = 19.7º, which corresponds to the (101) planes of the PVA crystals [20], is reduced after the intra-sulfonation process. This shows a relaxation of the crystalline domains in sPVA matrix due to the grafting of sulfonic acid groups as lateral chains in the backbone of PVA.
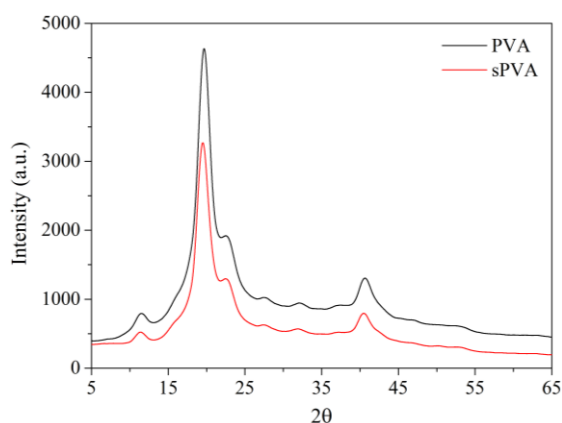
Figure 4.3. Comparison of XRD patterns of the PVA and sPVA samples

Figure 4.4 shows the XPS spectrum of sPVA in which the S2p peak characteristic of the sulfur atoms appears at 168 eV [8], [21], confirming the successful sulfonation of the polymeric matrix.
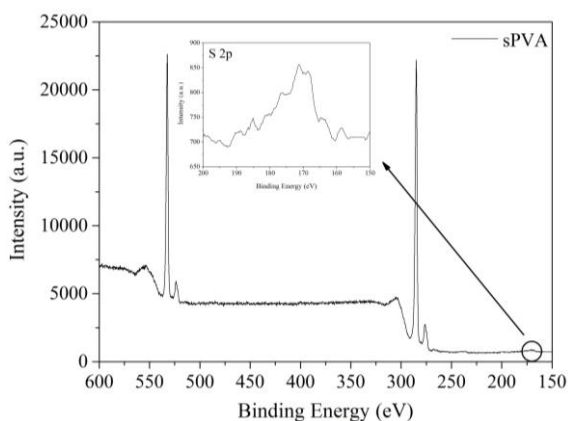
Figure 4.4. XPS spectrum of the sPVA sample. Inset graph shows a magnification of the S2p peak associated with the sulfur atoms

The sulfonation degree (DS) of sPVA was determined from the results of ICP-OES analysis. As expected, a low elemental sulfur content, 0.73 ± 0.02 mg/L, was found in the sPVA sample, corresponding to a DS of 0.1 %.

Thermal characterization

Figure 4.5 compares the thermogravimetric (TG) and first-order derivative (DTG) curves of PVA and sPVA samples. For PVA, A small weight loss of 5% from 25 to 200 °C was observed, corresponding to the evaporation of both weakly physical bond water and strongly chemical bond water. The second decomposition stage, from 200 to 400 ºC, is attributed to dehydration reactions that involve the elimination of the side groups (hydroxyl groups) from the main polymer chain with the loss of water molecules. Consequently, unsaturations appear in the main chain, which progressively turn into a polyene structure [22], [23]. The total weight loss corresponding to this stage is about 60%. The last stage, from 375 to 550 ºC, shows two different decomposition peaks attributed to the breakage and decomposition of the main polymer chain. The weight loss for these two peaks is 22% and 11%, respectively. Once the polyene structure is formed during the decomposition process, this structure is easy to attack via chain-scission turning into low molecular weight structures [22]–[24]. The decomposition of sPVA shows a similar behavior than PVA. However, it is known that the presence of acidic conditions can promote and accelerate the elimination reactions by protonation of -OH groups [22]. The presence of sulfonic acid groups ($-SO_3H$) in the structure of sPVA shifts the decomposition processes to lower temperatures by catalytic effect. The first and the second decomposition stage, attributed to the evaporation of water and elimination reactions, appear overlapped. The total weight loss of both stages is 21%. The decomposition of the main polymeric chain is observed between 400 and 500 ºC, with a weight loss of 52%. Additionally, a loss 28 wt.% is observed in the range from 225 to 350 ºC, attributed to the desulfonation of the sPVA matrix.
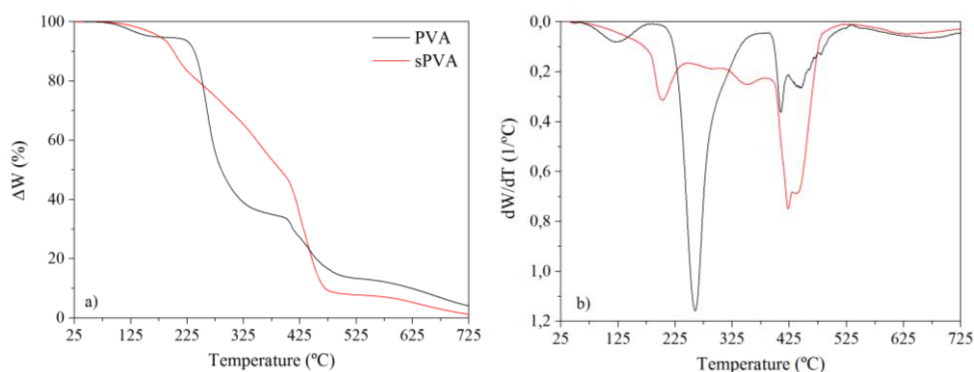
Figure 4.5. TGA and DTG curves of the PVA and sPVA samples

Graphene Oxide (GO)

Structural characterization

The oxidation process of graphite to GO was confirmed by FT-IR analysis. Figure 4.6 shows the spectrum of GO. The broad band observed between 3000 and 3600 cm^{-1} is attributed to the -OH stretching vibration of the alcohol and carboxylic acid groups. The bands at 2913 cm^{-1} and 1372 cm^{-1} are assigned to the stretching and bending vibration of the aliphatic C-H, respectively. The C=O stretching vibration of the carboxylic groups is found at 1717 cm^{-1}. At 1618 cm^{-1}, a band assigned to the aromatic carbon double-bond vibration (C=C) is shown; and the band at 1224 cm^{-}1 is attributed to the C-O stretching vibrations of the carboxylic acid groups. Furthermore, the bands at 1039 and 985 cm^{-1} are related to the vibrations of the epoxide groups in GO [7], [25]–[30]. These results confirm the attachment of oxygen containing groups in the carbon lattice of GO.
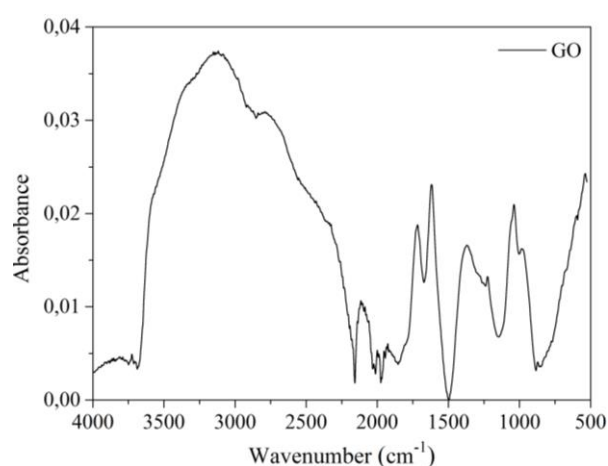
Figure 4.6. FT-IR spectrum of GO

Raman spectroscopy gives information about the crystal structure, disorder and defects in graphene-based materials [31]. Figure 4.7 compares the Raman spectra of graphite and GO. Graphite shows a prominent peak at 1561 cm^{-1} attributed to the G band which indicates a regular microstructure. In contrast, two different peaks can be distinguish in the spectrum of GO. The G band at 1586 cm^{-1}, wider and shifted to higher wavelengths compared to graphite; and a new peak at 1345 cm^{-1} attributed to the D band. The G band is associated to the vibration of sp^2 carbon in the graphitic 2D hexagonal lattice, and the pronounced D band is related to the vibrations of sp^3 carbon atoms of the structural imperfections created by the attachment of oxygen functional groups on the carbon basal plane, amorphous carbon, or edges that can break the symmetry [32]. These results also evidence the successful oxidation of graphite in GO.

_____

104
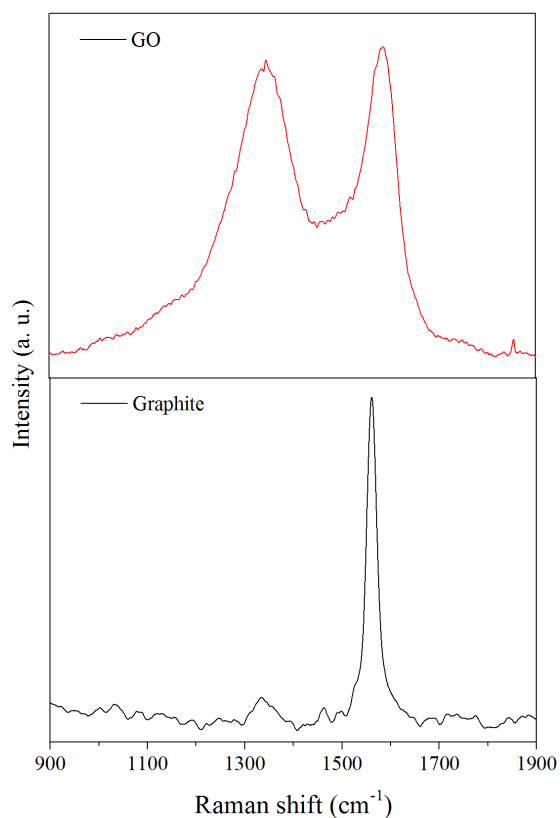
Figure 4.7. Raman spectra of the graphite and GO

Figure 4.8 compares the XRD patterns of graphite and GO. Graphite shows a sharp diffraction peak at $2\theta = 26.6º$, with a distance between layers of 0.33 nm corresponding to the (002) plane, indicating a highly organized crystal structure [7]. The chemical oxidation of graphite disturbs the ordering of layers due to the introduction of oxygen functional groups between layers [26]. These functional groups increase the inter-planar distance between the sheets to 0.75 nm, and hence the peak related to the (001) plane is shifted to 11.9º [33]. These results are in close agreement with those obtained by Raman.
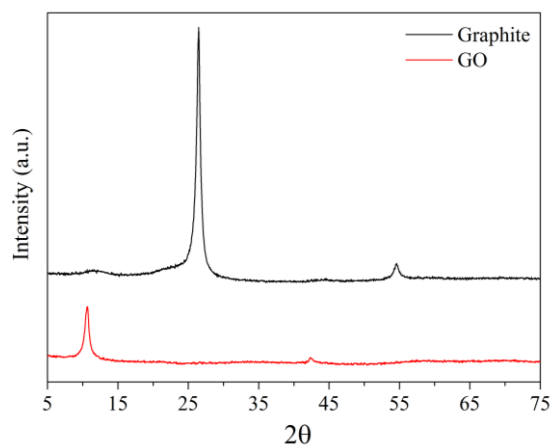
Figure 4.8. X-ray diffraction patterns of the graphite and GO

Morphological characterization

The morphology of the synthesized GO was characterized by SEM and TEM analysis, as shown in Figure 4.9. Single flakes of GO with a layered morphology were observed in the SEM image (Figure 4.9a) confirming a good exfoliation of the GO. The TEM image (Figure 4.9b) shows a sheet-like two dimensional structure with some wrinkles, darker lines, due to its reduced thickness [31], [34].
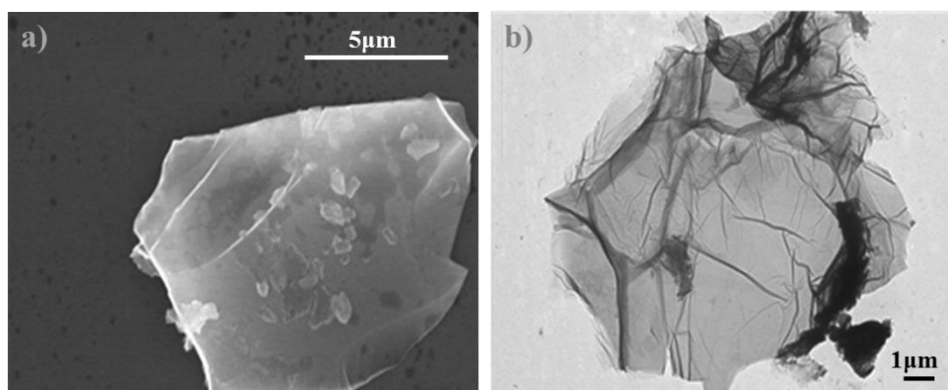
Figure 4.9. a) SEM and b) TEM images of the exfoliated GO

Membrane characterization

Structural characterization

FTIR

Figure 4.10 compares the FTIR spectra of all prepared PVA-based membranes. FTIR analysis was conducted in order to check the effectiveness of the crosslinking reaction as well as to identify the inter- and intra-molecular hydrogen bonding interactions between the hydroxyl groups of the polymer matrix and the oxygen functional groups of GO.
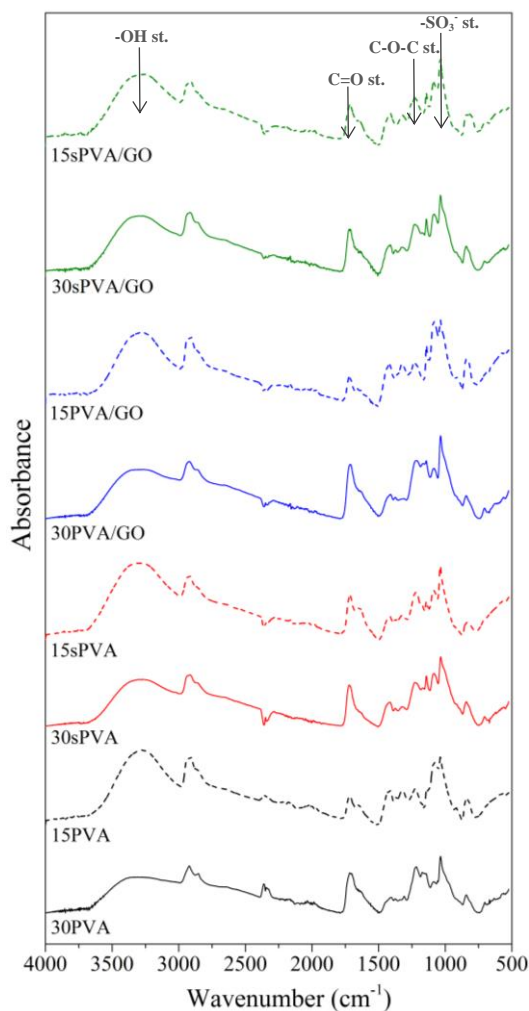
Figure 4.10. FT-IR spectra of the PVA-based crosslinked membranes

The broad absorption band observed around 3400 cm^{-1} is attributed to the -OH stretching vibration, which involves the hydroxyl band of the free and hydrogen bonded alcohols and the carboxylic acid band of the GO in the case of the composites. The characteristic absorption bands for the methylene groups of PVA and sPVA matrix appear at 2950 cm^{-1} and 2905 cm^{-1} and are assigned to the asymmetric and symmetric C-H stretching vibration, respectively. All membranes showed an absorption band between 1710 cm^{-1} and 1730 cm^{-1} corresponding to the C=O stretching vibration of the ester groups (-CO-O-) of SSA. The intensity of the carbonyl band increases quantitatively as the SSA content increases [35]. The presence of a low intensity band at 1650 cm^{-1} is associated with the bending vibration of the H_2O molecules, which denotes the presence of water in the membranes [15]. The stretching vibration of the aromatic sp^2 carbon bonds (C=C) of GO at 1618 cm^{-1} in the spectra of the PVA/GO and sPVA/GO composites [30]. The bands at 1420 cm^{-1} and 1330 cm^{-1} are ascribed to the scissoring and wagging vibrations of CH_2 groups, respectively. Additionally, two new bands appear at 1120 cm^{-1} and 1240 cm^{-1} attributed to the C-O-C stretching vibration of the new ester bonds formed during the crosslinking reaction [8]. The C-O characteristic vibration of the alcohols from the polymer matrix and the GO is also visible at 1086 cm^{-1}. The absorption band at 1037 cm^{-1} present in all spectra indicates the presence of sulfonic acid groups (-SO_3H) introduced by sPVA and SSA. In addition, the bands at 916 cm^{-1} and 840 cm^{-1} result from the OH out-of-plane motion of the carboxylic group in the SSA [25], and from the rocking vibration of CH_2 groups [36], respectively. Therefore, the changes observed in the spectra clearly evidence that the GO was incorporated into the polymer matrix and the crosslinking reaction occurred successfully between the hydroxyl groups of PVA or sPVA and the carboxylic acid groups of SSA.

In addition, a deep study of the relative intensities of the main functional groups in the membranes was carried out. The band intensity of the -OH, C=O, C-O-C and sulfonic acid groups (-SO_3H) was normalized respect to the intensity of the band of CH_2 groups of the polymer backbone ($v \sim 2950$ cm^{-1}), and the relative intensities were obtained as follows [37]

$$I_{-OH} = \frac{Abs_{3400}}{Abs_{2950}} \qquad I_{C=O} = \frac{Abs_{1720}}{Abs_{2950}}$$

$$I_{C-O-C} = \frac{Abs_{1240}}{Abs_{2950}} \qquad I_{-SO_3H} = \frac{Abs_{1037}}{Abs_{2950}}$$

The position and relative intensity obtained for each band are summarized in Table 4.3.

Table 4.3. Position and relative intensities of the -OH , C=O, C-O-C and -SO$_3^-$ bands

Membrane	-OH st.		C=O st.	
	ν_{-OH} (cm^{-1})	I-$_{OH}$	$\nu_{C=O}$ (cm^{-1})	I$_{C=O}$
15PVA	3276	1.28	1720	0.36
15sPVA	3319	1.01	1719	0.92
30PVA	3336	0.78	1716	1.82
30sPVA	3392	0.05	1718	2.08
15PVA/GO	3280	1.12	1720	0.42
15sPVA/GO	3267	1.12	1720	0.49
30PVA/GO	3307	0.79	1712	1.71
30sPVA/GO	3350	1.06	1710	2.15

Membrane	-C-O-C st.		–SO$_3^-$ st.	
	ν_{C-O-C} (cm^{-1})	I$_{C-O-}$	$\nu_{-SO_3}^-$ (cm^{-1})	I$_{-SO_3}^-$
15PVA	1230	1.29	1037	2.72
15sPVA	1228	1.81	1036	3.89
30PVA	1217	2.64	1036	3.62
30sPVA	1217	3.97	1034	5.37
15PVA/GO	1232	1.35	1036	2.82
15sPVA/GO	1234	1.45	1036	3.42
30PVA/GO	1213	2.51	1036	3.54
30sPVA/GO	1215	3.11	1037	4.34

The results show that higher crosslinking degree shifts the -OH band towards higher wavenumbers and reduce its intensity. This behaviour is because the hydroxyl groups react with the SSA to form new covalent bonds during the crosslinking reaction [7], [19], [22], [37]–[39]. Moreover, the membranes with higher crosslinking degree also undergo a considerable increasing of the intensity of the C=O and C-O-C bands, attributed to the formation of ester groups derived from the crosslinking reaction [16], [37]. The C=O and C-O-C bands are also shifted to lower frequencies in the membranes crosslinked at 30 wt.%, indicating an increase of the hydrogen bonding interactions between the ester and the hydroxyl groups of the polymer matrix. The use of SSA as a crosslinker agent also provides -SO$_3$H groups to the membranes by inter-

sulfonation of the polymer matrix. Thus, the intensity of the -SO$_3^-$ band is increased in the membranes with higher crosslinking degree [37].

sPVA-based membranes show a further decrease of the intensity of the -OH band due to the replacement of the hydroxyl groups by -SO$_3$H groups in the intra-sulfonation process. This effect is also evidenced by the shift of the -OH band towards higher frequencies, which is related to the reduction of hydrogen bonding interactions between the hydroxyl groups. Moreover, the intra-sulfonation of the polymer matrix was also corroborated by the increment of the -SO$_3^-$ band intensity.

On the other hand, the GO composites show a shift of the -OH band towards lower frequencies, confirming the good interfacial adhesion between the polymer matrix and the filler favored by the increase on hydrogen bonding interactions [40].

XRD

The structural changes induced by the crosslinking reaction and the addition of GO were characterized by XRD. Figure 4.11 compares the XRD diffraction patterns of *X*PVA, *X*sPVA, *X*PVA/GO and *X*sPVA/GO membranes with the pure PVA, sPVA and GO samples.
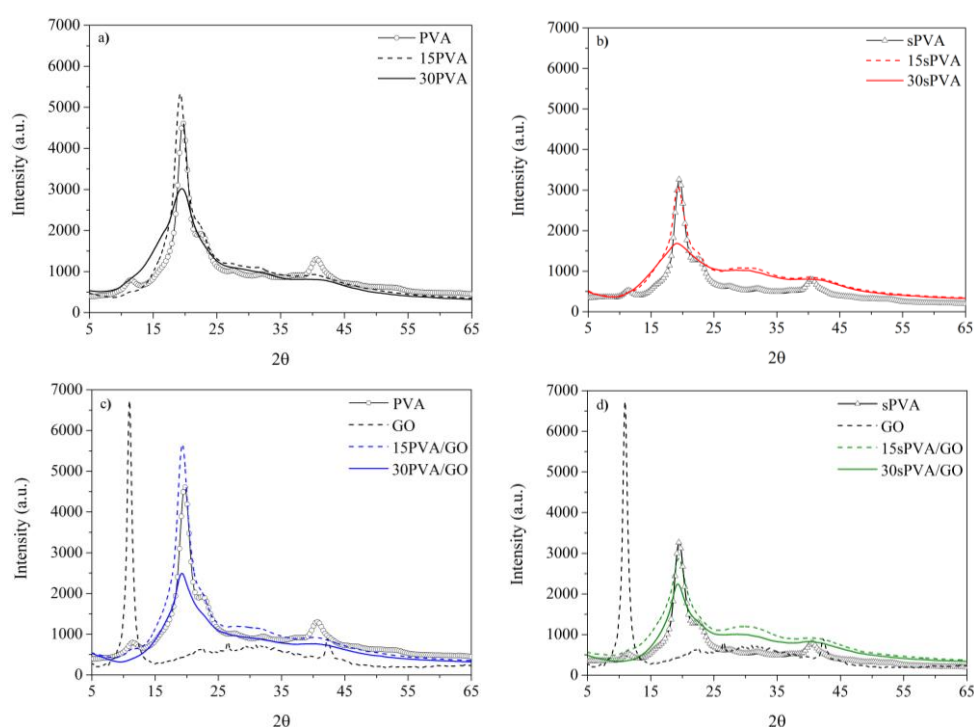
Figure 4.11. Comparison of the X-ray patterns of the a) PVA, b) sPVA and c) d) composites with the starting materials PVA, sPVA and GO

In general, when a polymer contains a crystalline region, the X-ray diffraction peaks are sharp and their intensities are high, whereas the peaks become broader for amorphous polymers [41]. The XRD spectrum of pure PVA shows a diffraction peak at $2\theta = 19.7°$, which corresponds to the crystalline phase of the polymer [39], [42], [43]. This main diffraction peak is also present in all the PVA-based membranes. However, the intensity and the width of the PVA peak are influenced by the crosslinking degree, the sulfonation of the polymer matrix and the addition of GO in the membranes.

The peak in the membranes with higher crosslinking degree (30 wt.%) becomes broader and less intense than that for the pure PVA and the membranes crosslinked at

15 wt.%, as shown in Figure 4.11a. Hence, a high crosslinking degrees lead to increase the amorphous character of the membranes [41], [42]. In contrast, the membrane 15PVA shows higher peak intensity than the pure PVA, which is attributed to more ordered structures or crystallinity domains.

The intra-sulfonation of the polymer matrix strongly increases the amorphous character of both the sPVA polymer and the crosslinked sPVA membranes. This change in the structure is evidenced by sharp decline of the main peak intensity, as shown in Figure 4.11b.

Finally, Figure 4.11c and d depict the XRD patterns of composite membranes, exhibiting only the diffraction peak associated to PVA or sPVA pattern. The peak corresponding to GO does not appear, which clearly demonstrates its fully exfoliation into the polymer matrix [7], [12], [26], [28].

Morphological characterization

Scanning and transmission electron microscopy studies are perhaps the two most common means to assess the state of dispersion of GO nano-platelets in a polymer matrix. Figure 4.12 and Figure 4.13 show the cross-sectional SEM images of *X*PVA, *X*PVA/GO, *X*sPVA and *X*sPVA/GO membranes and the TEM images of the 15PVA/GO composite, respectively.

From the SEM images can be seen that the cross-sectional surface of sPVA membranes is more compact and smoother than PVA membranes. The higher rigidity of sPVA membranes leads to a cleanest fracture surface. In contrast, the composites exhibit a fibrillary morphology with bright regions attributed to the high conductivity of the GO [26]. Hence, the SEM images confirm the good dispersion of the GO nano-platelets in the PVA/GO and sPVA/GO composites [8], [43].

Additionally, the TEM images of the 15PVA/GO composite confirm a good exfoliation of the GO nano-platelets into the polymer matrix.
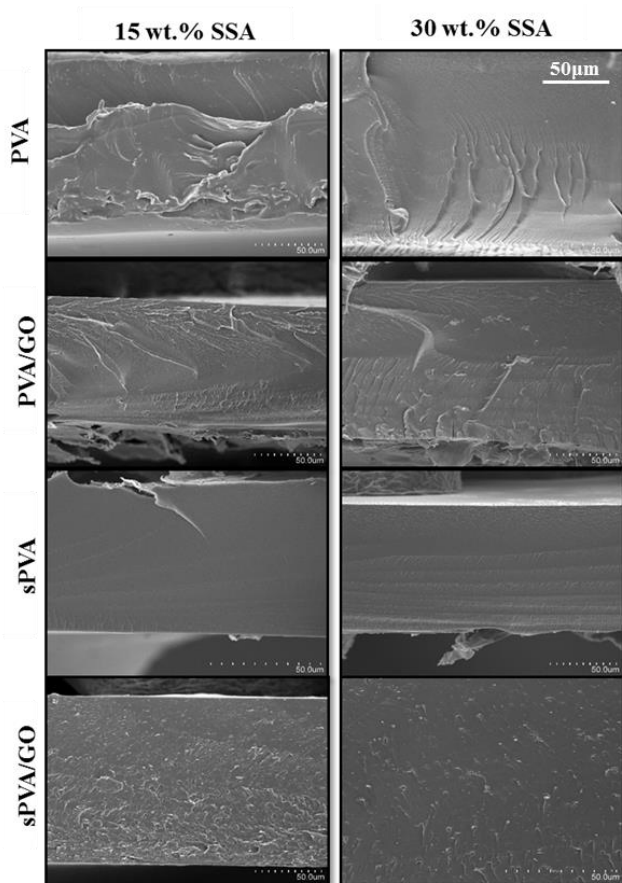
Figure 4.12. Cross-sectional SEM images of the *X*PVA, *X*PVA/GO, *X*sPVA and *X*sPVA/GO membranes
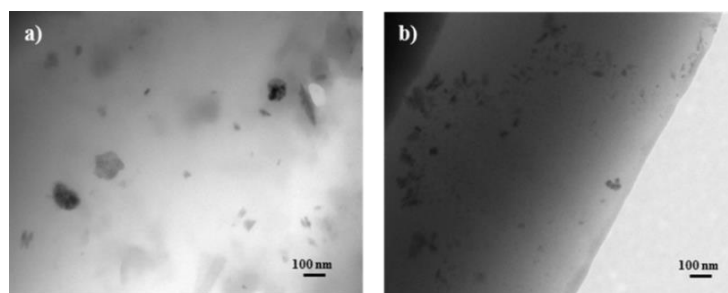
Figure 4.13. TEM images of the 15PVA/GO composite taken at a) 25K× and b) 20K× magnification

113

Thermal characterization

The thermal stability of membranes was investigated by TGA. Figure 4.14 shows the thermogravimetric (TG) and the first-order derivative (DTG) curves of the *X*PVA, *X*PVA/GO, *X*sPVA and *X*sPVA/GO membranes.
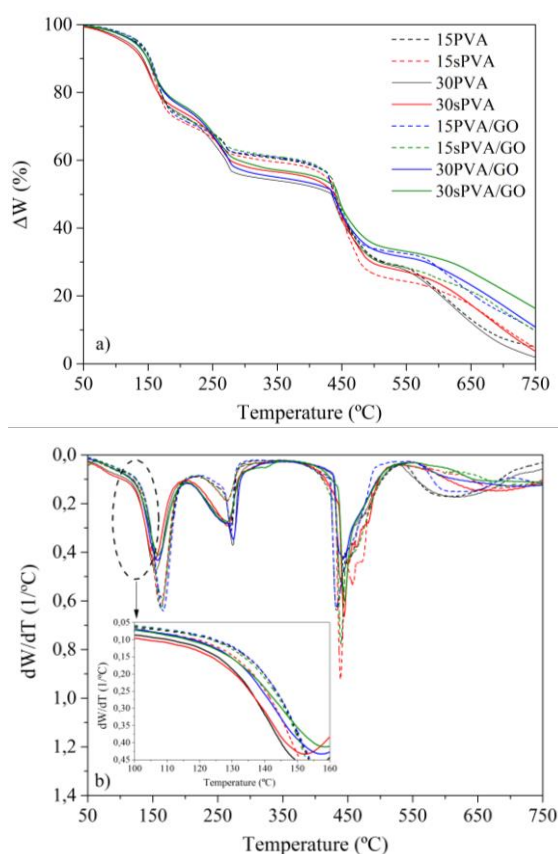
Figure 4.14. Comparison of the a) TG and b) DTG curves of crosslinked membranes. The inset graph in DTG curves shows a magnification of the first decomposition stage

All membranes exhibit three-stage weight losses, in a similar way as the pure PVA and sPVA. The first decomposition stage, occurred between 50 and 200 ºC, is due to the decomposition of the hydroxyl groups of the polymer matrix through elimination reactions to form polyene structures [9], [22]. The second stage takes place around 200-350 ºC and it is attributed to thermal desulfonation process. In this region, it is possible to differentiate two decomposition peaks for the *X*sPVA and *X*sPVA/GO membranes; the former is associated to the loss of the sulfonic acid groups introduced

by SSA (inter-sulfonation), and the later to the desulfonation of the sPVA matrix (intra-sulfonation) [22], [24], [37], [44]. Finally, the third decomposition stage is observed in the range from 350 to 750 ºC and is associated to the breakage and decomposition of the main chain by means of chain-scission mechanism [22], [41].

Table 4.4 summarizes the temperature weight losses extracted from the thermograms curves of each membrane.

Table 4.4. Temperature dependent weight loss values extracted from the thermograms of the crosslinked membranes

Membrane	Stage I		Stage II (ºC/%)				Stage III	
	T_{peak}	ΔW	$T_{peak\ I}$	ΔW_I	$T_{peak\ II}$	ΔW_{II}	T_{peak}	ΔW
15PVA	164	28	270	11	-	-	432	32
15sPVA	162	29	264	9	320	2	439	35
30PVA	154	26	273	20	-	-	439	25
30sPVA	152	25	265	15	310	2	444	29
15PVA/GO	166	29	269	9	-	-	432	28
15sPVA/GO	163	28	265	9	322	2	439	32
30PVA/GO	157	24	274	21	-	-	443	24
30sPVA/GO	158	23	264	16	325	3	445	24

The introduction of sulfonic acid groups by the crosslinking reaction with SSA causes remarkable changes in the thermal stability of the membranes. It could be expected that the membranes with higher concentration of SSA would show better thermal stability than those with lower concentration. However, the results show the opposite trend. This is due to the fact that the elimination reactions of the hydroxyl groups under acidic conditions are catalyzed [22]. Moreover, the lower amount of hydroxyl groups in the membranes with higher crosslinking degree reduces the hydrogen bonding interactions between the polymer chains responsible of the structure stabilization. Therefore, the thermal stability not only is controlled by the catalytic effect of the acidic groups contained in the membranes, but also by the hydrogen bonding interactions between the polymer chains. Similarly to SSA, the sulfonation of the polymer matrix also decreases the thermal stability of the sPVA membranes [22].

On the other hand, the addition of GO increases the thermal stability of the composites. The oxygen-containing groups of GO favors the interfacial adhesion between the

polymer matrix and the filler via hydrogen bonding interactions increasing the stabilization of the structure, in agreement with the results obtained by FT-IR.

Mechanical characterization

The mechanical properties of the membranes were evaluated from the stress-strain curves shown in Figure 4.15a measured at room temperature. The values of tensile strength (MPa), Young´s modulus (GPa) and elongation at break (%) extracted from the stress-strain curves are compared in Figure 4.15a, b and c.
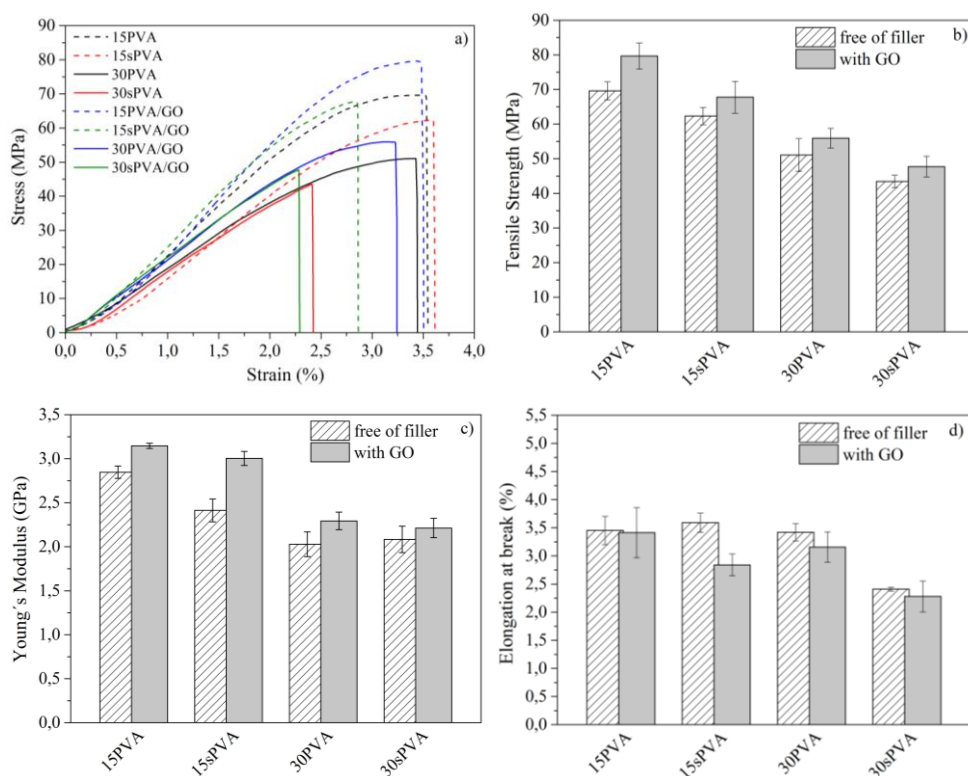
Figure 4.15. Comparison of the a) Stress-strain curves b) Elongation at break, b) tensile strength, and c) Young´s modulus values of the membranes

The crosslinking degree strongly affects to the mechanical behavior of the membranes, showing the membranes crosslinked at 30 wt.% of SSA lower mechanical properties than those crosslinked at 15 wt.%. This is because in the 30PVA and 30sPVA membranes the hydrogen bond interactions between the hydroxyl groups of the polymer matrix that stabilizes the structure are reduced compared to the 15PVA and

15sPVA membranes, resulting in a non-uniform stress distribution over the sample and so decreases the values of tensile strength and the Young modulus. Moreover, the higher amount of inter-chain covalent bonds in the 30PVA and 30sPVA membranes greatly restricts the movement of the polymer chains so the elongation at break also decreases [45]. Likewise, the membranes become more brittle when the hydroxyl groups are replaced by sulfonic acid groups by direct sulfonation of the polymer matrix, showing a slightly decrease of their mechanical performance.

In addition, it is evident that addition of the GO nano-platelets improves the tensile strength and Young modulus of the composites. The good interfacial adhesion between the inorganic filler (GO) and the polymer (PVA and sPVA) via hydrogen bonding interactions facilitates the stress transfer across filler-matrix interface. These interactions between the GO nano-platelets and the polymer matrix were previously confirmed by FTIR measurements. However, the elongation at break decreases with the addition of GO, indicating that the composites are more stiff and brittle than the membranes free-standing of GO. The addition of GO into the polymer matrix restricts the mobility of the polymer chains due to the strong hydrogen bonding interactions between them [7], [46], [47].

Proton conductivity (σ_{prot})

Proton conductivity (σ_{prot}) of a PEM is an important parameter to assess the suitability of a membrane for fuel cell applications. The sulfonic acid groups ($-SO_3H$) of the crosslinked membranes can be dissociated under hydrated conditions and act as a proton carriers through the membrane. Therefore, the effect of both the bi-sulfonation of PVA and the addition of GO on the proton conductivity were studied. Figure 4.16 shows the values of proton conductivity of all membranes measured at 25 ºC.
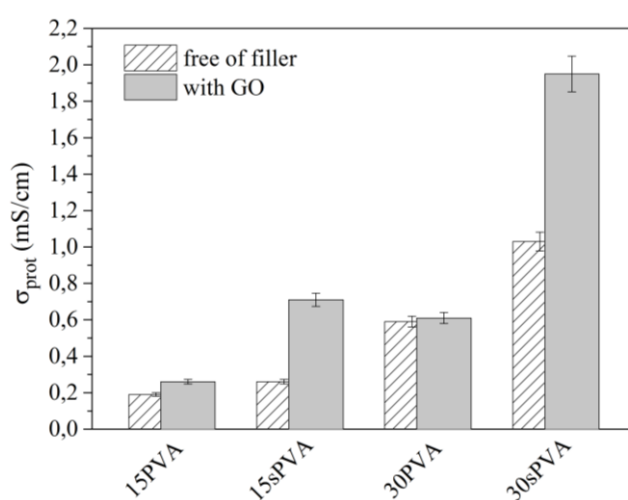
Figure 4.16. Evolution of proton conductivity (σ_{prot}) as a function of membrane composition measured at 25 ºC

In general, the proton conductivity increases with increasing the concentration of sulfonic acid groups in the membrane. Therefore both the increasing of the crosslinking degree and the modification of the PVA by intra-sulfonation improves the proton conductivity of the crosslinked membranes [8], [35], [41].

The proton conductivity of the 15PVA and 30PVA membranes is nearly unaffected by the addition of GO. However, a strong improvement can be observed when the polymer matrix is modified by intra-sulfonation [7]. The highest value of proton conductivity is achieved for the 30sPVA/GO composite, showing an improvement of 89 % compared to its homologue filler-free 30sPVA membrane. Therefore, not only the proton conductivity of the PVA-membranes is affected by the addition of GO, but also it is crucial an optimal concentration of sulfonic groups in their structure.

Conclusions

Protons conducting composite membranes based on PVA modified by double sulfonation were prepared by solution-casting method. The effect of the crosslinking degree, the intra-sulfonation of the polymer matrix and the addition of GO on the membrane properties were evaluated. FT-IR spectra were confirmed the chemical crosslinking of the polymer by SSA and also indicated the existence of inter- molecular interactions via hydrogen bonding between the components. SEM and TEM images showed a good dispersion of GO into the polymer matrix, resulting in an improvement of the thermal and mechanical stability of the composites. Among the eight tested membranes, the highest proton conductivity was achieved for the 30sPVA/GO composite. This indicates that the introduction of a great amount of sulfonic acid groups in the structure in combination with the addition of GO strongly increases the proton conductivity of the membranes. Therefore, it can be conclude that the strategy followed in this studied, bi-sulfonation and addition of GO, is a suitable and easy procedure to prepare proton exchange membranes for fuel cells applications. Furthermore, the proton-conducting properties and the electrochemical behavior of these composite membranes will be the subject of extensive investigation in the second part of this study.

Acknowledgements

References

[1] Shripad T. Revankar and P. Majumdar, *Fuel Cells: Principles, Design, and Analysis*. CRC Press, 2016.

[2] F. Barbir, *PEM Fuel Cells: Theory and Practice*, Elsevier. 2013.

[3] H. Zhang and P. K. Shen, "Recent development of polymer electrolyte membranes for fuel cells," Chem. Rev., vol. 112, no. 5, pp. 2780–2832, 2012.

[4] S. Patachia, A. J. M. Valente, A. Papanceaa and Victor M. M. Lobo, *Poly (Vinyl Alcohol) (PVA)-Based Polymer Membranes*. Nova Science Publishes, Inc., 2009.

[5] J. Maiti, N. Kakati, S. H. Lee, S. H. Jee, B. Viswanathan, and Y. S. Yoon, "Where do poly(vinyl alcohol) based membranes stand in relation to Nafion® for direct methanol fuel cell applications?," J. Power Sources, vol. 216, pp. 48–66, 2012.

[6] Y.-S. Ye, J. Rick, and B.-J. Hwang, "Water Soluble Polymers as Proton Exchange Membranes for Fuel Cells," Polymers (Basel)., vol. 4, pp. 913–963, 2012.

[7] H. Beydaghi, M. Javanbakht, and E. Kowsari, "Synthesis and Characterization of Poly(vinyl alcohol)/Sulfonated Graphene Oxide Nanocomposite Membranes for Use in Proton Exchange Membrane Fuel Cells (PEMFCs)," Ind. Eng. Chem. Res., vol. 53, no. 43, pp. 16621–16632, 2014.

[8] M. Yoo, M. Kim, Y. Hwang, and J. Kim, "Fabrication of highly selective PVA-g-GO/SPVA membranes via cross-linking method for direct methanol fuel cells," Ionics (Kiel)., vol. 20, no. 6, pp. 875–886, 2014.

[9] S. Yun, H. Im, Y. Heo, and J. Kim, "Crosslinked sulfonated poly(vinyl alcohol)/sulfonated multi-walled carbon nanotubes nanocomposite membranes for direct methanol fuel cells," J. Memb. Sci., vol. 380, no. 1–2, pp. 208–215, 2011.

[10] W. S. Hummers and R. E. Offeman, "Preparation of Graphitic Oxide," J. Am. Chem. Soc., vol. 80, no. 6, pp. 1339–1339, 1958.

[11] L. Shahriary and A. A. Athawale, "Graphene Oxide Synthesized by using Modified Hummers Approach," Int. J. Renew. Energy Environ. Eng., vol. 2, no. 1, pp. 58–63, 2014.

[12] J. Liang, Y. Huang, L. Zhang, Y. Wang, Y. Ma, T. Guo, and Y. Chen, "Molecular-Level Dispersion of Graphene into Poly(vinyl alcohol) and Effective Reinforcement of their Nanocomposites," Adv. Funct. Mater., vol. 19, no. 14, pp. 2297–2302, Jul. 2009.

[13] X. Qian, N. Gu, Z. Cheng, X. Yang, E. Wang, and S. Dong, "Methods to study the ionic conductivity of polymeric electrolytes using a.c. impedance spectroscopy," J. Solid State Electrochem., vol. 6, no. 1, pp. 8–15, 2001.

[14] R. Sengupta, S. Chakraborty, S. Bandyopadhyay, S. Dasgupta, R. Mukhopadhyay, K. Auddy, and A. S. Deuri, "A Short Review on Rubber / Clay Nanocomposites With Emphasis on Mechanical Properties," Engineering, vol. 47, pp. 21–25, 2007.

[15] A. M. Shehap, "Thermal and Spectroscopic Studies of Polyvinyl Alcohol/Sodium Carboxy Methyl Cellulose Blends," Egypt. J. Solids, vol. 31, no. 31, pp. 75–91, 2008.

[16] H. S. Mansur, C. M. Sadahira, A. N. Souza, and A. A. P. Mansur, "FTIR spectroscopy characterization of poly (vinyl alcohol) hydrogel with different hydrolysis degree and chemically crosslinked with glutaraldehyde," Mater. Sci. Eng. C, vol. 28, no. 4, pp. 539–548, 2008.

[17] J. M. Gohil, A. Bhattacharya, and P. Ray, "Studies on the cross-linking of poly (vinyl alcohol)," J. Polym. Res., vol. 13, no. 2, pp. 161–169, 2006.

[18] L. Daniliuc and C. David, "Intermolecular interactions in blends of poly(vinyl alcohol) with poly(acrylic acid): 2. Correlation between the states of sorbed water and the interactions in homopolymers and their blends," Polymer (Guildf)., vol. 37, no. 23, pp. 5219–5227, 1996.

[19] C.-Y. Tsenga, Y.-S. Yea, K.-Y. Kaoa, J. Josephb, W.-C. Shena, J. Ricka, and B.-J. Hwanga, "Interpenetrating network-forming sulfonated poly(vinyl alcohol) proton exchange membranes for direct methanol fuel cell applications," Int. J. Hydrogen Energy, vol. 36, no. 18, pp. 11936–11945, 2011.

[20] H. E. Assender and A. H. Windle, "Crystallinity in poly(vinyl alcohol). 1. An X-ray diffraction study of atactic PVOH," Polymer (Guildf)., vol. 39, no. 18, pp. 4295–4302, Jan. 1998.

[21] R. Kumar, M. Mamlouk, and K. Scott, "Sulfonated polyether ether ketone - sulfonated graphene oxide composite membranes for polymer electrolyte fuel cells," RSC Adv., vol. 4, no. 2, pp. 617–623, 2014.

[22] J.M. Morancho, , J.M. Salla, A. Cadenato, X. Fernández-Francos, X. Ramis, P. Colomer, Y. Calventus, and R. Ruíz, "Kinetic studies of the degradation of poly(vinyl alcohol)-based proton-conducting membranes at low temperatures," Thermochim. Acta, vol. 521, no. 1–2, pp. 139–147, 2011.

[23] Z. Peng and L. X. Kong, "A thermal degradation mechanism of polyvinyl alcohol/silica nanocomposites," Polym. Degrad. Stab., vol. 92, no. 6, pp. 1061–1071, 2007.

[24] C. C. Yang, W. C. Chien, and Y. J. Li, "Direct methanol fuel cell based on poly(vinyl alcohol)/titanium oxide nanotubes/poly(styrene sulfonic acid) (PVA/nt-TiO2/PSSA) composite polymer membrane," J. Power Sources, vol. 195, no. 11, pp. 3407–3415, 2010.

[25] G. Socrates, *Infrared and Raman characteristic group frequencies*. Wiley, 2004.

[26] S. Khilari, S. Pandit, M. M. Ghangrekar, D. Pradhan, and D. Das, "Graphene oxide impregnated PVA-STA composite polymer electrolyte membrane separator for power generation in single chambered Microbial Fuel Cell," Ind. Eng. Chem. Res., pp. 11597–11606, 2013.

[27] O. García-Valdez, R. Ledezma-Rodríguez, E. Saldívar-Guerra, L. Yate, S. Moya, and R. F. Ziolo, "Graphene oxide modification with graft polymers via nitroxide mediated radical polymerization," Polymer (Guildf)., vol. 55, no. 10, pp. 2347–2355, 2014.

[28] C. Bao, Y. Guo, L. Song, and Y. Hu, "Poly(vinyl alcohol) nanocomposites based on graphene and graphite oxide: a comparative investigation of property and mechanism," J. Mater. Chem., vol. 21, no. 36, pp. 13942–13950, 2011.

[29] G. Gonçalves, Paula A. A. P. Marques, A. Barros-Timmons, I. Bdkin, Manoj K. Singh, N. Emamic and J. Grácioa, "Graphene oxide modified with PMMA via ATRP as a reinforcement filler," J. Mater. Chem., vol. 20, no. 44, pp. 9927–9934, 2010.

[30] S. Morimune, T. Nishino, and T. Goto, "Poly(vinyl alcohol)/graphene oxide nanocomposites prepared by a simple eco-process," Polym. J., vol. 44, no. 10, pp. 1056–1063, Oct. 2012.

[31] G. Sobon, J. Sotor, J. Jagiello, R. Kozinski, M. Zdrojek, M. Holdynski, P. Paletko, J. Boguslawski, L. Lipinska, and K. M. Abramski, "Graphene Oxide vs Reduced Graphene Oxide as saturable absorbers for Er-doped passively mode-locked fiber laser," Opt. Express, vol. 20, no. 17, p. 19463, 2012.

[32] K. N. Kudin, B. Ozbas, H. C. Schniepp, R. K. Prud'homme, I. A. Aksay, and R. Car, "Raman spectra of graphite oxide and functionalized graphene sheets.," Nano Lett., vol. 8, no. 1, pp. 36–41, Jan. 2008.

[33] J. Guo, L. Ren, R. Wang, C. Zhang, Y. Yang, and T. Liu, "Water dispersible graphene noncovalently functionalized with tryptophan and its poly(vinyl alcohol) nanocomposite," Compos. Part B Eng., vol. 42, no. 8, pp. 2130–2135, 2011.

[34] X. Zhao, Q. Zhang, D. Chen, and P. Lu, "Enhanced mechanical properties of graphene-based polyvinyl alcohol composites," Macromolecules, vol. 43, no. 5, pp. 2357–2363, 2010.

[35] J. W. Rhim, H. B. Park, C. S. Lee, J. H. Jun, D. S. Kim, and Y. M. Lee, "Crosslinked poly(vinyl alcohol) membranes containing sulfonic acid group: Proton and methanol transport through membranes," J. Memb. Sci., vol. 238, no. 1–2, pp. 143–151, 2004.

[36] O. W. Guirguis and M. T. H. Moselhey, "Optical study of poly(vinyl alcohol)/hydroxypropyl methylcellulose blends," J. Mater. Sci., vol. 46, no. 17, pp. 5775–5789, 2011.

[37] A. Martínez-Felipe, C. Moliner-Estopiñán, C. T. Imrie, and A. Ribes-Greus, "Characterization of crosslinked poly(vinyl alcohol)-based membranes with different hydrolysis degrees for their use as electrolytes in direct methanol fuel cells," J. Appl. Polym. Sci., vol. 124, no. 2, pp. 1000–1011, Apr. 2012.

[38] E. Pretsch, P. Bühlmann, and M. Badertscher, *Structure Determination of Organic Compounds*. Springer, 2013.

[39] H. J. Salavagione, G. Martínez, and M. a. Gómez, "Synthesis of poly(vinyl alcohol)/reduced graphite oxide nanocomposites with improved thermal and electrical properties," J. Mater. Chem., vol. 19, no. 28, p. 5027, 2009.

[40] X. Yang, L. Li, S. Shang, and X. ming Tao, "Synthesis and characterization of layer-aligned poly(vinyl alcohol)/graphene nanocomposites," Polymer (Guildf)., vol. 51, no. 15, pp. 3431–3435, 2010.

[41] D. S. Kim, H. B. Park, J. W. Rhim, and Y. M. Lee, "Preparation and characterization of crosslinked PVA/SiO2 hybrid membranes containing sulfonic acid groups for direct methanol fuel cell applications," J. Memb. Sci., vol. 240, no. 1–2, pp. 37–48, 2004.

[42] C. C. Yang, "Synthesis and characterization of the cross-linked PVA/TiO2 composite polymer membrane for alkaline DMFC," J. Memb. Sci., vol. 288, no. 1–2, pp. 51–60, 2007.

[43] Y.-S. Yea, M.-Y. Chenga, X.-L. Xiec, J. Ricka, Y.-J. Huangb, F.-C. Changb, and B.-J. Hwanga, "Alkali doped polyvinyl alcohol/graphene electrolyte for direct methanol alkaline fuel cells," J. Power Sources, vol. 239, pp. 424–432, 2013.

[44] S. Zhong, X. Cui, Y. Gao, W. Liu, and S. Dou, "Fabrication and properties of poly(vinyl alcohol)-based polymer electrolyte membranes for direct methanol fuel cell applications," Int. J. Hydrogen Energy, vol. 39, no. 31, pp. 17857–17864, 2014.

[45] D. Moura, S. G. Caridade, M. P. Sousa, E. Cunha, H. C. Rocha, J. F. Mano, M. C. Paivac and N. M. Alves, "High performance free-standing films by layer-by-layer assembly of graphene flakes and ribbons with natural polymers †," J. Mater. Chem. B, vol. 4, pp. 7718–7730, 2016.

[46] H. Beydaghi, M. Javanbakht, and E. Kowsari, "Preparation and physic-chemical performance study of proton exchange membranes based on phenyl sulfonated graphene oxide nanosheets decorated with iron titanate nanoparticles," Polymer (Guildf)., vol. 87, pp. 26–37, 2016.

[47] S. Yao, Y. Li, Z. Zhou, and H. Yan, "Graphene oxide-assisted preparation of poly(vinyl alcohol)/carbon nanotube/reduced graphene oxide nanofibers with high carbon content by electrospinning technology," RSC Adv., vol. 5, no. 111, pp. 91878–91887, 2015.

[48] M. Bhattacharya, "Polymer nanocomposites-A comparison between carbon nanotubes, graphene, and clay as nanofillers," Materials (Basel)., vol. 9, no. 4, pp. 1–35, 2016.

4.3. Contribution II:

Bi-sulfonation of poly(vinyl alcohol)/graphene oxide composite membranes for Proton Exchange Membrane Fuel Cell applications. Part 2: Functional membrane properties

Bi-sulfonation of poly(vinyl alcohol)/graphene oxide composite membranes for Proton Exchange Membrane Fuel Cell applications. Part 2: Functional membrane properties

S. C. Sánchez-Ballester[a], A. Ribes-Greus[a], V. Soria[b], G. Rydzek[c] and K. Ariga[c]

[a]Instituto de Tecnología de Materiales (ITM), Universitat Politècnica de València, Valencia, Spain

[b]ICMUV, Universitat de València, Burjassot, Valencia, Spain

[c]World Premier International (WPI) Research Center for Materials Nanoarchitectonics (MANA), National Institute for Materials Science (NIMS), Tsukuba, Japan.

Abstract

A set of crosslinked membranes based on poly(vinyl alcohol) (PVA) and graphene oxide (GO) were prepared by solution-casting method. PVA was modified by direct sulfonation with propane sultone (intra-sulfonation), and further reticulated with sulfosuccinic acid (SSA) (inter-sulfonation) in order to improve its proton conductivity and dimensional stability. The effect of the bi-sulfonation of the polymer matrix and the addition of GO on the proton-conducting properties of the membranes was studied by water contact angle, water uptake, swelling ratio, ion exchange capacity, proton conductivity and H_2-O_2 fuel cell tests. The results reveal that the double sulfonation of PVA matrix and the addition of GO nano-platelets are an effective methodology to enhance the functional properties of membranes. In particular, the 30sPVA/GO composite shows an improvement of 140 % in proton conductivity at 50 ºC respect to the 30PVA membrane free-standing of GO. Moreover, the 30sPVA/GO composite also showed the maximum power density in the fuel cell performance test (13.9 mW/cm^2). The experimental results demonstrate that both the introduction of sulfonic acid groups to the PVA matrix by the bi-sulfonation process, and the addition of GO are a promising strategy to prepare feasible PVA-based membranes for fuel cell applications.

Keywords: poly(vinyl alcohol), graphene oxide, inter- and intra-sulfonation, proton exchange membranes, proton conduction, fuel cell

Introduction

Fuel Cells (FCs) have attracted considerable attention over the past two decades due to certain inherent advantages that the electrochemical conversion show compared to the thermal combustion processes. Among these advantages, electrochemical processes are more feasible, environmentally friendly and sustainable [1], [2].

An individual proton exchange membrane fuel cell (PEMFC) converts chemical energy to electrical energy through an electrochemical reaction. The main elements in a PEMFC are the electrodes and the proton exchange membrane (PEM) used as a solid electrolyte. The electrode where the fuel oxidation occurs is called anode, and the electrode where the reduction of oxygen occurs is called cathode. PEM constitutes an important part of a fuel cell, since it is involved in three vital functions of this device: it is the physical barrier which separates the reactants present in the anode from those present in the cathode, acts as a proton conducting medium and must be an electrical insulator preventing the transport of electrons through it [1]-[3].

Currently, Nafion® is the perfluorosulfonic acid (PFSA) ionomer most widely used as electrolyte in PEMFCs due to its excellent chemical, mechanical and thermal stability, as well as its high proton conductivity when fully hydrated. However, Nafion® presents several disadvantages such as high cost, difficulty in its synthesis and processing, and decreasing in proton conductivity above 80 ºC operation. Additionally, a critical drawback with its application in direct methanol fuel cells (DMFC) is its high methanol permeability ($\sim 10^{-6}$ cm^2/s) which reduces drastically the DMFC performance [1], [4].

In order to overcome these drawbacks, different paths have been followed for the development of alternative membranes to Nafion®, such as modification of perfluorinated polymer membranes, functionalization of hydrocarbon polymers and preparation of organic-inorganic composite membranes. The preparation of organic/inorganic composite membranes has been revealed as an emerging research field, having the possibility to combine specific properties of both the polymer matrix and the inorganic filler. In this way, we have focussed our interest in the preparation of hybrid membranes based on poly (vinyl alcohol) (PVA) and graphene oxide (GO) with high proton conductivity for FC applications.

PVA-based membranes are considered as alternative to Nafion® because its low cost, flexibility, good membrane-forming properties and high methanol selectivity [5]. However, PVA membranes are poor proton conductors compared with Nafion because they do not have negative charges ions in their structure. The technologies available today allow balancing some of the characteristics needed in a PEM by introduction of negative functional groups while inducing singular morphologies simultaneously. In this contribution, the introduction of negative charged groups into the PVA membrane was achieved by means of a two-step bi-sulfonation process: a first direct intra-sulfonation of PVA backbone followed by an inter-sulfonation and crosslinking

process using sulfosuccinic acid (SSA) as crosslinking agent [6]-[10]. Thus, the accommodation of the hydrophilic -SO$_3$H negative ions in two different regions of the membrane could contribute to facilitate the proton transport.

On the other hand, one of the most effective methods used to overcome the limitations of PFSA membranes is the preparation of organic-inorganic composite membranes. Membranes modified with carbon fillers have shown encouraging results for PEMFCs applications [9]. Among the different types of carbon fillers, graphene oxide (GO) has emerged as an attractive nanofiller due to its ability to enhance the mechanical, thermal, and electrical properties of the polymer composites [11]. Moreover, the presences of oxygen functional groups (hydroxyl, epoxy and carboxyl) in its structure make easy to disperse GO in polar polymers such as PVA. Upon incorporation of GO platelets within a PVA polymer matrix, a new morphology is generated with a unique structure. The high surface area of GO and its electronic insulating properties contribute not only to improve the dimensional stability of a PEM, but also its proton conductivity.

The present work highlights the importance of the modification of commercial PVA functionalized by means of two-step bi-sulfonation process. In this regard, pure PVA was slightly intra-sulfonated (0.1 %) by direct grafting of alkyl-sulfonated chains on the polymer backbone. Next, the membranes were prepared by solution-casting method and further crosslinked with sulfosuccinic acid (SSA). The SSA crosslinking agent confers dimensional stability and introduces inter-chain sulfonic acid groups responsible of the proton conduction. Both kinds of sulfonation allow us to design new morphologies with more hydrophilic nanophases randomly distributed through the membrane [12]. Moreover, in order to study the effect of the addition of GO on the functional properties of the PVA membranes, a set of composite membranes based on PVA/GO were prepared. In the preceding study (see Contribution I) [13], the synthesis and the structural, morphological, thermal and mechanical characterization of the functionalized PVA membranes were deeply studied and reported. In this work, we focused our interest on the functional properties of the membrane regarding to fuel cell applications. The properties were evaluated in terms of water contact angle, water uptake (WU) and swelling ratio (SW), ion exchange capacity (IEC), proton conductivity (σ_{prot}) and H$_2$-O$_2$ fuel cell performance. The experiments were conducted on eight different crosslinked membranes, and the functional properties were determined as a function of the crosslinking degree (15 or 30 SSA wt%), the intra-sulfonation of the matrix (sPVA) and the addition of GO.

Experimental

Chemicals

Graphite powder (particle size < 20 μm), sodium nitrate (NaNO$_3$, ≥ 99.0%), sodium hydride (NaH, dry 95%), 1,3-propane sultone (97%), poly(vinyl alcohol) (PVA, molecular weight 130000 g/mol degree of hydrolysis, min. 99%), and sulfosuccinic acid (SSA, 70 wt.% solution in water) were purchased from Sigma-Aldrich. Concentrated sulfuric acid (H$_2$SO$_4$, 95%), hydrogen peroxide (H$_2$O$_2$, 30% w/w), ethanol absolute (EtOH), hydrochloric acid (HCl, 37%), potassium permanganate (KMnO$_4$, extra pure), sodium chloride (NaCl) and sodium hydroxide (NaOH, ≥ 98%) were purchased from Scharlab.

Preparation of crosslinked membranes

A set of crosslinked membranes identified as *X*PVA, *X*sPVA, *X*PVA/GO and *X*sPVA/GO (where *X* represents the weight percentage of crosslinking agent and s denotes the intra-sulfonation of the PVA chains) were prepared by solution-casting method. The sulfonation reaction of PVA was carried out in two steps according to the procedure described in Contribution I [9], [10], [13]. First, 5 wt.% of PVA and sPVA aqueous solutions were prepared by dissolving the polymer in water and refluxing at 90 ºC for 6 hours. For the preparation of composite membranes (*X*PVA/GO and *X*sPVA/GO), a dispersion of 1 wt.% of GO was added to the polymer solution. GO was previously prepared from graphite powder using the Modified Hummers Method (MHM) [14], [15]. After that, SSA was added at two different concentrations (15 and 30 wt.%) in all cases and was vigorously stirred at room temperature for 24 hours. The homogeneous solutions were poured onto a Teflon plate and the cast membranes were allowed to dry at room temperature. The dried membranes were peeled off the plates and then crosslinked at 110 ºC for 2 hours.

Characterization techniques

Water contact angle

The wettability of composites was measured according to its water contact angle. Hence, static contact angle was evaluated using a *Theta Optical Tensiometer (KSV Instruments, Ltd)* and electrooptics comprising a CCD camera connected to a computer at room temperature. The distilled water (2 μL) was dropped on the sample surface at five different sites and the average value was taken as the representative value.

Water Uptake (WU) and Swelling ratio (SW)

The absorption of water was evaluated by performing swelling tests. Rectangular specimens of 4 x 1 cm^2 were dried at 60 ℃ under vacuum for 12 hours, and the weight of the dried composite was measured in a microbalance. The composites were immersed in tests tubes containing distilled water at 30 ℃. The absorption of water was measured gravimetrically at different times, taken out, wiped with tissue paper, and immediately weighted the sample on a microbalance. The samples were weighted until no further gain weight was observed, denoting that the equilibrium condition was achieved. The water uptake, WU (%), was calculated as the mass difference between the samples exposed to water (M_{eq}) and the dry sample (M_{dry}). The results were normalized respect to the mass of the dried sample by

$$(\mathbf{WU})_{\mathbf{eq}}\ (\%) = \frac{\mathbf{M_{eq}} - \mathbf{M_{dry}}}{\mathbf{M_{dry}}} \times \mathbf{100}$$

The swelling ratio (SW) was calculated from the change in length between the fully hydrated at equilibrium and dry composites, L_{eq} and L_{dry}, respectively, as follows

$$\mathbf{SW_{eq}}(\%) = \frac{\mathbf{L_{eq}} - \mathbf{L_{dry}}}{\mathbf{L_{dry}}} \times \mathbf{100}$$

Ion Exchange Capacity (IEC)

The IEC of each composite was determined by titration method. The pre-weighted dry sample was soaked in a 0.5 M HCl solution for 24 hours at room temperature to obtain its protonated form. The sample was washed with an excess amount of distilled water and then was immersed in a 2M NaCl solution for 24 hours at room temperature to exchange H$^+$ with Na$^+$ ions. The amount of H$^+$ liberated was estimated by acid-base titration against a standard 0.1 N (0.0955 ± 0.0009 N) NaOH solution with phenolphthalein as the indicator. The IEC values were calculated using the following equation

$$\mathbf{IEC(mequiv/g)} = \frac{\mathbf{N_{NaOH}} \times \mathbf{V_{NaOH}}}{\mathbf{W_{dry}}}$$

where N_{NaOH} is the normality of the titrant in mequiv/L, V_{NaOH} is the added titrant volume in *liters* (L), and W_{dry} is the dry mass of sample in *grams* (g).

Conductivity measurements

Conductivity of the composites was measured with a *Novocontrol Broadband Dielectric Spectrometer (BDS)* in the frequency range of 10^{-1} to 10^{7} Hz using an *Alpha-A Frequency Response Analyzer (Novocontrol)*.

The proton conductivity (σ_{prot}) was measured using a *BDS-1308 (Novocontrol)* liquid parallel plate sample cell. The samples were previously equilibrated with Mili-Q water to ensure fully hydrated state. The measurements were performed at 30, 50, 70 and 90 ºC. The proton conductivity (in S/cm) of the membranes was calculated using

$$\sigma_{prot} = \frac{L}{RA}$$

where *L* is the thickness of the conducting membranes in *centimeters* (cm), *A* the area of the electrode in contact with the sample in cm^2, and *R* the protonic resistance in *ohms* (Ω), taken from the Bode plot at high frequencies [16].

Electrical conductivity was measured at 30 ºC using a *BDS-1200 (Novocontrol)*, parallel-plate capacitor cell with two gold-plated electrodes. The electrical conductivity was taken at low frequencies, where the measured real part of the conductivity (σ') reaches a plateau which corresponds directly to the DC conductivity (σ_0).

H_2-O_2 fuel cell test

The performance of the composites in a fuel cell was tested by measuring the polarizations curves. The samples were equilibrated with Mili-Q water during 24 hours and then were sandwiched between two sheets of gas diffusion electrodes (*Fuels Cells Etc*, 4 mg/cm^2 Platinum Black). The electrochemical performances were evaluated with a single-cell fixture having an active area of 16 cm^2. The fuel cell was operated with hydrogen and oxygen at 25 ºC and atmospheric pressure.

Results and discussion

Water contact angle

The hydrophilic nature of the membranes surface was studied by water contact angle measurements. A low contact angle means that the solid is well wetted by the liquid and the membrane surface is more hydrophilic, while a high contact angle indicates higher hydrophobic character of the surface [17].

Figure 4.17 shows the comparison of water contact angle values and the pictures of the water droplets on membranes.
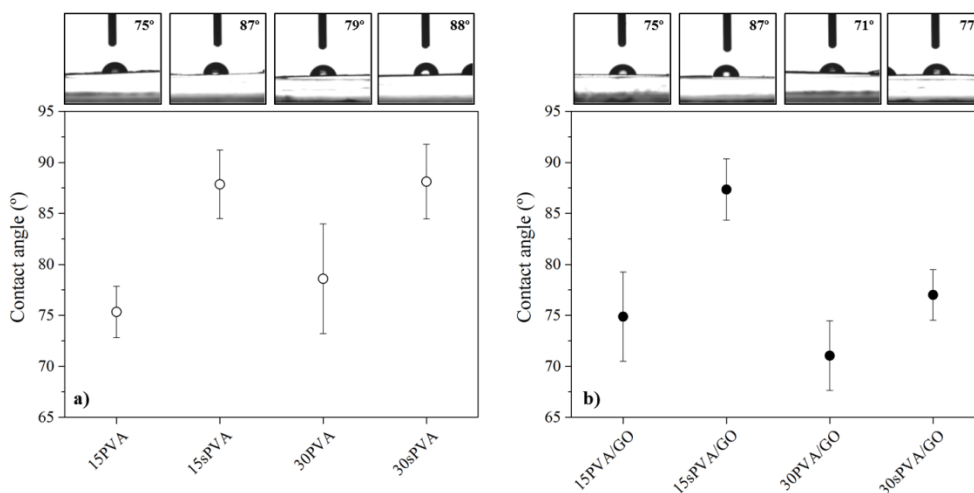
Figure 4.17. Water contact angle values and the pictures of the water droplets on membranes

According to the results shown in Figure 4.17a, the water contact angle is not affected by the crosslinking degree of the membrane, exhibiting similar values the membranes crosslinked with a 15 wt.% and at 30 wt.% of SSA. In contrast, the intra-sulfonation of the polymer matrix considerably increases the water contact angle of the membranes. The 15sPVA and 30sPVA membranes show an increase on the water contact angle of the 16 % and 13 % compared to the 15PVA and 30PVA membranes, respectively. The strong hydrogen bonding interactions between the sulfonic acid groups ($-SO_3H$) and the hydroxyl groups ($-OH$) of the polymer matrix reduce the hydrophilic groups available to interact with the water molecules in the membrane surface. The surface becomes more hydrophobic increasing the water contact angle values [18].

On the other hand, the addition of GO strongly decreases the water contact angle values of the 30PVA/GO and 30sPVA/GO membranes as shown in Figure 4.17b, indicating an increase of the hydrophilic character of the membrane surface. This effect

might be due to the hydrophilic oxygen functional groups (hydroxyl, epoxy and carboxylic acid groups) introduced by GO [11], [19]. However, this increase of the hydrophilic character is not observed in the membranes with lower crosslinking degree (15PVA/GO and 15sPVA/GO), showing the same values of water contact angle than their homologue membranes free-standing of GO (15PVA and 15sPVA).

Water Uptake (WU) and Swelling ratio (SW)

Water uptake and swelling ratio are directly related to proton conductivity and dimensional stability of PEMs, respectively. The absorbed water helps protons go through the membrane, and therefore higher water uptake in general improves the proton conductivity. However, an excess of absorbed water can lead to undesired effects such as low dimensional and mechanical stability, which reduce the membrane performance. Therefore, it is vital to have the optimal water uptake in PEMs.

The WU and SW of membranes were measured at 30 ºC and the results are summarized in Table 4.5.

Table 4.5. Water Uptake (WU) and Swelling ratio (SW) values of the membranes measured at 30 ºC

Membrane	WU (%)	SW (%)
15PVA	44.3 ± 0.7	10.0 ± 1.4
15sPVA	37.9 ± 0.8	8.9 ± 0.7
30PVA	42.8 ± 0.2	9.4 ± 1.2
30sPVA	34.3 ± 0.7	8.1 ± 0.9
15PVA/GO	41.0 ± 0.8	7.5 ± 0.9
15sPVA/GO	33.6 ± 0.7	6.9 ± 0.9
30PVA/GO	33.0 ± 0.6	6.7 ± 0.7
30sPVA/GO	31.8 ± 0.6	6.3 ± 1.0

In general, the water uptake of the membranes decreases with increasing the crosslinking degree. An increase on the crosslinking degree restricts the mobility of polymer chains since new covalent bonds are formed during the crosslinking reaction. Thus, membranes become more compact and the free volume able to accommodate water molecules is reduced [20].

Moreover, sPVA-based membranes show lesser values of water uptake than that membranes prepared from PVA. Similarly to the crosslinking effect, the strong intermolecular interactions between the hydroxyl groups (-OH) and the sulfonic acid groups (-SO$_3$H) of the sPVA matrix compact the membrane structure and limit the mobility of the chains, decreasing the water absorption [9], [21]. This trend is consistent with the values of water contact angle obtained for the sPVA-based membranes.

The composite membranes show a decrease of the water uptake. The laminar structure of GO acts as a barrier to water molecules, limiting the water uptake and the dimensional changes of the composites [22], [23]. The swelling ratio values exhibit the same trend than the water uptake in all cases.

Ion Exchange Capacity (IEC)

The IEC is defined by the number of moles of exchangeable groups per unit of mass of dry polymer. Therefore, it is closely related to the number of available active sites for proton transfer and consequently with the proton conductivity in PEMs. The IEC of the membranes was measured and the values are summarized in Table 4.6.

Table 4.6. Ion exchange capacity (IEC) values of the crosslinked membranes

Membrane	IEC (mequiv/g)
15PVA	0.67 ± 0.03
15sPVA	0.69 ± 0.00
30PVA	1.00 ± 0.16
30sPVA	1.06 ± 0.15
15PVA/GO	0.61 ± 0.04
15sPVA/GO	0.66 ± 0.01
30PVA/GO	0.97 ± 0.08
30sPVA/GO	1.02 ± 0.06

As it was expected, the IEC is sharply influenced both by the crosslinking degree and the sulfonation process of the polymer matrix, showing the highest value of IEC the 30sPVA membrane (1.06 mequiv/g). This can be attributed to the greater amount of sulfonic acid groups (-SO$_3$H) introduced by the SSA and the sPVA that increase the number of active sites for proton transport across the membrane [7]. However, the

addition of GO slightly decreases the IEC of the composites, effect due to the weaker acidic character of the carboxylic acid groups (-COOH) contained in GO compared to -SO$_3$H groups [9], [24].

Proton Conductivity (σ_{prot})

The proton conductivity in PEMs is usually related to the degree of hydration. Proton transport in sulfonated PEMs is mainly described by two mechanisms: Grotthus mechanism, in which protons jump between bonded-water molecules (H$_3$O$^+$SO$_3^-$) followed by a local molecular rearrangement to allow the next jump [25], and Vehicular mechanism, which assumes that the protons diffuse together with free water molecules by forming the complex H$_3$O$^+$. Under fully hydrated conditions, both mechanisms become significant and an effective proton transfer occurs by water transport pathways [26].

The proton conductivity of the membranes was studied from impedance measurements in the temperature range from 30 to 90 ºC. In order to calculate the proton conductivity, the protonic resistance R was taken from the Bode plot in the high frequencies range, in which the value of log |Z| becomes constant and the phase angle reaches its maximum value [16]. Figure 4.18 shows the Bode diagrams of the pre-hydrated membranes measured at 30 ºC as an example.

.
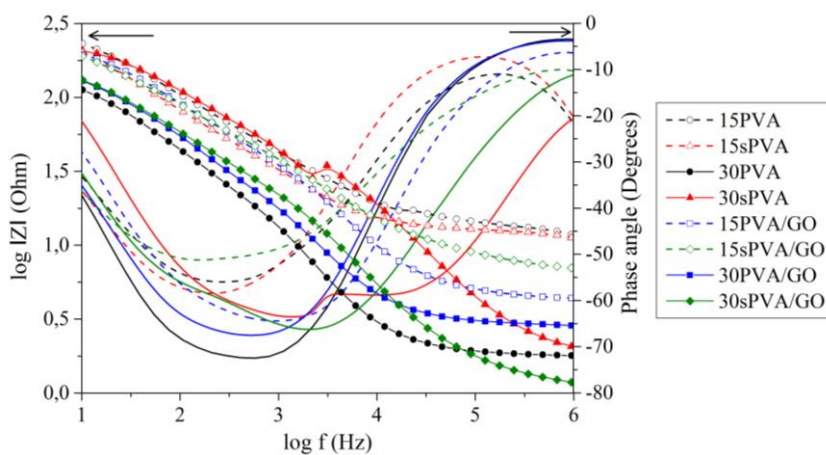
Figure 4.18. Bode diagram of the pre-hydrated membranes measured at 30 ºC

The obtained values of proton conductivity for the pre-hydrated membranes are listed in Table 4.7, and the evolution of the proton conductivity as a function of temperature is also shown in Figure 4.19.

Table 4.7. Values of proton conductivity (σ_{prot}) of the pre-hydrated membranes measured at different temperature

Membrane	σ_{prot} (mS/cm)			
	30º	50ºC	70ºC	90ºC
15PVA	0.21	0.75	1.37	0.98
15sPVA	0.23	0.71	1.61	1.54
30PVA	1.60	3.50	6.72	8.94
30sPVA	2.46	7.89	13.49	15.16
15PVA/GO	0.88	2.26	4.57	4.90
15sPVA/GO	0.97	2.23	6.16	6.24
30PVA/GO	1.61	3.39	6.93	11.82
30sPVA/GO	4.96	8.42	15.80	20.96
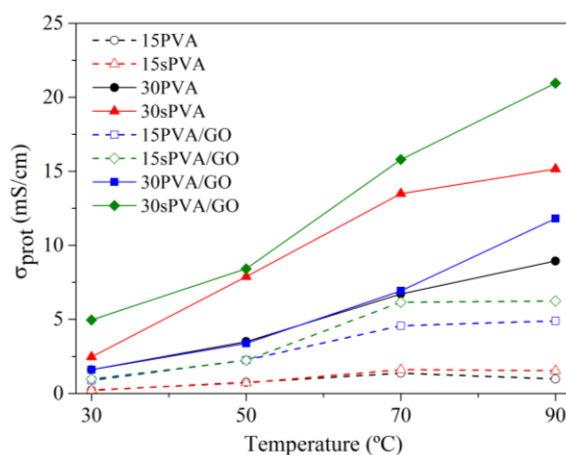
Figure 4.19. Evolution of proton conductivity (σ_{prot}) of the pre-hydrated membranes as a function of temperature

As expected, the proton conductivity of membranes increases gradually with temperature. An increase of temperature promotes the polymer chains mobility, enhancing the proton conduction through the membrane [20]. It was found a gradually increase, from 30 ºC to 90 ºC, of the proton conductivity for the membranes with

higher crosslinking degree. However, the membranes with lower crosslinking degree show a slight decrease (15PVA and 15sPVA) or almost no variation (15PVA/GO and 15sPVA/GO) of the proton conductivity beyond 70 ℃. This behavior can be associated to the evaporation of the higher amount of free water that these membranes contain in their structure, in agreement with the water uptake results [27], [28].

According to the results, the proton conductivity is strongly influenced by the crosslinking degree. The membranes with lower crosslinking degree show the lowest values of proton conductivity, despite their high water uptake values. In contrast, the introduction of higher concentration of sulfonic acid groups in the membranes crosslinked at 30 wt.% of SSA sharply improves the proton conductivity. Similar behaviour is observed in the membranes prepared from sPVA. It was found an increase of 125 % in the proton conductivity at 50 ℃ for the 30sPVA membrane compared to the 30PVA membrane. This increase is attributed to the higher concentration of sulfonic acid groups in the sPVA-based membranes, which are directly involved in the proton conduction [21].

Finally, a significant enhancement of proton conductivity can be observed in the composite membranes. The addition of GO to the bi-sulfonated membrane with higher crosslinking degree, 30sPVA/GO, leads to reach the highest value of proton conductivity (20.96 mS/cm at 90 ℃). Therefore, from these results it may be conclude that the addition of GO into the polymer matrix favorably contributes to the proton mobility.

The dependence of proton conductivity with temperature was fitted using the Arrhenius equation,

$$\log \sigma_{prot} = \log \sigma_0 - \frac{E_a}{RT}$$

where σ_{prot} is the proton conductivity (S/cm), σ_0 is a pre-exponential factor, E_a is the activation energy (kJ/mol), R is the universal gas constant (8.314 J/mol K), and T is the absolute temperature (K). The slope of log σ vs 1000/T gives the activation energy of proton conductivity, which is equivalent to the minimum energy required for the proton conduction. Figure 4.20 shows the Arrhenius plot for the pre-hydrated membranes.
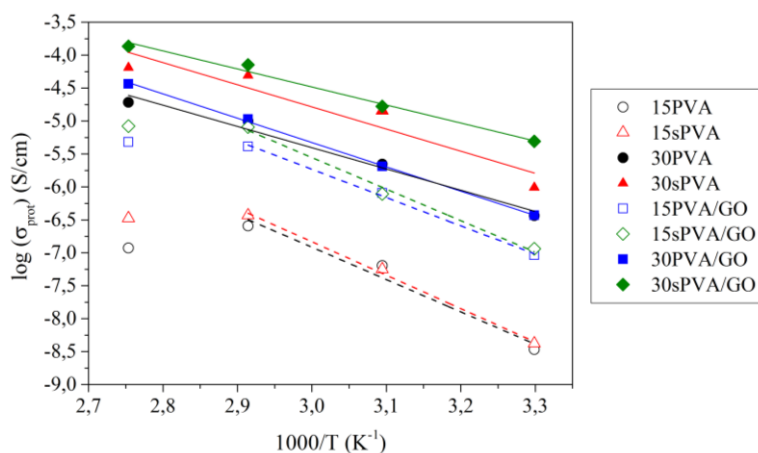
Figure 4.20. Arrhenius plot of the pre-hydrated membranes

As it can be seen, a linear correlation between σ_{prot} and T is observed in all the range of temperature (from 30 to 90 ºC) for the membranes crosslinked at 30 wt.% of SSA. However, when the concentration of the SSA is reduced to 15 wt.%, the linear trend is only seen from 30 to 70 ºC. Table 4.8 lists the values of activation energy obtained from the Arrhenius plot for each membrane. The E_a values range from 22.8 to 42.2 kJ/mol. A strong decrease of E_a is observed for the composite membranes, showing the lowest value the 30sPVA/GO composite (22.8 kJ/mol). This supports the hypothesis that the presence of GO nano-platelets enhances the proton conductivity by comparison with similar membranes free-standing of GO.

Table 4.8. Values of activation energy (E_a) for proton conductivity of the pre-hydrated membranes

Membrane	E_a (kJ/mol)
15PVA	40.8
15sPVA	42.2
30PVA	26.8
30sPVA	27.9
15PVA/GO	35.7
15sPVA/GO	39.8
30PVA/GO	30.7
30sPVA/GO	22.8

A high electrical conductivity is an undesirable property in PEMs, since a PEM must avoid the pass of the electrons through the membrane preserving its electrical resistance [23]. As shown in Table 4.9, the membranes exhibit low electrical conductivities (~10^{-10} S/cm), which corroborates the insulator property of the prepared membranes [29].

Table 4.9. Electrical conductivity (σ_{elec}) values of the membranes measured at 30 ºC

Membrane	σ_{elec} x10^{10} (S/cm)
15PVA	0.03
15sPVA	0.12
30PVA	0.10
30sPVA	0.14
15PVA/GO	0.16
15sPVA/GO	1.02
30PVA/GO	0.18
30sPVA/GO	1.47

H_2-O_2 fuel cell test

The performance of the membranes in a H_2-O_2 fuel cell was studied from the polarization curves measured at 25 ºC shown in Figure 4.21. As comparison the membrane Nafion 117 was also measured at the same conditions and its polarization curves are shown in Figure 4.21.
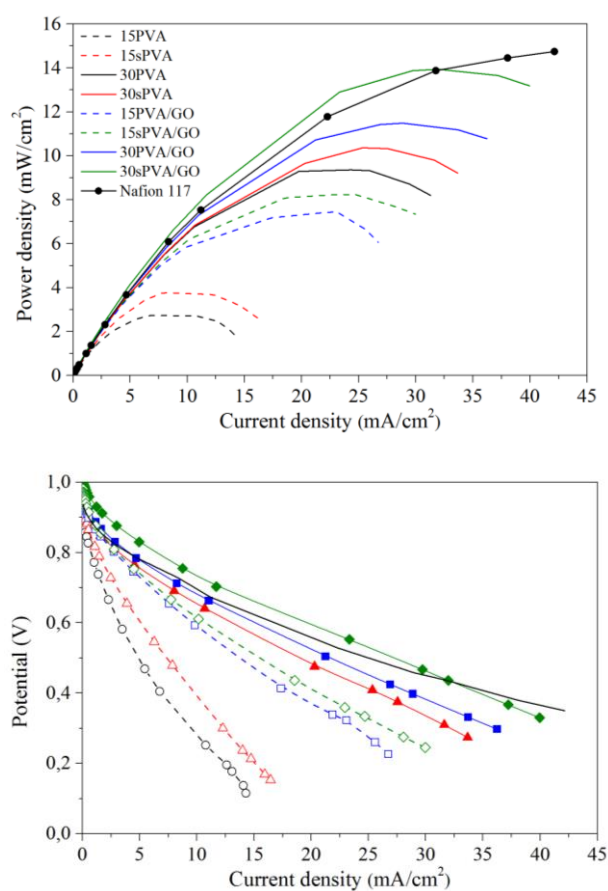
Figure 4.21. Polarization curves of the crosslinked membranes compared to Nafion 117 measured at 25 ºC

Table 4.10 summarizes the values of maximum power density (P_{max}) obtained for each membrane.

Table 4.10. Maximum power density (P_{max}) values obtained for the membranes at 25 ºC

Membrane	P_{max} (mW/cm^2)
15PVA	2.7 ± 0.2
15sPVA	3.7 ± 0.2
30PVA	9.4 ± 0.4
30sPVA	10.4 ± 0.5
15PVA/GO	7.4 ± 0.1
15sPVA/GO	8.3 ± 0.3
30PVA/GO	11.4 ± 0.1
30sPVA/GO	13.9 ± 0.5

According to the results, the crosslinking degree strongly affects to the performance of the membranes in the fuel cell. The highest values of P_{max} were obtained for the membranes crosslinked at 30 wt.% of SSA due to the higher concentration of active groups for the proton transport (sulfonic acid groups, -SO_3H) in their structure. This effect is accentuated with the intra-sulfonation of the polymer matrix and the addition of GO. The 30sPVA/GO composite reaches the maximum value of P_{max} (13.9 mW/cm^2) among all the assayed membranes. This increase of the amount of sulfonic acid groups in the bi-sulfonated composite results in an improvement of the performance in the fuel cell due to the enhancement of the proton conduction via Grotthus mechanism. Moreover, the composites show improved performance due to the homogeneous dispersion of the GO nano-platelets into the polymeric matrix which are able to form continuous and well-connected proton-conducting channels [30]. The obtained results are comparable with that for Nafion 117 (14.7 mW/cm^2) measured at the same operating conditions. Therefore, it can be conclude that the prepared composites are good candidates to be used as PEMs in H_2-O_2 fuel cells.

Conclusions

Four types of PVA-based crosslinked membranes at different sulfonation levels (15PVA, 15sPVA, 30PVA and 30sPVA) were prepared by solution-casting method. The effect of the intra- and inter-sulfonation of the polymer matrix was evaluated as a novel procedure to enhance the functional properties of the prepared membranes for their use in fuel cell applications. The effect of the addition of GO (1wt.%) was also studied by the preparation of their analogues 15PVA/GO, 15sPVA/GO, 30PVA/GO and 30sPVA/GO composites. The proton-conducting properties of the bi-sulfonated PVA membranes are directly influenced by the degree of sulfonation and the addition of GO in the polymer matrix. The water uptake and swelling ratio decrease as the sulfonation degree increases as well as with the addition of GO in the composite membranes. As expected, the proton conductivity values increase with temperature in all cases, showing the highest values at 90 °C. The bi-sulfonation of the polymer matrix in the 30sPVA membrane show an increase of 69 % of proton conductivity at 90 °C compared to the 30PVA membrane, even showing lower values of water uptake. The same behaviour is observed for the composites, increasing the proton conductivity from 11.82 mS/cm for the 30PVA/GO composite to 20.96 mS/cm for 30sPVA/GO composite at 90 °C. Therefore, it can be conclude that increasing the active ionic sites via intra- and inter-sulfonation of the polymer matrix results in an improvement of the proton-conducting properties of the assayed membranes. Likewise, the addition of GO favours the proton mobility through the membrane by formation of well-connected proton-conducting channels, while the effective management of water in the composites avoids an excess of water uptake enhancing their dimensional stability.

Acknowledgements

References

[1] J. Zhang, L. Zhang, H. Liu, A. Sun, and R. S. Liu, *Electrochemical Technologies for Energy Storage and Conversion*. Wiley, 2012.

[2] Z. Qi, *Electrochemical Energy Storage and Conversion Proton Exchange Membrane*. CRC Press, 2013.

[3] S. Javaid and T. Matsuura, *Polymer Membranes for Fuel Cells*. Springer, 2009.

[4] T. Schultz, S. Zhou, and K. Sundmacher, "Current Status of and Recent Developments in the Direct Methanol Fuel Cell," Chem. Eng. Technol., vol. 24, no. 12, pp. 1223–1233, 2001.

[5] S. Patachia, A. J. M. Valente, A. Papanceaa and Victor M. M. Lobo, *Poly (Vinyl Alcohol) (PVA)-Based Polymer Membranes*. Nova Science Publishes, Inc., 2009.

[6] J.M. Morancho, , J.M. Salla, A. Cadenato, X. Fernández-Francos, X. Ramis, P. Colomer, Y. Calventus, and R. Ruíz, "Kinetic studies of the degradation of poly(vinyl alcohol)-based proton-conducting membranes at low temperatures," Thermochim. Acta, vol. 521, no. 1–2, pp. 139–147, 2011.

[7] D. S. Kim, H. B. Park, J. W. Rhim, and Y. M. Lee, "Preparation and characterization of crosslinked PVA/SiO2 hybrid membranes containing sulfonic acid groups for direct methanol fuel cell applications," J. Memb. Sci., vol. 240, no. 1–2, pp. 37–48, 2004.

[8] A. Martínez-Felipe, C. Moliner-Estopiñán, C. T. Imrie, and A. Ribes-Greus, "Characterization of crosslinked poly(vinyl alcohol)-based membranes with different hydrolysis degrees for their use as electrolytes in direct methanol fuel cells," J. Appl. Polym. Sci., vol. 124, no. 2, pp. 1000–1011, Apr. 2012.

[9] M. Yoo, M. Kim, Y. Hwang, and J. Kim, "Fabrication of highly selective PVA-g-GO/SPVA membranes via cross-linking method for direct methanol fuel cells," Ionics (Kiel)., vol. 20, no. 6, pp. 875–886, 2014.

[10] S. Yun, H. Im, Y. Heo, and J. Kim, "Crosslinked sulfonated poly(vinyl alcohol)/sulfonated multi-walled carbon nanotubes nanocomposite membranes for direct methanol fuel cells," J. Memb. Sci., vol. 380, no. 1–2, pp. 208–215, 2011.

[11] A. Ammar, A. M. Al-Enizi, M. A. AlMaadeed, and A. Karim, "Influence of graphene oxide on mechanical, morphological, barrier, and electrical properties of polymer membranes," Arab. J. Chem., vol. 9, no. 2, pp. 274–286, 2016.

[12] Y. Hu, X. Li, L. Yan, and B. Yue, "Improving the Overall Characteristics of Proton Exchange Membranes via Nanophase Separation Technologies: A Progress Review," Fuel Cells, no. 1, pp. 3–17, 2017.

[13] S. C. Sánchez-Ballester, A. Ribes-Greus, V. Soria, G. Rydzek, and K. Ariga, "Bi-sulfonation of poly(vinyl alcohol)/Graphene oxide composite membranes for Proton Exchange Membrane Fuel Cell applications. Part 1: Membrane preparation and characterization," *In Preparation*.

[14] W. S. Hummers and R. E. Offeman, "Preparation of Graphitic Oxide," J. Am. Chem. Soc., vol. 80, no. 6, pp. 1339–1339, 1958.

[15] L. Shahriary and A. A. Athawale, "Graphene Oxide Synthesized by using Modified Hummers Approach," Int. J. Renew. Energy Environ. Eng., vol. 2, no. 1, pp. 58–63, 2014.

[16] X. Qian, N. Gu, Z. Cheng, X. Yang, E. Wang, and S. Dong, "Methods to study the ionic conductivity of polymeric electrolytes using a.c. impedance spectroscopy," J. Solid State Electrochem., vol. 6, no. 1, pp. 8–15, 2001.

[17] K. L. Mittal, Advances in Contact Angle, *Wettability and Adhesion, Volume Two*. Wiley, 2015.

[18] Y.-H. Su, Y.-L. Liu, Y.-M. Sun, J.-Y. Lai, D.-M. Wang, Y. Gao, B. Liu, and M. D. Guiver, "Proton exchange membranes modified with sulfonated silica nanoparticles for direct methanol fuel cells☆," J. Memb. Sci., vol. 296, no. 1–2, pp. 21–28, 2007.

[19] T. Jose, S. C. George, M. Mg, and S. Thomas, "Functionalized MWCNT and PVA Nanocomposite Membranes for Dielectric and Pervaporation Applications Chemical Engineering & Process Technology," J Chem Eng Process Technol, vol. 6, no. 3, pp. 1–8, 2015.

[20] C.-Y. Tseng, Y.-S. Ye, K.-Y. Kao, J. Joseph, W.-C. Shen, J. Rick, and B.-J. Hwang, "Interpenetrating network-forming sulfonated poly(vinyl alcohol) proton exchange membranes for direct methanol fuel cell applications," Int. J. Hydrogen Energy, vol. 36, no. 18, pp. 11936–11945, 2011.

[21] N. Seeponkai and J. Wootthikanokkhan, "Proton conductivity and methanol permeability of sulfonated poly(vinyl alcohol) membranes modified by using sulfoacetic acid and poly(acrylic acid)," J. Appl. Polym. Sci., vol. 105, no. 2, pp. 838–845, Jul. 2007.

[22] M.-Y. Lim, H. Shin, D. M. Shin, S.-S. Lee, and J.-C. Lee, "Poly(vinyl alcohol) nanocomposites containing reduced graphene oxide coated with tannic acid for humidity sensor," Polymer (Guildf)., vol. 84, pp. 89–98, 2016.

[23] L. Wang, J. Kang, J.-D. Nam, J. Suhr, A. K. Prasad, and S. G. Advani, "Composite Membrane Based on Graphene Oxide Sheets and Nafion for Polymer Electrolyte Membrane Fuel Cells," ECS Electrochem. Lett., vol. 4, no. 1, pp. F1–F4, 2014.

[24] Y. He, J. Wang, H. Zhang, T. Zhang, B. Zhang, S. Caob, and J. Liu, "Polydopamine-modified graphene oxide nanocomposite membrane for proton exchange membrane fuel cell under anhydrous conditions," J. Mater. Chem. A, vol. 2, no. 25, pp. 9548–9558, 2014.

[25] G. A. Ludueña, T. D. Kühne, and D. Sebastiani, "Mixed Grotthuss and vehicle transport mechanism in proton conducting polymers from Ab initio molecular dynamics simulations," Chem. Mater., vol. 23, no. 6, pp. 1424–1429, 2011.

[26] W. Liu, M. J. Janik, and R. H. Colby, *Polymers for Energy Storage and Delivery: Polyelectrolytes for Batteries and Fuel Cells*, vol. 1096. 2012.

[27] J. Chen, Q. Guo, D. Li, J. Tong, and X. Li, "Properties improvement of SPEEK based proton exchange membranes by doping of ionic liquids and Y 2O 3," Prog. Nat. Sci. Mater. Int., vol. 22, no. 1, pp. 26–30, 2012.

[28] H. Beydaghi, M. Javanbakht, and E. Kowsari, "Preparation and physic-chemical performance study of proton exchange membranes based on phenyl sulfonated graphene oxide nanosheets decorated with iron titanate nanoparticles," Polymer (Guildf)., vol. 87, pp. 26–37, 2016.

[29] S. Mo, L. Peng, C. Yuan, C. Zhao, W. Tang, C. Ma, J. Shen, W. Yang, Y. Yu, Y. Min, and A. J. Epstein., "Enhanced properties of poly(vinyl alcohol) composite films with functionalized graphene," RSC Adv., vol. 5, no. 118, pp. 97738–97745, 2015.

[30] Y.-S. Ye, M.-Y. Cheng, X.-L. Xie, J. Rick, Y.-J. Huang, F.-C. Chang, and B.-J. Hwang, "Alkali doped polyvinyl alcohol/graphene electrolyte for direct methanol alkaline fuel cells," J. Power Sources, vol. 239, pp. 424–432, 2013.

4.4. Contribution III:

Effect of the multiple sulfonation on the proton conductivity properties of poly(vinyl alcohol)/graphene oxide composite membranes

Effect of the multiple sulfonation on the proton conductivity properties of poly(vinyl alcohol)/graphene oxide composite membranes

S. C. Sánchez-Ballester[a], O. Santiago[d,e], T. J. Leo[d], E. Navarro[e], A. Ribes-Greus[a], V. Soria[b], G. Rydzek[c] and K. Ariga[c]

[a]Instituto de Tecnología de Materiales (ITM), Universitat Politècnica de València, Valencia, Spain
[b]ICMUV, Universitat de València, Burjassot, Valencia, Spain
[c]World Premier International Center for Materials Nanoarchitectonics (MANA), National Institute for Materials Science (NIMS), Tsukuba, Japan.
[d]ETSI Navales, Universidad Politécnica de Madrid, Madrid, Spain.
[e]ETS Ingeniería Aeronáutica y del Espacio, Universidad Politécnica de Madrid, Madrid, Spain

Abstract

The evaluation of the proton-conducting properties of hybrid organic-inorganic composite membranes based on poly(vinyl alcohol) (PVA) and graphene oxide (GO) was carried out. A two-step methodology in which PVA matrix was first intra-sulfonated (0.1 %) with propane sultone and subsequently inter-sulfonated using sulfosuccinic acid (SSA) as a crosslinking agent was followed in order to enhance the proton conductivity of the studied composites. In addition, graphene oxide was further sulfonated (sulfonation degree of 10 %) via substitution reaction with diazonium salt of sulfanilic acid in order to provide additional proton-conducting channels to the structure. Then, the PVA-based composite membranes were prepared by solution-casting method. The resulting sGO composites showed better mechanical properties and lower water and methanol uptake compared to those prepared with GO. The proton conductivity and methanol permeability of the hybrid composites were tested in order to evaluate their potential for DMFC applications. Among all the studied composites, the 30PVA/sGO composite showed the best performance, exhibiting high proton conductivity (17.01 mS/cm at 90 ℃), low methanol permeability (1.84×10^{-8} cm^2/s at 30 ℃) and high OCV values in DMFC test (0.76 V at 50 ℃ and a 2M methanol feed concentration), indicating that is a good candidate to be used as PEM in DMFC applications.

Keywords: poly(vinyl alcohol), sulfonated graphene oxide, hybrid organic-inorganic composites, multiple sulfonation, proton exchange membranes, direct methanol fuel cells

Introduction

Direct methanol fuel cells (DMFCs) are considered as one of the most promising power sources for portable or mobile applications, due to its high energy efficiency, low operating temperature conditions and low environmental impact. The proton exchange membrane (PEM) is the core component in a DMFC through which the protons are transferred from the anode to the cathode and it acts as an electronic insulator and barrier to fuel molecules.

Currently, the perfluorosulfonic acid membrane Nafion® is the most used electrolyte in DMFCs due to its high proton conductivity (0.1 S/cm) at a fully hydrated state and its excellent mechanical and thermal stability [1], [2]. However, its high manufacturing cost and high methanol permeability ($\sim 10^{-6}$ cm^2/s) limits its application. In order to bring down the cost of PEMs, non-fluorinated membranes, such as hydrocarbon based PEMs, have been considered as one of the most attractive alternatives to Nafion® [4], [5]. Polyvinyl alcohol (PVA) based membranes stand out among the different types of hydrocarbon based PEMs for DMFC applications due to its low cost and high performance in hydro-alcoholic environments. However, pure PVA does not possess any protonic conductivity. Therefore, the development of different strategies such as the incorporation of fillers to the polymer matrix in order to prepare hybrid organic-inorganic composite membranes with improved proton conductivity has been investigated in order overcome this drawback [5].

Fillers can be classified in organic and inorganic compounds. Organic fillers containing sulfonic acid groups, such as sulfonated poly(propylene oxide), block effectively the methanol permeability but also decrease the proton conductivity of the membranes [6], [7]. While the addition of inorganic fillers, which can be classified as proton conductive fillers, hydrophilic fillers or hydrophilic and proton conductive bifunctional fillers, increase the proton conductivity at the same time that limit methanol permeability [8]–[10].

Graphene oxide (GO) has been used extensively as inorganic filler in PEMs. GO is a two-dimensional single layered homologue of graphene containing various oxygen functional groups (epoxy, carbonyl and hydroxyl) widely used in supercapacitors, biosensors and photovoltaic cells applications. The incorporation of GO into a polymer matrix improves many of the physical and chemical membrane properties, including mechanical strength and proton conductivity [11]. Recently, the preparation, characterization and performance of PVA/GO nanocomposite membranes were widely investigated [12]. In addition, GO can be sulfonated and transformed in a highly hydrophilic and proton-conductive bifunctional filler. The sulfonation of the GO (sGO) can improve the proton conductivity and the performance of composite membranes in a fuel cell [13]. The presence of sulfonic acid groups (-SO$_3$H) on the GO surface provides extra pathways for proton conduction, improving the connectivity and arrangements of ionic conducting domains.

Sulfonated graphene oxide (sGO) has been extensively used to promote proton conductivity in some polymer matrix composites. Y. Heo et al. synthesized a novel composite membrane of sulfonated graphene oxide (sGO) and SPEEK with various sulfonated graphene oxide contents [14]. It was found that the sulfonation of graphene oxide induces an increase in the number of sulfonic groups ($-SO_3H$), which significantly increases the proton conductivity of sulfonated graphene oxide/SPEEK membrane. In addition, a considerable increase of the methanol selectivity was observed making the composite membrane good candidates for use in DMFCs. F.-C. Chang et al. prepared sGO/Nafion composite membranes with low methanol-crossover and water uptake with improved proton conductivity at low relative humidity [15]. V. Baglio et al. prepared composite membranes by incorporation of organo-modified GO containing sulfonilic terminal groups to Nafion polymer [16], which significantly reduce the ohmic losses at high temperatures in DMFC test. A. Sirivat et al. have developed novel proton exchange membranes consisting in sGO embebed in sulfonated polysulfone (-sPSF). The membrane exhibited the higher proton conductivity and lower methanol permeability of 4.27×10^{-3} S/cm and 3.48×10^{-7} cm^2/s, respectively, than Nafion 117 [17]. H. Beydaghi et al. prepared PVA-based composite membranes using iron oxide (Fe_3O_4) nanoparticles are deposited onto sulfonated graphene oxide (sGO) nanosheets in order to orientate the sGO/Fe_3O_4 nanosheets to the through-plane direction of the membrane by applying a magnetic field. It was found higher proton conductivity, methanol permeability, and selectivity in aligned membranes compared to a nonaligned ones [18].

The aim of the present study was to evaluate the suitability of the modification of PVA by intra- and inter-sulfonation, as well as the effect of the addition of the sGO filler on the proton conductive properties of the prepared hybrid organic-inorganic composite membranes. The key point of our strategy was to make a high contrast in polarity between hydrophilic and hydrophobic domains by introduction of sulfonated units only at the end of side chain groups, in a similar way that the proposed by Hay and coworkers [19]. Hey et al. saw that a large excess of chlorosulfuric acid in dichloromethane at room temperature allows the selective and quantitative introduction of sulfonic acid groups only on the end groups. In our case, the methodology followed for the distribution of sulfonic acid groups units was different. First, commercial PVA was slightly sulfonated (0.1 %) and then was further crosslinked using sulfosuccinic acid (SSA) at two different concentrations, 15 and 30 wt.%, as a sulfonated crosslinking agent. Finally, the hybrid organic-inorganic composites were prepared by direct dispersion of the sGO nanoplatelets (sulfonation degree of 10 %) into the polymer matrix using the solution-casting method. The evaluation of the proton transport properties of the prepared composites was carried out as a function of the water contact angle, water and methanol uptake (WU/MU), ion exchange capacity (IEC), proton conductivity (σ_{prot}) and the performance in a H_2-O_2 fuel cell. Furthermore, their methanol permeability and their performance in a DMFC were also investigated.

Experimental

Chemicals

Graphite powder (particle size < 20 μm), sodium nitrate (NaNO$_3$, ≥99.0%), sodium hydride (NaH, dry 95%), 1,3-propane sultone (97%), poly(vinyl alcohol) (PVA, molecular weight 130000 g/mol, degree of hydrolysis min. 99%), sulfanilic acid (99%), sodium nitrite (NaNO$_2$, 99.5%) and sulfosuccinic acid (SSA, 70 wt.% solution in water) were purchased from Sigma-Aldrich. Concentrated sulfuric acid (H$_2$SO$_4$, 95%), hydrogen peroxide (H$_2$O$_2$, 30% w/w), ethanol absolute (EtOH), hydrochloric acid (HCl, 37%), potassium permanganate (KMnO$_4$, extra pure), sodium chloride (NaCl), sodium hydroxide (NaOH, ≥ 98%) and methanol (MeOH) were purchased from Scharlau.

Synthesis of materials

Synthesis of sulfonated poly(vinyl alcohol) (sPVA)

The synthesis of sPVA was carried out in two steps [20], [21]. First, 10 g of commercial PVA were added in 250 mL of EtOH. Successively, 4.8 g of NaH were slowly added to the PVA dispersion under constant mechanical stirring at room temperature. Then, 5 g of 1,3-propane sultone were added dropwise and the dispersion was stirred at 80 °C for 24 hours. In a second step, the obtained sodium sulfonated salt was transformed in the protonated form by immersion in HCl solution for 12 hours. The sPVA powder was filtered, washed with ethanol and finally dried for 4 hours in a vacuum oven at 50 °C.

Synthesis of sulfonated graphene oxide (sGO)

Graphene oxide (GO) was prepared by the Modified Hummers Method (MHM) using graphite powder as the starting material [22]. sGO was achieved by functionalization of GO via free radical addition using sulfanilic acid diazonium salt as adduct, as shown in Scheme 4.4. Briefly, 50 mg of GO were added to 8 mL 0.06 M sulfanilic acid solution at 70 °C. Under continuous stirring, 2 mL 6×10^{-3} M sodium nitrite solution was added dropwise and the mixture held at 70 °C for 12 hours. The sulfanilic acid diazonium salt obtained from the reaction of sulfanilic acid with sodium nitrite was become in aryl radical by transfer of a delocalized electron from the GO. The aryl radical reacts rapidly with the carbon atoms in the GO layers to form new covalent bonds, changing the hybridization from sp^2 to sp^3 [15]. The final product was washed several times with pure water and centrifuged until the pH reached 7.
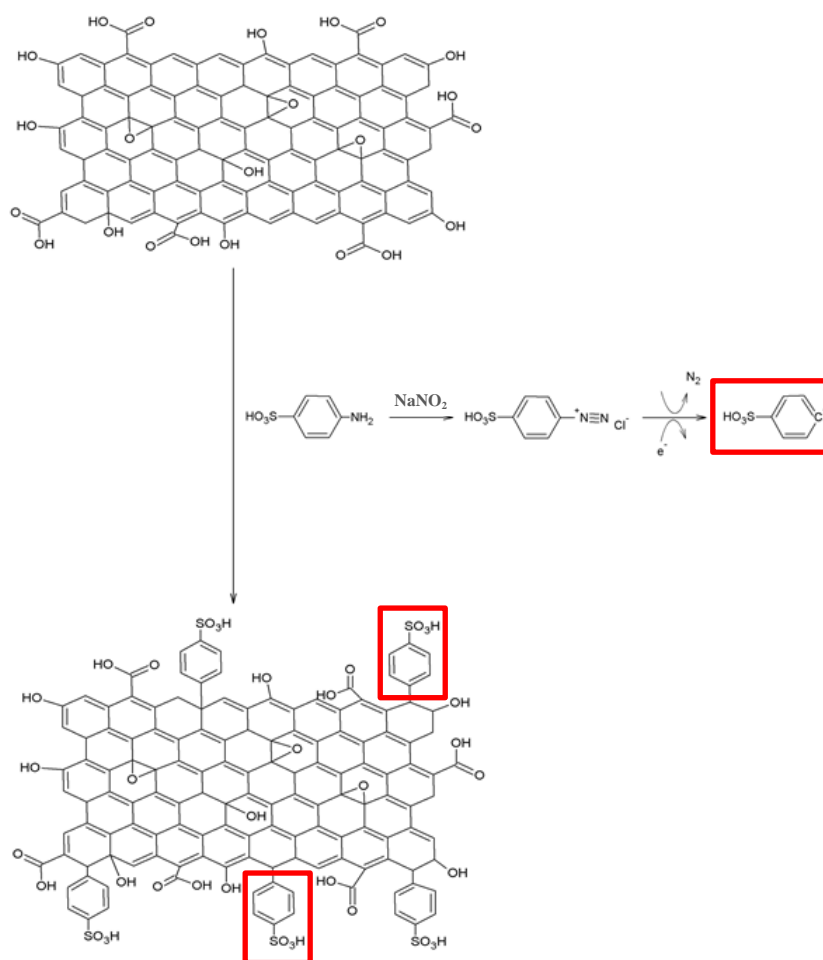
Scheme 4.4. Schematic diagram of the synthesis of sGO

Preparation of the composite membranes

sGO composite membranes, identified as *X*PVA/sGO and *X*sPVA/sGO, where *X* represents the weight percentage of SSA and *s* the intra-sulfonation of the polymer matrix, were prepared by solution-casting method. The three-steps methodology followed for the preparation of the crosslinked membranes was previously described in Contribution I [11]. First, 5 wt.% of PVA and sPVA aqueous solutions were prepared by dissolving the polymer in water and refluxing at 90 °C for 6 hours. A dispersion of sGO in distilled water (1 wt.% respect polymer) was sonicated to obtain an homogeneous dispersion and was then added to the PVA and sPVA solutions

previously prepared. Lastly, the solutions were mixed with SSA at two different concentration (15 and 30 wt.% respect polymer) and vigorously stirred at room temperature for 24 hours. The homogeneous solutions were poured onto a Teflon plate and the cast membranes were allowed to dry at room temperature. The dried membranes were peeled off the plates and were crosslinked at 110 ºC for 2 hours. The average thickness of membranes was 103 ± 26 μm. Table 4.11 shows the experimental composition and nomenclature of each composite.

Table 4.11. Experimental composition and nomenclature of each composite membrane

Composite	PVA (wt.%)	sPVA (wt.%)	sGO (wt.%)	SSA (wt.%)
15PVA/sGO	83.99	–	1.00	15.00
15sPVA/sGO	–	84.11	1.01	14.89
30PVA/sGO	68.88	–	0.99	30.13
30sPVA/sGO	–	69.14	1.01	29.85

Characterization techniques

Fourier Transform Infrared (FTIR) spectra were recorded with a *Thermo Nicolet 5700 FTIR*. The IR spectra were collected after 64 scans in the 4000-400 cm^{-1} region using the attenuated total reflectance (ATR) mode at a resolution of 4 cm^{-1}. Backgrounds spectra were collected before each series of experiments. All the experiments were performed three times and the average was taken as the representative value.

Raman spectroscopy analysis was carried out using a *Horiba XploRA-One* Raman microscope. Raman excitation source was provided by a 532 nm laser. Spectra were recorded from 200 to 3500 cm^{-1}.

X-Ray diffraction measurements were conducted using a *D8 Advance A25 Bruker* diffractometer in order to study the structure of the synthesized sGO and to corroborate the fully exfoliation of sGO into PVA and sPVA membranes. Copper K_α ($\lambda_{K\alpha} = 0.15418$ nm) radiation was used with a power setting of 40 kV and 40 mA. Data were collected from 5 to 75º with a scanning step of 0.01 º and a scan rate of 0.02 º/s.

The XPS spectrum was recorded using a multianalysis system *SCALAB 210* using a monochromatic Mg excitation line at 1253.6 eV.

The cross-sectional morphology of the composites was studied using a *Hitachi SU8000* Field Emission-Scanning Electron Microscope (FE-SEM) with an acceleration voltage of 20 kV. For this purpose, the samples were prepared by immersing the films in liquid nitrogen for 10 minutes before fracture and next coated with a gold/palladium alloy

before analysis. The composition of sGO was investigated by energy dispersive X-ray spectroscopy (EDX).

Transmission Electron Microscopy (TEM) was performed with a *JEOL JEM-1010* microscope operating at an accelerating voltage of 100 kV. Composite membranes were observed as ultrathin sections cut with an ultra-microtome *Leica EM UC6* and further transferred to copper grills.

The degradation process and the thermal stability of the membranes were investigated by Thermogravimetric Analysis (TGA) on a *TA Instruments TGA Q-500* analyzer. Measurements were carried out under nitrogen atmosphere at 10 °C/min heating rate covering from 25 to 800 °C temperature range.

The wettability of the membranes was characterized according to its water contact angle. Hence contact angle was evaluated using a *Theta Optical Tensiometer (KSV Instruments, Ltd)* and electrooptics comprising a CCD camera connected to a computer at room temperature. The distilled water (2 μL) was dropped on the sample surface at five different sites and the average value was taken as the representative value.

The stress-strain curves of membranes were obtained using a *MTS QTest 1/L Elite* Dynamometer. The membranes were cut into tensile specimens dog-bone shaped with the gauge length and width of 15 mm x 5 mm, respectively. Tests were conducted with a 100 N load cell under a strain rate of 5 mm/min at room temperature. The values were calculated as average over seven specimens of each membrane.

Water and Methanol Uptake (WU/MU)

The absorption of water and methanol was evaluated by performing swelling tests on the composites. Rectangular specimens of 4 x 1 cm^2 were dried at 60 °C under vacuum for 12 hours, and the weight of the dried membranes was measured in a microbalance. The membranes were immersed in tests tubes containing distilled water and 2M methanol solution at 30, 35, 40 and 45 °C to simulate the behavior of the materials in a DMFC environment. The absorption of the solvents was measured gravimetrically at different times, taken out, wiped with tissue paper, and immediately weighted the membrane on a microbalance. The membranes were immersed in the water and methanol solutions until no further gain weight were observed, meaning the achievement of equilibrium condition. The water and methanol uptake, WU and MU (%), was calculated as the mass difference between the samples exposed to the solvent (M_{eq}) and the dry sample (M_{dry}). The results were normalized respect to the mass of the dried sample according to,

$$(\textbf{WU/MU})_{\textbf{eq}}\ (\%) = \frac{\textbf{M}_{\textbf{eq}} - \textbf{M}_{\textbf{dry}}}{\textbf{M}_{\textbf{dry}}} \times \textbf{100}$$

Ion Exchange Capacity (IEC)

The IEC of each composite was determined by titration method. The pre-weighted dry sample was soaked in a 0.5 M HCl solution for 24 hours at room temperature to obtain its protonated form. The sample was washed with an excess amount of distilled water and then was immersed in a 2M NaCl solution for 24 hours at room temperature to exchange H^+ with Na^+ ions. The amount of H^+ liberated was estimated by acid-base titration against a standard 0.1 N (0.0955 ± 0.0009 N) NaOH solution with phenolphthalein as the indicator. The IEC values were calculated using the following equation

$$IEC\ (mequiv/g) = \frac{N_{NaOH} \times V_{NaOH}}{W_{dry}}$$

where N_{NaOH} is the normality of the titrant in mequiv/L, V_{NaOH} is the added titrant volume in *liters* (L), and W_{dry} is the dry mass of sample in *grams* (g).

Conductivity measurements

The conductivity of the membranes was measured with a *Novocontrol Broadband Dielectric Spectrometer (BDS)* in the frequency range of 10^{-1} to 10^7 Hz using an *Alpha-A Frequency Response Analyzer (Novocontrol)*.

The proton conductivity (σ_{prot}) was measured using a *BDS-1308 (Novocontrol)* liquid parallel plate sample cell. The membranes were previously equilibrated with Mili-Q water to ensure fully hydrated state. The measurements were performed at 30, 50, 70 and 90 ºC. The proton conductivity (S/cm) of the membranes was calculated according to

$$\sigma_{prot} = \frac{L}{RA}$$

where L is the thickness of the conducting membranes in *centimeters* (cm), A the area of the electrode in contact with the sample in cm^2, and R the protonic resistance in *ohms* (Ω), taken from the Bode plot at high frequencies [23].

The electrical conductivity (σ_{elec}) was measured at 30 ºC using a *BDS-1200 (Novocontrol)*, parallel-plate capacitor with two gold-plated electrodes system, as dielectric cell test. The electrical conductivity was taken at low frequencies, where the measured real part of the conductivity (σ') reaches a plateau which directly corresponds to the DC conductivity (σ_0).

Methanol diffusion coefficients (D_{MeOH})

The methanol diffusion coefficients (D_{MeOH}) through the composites were tested by a home-made gravimetric permeation cell. The composites were cut into disks of 15 mm in diameter. The cell was filled with methanol solution (2M) and then was quickly assembled with the sample clamped to seal the pathway of the solvent. The sealed cell was immediately put on an analytical balance that was in a constant temperature chamber. The weight loss, related to the methanol diffused through the membrane, was recorded as a function of time. The diffusion coefficients were obtained from the transient state, which is valid for short times, using the Rogers equation [24],

$$\ln\left(F\ t^{\frac{1}{2}}\right) = \ln\left[2\,c_1\left(\frac{D}{\pi}\right)^{1/2}\right] - \frac{l^2}{4Dt}$$

where F is the permeation flux in $g \cdot cm^{-2} \cdot s^{-1}$, t is the time in *seconds* (s), c_1 is the penetrant concentration at x = 0, l is the thickness of the sample in *centimeters* (cm), and D is a constant diffusion coefficient in cm^2/s. The plot of $\ln(F\ t^{1/2})$ vs $(1/t)$ gives the slope $(-l^2/4D)$ from which the value of D_{MeOH} can be estimated.

Fuel cell tests

H_2-O_2 fuel cell tests

The performance of the composites in a fuel cell was tested by measuring the polarizations curves. The samples were equilibrated with Mili-Q water during 24 hours and then were sandwiched between two sheets of gas diffusion electrodes (*Fuels Cells Etc*, 4 mg/cm^2 Platinum Black). The electrochemical performances were evaluated with a single-cell fixture having an active area of 16 cm^2. The fuel cell was operated with hydrogen and oxygen at 25 ºC and atmospheric pressure.

Direct Methanol Fuel Cell test

Tests in a single DMFC with commercial electrodes, Pt/C (1 mg/cm^2) for the cathode and Pt-Ru/C (3 mg/cm^2) for the anode, were carried out. To do this, performance at methanol concentrations from 1 M to 4 M concentration range was studied, which allows determining the concentration range where the power density is maximum. The membrane-electrode assembly was carried out by pressing with the ending plates, without any ionomer.

Results and discussion

sGO characterization

The sulfonation of graphene oxide was confirmed by Raman, XRD, XPS, TGA and EDX analysis. Figure 4.22 compares the Raman spectra of the GO and sGO. GO shows the typical bands at 1345 and 1586 cm^{-1} corresponding to the D and G bands, respectively [25]. The intensity ratio of I(D)/I(G) gives information about structural changes during a chemical process. After sulfonation process, the value of the intensity ratio of GO increases from 0.97 to 1.04. Hence, this increase can be attributed to the increment of sp^3 domains by the introduction of phenyl sulfonated groups on the basal carbon plane, decreasing the original π network of GO [26], [27].
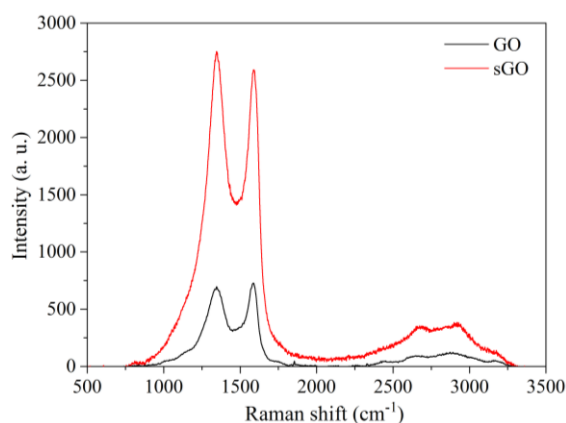
Figure 4.22. Raman spectra of GO and sGO platelets

The chemical and microstructural modification of the GO was studied by XRD. Figure 4.23a compares the XRD patterns of the GO and sGO nano-platelets. GO shows a diffraction peak at $2\theta = 11.9º$ corresponding to the (001) plane with an interlayer spacing of 0.75 nm. The sGO pattern does not show significant differences from the pattern of GO, indicating that the functionalization of GO not greatly affects its crystal structure [28].

The surface modification of GO by sulfonation was also corroborated by XPS. Figure 4.23b shows the XPS spectrum of sGO. Three different peaks can be distinguished in the spectrum. The peak at 532.97 eV is attributed to the O1s signal, at 286.88 eV is observed the C1s peak, and finally the S2p peak at 168.44 eV which is associated to the sulfur atoms [14], confirming the successful sulfonation of the GO.
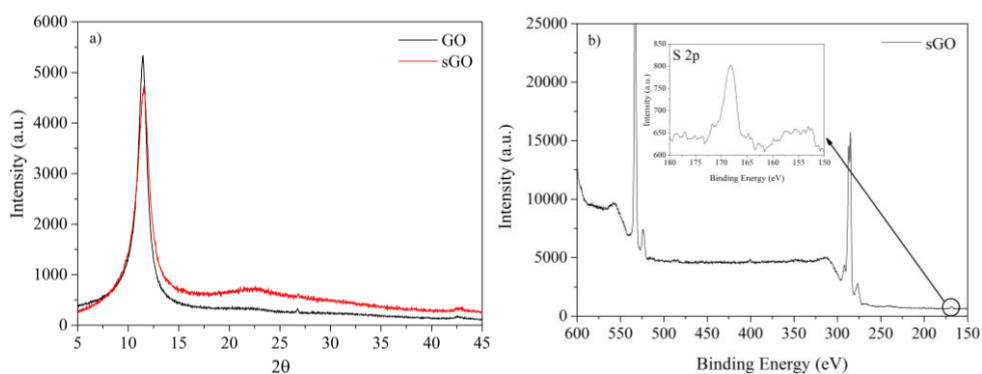
Figure 4.23. a) XRD patterns of GO and sGO nano-platelets, and b) XPS spectrum of sGO, inset graph shows a magnification of the S2p peak associated with the sulfur atoms

The thermogravimetric (TG) and the first-order derivative (DTG) curves of GO and sGO measured under nitrogen atmosphere are shown in Figure 4.24a and b, respectively. The GO curves exhibit two main decomposition stages. The former, occurred from 25 ℃ to 175 ℃, is attributed to the evaporation of absorbed water and shows a weight loss of 18 %. The latter shows a weight loss of 67 % at 219 ℃ and is due to the decomposition of the labile oxygen-containing groups of GO. In contrast, besides the two decomposition stages observed for GO, sGO curves also show at 364 ℃ a weight loss of 42 % attributed to the desulfonation of the graphitic structure, which confirms the attachment of sulfonic acid groups in GO surface [29]. Moreover, the residue content increases after sulfonation process. The decomposition of the sulfonic acid groups may promote carbonization of the polymer, being responsible for the high residue content of the sGO in comparison with GO.
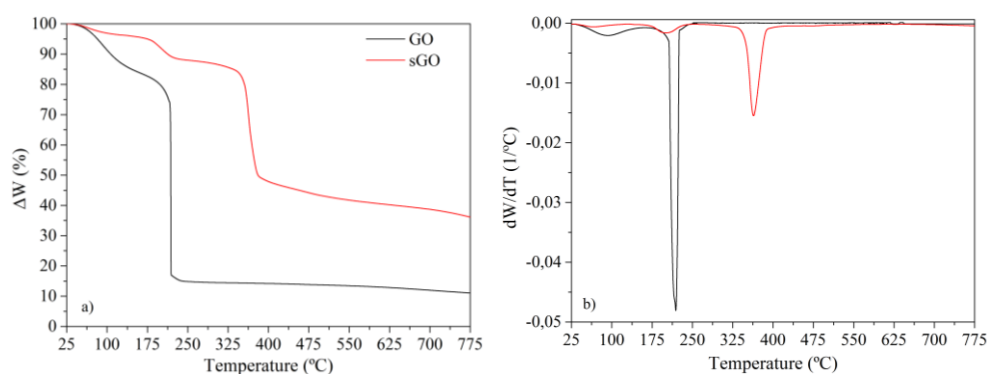
Figure 4.24. (a) TG and (b) DTG curves of the GO and sGO nano-platelets

Finally, the percentage of sulfur in sGO was determined by EDX. Figure 4.25 shows the EDX spectrum of the sGO sample with the characteristic peaks of carbon, oxygen and sulfur. The content of sulfur obtained from the EDX analysis for the synthesized sGO nano-platelets was 3.9 ± 0.2 wt.%, which corresponds to a degree of sulfonation (proportion of -SO$_3$H groups attached to the structure of GO) of 10 %.

Element	wt.%
C	57.2 ± 0.3
O	38.3 ± 0.5
S	3.9 ± 0.2
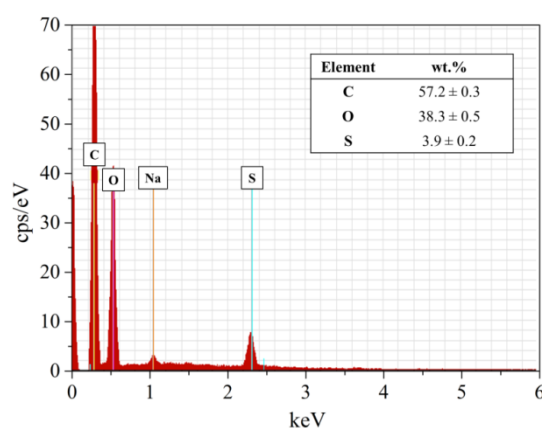
Figure 4.25. EDX elemental composition of the sGO nano-platelets

Composites characterization

Structural characterization

FTIR analysis was conducted in order to identify the intra- and inter-molecular hydrogen bonding interactions between the polymer matrix and the filler, and to confirm the crosslinking reaction with the SSA in the composites. Figure 4.26 compares the FT-IR spectra of all prepared sGO composites. The broad band observed between 3000 cm^{-1} and 3700 cm^{-1} is characteristic of the stretching vibration of the free and hydrogen bonded hydroxyl groups (-OH) [30]. The -OH vibration band for the composites with higher crosslinking degree is shifted to higher wavenumbers and its intensity decreases. This confirms the reduction of the hydroxyl groups by crosslinking reaction with SSA through esterification reactions, in which new covalent bonds are formed [31], [32]. At 2800 and 2900 cm^{-1} appear the symmetric and asymmetric stretching bands of the methylene groups (C-H) of the PVA and sPVA backbones, respectively [30]. The band at 1710 cm^{-1} is attributed to the stretching vibration of the carbonyl (C=O) contained in the ester groups of the SSA and the carboxylic acid groups of the sGO [28]. As the hydroxyl band, the carbonyl band also is influenced by the crosslinking reaction, showing an increase of intensity in the composites with higher crosslinking degree [32], [33]. Moreover, at 1220 cm^{-1} is visible the C-O-C

stretching vibration band of the new ester bonds formed during the crosslinking process [20], [30], [34]. The characteristic C-O vibration band of the alcohols from the polymer matrix (PVA and sPVA) and the sGO is also visible at 1086 cm^{-1}. Finally, at 1033 cm^{-1} appears the stretching vibration band of the sulfonic acid groups (-SO$_3$H) introduced by sGO, sPVA and SSA [32]. Therefore, the changes observed in the spectra evidence the dispersion of the GO nano-platelets into the polymer matrix and the successful crosslinking reaction between the hydroxyl groups of the polymer matrix and the SSA at two different concentrations.
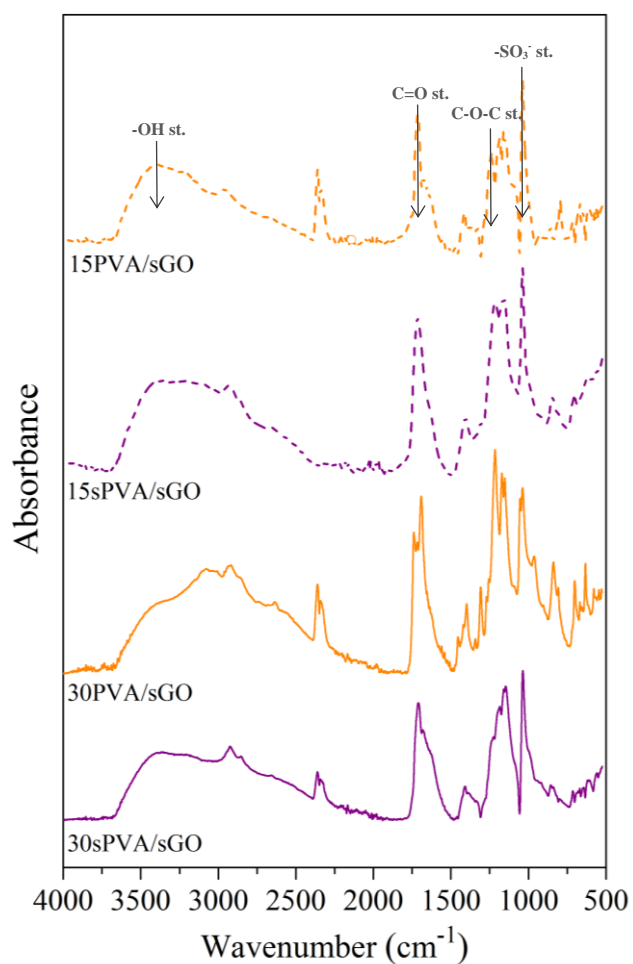
Figure 4.26. Comparison of FTIR spectra of the sGO composites

XRD

The X-Ray diffraction measurements were performed in order to examine the crystal structure of the sGO composite membranes, and to check whether the sGO nano-platelets were fully exfoliated into the polymer matrix. Figure 4.27 compares the XRD patterns of the composite membranes with pure PVA and sGO. The membranes show a main peak at 19.7º corresponding to the crystalline phase of the PVA matrix, as observed in the previously GO composites studied in Contribution I [11]. Compared to pure PVA, the intensity of the main peak in the composites with higher crosslinking degree is strongly reduced and becomes broader [35]. This behaviour is attributed to the reduction of the hydroxyl groups of the polymer matrix by reaction with SSA during the crosslinking reaction, causing an increase of the amorphous character of composites [36]. Likewise, the sulfonation of the polymer matrix also decreases the crystalline character of the membranes, being the intensity of the main peak in the *X*sPVA/sGO composites much smaller than in *X*PVA/GO composites.

Finally, as can be observed in Figure 4.27, the diffraction peak of pure sGO appears at 11.6º. However, this peak is not perceptible in the composites, meaning a fully exfoliation of the sGO nano-platelets into the polymer matrix [13], [37].
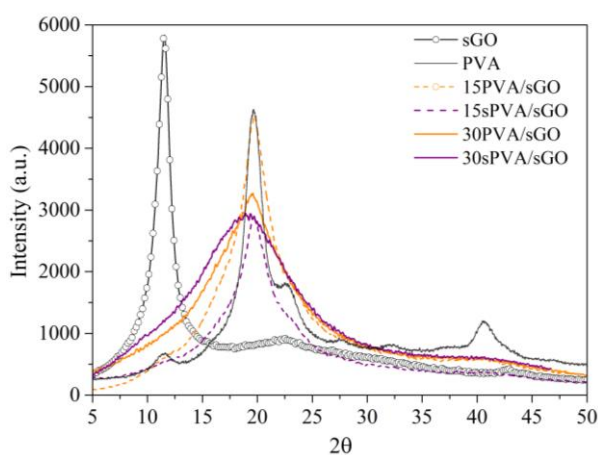
Figure 4.27. Comparison of XRD patterns of the sGO composite membranes with pure PVA and sGO

Morphological characterization

The morphological characterization of the composites was carried out by FE-SEM. Figure 4.28 shows the cross-sectional images of the sGO composites. The sGO is distinguished in the images as the bright region; this effect is due to its higher conductivity compared to the polymer matrix [38]. The SEM images show a uniform distribution of the sGO nano-platelets into the polymer matrix, which can be attributed to the good interfacial adhesion between polymer matrix and the filler via hydrogen bonding interactions [13], [14], [26].
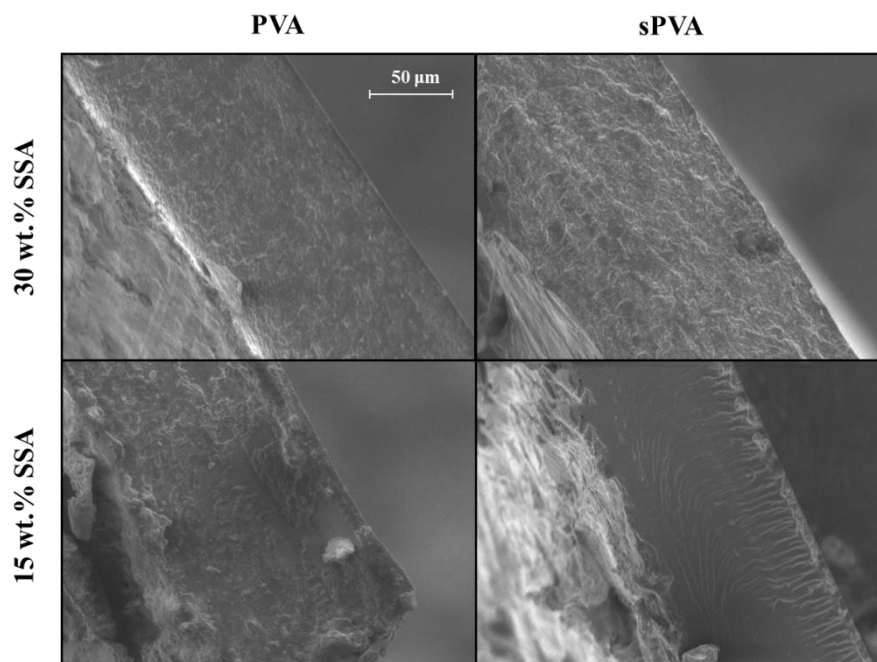
Figure 4.28. SEM cross-sectional images of the sGO composites

In addition, TEM was also used in order to assess the state of exfoliation of sGO in the polymer matrix. Figure 4.29 shows the TEM images of the 30PVA/sGO and 30sPVA/sGO composites. The images show a good exfoliation of the sGO nano-platelets into the polymer matrix, despite some agglomerates are present due to the strong π-π stacking interactions between sGO nano-platelets [38], [39].

30PVA/sGO **30sPVA/sGO**
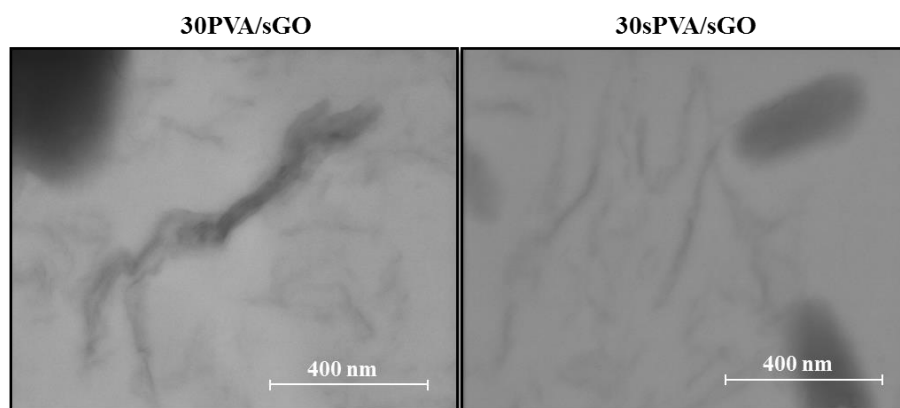
Figure 4.29. TEM images of the 30PVA/sGO and 30sPVA/sGO composites observed at 120k magnification

In order to evaluate which composite is the best candidate to be used as PEM in DMFCs, the sGO composites were compared with the previously prepared GO composites in the Contribution I in terms of thermal and mechanical stability, and proton-conducting properties.

Thermal characterization

The thermal stability of the composite membranes was evaluated through thermogravimetric analysis. Figure 4.30 compares the thermogravimetric (TG) and the first-order derivative (DTG) curves of the sGO and GO composites.
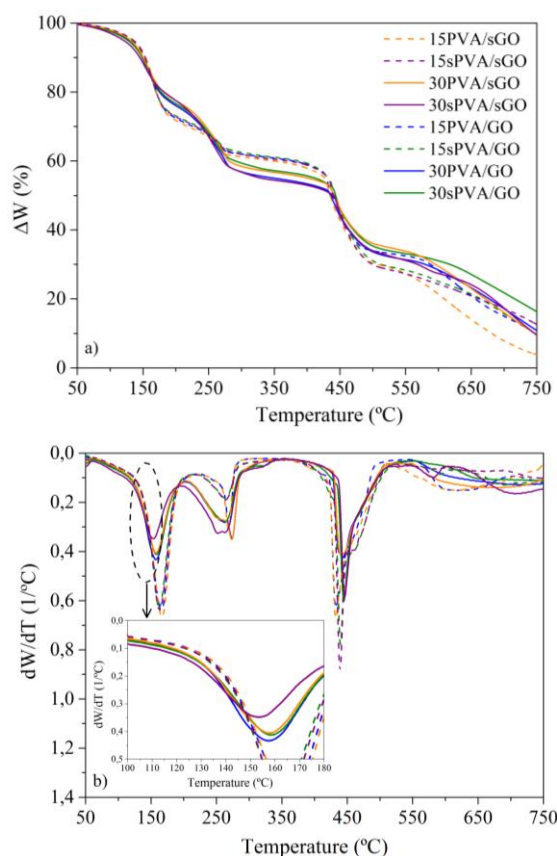
Figure 4.30. Comparison of a) TGA and b) DTG curves of the sGO and GO composites. The inset graph in DTG curves shows a magnification of the first decomposition stage

All the composites showed the same decomposition pattern with three main weight loss stages which appear as three major peaks in DTG curves. The first decomposition stage, from 50 to 200 ºC, is associated to the elimination reactions of the hydroxyl side-chain groups of the polymer matrix. In this stage, the weight loss observed for the composite membranes ranges from 20 to 30 % depending of their crosslinking degree. The membranes with lower crosslinking degree show a stronger weigh loss due to the higher amount of hydroxyl groups contained in its structure [40]. The second stage

takes place within 200 to 350 ºC and it is attributed to the decomposition of the sulfonic acid groups ($-SO_3H$) [34]. In sPVA composites, two different contributions can be distinguish in this stage, the degradation of sulfonic acid groups of SSA at 270 ºC, and the desulfonation of the sPVA matrix at 320 ºC. Moreover, the membranes with higher crosslinking degree (30wt.%), exhibit a weight loss two times higher than those crosslinked at 15wt.%, effect due to the higher amount of sulfonic acid groups introduced by SSA. The last decomposition stage, occurred between 350 and 600 ºC, is associated to the cleavage of the polymer backbone by chain scission [34], reflecting a weight loss of about 60 %. Table 4.12 summarizes the temperature weight losses extracted from the thermograms curves of each composite.

Table 4.12. Temperature dependent weight loss values extracted from the thermograms of the crosslinked membranes

Composite	Stage I		Stage II (ºC/%)				Stage III	
	T_{peak}	ΔW	$T_{peak\,I}$	ΔW_I	$T_{peak\,II}$	ΔW_{II}	T_{peak}	ΔW
15PVA/sGO	167	30	269	9	-	-	433	31
15sPVA/sGO	163	28	264	9	319	2	439	32
30PVA/sGO	157	22	274	21	-	-	444	22
30sPVA/sGO	153	21	263	21	322	3	446	27
15PVA/GO	166	29	269	9	-	-	432	28
15sPVA/GO	163	28	265	9	322	2	439	32
30PVA/GO	157	24	274	21	-	-	443	24
30sPVA/GO	158	23	264	16	325	3	445	24

According to the results, the composites with lower crosslinking degree show higher thermal stability. This effect is due to the higher amount of hydroxyl groups which stabilize the structure by hydrogen-bonding interactions, in agreement with the FTIR results. On the other hand, the sulfonation of the filler (sGO) does not contribute to enhance the thermal stability of the composites. In addition to show the 30sPVA/sGO composite a strong decrease of the thermal stability due to the catalytic effect that the excess of sulfonic acid groups produce on elimination reactions [40].

Mechanical characterization

The mechanical properties of sGO composites were evaluated from their stress-strain curves measured at room temperature, and compared with the results obtained for the GO composites previously studied in Contribution II [12] as shown in Figure 4.31.
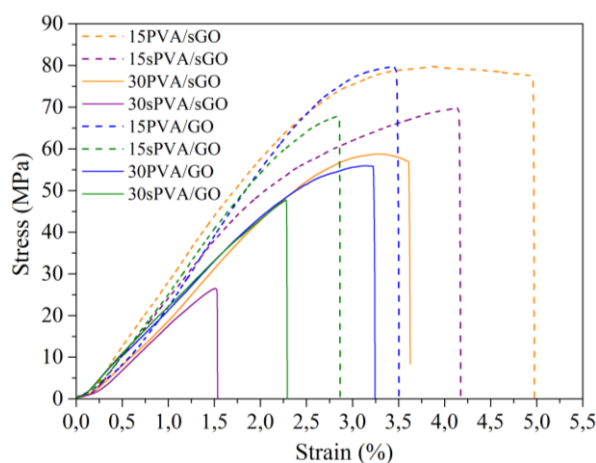
Figure 4.31. Stress-strain curves of sGO and GO composite membranes

Table 4.13 shows the values of tensile strength, Young´s modulus and elongation at break obtained from the stress-strain curves of the composites.

Table 4.13. Values of the mechanical properties of the sGO and GO composite membranes

Composite	Tensile Strength (MPa)	Young´s Modulus (GPa)	Elongation at break (%)
15PVA/sGO	81 ± 3	3.1 ± 0.3	5.0 ± 0.3
15sPVA/sGO	70 ± 2	2.8 ± 0.2	4.2 ± 0.2
30PVA/sGO	59 ± 3	2.4 ± 0.1	3.6 ± 0.3
30sPVA/sGO	27 ± 5	2.1 ± 0.1	1.5 ± 0.2
15PVA/GO	80 ± 4	3.1 ± 0.0	3.4 ± 0.4
15sPVA/GO	68 ± 5	3.0 ± 0.1	2.8 ± 0.2
30PVA/GO	56 ± 3	2.3 ± 0.1	3.2 ± 0.3
30sPVA/GO	48 ± 3	2.2 ± 0.3	2.3 ± 0.3

It could be expected that an increase of crosslinking degree enhances the mechanical properties of the composites. However, the results show the opposite trend. As shown in Table 4.13, the composites with lower crosslinking degree show the highest values of tensile strength, Young´s modulus and elongation at break. The higher amount of hydroxyl groups in the 15PVA/sGO, 15sPVA/sGO, 15PVA/GO and 15sPVA/GO composites stabilizes the structure via hydrogen bonding interactions, resulting in an enhancement of the mechanical properties [42].

The sulfonation of the filler (sGO) improves the mechanical properties of the composites. In comparison, the sulfonic acid groups (-SO$_3$H) introduced in sGO have stronger interaction via hydrogen bonding with the hydroxyl groups (-OH) of PVA matrix than the carboxylic acid groups (-COOH) of the GO. This increase the interfacial adhesion between the filler (sGO) and the polymer matrix, which facilitates the stress transfer across filler-polymer matrix interface improving the mechanical properties of the sGO composites [13], [41].

Nevertheless, the multiple sulfonation in the 15sPVA/sGO and 30sPVA/sGO composites considerable decreases their mechanical behaviour. This effect is much more severe in 30sPVA/sGO composite, exhibiting the lowest values of tensile strength, Young´s modulus and elongation at break. From these results it can be conclude that the multiple sulfonation of the polymer matrix (intra- and inter-sulfonation) and the filler results in a brittle composite with weakened mechanical properties.

Proton-conducting properties

Water Contact Angle

The hydrophilicity of the composites surface was studied by water contact angle. In general, membrane surface hydrophilicity is higher when the contact angle is smaller. Figure 4.32 shows the values of water contact angle and the differences in shape of water droplets onto the surface of the sGO and GO composites.
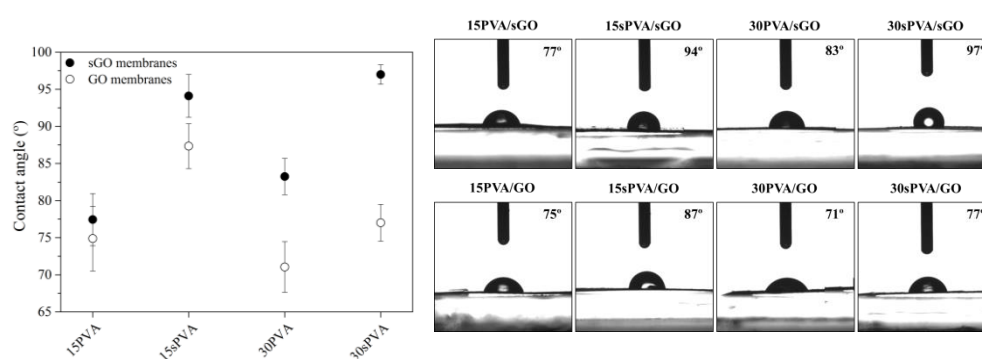
Figure 4.32. Values of water contact angle and differences in shape of water droplets onto the surface of the sGO and GO composites

The results show a considerable increase in the values of water contact angle when the GO is functionalized by sulfonation, indicating an increment of the hydrophobic character of the membrane surface. The 15PVA/sGO, 15sPVA/sGO, 30PVA/sGO and 30sPVA/sGO composites undergoes an increment of water contact angle of 3, 8, 17 and 26 %, respectively, compared to their homologue composites prepared with GO. This evidence the existence of a nano-phase separated morphology in which the hydrophilic groups (sulfonic acid groups and hydroxyl groups) are placed into the interior of the structure interacting each other via hydrogen bonding, whereas the hydrophobic groups are arranged on the surface of the composites [43]. Notice that this effect is more accentuated both in the composites with higher crosslinking degree and the composites prepared from sPVA matrix. The reduction of hydroxyl groups by either crosslinking reaction or functionalization of the polymer matrix (sPVA) further reduce the hydrophilic character of the membranes increasing the water contact angle values.

Water and Methanol Uptake (WU/MU)

Water uptake greatly affects to the proton-conducting properties of proton exchange membranes. In general, a high water uptake leads to an improvement of proton conductivity since protons are transported through the membrane with the water molecules. However, an excess of water can cause undesired side effects including high methanol permeability, low dimensional stability and low mechanical integrity [15], [44], [45].

The water and methanol uptake of the sGO composites were measured as a function of temperature, and the results were compared with those obtained for the GO composites [12]. Table 4.14 lists the values of water and 2M methanol uptake measured at 30, 35, 40 and 45 ºC for the composites.

Table 4.14. Water uptake and methanol uptake values of the composites as a function of temperature

Composite	Water Uptake (%)			
	30ºC	35ºC	40ºC	45ºC
15PVA/sGO	39.2 ± 0.9	42.5 ± 0.7	44.9 ± 0.4	45.3 ± 0.8
15sPVA/sGO	26.6 ± 0.8	29.2 ± 0.5	32.1 ± 0.6	33.5 ± 0.7
30PVA/sGO	31.9 ± 0.6	32.6 ± 0.3	33.7 ± 0.7	37.9 ± 0.9
30sPVA/sGO	22.2 ± 0.1	25.4 ± 0.3	27.6 ± 0.4	29.9 ± 0.5
15PVA/GO	41.0 ± 0.8	44.0 ± 0.2	46.8 ± 0.4	49.2 ± 0.5
15sPVA/GO	33.6 ± 0.7	36.0 ± 0.8	39.6 ± 0.5	43.0 ± 0.7
30PVA/GO	33.0 ± 0.6	36.2 ± 0.8	37.8 ± 0.9	42.9 ± 0.5
30sPVA/GO	31.8 ± 0.6	33.2 ± 0.7	35.9 ± 0.7	38.3 ± 0.9

Composite	Methanol Uptake (%)			
	30ºC	35ºC	40ºC	45ºC
15PVA/sGO	38.4 ± 0.2	40.1 ± 0.7	41.1 ± 0.9	43.8 ± 0.4
15sPVA/sGO	25.0 ± 0.3	27.7 ± 0.4	28.9 ± 0.5	31.5 ± 0.6
30PVA/sGO	30.3 ± 0.5	31.6 ± 0.4	32.2 ± 0.6	36.1 ± 0.9
30sPVA/sGO	21.6 ± 0.1	24.2 ± 0.2	26.5 ± 0.3	27.7 ± 0.2
15PVA/GO	39.7 ± 0.9	42.9 ± 0.4	46.0 ± 0.3	48.2 ± 0.4
15sPVA/GO	32.5 ± 0.6	34.1 ± 0.3	37.0 ± 0.8	39.1 ± 0.3
30PVA/GO	31.7 ± 0.5	34.4 ± 0.7	37.4 ± 0.8	41.0 ± 0.4
30sPVA/GO	29.7 ± 0.4	31.7 ± 0.6	33.3 ± 0.7	34.4 ± 0.7

In addition, Figure 4.33 depicts the evolution of the water and methanol uptake of the composites as a function of temperature.
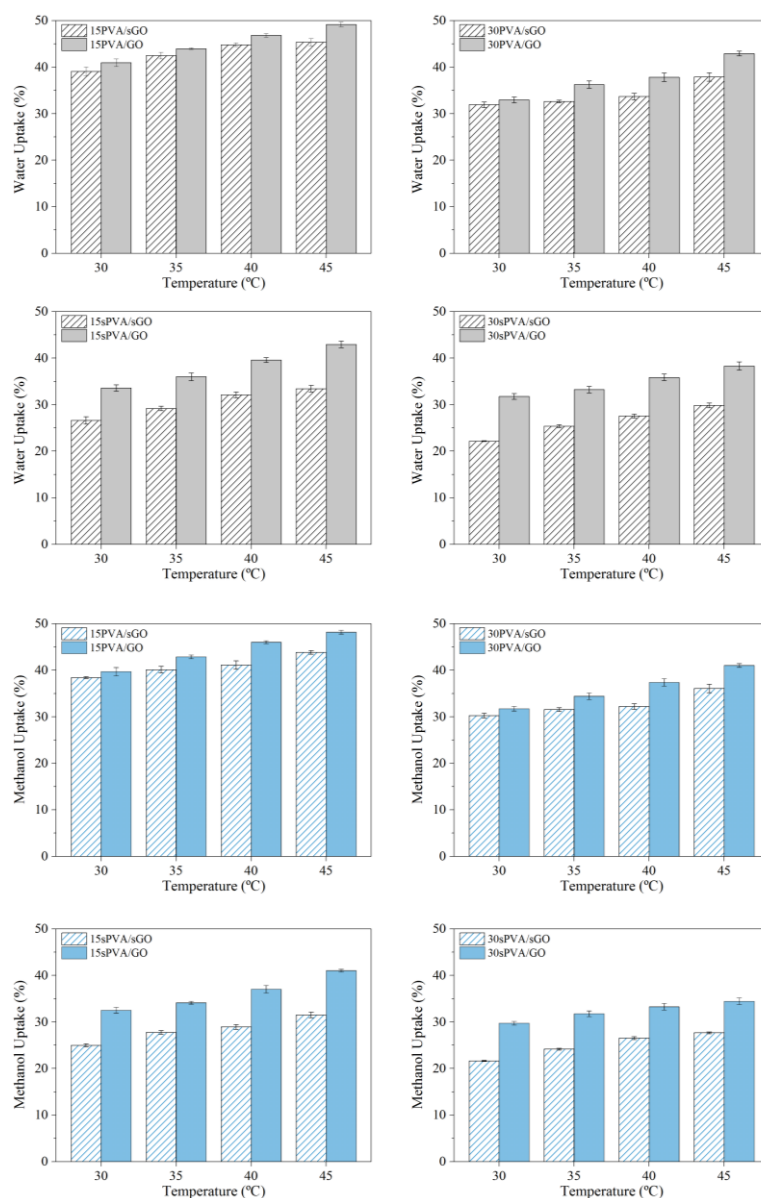
Figure 4.33. Evolution of water uptake (WU) and methanol uptake (MU) of the composites as a function of temperature

All the composites show an increasing trend of water uptake with temperature. An increase in temperature favors the mobility of the polymer chains resulting in a larger free volume to accommodate water molecules [44], [46]. Moreover, the degree of crosslink directly affects to the absorption properties of the composites. When the composites are crosslinked at 30 wt% of SSA the mobility of the polymer chains is strongly reduced due to the formation of a greater amount of covalent bonds during the crosslinking reaction than in the composites crosslinked at 15 wt.% of SSA. Therefore, the composites become more compact and rigid, hindering the absorption of water molecules [44], [47]. On the other hand, both the sulfonation of the polymer matrix (sPVA) and the filler (sGO) strongly reduces the water uptake of the composites. The existence of strong hydrogen bonding interactions between the sulfonic acid groups and the remaining hydroxyl groups improves the interfacial adhesion and compatibility between the filler and the polymer matrix. This results in a more compact structure in the composites with narrower water transferring channels, showing lower water absorption and improved dimensional stability [18], [41]. These results are in agreement with the obtained values of water contact angle.

Finally, methanol uptake shows a similar trend as the water uptake, as shown in Figure 4.33. However, all the composites exhibit methanol uptake values lower than those for water uptake, confirming that the PVA matrix has higher affinity towards water rather than methanol [43].

Ion Exchange Capacity (IEC)

The IEC is a measure the ion exchangeable sites in proton exchange membranes that is directly related to proton conductivity. Figure 4.34 compares the values of IEC obtained for the sGO and the GO composite membranes measured at room temperature. According to the results, the IEC values increase with increasing the concentration of sulfonic acid groups (-SO_3H) in the composites. In this context, the sGO composites show higher IEC values that those prepared with GO, since the acidic character of the sulfonic acid groups (-SO_3H) of the sGO is stronger than the carboxylic acid groups (-COOH) present in GO [13], [14]. The IEC values of sGO and GO composites range from 0.71 to 1.15 mequiv/g and 0.61 to 1.02 mequiv/g, respectively. The 30sPVA/sGO composite exhibits the highest value of IEC, exhibiting an increase of 19 % respect to the 30PVA/GO composite. This result is attributed to the triple sulfonation of the membrane by means of the crosslinker agent (SSA), polymer matrix (sPVA) and filler (sGO).
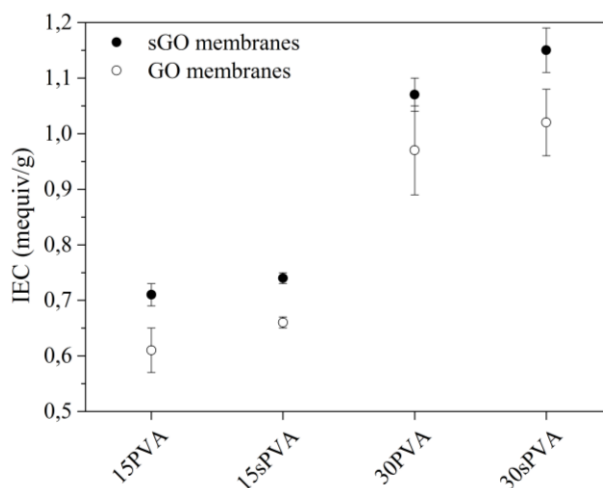
Figure 4.34. Comparison of the Ion Exchange Capacity (IEC) values of the sGO and GO composites

Proton Conductivity (σ_{prot})

Proton conductivity is a very important factor to determine the performance of a PEM in a fuel cell. The proton mobility in PEMs is strongly influenced by the water uptake. Water molecules can exist in two different forms in hydrated membranes: linked-water and free water. The mechanisms through which water molecules transport the protons are Grotthus and Vehicular mechanisms. In Grotthus mechanism the protons jump from one linked-water molecule ($H_3O^+SO_3^-$) to the next molecule, while in the Vehicular mechanism the protons diffuse together with the free water molecules by forming the complex H_3O^+ [48].

The proton conductivity of composites was studied from impedance measurements in the temperature range from 30 to 90 ºC. Bode diagram plots the log |Z| versus log f. In order to calculate the proton conductivity, the protonic resistance R was taken from the Bode plot in the high frequencies range, in which the value of log |Z| becomes constant and the phase angle reaches its maximum value [23]. Figure 4.35 shows the Bode diagrams of the pre-hydrated composites measured at 30 ºC as an example.
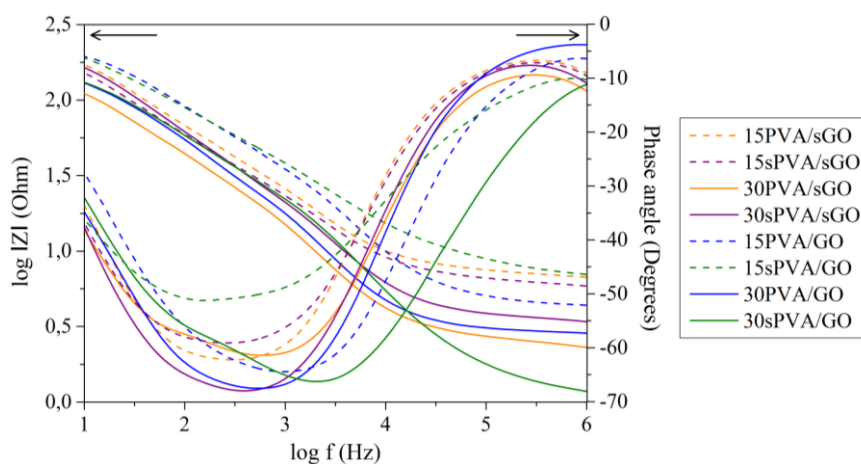
Figure 4.35. Bode diagram of the pre-hydrated composites measured at 30 ºC

The obtained values of proton conductivity of the pre-hydrated composites are listed in Table 4.15, and the evolution of the proton conductivity as a function of temperature is also shown in Figure 4.36.

Table 4.15. Proton conductivity (σ_{prot}) values of the pre-hydrated composites measured at 30, 50, 70 and 90 ºC

Composite	σ_{prot} (mS/cm)			
	30 ºC	50 ºC	70 ºC	90 ºC
15PVA/sGO	0.80	1.45	1.63	1.08
15sPVA/sGO	0.70	1.72	3.02	2.11
30PVA/sGO	2.18	7.38	15.34	17.01
30sPVA/sGO	1.38	5.22	11.48	13.54
15PVA/GO	0.88	2.26	4.57	4.90
15sPVA/GO	0.97	2.23	6.16	6.24
30PVA/GO	1.61	3.39	6.93	11.82
30sPVA/GO	4.96	8.42	15.80	20.96
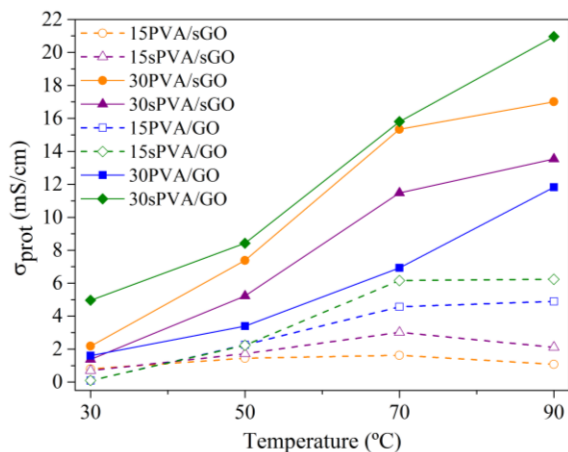
Figure 4.36. Evolution of proton conductivity (σ_{prot}) of pre-hydrated composite membranes as a function of temperature

In general, the temperature contributes to enhance the proton conductivity of the composites. The mobility of the polymer chains is favored with temperature, promoting the proton transport through the membrane. It can be clearly seen that the composites with higher crosslinking degree show a positive temperature dependence of proton conductivity from 30 to 90 ºC. In contrast, the proton conductivity of the composites with lower crosslinking degree exhibit a slightly decrease or no vary above 70 ºC, which is attributed to the evaporation of the higher amount of free water contained in these membranes [41], [46].

The crosslinking degree strongly affects to proton conductivity of the composites, since the crosslinking agent SSA contains sulfonic acid groups in its structure that favor the proton conduction. Thus, the composites crosslinked at 30 wt.% of SSA show the higher values of proton conductivity [33], [49]. In addition, the proton conductivity increases in all cases by sulfonation of the polymer matrix except for the 30sPVA/sGO composite, which shows lower values of proton conductivity than the 30PVA/sGO composite. This can be attributed to the low water uptake (22 % at 30 ºC) that 30sPVA/sGO composite membrane shows. Hence, not only the introduction of sulfonic acid groups is a requirement, but also it is needed an appropriate water uptake to reach high values of proton conductivity in composite membranes [20].

It is noteworthy that the sulfonation of the filler (sGO) does not significantly affect to the proton conductivity of the composites. Only it is possible to observe a strongly increase of the proton conductivity for the 30PVA/sGO composite in all the range of temperature.

The dependence of proton conductivity with temperature can be taken as an indicator for a particular type of proton conduction mechanism. Generally, it can be distinguish two different systems, those that show linearity in log σ_{prot} versus 1/T according to Arrhenius behaviour, or those which present a curvature, diverting from the linear Arrhenius behaviour. In the latter case, empirical equations derived from the free volume theory, as for example the Vogel-Tamman-Fulcher (VTF) equation [50]–[53], are used for the experimental data fitting. The proton conductivity in polymer systems depends not only on the density of charge carriers, their type and mobility, but also on the macromolecular conformational changes affecting the free volume.

When the proton conductivity takes place through the Grotthus mechanism or proton hopping process, the temperature dependence is well fitted by the Arrhenius equation,

$$\log \sigma_{\mathbf{prot}} = \log \sigma_0 - \frac{E_a}{RT}$$

where σ_{prot} is the proton conductivity (*S/cm*), σ_0 is a pre-exponential factor, E_a is the activation energy (*kJ/mol*), *R* is the universal gas constant (*8.314 J/mol K*), and *T* is the absolute temperature (*K*).

In contrast, when the proton conductivity proceeds through Vehicular mechanism a non-linear behaviour is observed. In this case, the dependence of proton conductivity with temperature is best fitted with the VTF equation, indicating that segmental motions within the polymer play a significant role in the proton transport mechanism,

$$\log \sigma_{\mathbf{prot}} = \log \sigma_0 - \frac{B}{T - T_0}$$

where σ_{prot} and *T* are the proton conductivity (S/cm) and the absolute temperature (K), respectively. σ_0, *B* and T_0 are fitting parameters which correspond to the maximum number of charge carriers in the system, the pseudo-activation energy of vibration motion of macromolecular segments, and the so-called Vogel temperature below which rapid transport of protons vanishes, respectively.

In PEMs, the proton conduction at low water content is dominated by polymer segmental motion (VTF behaviour). However, at high water content, the proton transport mechanism is much more liquid-like with some polymeric influence, showing an Arrhenius behaviour. Therefore, the proton transfer is largely dependent on the water content in the membrane [54], [55].

The dependence of proton conductivity with temperature, $\log \sigma_{prot}$ versus $1/T$ plot, of the pre-hydrated composites is shown in Figure 4.37.
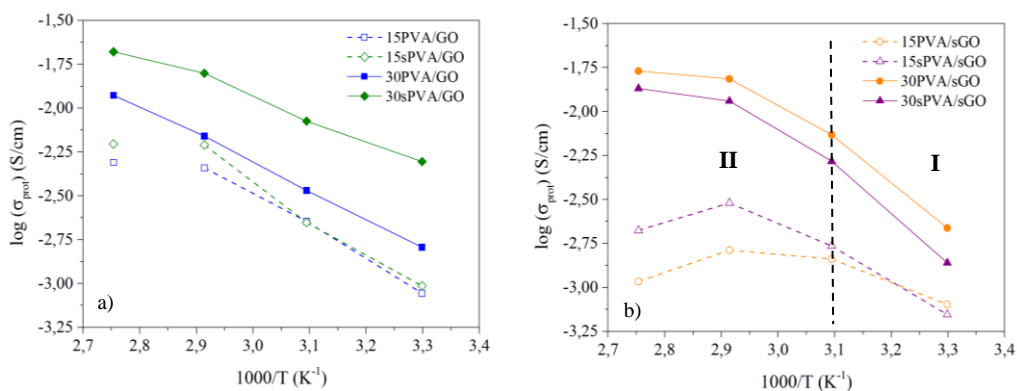
Figure 4.37. Plot of log σ_{prot} vs 1000/T for the pre-hydrated a) GO and b) sGO composites

According to the results shown in Figure 4.37a, the dependence of proton conductivity with temperature for the GO composites follows an Arrhenius behaviour, suggesting that proton conduction takes place by means of Grotthus mechanism. The 30PVA/GO and 30sPVA/GO composites show a linear dependence in all the range of temperature. Nevertheless, the 15PVA/GO and 15sPVA/GO composites exhibit no-linearity beyond 70 ºC, which can be attributed to the evaporation of the higher amount of water that these composites absorb [12].

In contrast, the dependence of proton conductivity of the sGO composites with temperature is not exactly linear in the range from 50 to 90 ºC, as shown in Figure 4.37b, suggesting non-Arrhenius behaviour. It is possible differentiate two different regions in the log σ_{prot} vs 1000/T plot, I and II. In region I, from 30 to 50 ºC, a typical Arrhenius behaviour is observed, in which the Grotthus mechanism is predominant for proton conduction. While in region II, from 50 to 90 ºC, the dependence of σ_{prot} with temperature shows the typical VTF behaviour, indicating that segmental motion of the polymer matrix becomes the dominate factor in the proton transfer mechanism. These results suggest that the proton conductivity at high temperature took place mainly via Vehicular mechanism, in agreement with the low values of water uptake obtained for the sGO composites. Similarly to GO composites, the 15PVA/sGO and 15sPVA/sGO composites show a sharp decrease of proton conductivity beyond 70 ºC attributed to the evaporation of free water.

In Table 4.16 are listed the fitting values of log σ_0, B and T_0 parameters to VFT equation for sGO composite with higher crosslinking degree (30PVA/sGO and 30sPVA/sGO).

Table 4.16. VFT fitting parameters for the 30PVA/sGO and 30sPVA/sGO membranes

Composite	log σ_0 (S/cm)	B (K)	T_0 (K)	R^2
30PVA/sGO	-1.29	0.34	272	0.97
30sPVA/sGO	-1.31	0.41	274	0.98

The experimental data shows a good fitting to VFT equation, as can be seen from the R^2 values. The multiple sulfonation in the 30sPVA/sGO composite leads to a decrease of the log σ_0, suggesting that in spite of the higher amount of charge carriers groups (-SO$_3$H groups) in its structure, their availability for proton conduction is restricted. This is directly related to the increase of T_0 that is associated to a higher rigidity of the 30sPVA/sGO composite in comparison with the 30PVA/sGO. The increase in rigidity hinders the segmental motion of the polymer chains in the 30sPVA/sGO composite decreasing its proton conductivity. Moreover, the parameter B, related to activation energy of motion of macromolecular segments, is higher for the 30sPVA/sGO composite, corroborating that the multiple-sulfonation restricts the polymer segmental motion [56].

Low electrical conductivity is also one of the requirements that a PEM must to meet in order to avoid the pass of electrons through the membrane. Table 4.17 shows the values of electrical conductivity (σ_{elec}) of the studied composites. All composites exhibit low electrical conductivity (10^{-10} S/cm), confirming that both the sGO and GO composites are good electrical insulators.

Table 4.17. Electrical conductivity (σ_{elec}) values of the composites measured at 30 ºC

Composite	$\sigma_{elec} \times 10^{10}$ (S/cm)
15PVA/sGO	1.38
15sPVA/sGO	9.43
30PVA/sGO	5.30
30sPVA/sGO	15.1
15PVA/GO	0.16
15sPVA/GO	1.02
30PVA/GO	0.18
30sPVA/GO	1.47

H_2-O_2 fuel Cell test

The performance of the composites in a hydrogen single cell was studied from the polarization curves measured at 25 ºC shown in Figure 4.38.
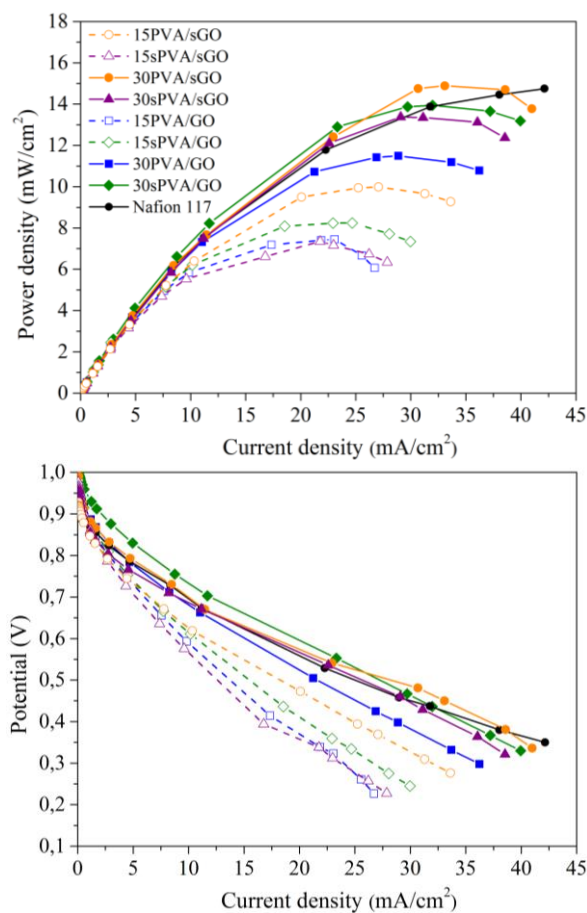
Figure 4.38. Comparison of the polarization curves of the sGO and GO composites with Nafion 117 at 25 ºC

The values of maximum power density (P_{max}) obtained for each composite are summarized in Table 4.18. According to the results, higher crosslinking degree affects positively to the performance of the composites in a H_2-O_2 fuel cell, showing the composites crosslinked at 30 wt.% of SSA the highest values of P_{max}. This improvement is attributed to the higher amount of sulfonic acid groups (-SO_3H)

introduced by SSA in the structure of the 30PVA/sGO, 30sPVA/sGO, 30PVA/GO and 30sPVA/GO composites, which enhance the proton conduction via Grotthus mechanism [32]. Among all the membranes with higher crosslinking degree, the 30PVA/sGO composite exhibits the highest value of P_{max} with an improvement of 30 % in comparison with the 30PVA/GO composite. In contrast, the multiple sulfonation in the 30sPVA/sGO composite does not improve its performance of fuel cell as can be expected, but rather it is decreased by a 8 % respect to the 30PVA/sGO composite, in agreement with the values of proton conductivity.

For comparison, Nafion 117 membrane was measured at the same operating conditions. The value of P_{max} obtained for Nafion 117 was 14.7 mW/cm^2, while the values for the composites range from 7.4 to 14.8 mW/cm^2, indicating that the prepared sGO and GO composites are feasible candidates to be used as PEMs in H_2-O_2 fuel cells.

Table 4.18. Maximum power density (P_{max}) values of the sGO and GO composites compared to Nafion 117 at 25 ºC

Composite	P_{max} (mW/cm^2)
15PVA/sGO	10.5 ± 0.3
15sPVA/sGO	7.4 ± 0.1
30PVA/sGO	14.8 ± 0.1
30sPVA/sGO	13.5 ± 0.2
15PVA/GO	7.4 ± 0.1
15sPVA/GO	8.3 ± 0.3
30PVA/GO	11.4 ± 0.1
30sPVA/GO	13.9 ± 0.5
Nafion 117	14.7 ± 0.3

Methanol diffusion coefficients (D$_{MeOH}$)

Methanol permeability is an important consideration in DMFC applications, since the crossover of methanol from the anode to the cathode leads to a lower cell voltage and decreased fuel efficiency. Hence, the methanol diffusion coefficients of the composites that shown the better performances in H$_2$-O$_2$ fuel cell test (30PVA/GO, 30PVA/sGO, 30sPVA/GO and 30sPVA/sGO composites) were measured at 30 ºC in order to evaluate the suitability of these composites as PEMs in DMFCs. Moreover, the obtained results were compared with their respective membranes free-standing of filler and with the Nafion 117 reference membrane measured at the same experimental conditions. The rate of mass loss of methanol through the membranes was recorded as a function of time as shown in Figure 4.39.
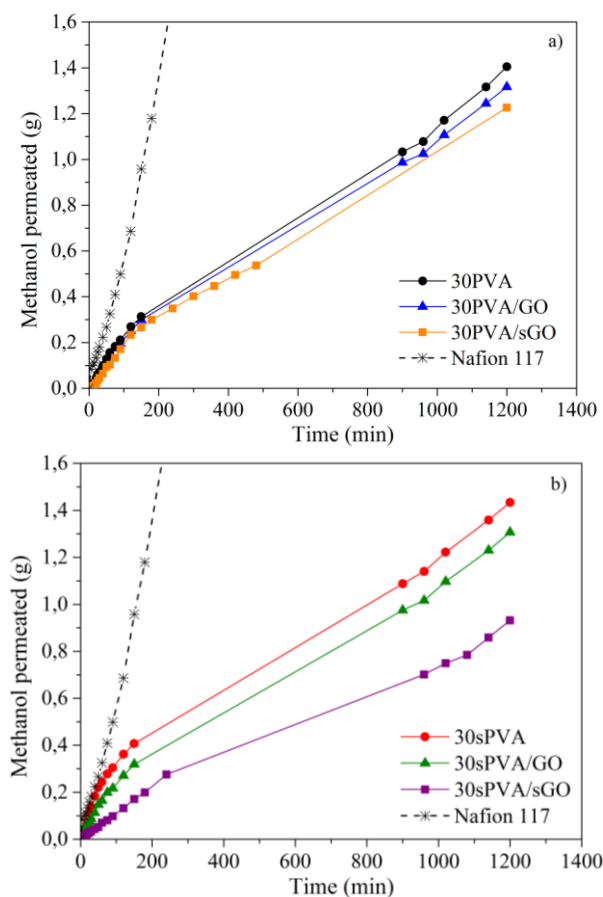
Figure 4.39. Comparison of permeation curves of the a) PVA-based and b) sPVA-based composites with their homologues free-standing of filler and Nafion 117 membrane

Table 4.19 lists the methanol diffusion coefficient values (D_{MeOH}) calculated for each of the assayed membrane.

Table 4.19. Methanol diffusion coefficients (D_{MeOH}) and methanol selectivity (Φ) values of the assayed membranes at 30 ºC

Composite	$D_{MeOH} \times 10^8$ (cm^2/s)	Φ (S·s·cm^{-3})
30PVA	3.39	0.47×10^5
30PVA/GO	1.98	0.80×10^5
30PVA/sGO	1.84	1.20×10^5
30sPVA	2.12	1.18×10^5
30sPVA/GO	1.62	3.10×10^5
30sPVA/sGO	0.99	1.41×10^5
Nafion 117	16.43	0.80×10^5

The methanol diffusion coefficients obtained for the PVA and sPVA-based membranes are about one order of magnitude lower than that of Nafion 117 membrane measured under the same experimental conditions, corroborating the low affinity of the PVA polymer for methanol [44], [57].

Among all the membranes, the sGO composites showed the lowest values of D_{MeOH}, 1.84×10^{-8} and 0.99×10^{-8} cm^2/s for the 30PVA/sGO and 30sPVA/sGO composites, respectively. These results suggest that the addition of sGO nanoplatelets into the polymer matrix reduces more effectively the methanol crossover through the membrane than the GO nanoplatelets. The sulfonic acid groups of the sGO nanoplatelets strongly interact with the hydroxyl groups of the polymer matrix improving the filler-matrix interfacial adhesion; this results in a compact structure of the composites and restricts their free volume to accommodate methanol molecules so reducing their methanol diffusion coefficients [15], [44], in agreement with the results obtained of methanol uptake.

In addition, an ideal PEM should also possess a high methanol selectivity (Φ), which is defined as the ratio of proton conductivity to methanol diffusion coefficient [44], for DMFCs applications. Table 4.19 also summarizes the methanol selectivity values calculated for each of the assayed membranes. According to the results, the incorporation of a nano-filler into the polymer matrix increases the Φ values of the composites compared to the membranes free-standing of filler [20]. This effect is enhanced by either the sulfonation of the polymer matrix (sPVA) or the filler (sGO), as a combination of lower methanol diffusion coefficients and higher proton conductivity

values [14], [18]. The highest value of Φ was obtained for the 30sPVA/GO membrane $(3.1 \times 10^5$ S·s·cm$^{-3})$, showing an improvement of 163 % in comparison with its homologue 30sPVA membrane free-standing of filler. However, the 30sPVA/sGO composite despite showing the lowest value of D_{MeOH}, it does not reach the highest value of methanol selectivity. This fact is attributed to the low proton conductivity, 1.38 mS/cm, that the 30sPVA/sGO composite shown [58]. Moreover, the composites exhibit higher methanol selectivity values than Nafion 117. It is noteworthy that though the proton conductivity of Nafion 117 is much higher than that of the composites, its high methanol diffusion coefficient leads to a sharp decrease of the methanol selectivity. Therefore, it can be conclude that the used of these composites as PEMs in DMFCs applications can mitigate the problem of methanol crossover.

DMFC test

Finally, the performance of the 30sPVA/GO and 30PVA/sGO composites PEMs was evaluated in a DMFC at 50 ºC with different concentrations of methanol. Among all the prepared composites, only the 30sPVA/GO and 30PVA/sGO composites were selected for the DMFC test due to their good performance in H$_2$-O$_2$ fuel cell and their high methanol selectivity. A first sifting using a 1M methanol concentration were conducted in order to corroborate that the addition of both GO and sGO nanoplatelets improves the maximum power density (P_{max}) of the composites in comparison with the base 30PVA membrane free-standing of filler. Figure 4.40 compares the DMFC polarization curves of the 30sPVA/GO and 30PVA/sGO composites with the base 30PVA membrane fed with a 1M methanol concentration.
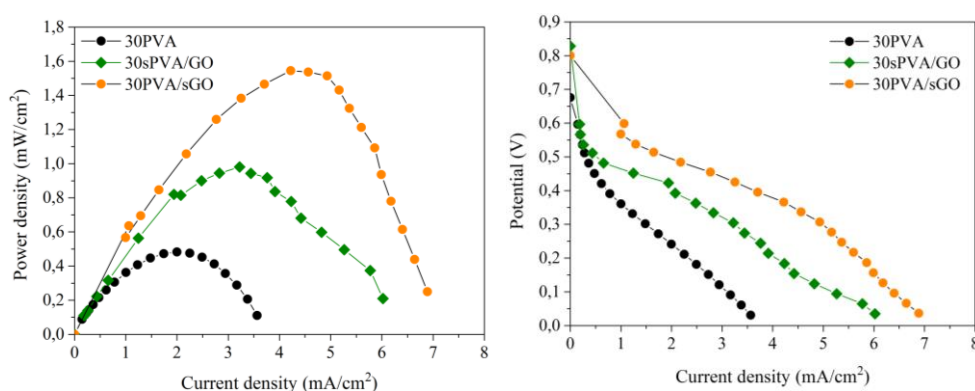
Figure 4.40. Comparison of the DMFC polarization curves of the 30sPVA/GO and 30PVA/sGO composites with the base 30PVA membrane fed with a 1M methanol concentration at 50 ºC

The results show an improvement of the DMFC performance for the 30sPVA/GO and 30PVA/sGO composites as compared to the base 30PVA membrane. However, the

highest P_{max} value (1.54 mW/cm^2) was reached for the 30PVA/sGO composite, showing an improvement of 57 % respect to the 30sPVA/GO composite and of 220 % for the 30PVA membrane.

In addition, the performance of the 30sPVA/GO and 30PVA/sGO composites in a DMFC was evaluated as a function of the concentration of the methanol fed. Figure 4.41 compares the polarization curves of each composite measured at different methanol feed concentration.
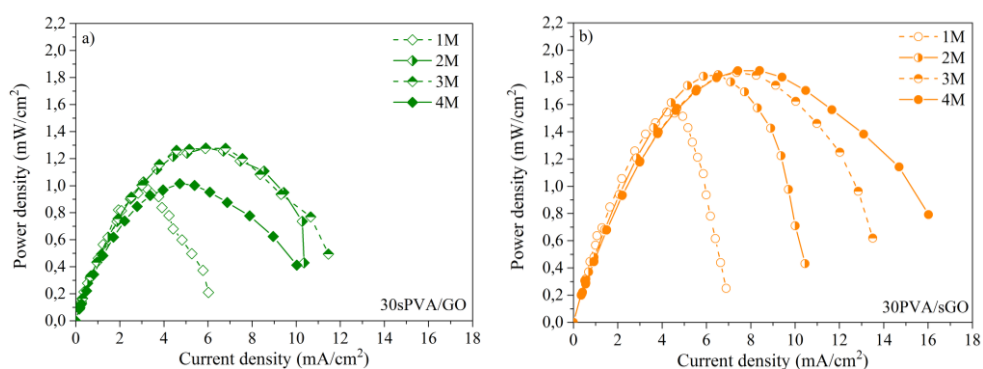
Figure 4.41. Comparison of the polarization curves of the a) 30sPVA/GO and b) 30PVA/sGO composites obtained in a DMFC operating at 50 ºC and fed with 1, 2, 3 and 4M methanol concentration

The average values of P_{max} obtained for the 30sPVA/GO and 30PVA/sGO composites at the different methanol feed concentration are compared in Figure 4.42.
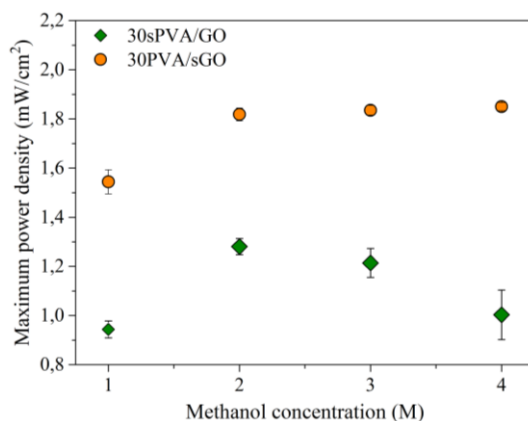
Figure 4.42. Maximum power density (P_{max}) average values of the 30sPVA/GO and 30PVA/sGO composites as a function of the methanol feed concentration

According to the results, a considerable increase of the P_{max} is observed with increasing the methanol concentration from 1M to 2M in both composites. It was found that the values of P_{max} for the 30sPVA/GO composite progressively decrease from 2M to 4M methanol concentration [59], [60]. Thus, 2M methanol concentration can be considered as the optimal feed concentration for the 30sPVA/GO composite since it reaches the highest value of P_{max} (1.28 mW/cm^2). In contrast, the values of P_{max} for the 30PVA/sGO composite remain practically constant (~1.83 mW/cm^2) beyond 2M methanol concentration, indicating a good methanol barrier property of the composite even at high methanol feed concentration.

The influence of methanol concentration on the OCV values for the 30PVA, 30sPVA/GO and 30PVA/sGO membranes were evaluated, and compared with the reference Nafion 117 membrane measured at the same operating conditions. Table 4.20 summarizes the values of OCV obtained for each membrane as a function of the methanol feed concentration.

Table 4.20. Open Circuit Voltage (OCV) values of the 30PVA, 30sPVA/GO, 30PVA/sGO and Nafion 117 membranes as a function of the methanol feed concentration

Membrane	OCV (V)			
	1M	2M	3M	4M
30PVA	0.67	-	-	-
30PVA/sGO	0.80	0.76	0.74	0.74
30sPVA/GO	0.83	0.76	0.69	0.69
Nafion 117	0.76	0.72	0.69	0.68

In general, the open circuit voltage (OCV) decreases when the concentration of methanol is higher due to the higher probability that methanol crossover occurs though the membrane creating a larger mixed potential on the cathode [61]. The 30sPVA/GO and 30PVA/sGO composites exhibit higher OCV values than the base 30PVA membrane at 1M methanol concentration and the Nafion 117 membrane in all the range of methanol concentration. This increase in the OCV is associated with a decrease of methanol crossover [41], [62], [63]. It is noteworthy that the 30PVA/sGO composite show higher OCV values in the range from 2M to 4M methanol concentration than the 30sPVA/GO composite. This can be related to the better DMFC performance that the 30PVA/sGO composite show in comparison with the 30sPVA/GO composite at higher methanol concentrations, probably by reduction of the mixed-potential losses. Therefore, it can be conclude that the PVA-based

composites prepared in this study, in particular the 30PVA/sGO composite, can be act as effective methanol barriers in DMFC.

Finally, the maximum power density values obtained with a 2M methanol feed concentration for the 30sPVA/GO (1.28 mW/cm^2) and 30PVA/sGO (1.82 mW/cm^2) membranes were compared with those obtained for Nafion 117 membrane (10.37 mW/cm^2) in the Figure 4.43. The results show a strong decrease of P$_{max}$ for both composites, 10 times lower than the Nafion 117 membrane, despite showing higher values of OCV. This effect can be attributed to the high proton conductivity that Nafion 117 membrane show (0.0144 S/cm at 50 ºC) measured under the same conditions that the studied composites.
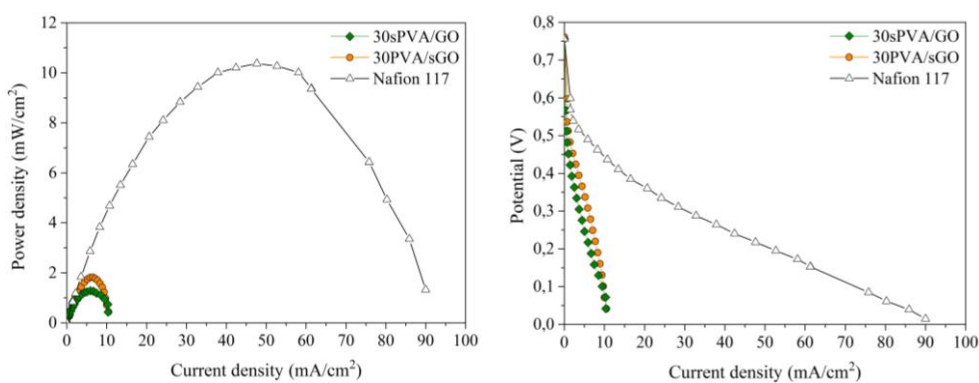
Figure 4.43. Comparison of the DMFC polarization curves of the 30sPVA/GO and the 30PVA/sGO composites with the Nafion 117 membrane operating at 50 ºC and with a methanol feed concentration of 2M

Conclusions

Hybrid organic-inorganic composites based on PVA with embedded sulfonated graphene oxide (sGO) were prepared by solution-casting method and their potential as proton exchange membranes for DMFC applications was evaluated. Additionally, the polymer matrix was structurally modified via bi-sulfonation in order to improve the proton conductivity of the prepared composites. To this end, the PVA matrix was first intra-sulfonated using propane sultone as sulfonating agent, and then further crosslinked with SSA at two different concentrations, 15 and 30 wt.%. It was expected that the dispersion of sGO nano-platelets into the PVA matrix could change the initial morphology of the composites creating new hydrophilic/hydrophobic domains that favor the proton conduction.

The results showed that the introduction of sGO nano-platelets enhance the mechanical properties of the composites as compared to those prepared with GO. The sulfonic acid groups contained in the sGO improve the interfacial adhesion between the filler and the polymer matrix via hydrogen bonding interactions so the stress transfer through the composite is favored. On the other hand, the water contact angle measurements reveal the existence of hydrophobic and hydrophilic domains in the composites, thus creating proton transport channels across the composite membrane. Moreover, the addition of sGO nano-platelets blocks more effectively the pass of solvent molecules through the membrane than those prepared from GO, showing lower values of water and methanol uptake.

The proton conductivity of the composites was investigated as a function of the type of filler added (GO or sGO) and temperature. As it was expected, proton conductivity increases with temperature in all cases. Moreover, it could be observed that the dependence of the proton conductivity with temperature for the GO composites follows an Arrhenius behaviour in all the range of temperature indicating that the proton conduction takes place through Grotthus mechanism. In contrast, for the sGO composites, a deviation from the Arrhenius behaviour is observed at high temperatures. In this case, the dependence of proton conductivity with the temperature fits to the typical VTF behaviour, denoting the prevalence of the Vehicular mechanism for the proton conduction. It is noteworthy that the multiple sulfonation proposed in this study was partially effective. When all the components were sulfonated, case of the 30sPVA/sGO composite, a strong decrease of the proton conductivity from 20.96 mS/cm for the 30sPVA/GO composite to 13.54 mS/cm for the 30sPVA/sGO composite at 90 °C was observed. Nevertheless, the values of maximum power density obtained from the H_2-O_2 fuel cell test were quite similar for the 30PVA/sGO composite (14.8 mW/cm^2) and the 30sPVA/sGO composite (13.5 mW/cm^2).

Finally, in order to evaluate the performance of the most promising composites in a DMFC, measurements of their methanol diffusion coefficients and DMFC tests were performed. The methanol permeation experiments showed a good methanol selectivity

for the 30PVA/sGO composite (1.20×10^5 S·s·cm^{-3}) and the 30sPVA/GO composite (3.10×10^5 S·s·cm^{-3}), behaving as an excellent methanol barrier. These results are in agreement with the high values of OCV that both composites shown (0.76 V) at 50 ℃ with a 2M methanol concentration, indicating lower methanol crossover. In spite of showing lower values of OCV, the reference Nafion 117 membrane achieved a much higher value of maximum power density (10.37 mW/cm^2) than the prepared composites in the DMFC test due to its high proton conductivity (0.0144 S/cm at 50 °C).

Acknowledgements

References

[1] K. Pourzare, Y. Mansourpanah, and S. Farhadi, "Advanced nanocomposite membranes for fuel cell applications : a comprehensive review," Biofuel Res. J., vol. 12, pp. 496–513, 2016.

[2] Walter Grot, *Fluorinated Ionomers*. Second Edition, Elsevier, 2008.

[3] Günther G. Scherer, *Fuel Cells I (Advances in Polymer Science)*, 1st ed. Springer, 2008.

[4] S. J. Peighambardoust, S. Rowshanzamir, and M. Amjadi, "Review of the proton exchange membranes for fuel cell applications," Int. J. Hydrogen Energy, vol. 35, no. 17, pp. 9349–9384, 2010.

[5] C. Houchins, G. J. Kleen, J. S. Spendelow, J. Kopasz, D. Peterson, N. L. Garland, D. L. Ho, J. Marcinkoski, K. E. Martin, R. Tyler, and D. C. Papageorgopoulos, "U.S. DOE Progress Towards Developing Low-Cost, High Performance, Durable Polymer Electrolyte Membranes for Fuel Cell Applications," Membranes (Basel)., vol. 2, no. 4, pp. 855–878, Dec. 2012.

[6] Y.-F. Lina, Y.-H. Hsiaoa, C.-Y. Yena, C.-L. Chiangb, C.-H. Leea, C.-C. Huanga, C.-C. M. Ma, "Sulfonated poly(propylene oxide) oligomers/Nafion® acid-base blend membranes for DMFC," J. Power Sources, vol. 172, no. 2, pp. 570–577, Oct. 2007.

[7] K. Dutta, S. Das, and P. P. Kundu, "Partially sulfonated polyaniline induced high ion-exchange capacity and selectivity of Nafion membrane for application in direct methanol fuel cells," J. Memb. Sci., vol. 473, pp. 94–101, Jan. 2015.

[8] Y.-T. Kim, K.-H. Kim, M.-K. Song, and H.-W. Rhee, "Nafion/ZrSPP composite membrane for high temperature operation of proton exchange membrane fuel cells," Curr. Appl. Phys., vol. 6, no. 4, pp. 612–615, Jul. 2006.

[9] D. H. Jung, S. Y. Cho, D. H. Peck, D. R. Shin, and J. S. Kim, "Preparation and performance of a Nafion®/montmorillonite nanocomposite membrane for direct methanol fuel cell," J. Power Sources, vol. 118, no. 1–2, pp. 205–211, May 2003.

[10] V. Baglio, A. S. Aricò, A. Di Blasi, V. Antonucci, P. L. Antonucci, and S. Licoccia, "Nafion–TiO_2 composite DMFC membranes: physico-chemical properties of the filler versus electrochemical performance," Electrochim. Acta, vol. 50, no. 5, pp. 1241–1246, Jan. 2005.

[11] S. C. Sánchez-Ballester, A. Ribes-Greus, V. Soria, G. Rydzek, K. Ariga, "Bi-sulfonation of poly(vinyl alcohol)/Graphene oxide composite membranes for Proton Exchange Membrane Fuel Cell applications. Part 1: Membrane preparation and characterization," *In Preparation*.

[12] S. C. Sánchez-Ballester, A. Ribes-Greus, V. Soria, G. Rydzek, K. Ariga "Bi-sulfonation of poly(vinyl alcohol)/Graphene oxide composite membranes for Proton Exchange Membrane Fuel Cell applications. Part 2: Functional membrane properties," *In Preparation*.

[13] H. Beydaghi, M. Javanbakht, and E. Kowsari, "Synthesis and Characterization of Poly(vinyl alcohol)/Sulfonated Graphene Oxide Nanocomposite Membranes for Use in Proton Exchange Membrane Fuel Cells (PEMFCs)," Ind. Eng. Chem. Res., vol. 53, no. 43, pp. 16621–16632, 2014.

[14] Y. Heo, H. Im, and J. Kim, "The effect of sulfonated graphene oxide on Sulfonated Poly (Ether Ether Ketone) membrane for direct methanol fuel cells," J. Memb. Sci., vol. 425–426, pp. 11–22, 2013.

[15] H. C. Chien, L. D. Tsai, C. P. Huang, C. Y. Kang, J. N. Lin, and F. C. Chang, "Sulfonated graphene oxide/Nafion composite membranes for high-performance direct methanol fuel cells," Int. J. Hydrogen Energy, vol. 38, no. 31, pp. 13792–13801, 2013.

[16] I. Nicotera, C. Simari, L. Coppola, P. Zygouri, D. Gournis, S. Brutti, F. D. Minuto, A. S. Aricò, D. Sebastian, and V. Baglio., "Sulfonated Graphene Oxide Platelets in Nafion Nanocomposite Membrane: Advantages for Application in Direct Methanol Fuel Cells," J. Phys. Chem. C, vol. 118, no. 42, pp. 24357–24368, 2014.

[17] P. Bunlengsuwan, N. Paradee, and A. Sirivat, "Influence of Sulfonated Graphene Oxide on Sulfonated Polysulfone Membrane for Direct Methanol Fuel Cell," Polym. Plast. Technol. Eng., 2017.

[18] H. Beydaghi and M. Javanbakht, "Aligned Nanocomposite Membranes Containing Sulfonated Graphene Oxide with Superior Ionic Conductivity for Direct Methanol Fuel Cell Application," Ind. Eng. Chem. Res., vol. 54, no. 28, pp. 7028–7037, 2015.

[19] S. Matsumura, Antisar R. Hlil, C. Lepiller, J. Gaudet, D. Guay, and Allan S. Hay, "Ionomers for Proton Exchange Membrane Fuel Cells with Sulfonic Acid Groups on the End Groups: Novel Linear Aromatic Poly(sulfide-ketone)s," Macromolecules, vol. 41, no. 2, pp. 277–280, 2008.

[20] M. Yoo, M. Kim, Y. Hwang, and J. Kim, "Fabrication of highly selective PVA-g-GO/SPVA membranes via cross-linking method for direct methanol fuel cells," Ionics (Kiel)., vol. 20, no. 6, pp. 875–886, 2014.

[21] S. Yun, H. Im, Y. Heo, and J. Kim, "Crosslinked sulfonated poly(vinyl alcohol)/sulfonated multi-walled carbon nanotubes nanocomposite membranes for direct methanol fuel cells," J. Memb. Sci., vol. 380, no. 1–2, pp. 208–215, 2011.

[22] W. S. Hummers and R. E. Offeman, "Preparation of Graphitic Oxide," J. Am. Chem. Soc., vol. 80, no. 6, pp. 1339–1339, 1958.

[23] X. Qian, N. Gu, Z. Cheng, X. Yang, E. Wang, and S. Dong, "Methods to study the ionic conductivity of polymeric electrolytes using a.c. impedance spectroscopy," J. Solid State Electrochem., vol. 6, no. 1, pp. 8–15, 2001.

[24] S. Xiao, C. Moresoli, J. Bovenkamp, and D. De Kee, "Sorption and permeation of organic environmental contaminants through PVC geomembranes," J. Appl. Polym. Sci., vol. 63, no. 9, pp. 1189–1197, 1997.

[25] L. Shahriary and A. A. Athawale, "Graphene Oxide Synthesized by using Modified Hummers Approach," Int. J. Renew. Energy Environ. Eng., vol. 2, no. 1, pp. 58–63, 2014.

[26] R. Kumar, M. Mamlouk, and K. Scott, "Sulfonated polyether ether ketone – sulfonated graphene oxide composite membranes for polymer electrolyte fuel cells," RSC Adv., vol. 4, no. 2, p. 617, 2014.

[27] K. Feng, B. Tang, and P. Wu, "Sulfonated graphene oxide – silica for highly selective Na fi on-based proton exchange," J. Mater. Chem. A Mater. energy Sustain., vol. 2, pp. 16083–16092, 2014.

[28] H. Hou, X. Hu, X. Liu, W. Hu, R. Meng, and L. Li, "Sulfonated graphene oxide with improved ionic performances," Ionics (Kiel)., vol. 21, no. 7, pp. 1919–1923, 2015.

[29] Ravikumar and K. Scott, "Freestanding sulfonated graphene oxide paper: a new polymer electrolyte for polymer electrolyte fuel cells," Chem. Commun., vol. 48, no. 45, pp. 1–11, 2012.

[30] H. S. Mansur, C. M. Sadahira, A. N. Souza, and A. A. P. Mansur, "FTIR spectroscopy characterization of poly (vinyl alcohol) hydrogel with different hydrolysis degree and chemically crosslinked with glutaraldehyde," Mater. Sci. Eng. C, vol. 28, no. 4, pp. 539–548, 2008.

[31] M. N. Hyder, R. Y. M. Huang, and P. Chen, "Composite poly(vinyl alcohol)-poly(sulfone) membranes crosslinked by trimesoyl chloride: Characterization and dehydration of ethylene glycol-water mixtures," J. Memb. Sci., vol. 326, no. 2, pp. 363–371, 2009.

[32] A. Martínez-Felipe, C. Moliner-Estopiñan, C. T. Imrie, A. Ribes-Greus, "Characterization of crosslinked PVA-based membranes with different hydrolysis degrees for their use as electrolytes in DMFCs," Polym. Polym. Compos., vol. 21, no. 7, pp. 449–456, 2013.

[33] J. W. Rhim, H. B. Park, C. S. Lee, J. H. Jun, D. S. Kim, and Y. M. Lee, "Crosslinked poly(vinyl alcohol) membranes containing sulfonic acid group:

Proton and methanol transport through membranes," J. Memb. Sci., vol. 238, no. 1–2, pp. 143–151, 2004.

[34] C.-C. Yang, "Fabrication and characterization of poly(vinyl alcohol)/montmorillonite/poly(styrene sulfonic acid) proton-conducting composite membranes for direct methanol fuel cells," Int. J. Hydrogen Energy, vol. 36, no. 7, pp. 4419–4431, 2011.

[35] H. J. Salavagione, G. Martínez, and M. a. Gómez, "Synthesis of poly(vinyl alcohol)/reduced graphite oxide nanocomposites with improved thermal and electrical properties," J. Mater. Chem., vol. 19, no. 28, p. 5027, 2009.

[36] C. C. Yang, "Synthesis and characterization of the cross-linked PVA/TiO2 composite polymer membrane for alkaline DMFC," J. Memb. Sci., vol. 288, no. 1–2, pp. 51–60, 2007.

[37] J. Liang, Y. Huang, L. Zhang, Y. Wang, Y. Ma, T. Guo, and Y. Chen, "Molecular-Level Dispersion of Graphene into Poly(vinyl alcohol) and Effective Reinforcement of their Nanocomposites," Adv. Funct. Mater., vol. 19, no. 14, pp. 2297–2302, Jul. 2009.

[38] Y.-S. Ye, M.-Y. Cheng, X.-L. Xie, J. Rick, Y.-J. Huang, F.-C. Chang, and B.-J. Hwang, "Alkali doped polyvinyl alcohol / graphene electrolyte for direct methanol alkaline fuel cells," J. Power Sources, vol. 239, pp. 424–432, 2013.

[39] J. R. Potts, D. R. Dreyer, C. W. Bielawski, and R. S. Ruoff, "Graphene-based polymer nanocomposites," Polymer (Guildf)., vol. 52, no. 1, pp. 5–25, 2011.

[40] J. M. Morancho, J. M. Salla, A. M. Cadenato, X. Fernández, X. Ramis, P. Colomer, R. Ruiz, and Y. Calventus, "Kinetic studies of the degradation of poly(vinyl alcohol)-based proton-conducting membranes at low temperatures," Thermochim. Acta, vol. 521, no. 1–2, pp. 139–147, 2011.

[41] H. Beydaghi, M. Javanbakht, and E. Kowsari, "Preparation and physic-chemical performance study of proton exchange membranes based on phenyl sulfonated graphene oxide nanosheets decorated with iron titanate nanoparticles," Polymer (Guildf)., vol. 87, pp. 26–37, 2016.

[42] S. Yao, Y. Li, Z. Zhou, and H. Yan, "Graphene oxide-assisted preparation of poly(vinyl alcohol)/carbon nanotube/reduced graphene oxide nanofibers with high carbon content by electrospinning technology," RSC Adv., vol. 5, no. 111, pp. 91878–91887, 2015.

[43] Y.-H. Su, Y.-L. Liu, Y.-M. Sun, J.-Y. Lai, D.-M. Wang, Y. Gao, B. Liu, and M. D. Guiver, "Proton exchange membranes modified with sulfonated silica nanoparticles for direct methanol fuel cells☆," J. Memb. Sci., vol. 296, no. 1–2, pp. 21–28, 2007.

[44] S. Zhong, X. Cui, Y. Gao, W. Liu, and S. Dou, "Fabrication and properties of poly(vinyl alcohol)-based polymer electrolyte membranes for direct methanol fuel cell applications," Int. J. Hydrogen Energy, vol. 39, no. 31, pp. 17857–17864, 2014.

[45] M. Erkartal, H. Usta, M. Citir, and U. Sen, "Proton conducting poly(vinyl alcohol) (PVA)/ poly(2-acrylamido-2-methylpropane sulfonic acid) (PAMPS)/ zeolitic imidazolate framework (ZIF) ternary composite membrane," J. Memb. Sci., vol. 499, pp. 156–163, 2016.

[46] J. Chen, Q. Guo, D. Li, J. Tong, and X. Li, "Properties improvement of SPEEK based proton exchange membranes by doping of ionic liquids and Y 2O 3," Prog. Nat. Sci. Mater. Int., vol. 22, no. 1, pp. 26–30, 2012.

[47] H. Beydaghi, M. Javanbakht, and A. Badiei, "Cross-linked poly(vinyl alcohol)/sulfonated nanoporous silica hybrid membranes for proton exchange membrane fuel cell," J. Nanostructure Chem., vol. 4, no. 2, p. 97, 2014.

[48] G. A. Ludueña, T. D. Kühne, and D. Sebastiani, "Mixed Grotthuss and vehicle transport mechanism in proton conducting polymers from Ab initio molecular dynamics simulations," Chem. Mater., vol. 23, no. 6, pp. 1424–1429, 2011.

[49] C. Ajith, A. P. Deshpande, and S. Varughese, "Proton conductivity in crosslinked hydrophilic ionic polymer system: Competitive hydration, crosslink heterogeneity, and ineffective domains," J. Polym. Sci. Part B Polym. Phys., vol. 54, no. 11, pp. 1087–1101, 2016.

[50] H. Vogel, "The law of the relationship between viscosity of liquids and the temperature," Phys. Zeitschrift, vol. 22, p. 645, 1921.

[51] G. Tammann and W. Hesse, "Die Abhängigkeit der Viscosität von der Temperatur bie unterkühlten Flüssigkeiten," Z. Anorg. Allg. Chem., vol. 156, p. 245, 1926.

[52] G. S. Fulcher, "Analysis of recent measurements of the viscosity of glasses," J. Am. Ceram. Soc., vol. 8, p. 339, 1925.

[53] M. Armand, "Polymer solid electrolytes - an overview," Solid State Ionics, vol. 9–10, no. PART 2, pp. 745–754, Dec. 1983.

[54] J. R. P. Jayakody, P. E. Stallwort , E. S. Mananga, J. Farrington-Zapata, and S. G. Greenbau, "High pressure NMR study of water self-diffusion in NAFION-117 membrane," J. Phys. Chem.: B, pp. 4260–4262, 2004.

[55] H. Gao and K. Lian, "Proton-conducting polymer electrolytes and their applications in solid supercapacitors: a review," RSC Adv., vol. 4, no. 62, p. 33091, 2014.

[56] Alabi, Akinleye Christopher, "I. Synthesis and proton conductivity studies of mesostructured organosilicates and bitriazole-polymer composites II. Targeted nanoparticles for siRNA delivery," PhD thesis, California Institute of Technology, 2009.

[57] C.-S. Wu, F.-Y. Lin, C.-Y. Chen, and P. P. Chu, "A polyvinyl alcohol/p-sulfonate phenolic resin composite proton conducting membrane," J. Power Sources, vol. 160, no. 2, pp. 1204–1210, Oct. 2006.

[58] S. Neelakandan, K. Noel Jacob, P. Kanagaraj, R. M. Sabarathinam, A. Muthumeenal, and A. Nagendran, "Effect of sulfonated graphene oxide on the performance enhancement of acid-base composite membranes for direct methanol fuel cells," RSC Adv., vol. 6, no. 57, pp. 51599–51608, 2016.

[59] J. G. Liu, T. S. Zhao, R. Chen, and C. W. Wong, "The effect of methanol concentration on the performance of a passive," DMFC, Electrochem. Commun., vol. 7, no. February, pp. 288–294, 2005.

[60] C. C. Yang, W. C. Chien, and Y. J. Li, "Direct methanol fuel cell based on poly(vinyl alcohol)/titanium oxide nanotubes/poly(styrene sulfonic acid) (PVA/nt-TiO2/PSSA) composite polymer membrane," J. Power Sources, vol. 195, no. 11, pp. 3407–3415, 2010.

[61] Q. Ye and T. S. Zhao, "Abrupt Decline in the Open-Circuit Voltage of Direct Methanol Fuel Cells at Critical Oxygen Feed Rate," J. Electrochem. Soc., vol. 152, no. 11, p. A2238, 2005.

[62] S. Mollá and V. Compañ, "Polyvinyl alcohol nanofiber reinforced Nafion membranes for fuel cell applications," J. Memb. Sci., vol. 372, no. 1–2, pp. 191–200, 2011.

[63] C.-Y. Tseng, Y.-S. Ye, K.-Y. Kao, J. Joseph, W.-C. Shen, J. Rick, and B.-J. Hwang, "Interpenetrating network-forming sulfonated poly(vinyl alcohol) proton exchange membranes for direct methanol fuel cell applications," Int. J. Hydrogen Energy, vol. 36, no. 18, pp. 11936–11945, 2011.

Layer-by-Layer assembled proton exchange composite membranes

Chapter 5

5.1. Summary

In this chapter, the Layer-by-Layer (LbL) assembly method is employed as alternative procedure for the preparation of proton exchange membranes (PEMs) with high methanol selectivity based on poly(vinyl alcohol) (PVA) and graphene oxide (GO) to use in DMFC applications.

As a first attempt, the 30PVA and 30sPVA membranes crosslinked at 30 wt.% of SSA were selected as a substrates for the preparation of the LbL composite membranes due to the good proton-conducting properties that these membranes showed in the studies undertaken in Chapter 4. However, their low mechanical stability did not allow performing the layer-by-layer assembly onto the substrates since these broke during the process. Therefore, the 15PVA and 15sPVA, with a lower crosslinking degree, membranes were finally chosen as substrates for the preparation of the hybrid organic-inorganic composites by the LbL assembly method.

Once selected the substrate, the composites were prepared by alternating deposition of layers of GO and polymer on the substrate surface. According to the forces responsible to keep the LbL assembled structure, two different types of LbL composites were prepared: Hydrogen-bonding LbL composites (**Contribution IV**) and Electrostatic LbL composites (**Contribution V**).

The LbL structure of the composites was characterized through structural (FTIR), morphological (SEM, AFM), thermal (TGA) and mechanical (Vickers hardness) measurements. Moreover, the effect of the sulfonation of the substrate, the number of deposited bilayers and the type of interactions involved for the stabilization of the LbL assembly was investigated on the proton-conducting properties by assays of water contact angle, water uptake (WU), ion exchange capacity (IEC), proton conductivity (σ_{prot}) and H_2-O_2 fuel cell test. Finally, the methanol diffusion coefficients (D_{MeOH}) of the composites were also evaluated in order to validate their potential as electrolytes in DMFCs.

LAYER-BY-LAYER ASSEMBLED COMPOSITE

Polymer layer

GO nano-platelets layer

Substrate membrane
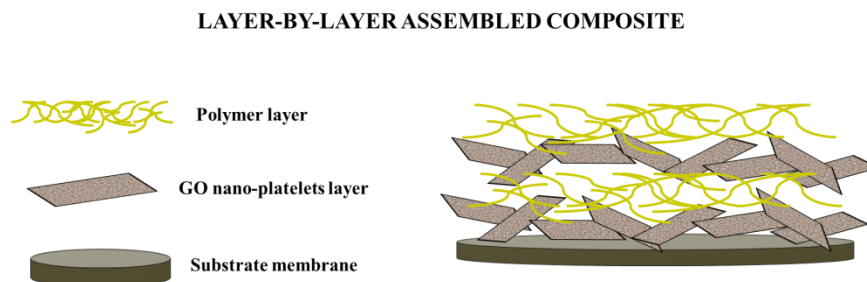
5.2. Contribution IV:

Layer-by-Layer assembly of poly(vinyl alcohol)/graphene oxide hybrid composite membranes via hydrogen-bonding interactions for direct methanol fuel cells

Layer-by-Layer assembly of poly(vinyl alcohol)/graphene oxide hybrid composite membranes via hydrogen-bonding interactions for direct methanol fuel cells

S. C. Sánchez-Ballester[a], L. Monreal[b], A. Ribes-Greus[a], V. Soria[c], G. Rydzek[d] and K. Ariga[d]

[a]Instituto de Tecnología de Materiales (ITM), Universitat Politècnica de València, Valencia, Spain
[b]Departament de Matemàtica Aplicada, Universitat Politècnica de València, Valencia, Spain
[c] ICMUV, Universitat de València, Burjassot, Valencia, Spain
[d] World Premier International (WPI) Research Center for Materials Nanoarchitectonics (MANA), National Institute for Materials Science (NIMS), Tsukuba, Japan.

Abstract

In this study, two kinds of hybrid organic-inorganic composite membranes based on graphene oxide (GO) and poly(vinyl alcohol) (PVA) were fabricated by Layer-by-Layer (LbL) assembly method for use as Proton Exchange Membranes (PEMs) in fuel cell applications. The multilayered membranes were constructed by deposition of GO/PVA and GO/sulfonated graphene oxide (sPVA) bilayers onto the surface of crosslinked 15PVA and 15sPVA substrates, respectively, through hydrogen-bonding interactions. The successful deposition of the bilayers onto the substrates was confirmed by FTIR, SEM and AFM analysis. Thermal and mechanical properties of the LbL composite membranes were investigated by means TGA and Vickers microhardness, respectively. Moreover, the proton-conducting properties were studied as a function of the deposited bilayers and the sulfonation of the substrate. The deposition of a single GO/sPVA bilayer onto the sulfonated substrate, $15sPVA(GO/sPVA)_1$ exhibited higher proton conductivity values up to 3.66 mS/cm bellow 70 ºC, which is superior than the previous 15sPVA/GO composite prepared by solvent casting method. Finally, the methanol diffusion coefficients of the LbL membranes were also measured as a preliminary assay to explore their feasibility as electrolytes in direct methanol fuel cells.

Keywords: poly(vinyl alcohol), graphene oxide, Layer-by-Layer assembly, hydrogen-bonding interaction, proton exchange membrane, proton conductivity, proton exchange membrane fuel cell

Introduction

Proton Exchange Membrane Fuel Cells (PEMFCs) have emerged as a promising clean power source for a wide range of applications [1]. The heart of a PEMFC is the proton exchange membrane (PEM), which provides a proton conductive media while acting as a barrier for the electrons [2]. The performance of a PEM is not only determined by the structure and characteristics of the material, but also by its morphology and hydration degree. Recently, two strategies have been reported to design PEMs with enhanced functional properties, particularly focused on improving their proton conductivity and water management.

The first strategy lies on the preparation of locally and densely sulfonated polymers [3]. In general, the modification of commercial polymers by sulfonation has been extensively reported, showing that the attachment of sulfonic acid moieties to a polymer matrix positively affects to the proton conductivity [3]-[20]. In contrast, the second strategy is focused on the manipulation of membrane morphology in order to create separated nano-phases. Different methodologies such as Layer-by-Layer assembly process, crosslinking reactions, block and graft copolymerization and heterogeneous blendings have been widely used to develop this type of morphology with nano-phase separation [21], [22]. This morphology provides an enhancement of the PEMs functional properties through the formation of two different domains: a hydrophilic domain that confers an optimal water uptake to the membrane as well as continuous ionic transport channels for the proton conduction, while the hydrophobic domain provides good dimensional stability, mechanical strength, and prevents the methanol crossover through the membrane when methanol is directly used as a fuel.

The methodology selected in this study for the preparation of the PEMs was the Layer-by-Layer (LbL) assembly method in combination with a final crosslinking process using glutaraldehyde (GA) as crosslinking agent. The LbL assembly can be based on different kinds of driving forces, such as such as electrostatic forces [23]-[25], hydrogen bonding [26]-[28], covalent bonding [29], [30], and other weak intermolecular interactions. Recently, an increasing interest has been focused on the construction of nanoscale LBL assembled materials driven by hydrogen bond formation, opening a new opportunity for the LBL technique.

The aim of this study was the preparation and characterization of hybrid organic-inorganic composite membranes based on poly(vinyl alcohol) (PVA) and graphene oxide (GO) for PEMFC applications by the LbL assembly method through hydrogen-bonding interactions. The interest of use inorganic fillers, as the graphene oxide, for the preparation of hybrid organic-inorganic composites is due to its capability to enhance the proton-conducting properties of PEMs. Exfoliated graphene oxide nano-platelets are extensively used for fuel cell applications since the oxygen-containing groups attached to its structure (hydroxyl, carboxyl and epoxy groups) allow it to be easy

dispersed in hydrophilic polymers, thus enhancing the interfacial adhesion between the GO and the polymer matrix [31].

For this purpose, two different crosslinked membranes, 15PVA and 15sPVA, were employ as a substrates for the LbL assembly process. The substrates were prepared using the solution-casting method, and further modified by inter-sulfonation with sulfosuccinic acid (SSA) at 15 wt.%, taking place the crosslinking and sulfonation of the polymer chains occur simultaneously. In order to study the effect of the sulfonation on the proton-conducting properties, composites based on sulfonated poly(vinyl alcohol) (sPVA) were also prepared. In this case, the pristine PVA was previously modified by randomly attachment of sulfonic acid groups along the main PVA chain, process denoted as intra-sulfonation. The LbL composite membranes were prepared by alternate deposition of GO/PVA and GO/sPVA bilayers on the 15PVA and 15sPVA substrates, respectively. Two sets of composites denoted as $15PVA(GO/PVA)_n$ and $15sPVA(GO/sPVA)_n$, where *n* refers to the number of deposited bilayer and varies between 1 and 3, were prepared. As a final step, the composites were crosslinked by immersion into a GA solution in order to keep assembled the structure. Both the effect of the number of bilayers deposited and the sulfonation on the structural (FTIR), thermal (TGA), morphological (SEM, AFM) and mechanical properties (Vickers hardness) was studied. Moreover, the proton transport properties were investigated in terms of water contact angle, water uptake (WU) and swelling ratio (SW), ion exchange capacity (IEC), proton conductivity (σ_{prot}) and their performance in a H_2-O_2 fuel cell. Finally, in order to evaluated the potential of the composites as PEMs in Direct Methanol Fuel Cells (DMFCs) a preliminary study of the methanol diffusion coefficients of the composites was carried out.

Experimental

Chemicals

Graphite powder (particle size < 20 μm), sodium nitrate (NaNO$_3$, ≥ 99.0%), sodium hydride (NaH, dry 95%), 1,3-propane sultone (97%), poly(vinyl alcohol) (PVA, molecular weight 130000 g/mol degree of hydrolysis, min. 99%), sulfosuccinic acid (SSA, 70 wt.% solution in water) and glutaraldehyde (GA, 25 wt.% solution in water) were purchased from Sigma-Aldrich. Concentrated sulfuric acid (H$_2$SO$_4$, 95%), hydrogen peroxide (H$_2$O$_2$, 30% w/w), ethanol absolute (EtOH), hydrochloric acid (HCl, 37%), potassium permanganate (KMnO$_4$, extra pure), sodium chloride (NaCl), sodium hydroxide (NaOH, ≥ 98%) and methanol (MeOH) were purchased from Scharlau.

Synthesis of sulfonated poly(vinyl alcohol) (sPVA)

sPVA was synthesized according to the procedure previously described in Contribution I and III [32], [33]. In a first step, 10 g of commercial PVA were added in 250 mL of EtOH, followed by the slow addition of 3.8 g of NaH under constant stirring. Next, 5g of propane sultone were added dropwise to the mixture and stirred at 80 ºC for 24 hours. The obtained sodium sulfonated salt was transformed to the protonated form by immersion in hydrochloric acid solution for 12 hours. The sPVA powder was filtered, washed with ethanol and finally dried for 4 hours in a vacuum oven at 50 ºC.

Synthesis of graphene oxide (GO)

GO was synthesized from graphite powder using the Modified Hummers Method (MHM) [34], [35]. Briefly, 2 g of graphite in 46 mL of concentrated H$_2$SO$_4$ were mixed with 1 g of NaNO$_3$ in an ice bath under constant stirring. After 5 minutes, 6 g of KMnO$_4$ were added gradually to the above solution while keeping the temperature below 20 ºC to prevent overheating. The ice bath was then removed and the mixture was stirred at 35 ºC for 30 minutes. The resulting solution was diluted by adding 92 mL of distilled water dropwise under constant stirring. Then, the temperature was increased at 98 ºC and 280 mL of distilled water was added under vigorous stirring. After 2 hours, the suspension was filtered and treated with 30% H$_2$O$_2$ solution. The resulting GO was washed several times with HCl and EtOH until the washings reach pH 7, followed by filtration. Finally, the powder was suspended in distilled water and sonicated for 3 hours, filtered and dried in a vacuum oven for 12 hours.

Preparation of substrate membranes

Two types of crosslinked membranes, 15PVA and 15sPVA, were prepared by solution casting method to use as substrate membranes in hydrogen-bonding LbL assembly. First, PVA and sPVA aqueous solution (5 wt.%) were prepared by dissolving the polymer in water and refluxing at 90 ºC for 6 hours. Then, the solutions were mixed with 15 wt.% of sulfosuccinic acid (SSA) and vigorously stirred at room temperature for 24 hours. The homogeneous solutions were poured onto a Teflon plate and the cast membranes were allowed to dry at room temperature. As the last step, the dried membranes were crosslinked at 110 ºC for 2 hours.

Preparation of Layer-by-Layer solutions

Polymer solutions (PVA and sPVA) were prepared dissolving 1 wt.% of polymer in Mili-Q water and refluxing at 90 ºC for 6 hours. GO aqueous dispersion (1 mg/mL) was prepared by dispersing GO powder in Mili-Q water by sonication during 30 minutes. The pH of the polymer solution and the GO dispersion was adjusted to 3.5. This pH was selected to promote the protonated form of the carboxylic acid groups (-COOH, $pK_a = 4.3$) of GO, in order to assemble the composite membranes via hydrogen bonding interactions [36].

Layer-by-Layer (LbL) assembly of composite membranes

Prior to the LbL assembly process, the substrate was conditioned in Mili-Q water (pH 3.5) for 15 minutes. Next, the substrate was alternately dipped in the GO dispersion and polymer solution for 30 minutes. After each dipping step, the membrane was rinsed with Mili-Q water for 5 minutes to remove weakly bonded molecules. The process was repeated to increase the number of deposited GO/polymer bilayers on the substrate surface. Scheme 5.1 shows schematically the one bilayer deposition process by the LbL assembly method based on hydrogen-bonding interactions. Finally, the composites were crosslinked by immersing in a 3 % solution of GA for 30 minutes at room temperature in order to fix the deposited bilayers. The composites were denoted as 15PVA(GO/PVA)$_n$ and 15sPVA(GO/sPVA)$_n$, where *n* represents the number of GO/PVA and GO/sPVA bilayers deposited, respectively.
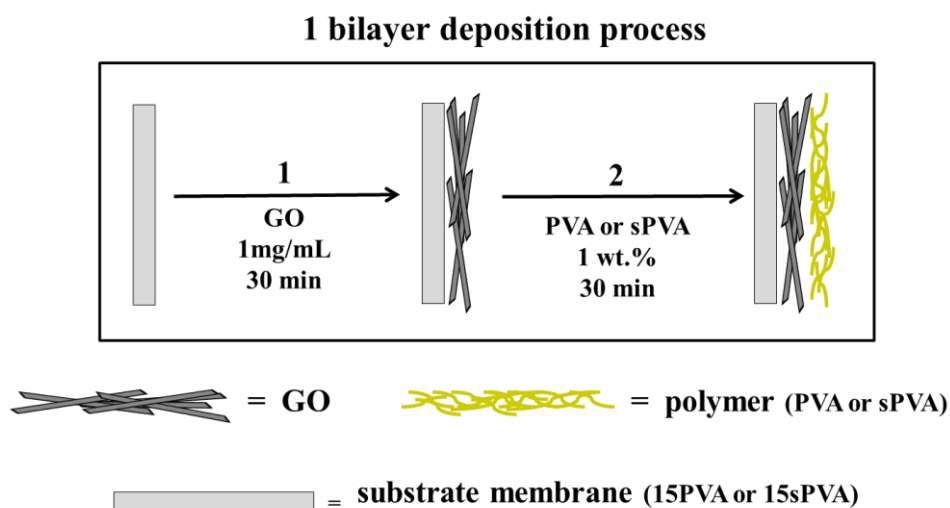
Scheme 5.1. Schematic representation of the one bilayer deposition process by LbL assembly method based on hydrogen-bonding interactions

Characterization techniques

Fourier Transform Infrared (FTIR) spectra were recorded with a *Thermo Nicolet 5700 FTIR*. The FTIR spectra were collected after 64 scans in the 4000-400 cm^{-1} region using the Attenuated Total Reflectance (ATR) mode at a resolution of 4 cm^{-1}. Backgrounds spectra were collected before each series of experiments. All the experiments were performed three times taken the average as the representative value.

The degradation process and thermal stability of the composites were investigated by Thermogravimetric Analysis (TGA) on a *TA Instruments TGA Q-500* analyzer. Measurements were carried out under nitrogen atmosphere at 10 ºC/min heating rate covering from 25 to 800 ºC temperature range.

The surface and cross-sectional morphology of the composites was studied using a *JEOL JSM-6300* scanning electron microscope with an acceleration voltage of 20 kV. The samples for cross-sectional analysis were prepared by immersing the films in liquid nitrogen for 10 minutes before fracture.

The morphology surface of composites was further studied using an Atomic Force Microscope (AFM) *Multimode Nanoscope IVa, Digital Instrument/ Veeco* operating in tapping mode at room temperature under ambient conditions.

Microhardness (MH) measurements were carried out using a Vickers indentor equipped with a *Leitz RZD-DO* microhardness tester. A load of 100 g was used, with a loading cycle of 25 s at room temperature. The hardness value was measured immediately after indentation. MH values (in MPa) were calculated according to the following relationship [37]

$$MH = 2 \sin 68° \left(\frac{P}{d^2} \right)$$

where P is the contact load in *newtons* (N) and d is the diagonal length of the projected indentation area in *millimeters* (mm). The experimental values were taken from the average of three measurements.

Water contact angle

The wettability of composites was measured according to its water contact angle. Hence, static contact angle was evaluated using a *Theta Optical Tensiometer (KSV Instruments, Ltd)* and electrooptics comprising a CCD camera connected to a computer at room temperature. The distilled water (2 μL) was dropped on the sample surface at five different sites and the average value was taken as the representative value.

Water Uptake (WU) and Swelling ratio (SW)

The absorption of water was evaluated by performing swelling tests. Rectangular specimens of 4 x 1 cm^2 were dried at 60 ºC under vacuum for 12 hours, and the weight of the dried composite was measured in a microbalance. The composites were immersed in tests tubes containing distilled water at 30 ºC. The absorption of water was measured gravimetrically at different times, taken out, wiped with tissue paper, and immediately weighted the sample on a microbalance. The samples were weighted until no further gain weight was observed, denoting that the equilibrium condition was achieved. The water uptake, WU (%), was calculated as the mass difference between the samples exposed to water (M_{eq}) and the dry sample (M_{dry}). The results were normalized respect to the mass of the dried sample by

$$WU_{eq}(\%) = \frac{M_{eq} - M_{dry}}{M_{dry}} \times 100$$

The swelling ratio (SW) was calculated from the change in length between the fully hydrated at equilibrium and dry composites, L_{eq} and L_{dry}, respectively, as follows

207

$$SW_{eq}(\%) = \frac{L_{eq} - L_{dry}}{L_{dry}} \times 100$$

Ion Exchange Capacity (IEC)

The IEC of each composite was determined by titration method. The pre-weighted dry sample was soaked in a 0.5 M HCl solution for 24 hours at room temperature to obtain its protonated form. The sample was washed with an excess amount of distilled water and then was immersed in a 2M NaCl solution for 24 hours at room temperature to exchange H^+ with Na^+ ions. The amount of H^+ liberated was estimated by acid-base titration against a standard 0.1 N (0.0955 ± 0.0009 N) NaOH solution with phenolphthalein as the indicator. The IEC values were calculated using the following equation,

$$IEC(mequiv/g) = \frac{N_{NaOH} \times V_{NaOH}}{W_{dry}}$$

where N_{NaOH} is the normality of the titrant in mequiv/L, V_{NaOH} is the added titrant volume in *liters* (L), and W_{dry} is the dry mass of sample in *grams* (g).

Conductivity measurements

Conductivity of the composites was measured with a *Novocontrol Broadband Dielectric Spectrometer (BDS)* in the frequency range of 10^{-1} to 10^7 Hz using an *Alpha-A Frequency Response Analyzer (Novocontrol)*.

The proton conductivity (σ_{prot}) was measured using a *BDS-1308 (Novocontrol)* liquid parallel plate sample cell. The samples were previously equilibrated with Mili-Q water to ensure fully hydrated state. The measurements were performed at 30, 50, 70 and 90 ºC. The proton conductivity (in S/cm) of the membranes was calculated using

$$\sigma_{prot} = \frac{L}{R\,A}$$

where *L* is the thickness of the conducting membranes in *centimeters* (cm), *A* the area of the electrode in contact with the sample in cm^2, and *R* the protonic resistance in *ohms* (Ω), taken from the Bode plot at high frequencies [38].

Electrical conductivity was measured at 30 ºC using a *BDS-1200 (Novocontrol)*, parallel-plate capacitor cell with two gold-plated electrodes. The electrical conductivity was taken at low frequencies, where the measured real part of the conductivity (σ') reaches a plateau which corresponds directly to the DC conductivity (σ_0).

H_2-O_2 fuel cell test

The performance of the composites in a fuel cell was tested by measuring the polarizations curves. The samples were equilibrated with Mili-Q water during 24 hours and then were sandwiched between two sheets of gas diffusion electrodes (*Fuels Cells Etc*, 4 mg/cm^2 Platinum Black). The electrochemical performances were evaluated with a single-cell fixture having an active area of 16 cm^2. The fuel cell was operated with hydrogen and oxygen at 25 ºC and atmospheric pressure.

Methanol diffusion coefficients (D_{MeOH})

The methanol diffusion coefficients (D_{MeOH}) through the composites were tested by a home-made gravimetric permeation cell. The composites were cut into disks of 15 mm in diameter. The cell was filled with methanol solution (2M) and then was quickly assembled with the sample clamped to seal the pathway of the solvent. The sealed cell was immediately put on an analytical balance that was in a constant temperature chamber. The weight loss, related to the methanol diffused through the membrane, was recorded as a function of time. The diffusion coefficients were obtained from the transient state, which is valid for short times, using the Rogers equation [39],

$$\ln\left(F\ t^{\frac{1}{2}}\right) = \ln\left[2c_1\left(\frac{D}{\pi}\right)^{1/2}\right] - \frac{l^2}{4Dt}$$

where *F* is the permeation flux in g·cm^{-2}·s^{-1}, t is the time in *seconds* (s), c_1 is the penetrant concentration at x = 0, *l* is the thickness of the sample in *centimeters* (cm), and *D* is a constant diffusion coefficient in cm^2/s. The plot of ln(F t$^{1/2}$) vs (1/t) gives the slope ($-l^2/4D$) from which the value of D_{MeOH} can be estimated.

Results and discussion

Structural characterization

FTIR analysis was carried out in order to verify the deposition of the GO/PVA and GO/sPVA bilayers on the surface of 15PVA and 15sPVA membranes, respectively, during the LbL assembly process. Figure 5.1 compares the FTIR spectra of the 15PVA and 15sPVA substrates before and after deposition of one and three bilayers with the spectrum of GO.
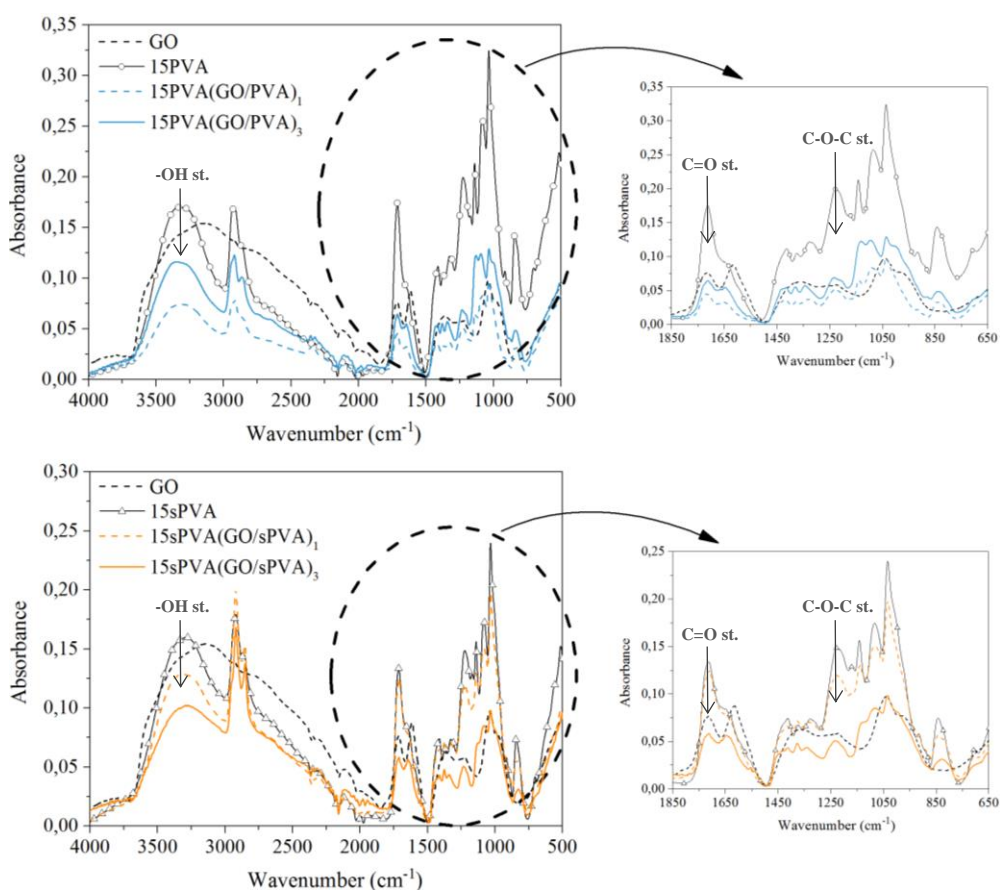
Figure 5.1. FTIR spectra of the 15PVA and 15sPVA membranes before and after deposition of one and three GO/PVA and GO/sPVA bilayers compared to the spectrum of GO

The FTIR spectra of the 15PVA and 15sPVA substrates show a broad band between 3000 and 3700 cm^{-1} characteristic of the stretching vibration of the hydroxyl groups (-OH) of the polymer matrix [40]. At 2800 and 2900 cm^{-1} appears the symmetric and asymmetric stretching band of the methylene groups (C-H), respectively [40]. Moreover, the band at 1710 cm^{-1} is attributed to the stretching vibration of the carbonyl groups, introduced by the SSA in the crosslinking reaction [41]. The absorption band at 1037 cm^{-1} is ascribed to the sulfonic acid groups (-SO$_3$H) of the SSA and sPVA.

After deposition of bilayers, the spectrum of the composites does not show substantially changes. The modification of the 15PVA and 15sPVA substrates by LbL assembly produces morphological changes on their surface, but it does not affect to the chemical structure of the whole assembly. It is observed that the intensity of the stretching vibration band of the hydroxyl groups at 3400 cm^{-1} decreases in the LbL composites; this might be due to the reaction of the hydroxyl groups during the final crosslinking process with GA to form new acetal bonds. In addition, the band at 1710 cm^{-1}, associated to the stretching vibration of the carbonyl groups from the SSA, is strongly decreased while a new band appears at 1646 cm^{-1}, corresponding to the stretching vibration of the aromatic double bonds (C=C) of GO [42]. These results combined with the appearance of a new band at 1234 cm^{-1}, attributed to a mixed contribution from the epoxy groups of GO and the acetal groups formed in the final crosslinking reaction with GA [32], evidence the successful deposition of the GO/PVA and GO/sPVA bilayers during the LbL assembly process.

Thermal characterization

The thermal stability of the composites was investigated by TGA. Figure 5.2 compares the thermogravimetric (TG) and the first-order derivative (DTG) curves of the 15PVA and 15sPVA substrates before and after deposition of one and three GO/PVA and GO/sPVA bilayers, respectively.
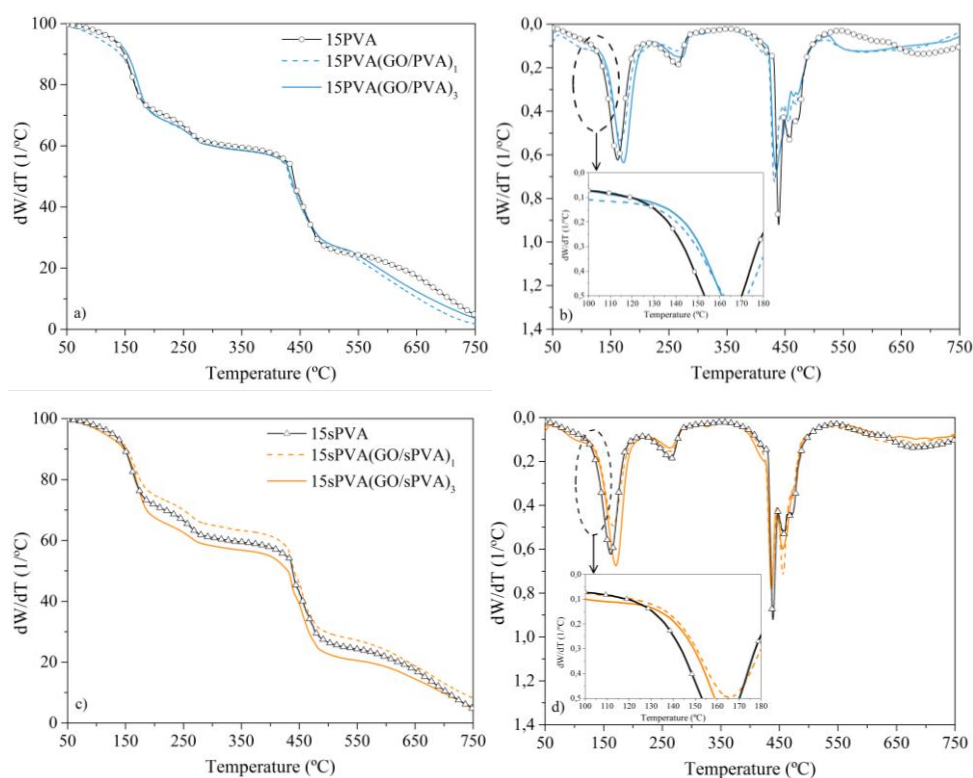
Figure 5.2. Comparison of TG (a, c) and DTG (b, d) curves of the 15PVA and 15sPVA substrates before and after deposition of one and three GO/PVA and GO/sPVA bilayers. The inset graph in DTG curves shows a magnification of the first decomposition stage

As can be seen in DTG curves, the LbL composites show the same decomposition pattern that their respective substrates. The first decomposition stage, ranging from 50 to 200 ºC, is due to the decomposition of the hydroxyl groups of the polymer matrix by elimination reactions [33], [43]. The second stage is attributed to the thermal desulfonation process and takes place around 200-350 ºC. This decomposition is due to both the loss of sulfonic acid groups introduce by the sulfosuccinic acid (SSA) during

the crosslinking reaction of the substrates and the sulfonic acid groups tethered to the PVA chains in the $15sPVA(GO/sPVA)_n$ composites [43]-[46]. The last decomposition stage is observed in the range of 350 and 500 ºC and is associated to the breakage and decomposition of the polymer main chain [43], [47]. Notice that beyond 500 ºC the thermal decomposition of the formed char takes place. Table 5.1 summarizes the temperature weight losses extracted from the thermograms curves of the composites.

Table 5.1. Temperature dependent weight loss values extracted from the thermograms of the hydrogen bonding LbL composites

Membrane	Stage I		Stage II (ºC/%)		Stage III	
	T_{peak}	ΔW	T_{peak}	ΔW	T_{peak}	ΔW
15PVA	164	28	270	11	432	32
$15PVA(GO/PVA)_1$	167	32	265	7	431	34
$15PVA(GO/PVA)_3$	172	32	266	7	435	32
15sPVA	162	29	264	9	439	35
$15sPVA(GO/sPVA)_1$	165	26	265	8	436	35
$15sPVA(GO/sPVA)_3$	171	33	265	8	437	36

The thermal stability of the LbL composites improves with increasing the number of bilayers. The value of the maximum temperature for the first decomposition stage of the $15PVA(GO/PVA)_3$ and $15sPVA(GO/sPVA)_3$ composites is about 8 and 9 °C higher than their substrates, respectively. Furthermore, the decomposition rate of the $15sPVA(GO/sPVA)_n$ composites is faster than the $15PVA(GO/PVA)_n$. This behaviour is promoted by the catalytic effect of the sulfonic acid groups of the sPVA. From these results it can be concluded that the thermal stability of the composites is improved with deposition of GO/PVA and GO/sPVA bilayers by stabilization of the structure via hydrogen-bonding interactions between the polymer matrix and the graphene oxide [48]-[50].

Morphological characterization

SEM measurements were carried out in order to confirm the deposition of GO/PVA and GO/sPVA bilayers onto the surface of the 15PVA and 15sPVA substrates. Figure 5.3 compares the membrane surface after deposition of one and three bilayers at two different magnifications (200× and 1.5K× for the inset image). The GO nano-platelets can be clearly observed uniformly deposited onto the surface of both substrates. The three-bilayer composites present a much covered surface than those with a single bilayer, which means that an increase of the deposited bilayers increases the efficiency of the process [51], [52].
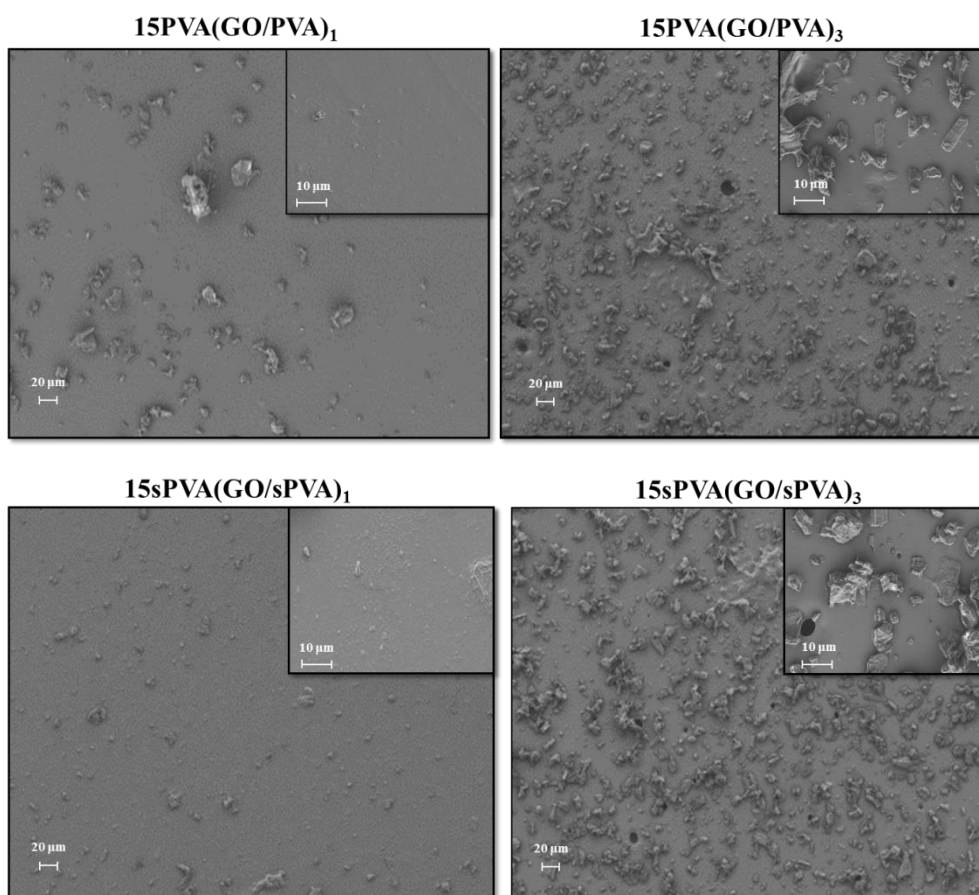
Figure 5.3. SEM images of the substrates surface after deposition of one and three GO/PVA and GO/sPVA bilayers (magnification 200×). Inset SEM images are at 1.5K× magnification

The cross-section morphology of the three-bilayer composites was also characterized by SEM as shown in Figure 5.4. The images clearly show a very thin dense layer light colored onto the surface of both substrates. A pronounced transition between the coating and the substrates is observed, showing a different morphology for each phase, substrate and deposited bilayers [49], [50].
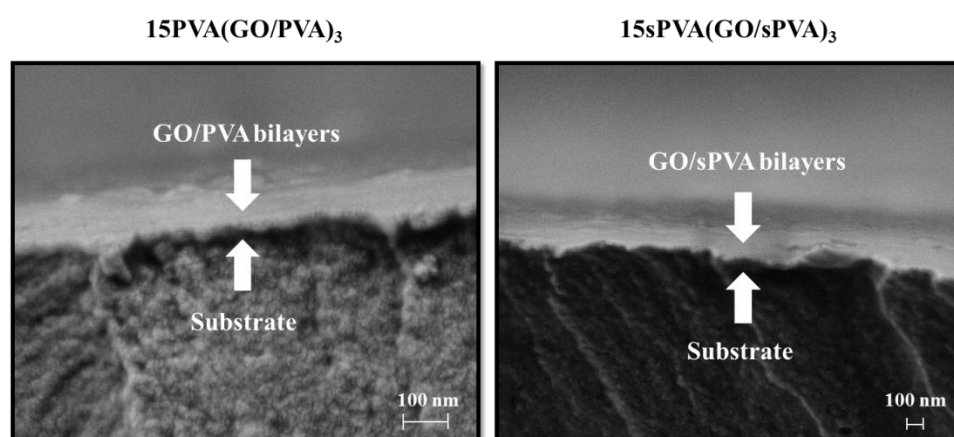
Figure 5.4. SEM images of the cross-section view of the 15PVA(GO/PVA)$_3$ and 15sPVA(GO/sPVA)$_3$ composites

Furthermore, the surface morphology of the composites was analyzed by AFM. Figure 5.5 shows the tapping-mode AFM images of the 15PVA and 15sPVA substrates and the 15PVA(GO/PVA)$_n$ and 15sPVA(GO/sPVA)$_n$ composites build-up from one and three bilayers. As expected, the substrates present a smooth surface with a cross-sectional profile almost planar (Figure 5.5a and d). In contrast, the LbL composites exhibit a rough morphology, showing some peaks which reveal the height of the GO nano-platelets deposited [26]. The homogeneous peak distribution observed in the cross-sectional profile plots confirms that the GO nano-platelets are fully exfoliated and dispersed onto the substrates surface. Moreover, it can be observed an increment of the average roughness (R_a) with increasing the number of deposited bilayers, showing a change in R_a from 0.4 to 8.1 nm for the 15PVA substrate and from 0.5 to 8.3 nm for the 15sPVA substrate after deposition of three bilayers. The total thickness of the coated was about 10 nm and 20 nm after deposition of one and three bilayers, respectively.
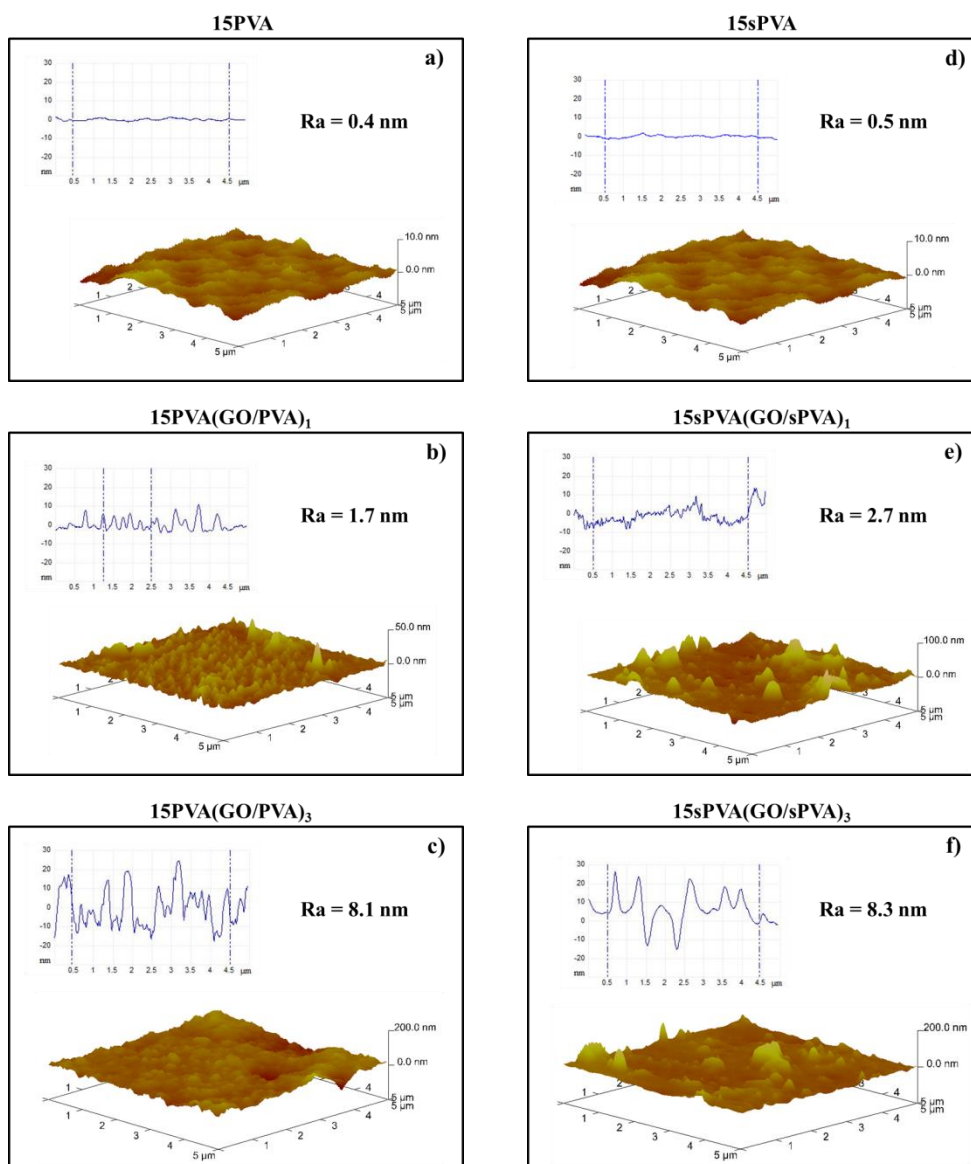
Figure 5.5. AFM images of the 15PVA and 15sPVA substrate membranes before and after deposition of one and three GO/PVA and GO/sPVA bilayers, respectively

### Mechanical characterization

The mechanical properties of the LbL composites were studied as a function of the deposited bilayers by means Vickers hardness tests. Table 5.2 shows the values of Vickers hardness of the 15PVA and 15sPVA substrates and their respective composites 15PVA(GO/PVA)$_n$ and 15sPVA(GO/sPVA)$_n$.

Table 5.2. Values of Vickers Hardness (HV) of the 15PVA(GO/PVA)$_n$ and 15sPVA(GO/sPVA)$_n$ composites and their respective substrates

Membrane	HV (MPa)
15PVA	148 ± 1
15PVA(GO/PVA)$_1$	150 ± 1
15PVA(GO/PVA)$_3$	202 ± 7
15sPVA	153 ± 3
15sPVA(GO/sPVA)$_1$	156 ± 1
15sPVA(GO/sPVA)$_3$	214 ± 4

The values of Vickers hardness increase with increasing the deposited bilayers, while a further increase can be observed for the composites based on sPVA, 15sPVA(GO/sPVA)$_n$. After deposition of a single bilayer, a very slight improvement of the hardness is observed. However, it is found that with the addition of three bilayers, the hardness sharply increases from 148 to 202 MPa and 153 to 214 MPa for the 15PVA(GO/PVA)$_n$ and 15sPVA(GO/sPVA)$_n$ composites, respectively. These results evidence an enhancement of the mechanical properties of the composites by deposition of GO layers. The high hardness of GO nano-platelets as well as the uniformly dispersion of GO onto the substrate of the membranes, corroborated by SEM analysis, improve the load transfer in the LbL composites [26], [52]. In addition, the final crosslinking process constrains the mobility of polymer chains increasing the hardness of the composites.

Water contact angle

The wettability of the substrates and the LbL composites was evaluated by water contact angle analysis. In general, surfaces showing contact angle higher than 90º are considered hydrophobic, and for contact angle lower than 90º hydrophilic. Figure 5.6 shows the differences in form of the water droplets onto the surface of the substrates

and the 15PVA(GO/PVA)$_n$ and 15sPVA(GO/sPVA)$_n$ composites, and their water contact angle values.
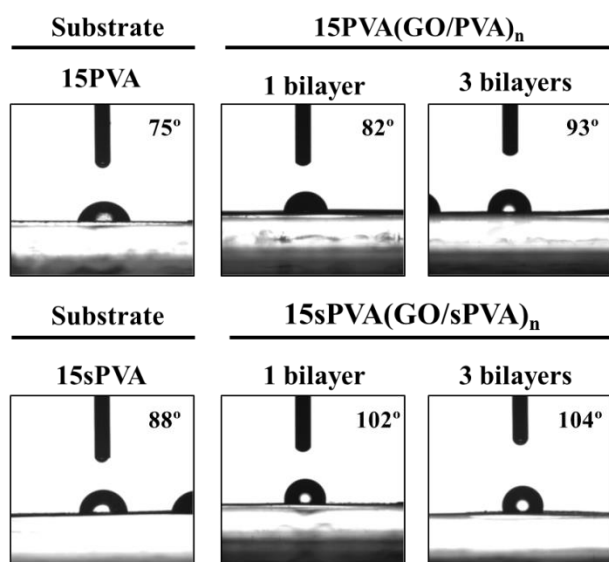
Figure 5.6. Water contact angle values and differences in shape of water droplets onto the surface of the 15PVA and 15sPVA substrates before and after deposition of one and three GO/PVA and GO/sPVA bilayers, respectively

It could be expected that after deposition of GO/PVA and GO/sPVA bilayers onto the surface of substrates would increase the hydrophilic character of the composites, since both the polymers (PVA and sPVA) and the nano-filler (GO) contain polar groups [53]. However, the opposite trend is observed. The hydrophobic character of the 15PVA and 15sPVA substrates surface increases gradually with increasing the number of deposited bilayers, which evidences the existence of a nano-phase separation morphology. The polar groups are placed into the interior of the structure interacting each other through hydrogen-bonding bonds to keep the bilayers assembled, while the non-polar groups remain situated in the surface. Additionally, the final crosslinking process also contributes to diminish the hydrophilicity of the composites since the remaining hydroxyl groups situated on the surface react with GA by acetylation reaction. Moreover, the sulfonation of the PVA also influences to the hydrophilicity character of the composites, showing the 15sPVA(GO/sPVA)$_n$ composites much higher values of water contact angle than that obtain for the 15PVA(GO/sPVA)$_n$ composites.

Water Uptake (WU) and Swelling ratio (SW)

In general, water uptake plays an important role in PEMs because it is directly related to proton conductivity. High water uptake leads to a high proton conductivity, due to water molecules act as a transportation medium for protons in the hydrophilic domains of the membrane [54], [55]. However, an excess of water absorption results in poor dimensional stability and mechanical stability. Consequently, it is essential to test the change of the water uptake and swelling ratio of the composites after modification by LbL assembly.

Figure 5.7a shows the evolution of water uptake of the 15PVA and 15sPVA substrates as a function of the number of bilayers deposited at 30 ℃.
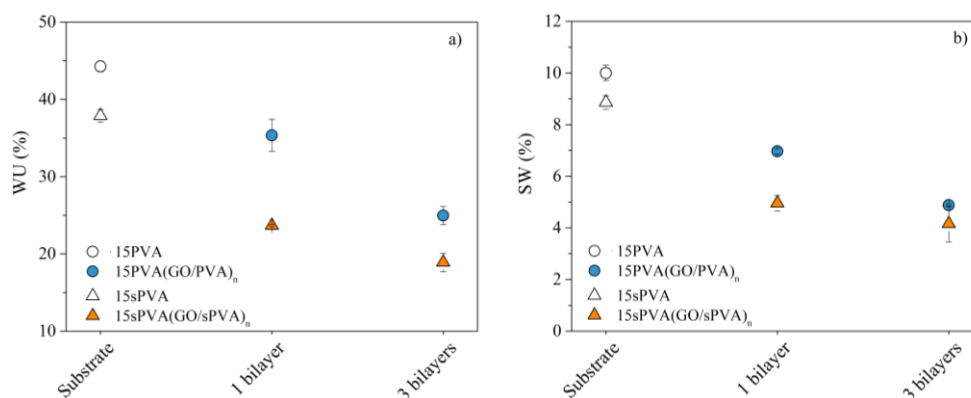
Figure 5.7. Evolution of the a) Water Uptake (WU) and b) Swelling ratio (SW) of the 15PVA(GO/PVA)$_n$ and 15sPVA(GO/sPVA)$_n$ composites as a function of the deposited bilayers at 30 ºC

The water uptake values strongly decrease with increasing the deposited bilayers [49]. After deposition of three bilayers, the WU decreases from 44 % to 28 % and from 38 % to 23 % for the 15PVA and 15sPVA substrates, respectively. This trend is consistent with the water contact angle values, which evidences that after deposition of GO/PVA and GO/sPVA bilayers the hydrophobic character of the composites increases. Moreover, it is noticed that the sulfonation of the polymer matrix strongly affects to the water uptake, as it was also observed for the composites prepared by solution-casting method in Contribution II [56]. The water uptake of 15sPVA(GO/sPVA)$_3$ is 23 %, whereas, its homologue prepared from the 15PVA substrate, 15PVA(GO/PVA)$_3$, shows a water uptake of 28 %.

Swelling ratio values show similar behaviour to water uptake, as shown in Figure 5.7b. It is observed a strongly enhancement of the dimensional stability after deposition of three bilayer, showing a decrease by almost half of the swelling ratio values as compared to their substrates.

Ion Exchange Capacity (IEC)

Ion exchange capacity measures the number of exchangeable groups that contribute to proton-conduction per unit of mass in a membrane. Therefore, usually IEC is related to the proton conductivity in PEMs.

Table 5.3 summarizes the IEC values obtained for the one and three-bilayer composites and their substrates. The IEC values increase with increasing the number of deposited bilayers. This trend can be attributed to the acidic character of the carboxylic acid groups (-COOH) contained in GO. However, this increase is more marked in the $15sPVA(GO/sPVA)_n$ composites, since the sulfonic acid groups (-SO_3H) introduced by deposition of sPVA layers strongly increase the acidity of the composites [57].

Table 5.3. Ion exchange capacity (IEC) values of one and three-bilayer composites and their substrates

Membrane	IEC (mequiv/g)
15PVA	0.67 ± 0.03
$15PVA(GO/PVA)_1$	0.82 ± 0.05
$15PVA(GO/PVA)_3$	0.88 ± 0.19
15sPVA	0.69 ± 0.00
$15sPVA(GO/sPVA)_1$	0.87 ± 0.02
$15sPVA(GO/sPVA)_3$	1.02 ± 0.01

Proton conductivity (σ_{prot})

Figure 5.8 shows the evolution of proton conductivity of the pre-hydrated $15PVA(GO/PVA)_n$ and $15sPVA(GO/sPVA)_n$ composites and their substrates as a function of the temperature.
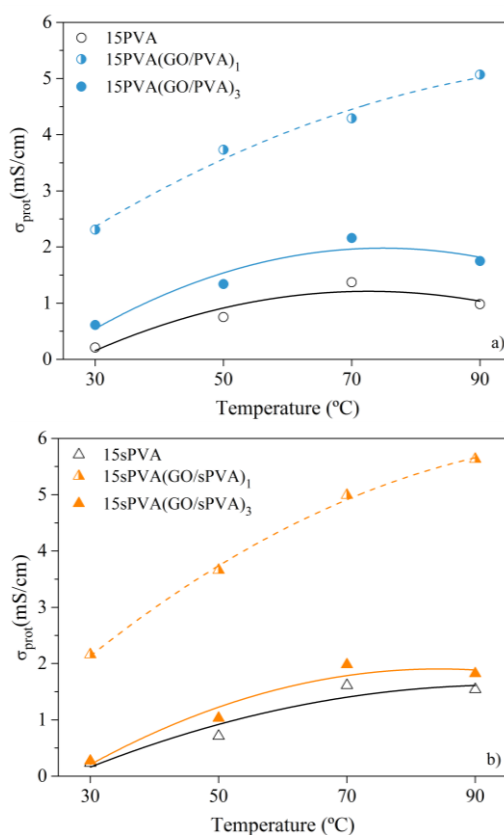
Figure 5.8. Evolution of the proton conductivity (σ_{prot}) of the pre-hydrated a) $15PVA(GO/PVA)_n$, b) $15sPVA(GO/sPVA)_n$ composites and their respective substrates as a function of temperature

The values of proton conductivity obtained for the pre-hydrated LbL composites measured at 30, 50, 70 and 90 ºC are listed in Table 5.4. For comparison, the values of proton conductivity of the 15PVA/GO and 15sPVA/GO composites previously prepared by solvent-casting method in Contribution II are also shown.

Table 5.4. Proton conductivity (σ_{prot}) values of the pre-hydrated LbL composites and their substrates measured as a function of temperature. The composites previously prepared by solution-casting (S-C) method are included for comparison

Membrane	σ_{prot} (mS/cm)			
	30 ºC	50 ºC	70 ºC	90 ºC
15PVA	0.21	0.75	1.37	0.98
15PVA(GO/PVA)$_1$	2.31	3.73	4.29	5.07
15PVA(GO/PVA)$_3$	0.61	1.34	2.16	1.75
15PVA/GO (S-C method)	0.88	2.26	4.57	4.90
15sPVA	0.23	0.71	1.61	1.54
15sPVA(GO/sPVA)$_1$	2.16	3.66	4.99	5.63
15sPVA(GO/sPVA)$_3$	0.27	1.03	1.98	1.82
15sPVA/GO (S-C method)	0.97	2.23	6.16	6.24

In general, an enhancement of the proton conductivity is observed with temperature. At higher temperature, the mobility of the polymer chains increases favoring the proton transport through the composites. However, both the substrates and the three-bilayer composites show a slightly decrease of proton conductivity above 70 ºC attributed to the water evaporation [58].

As can be clearly seen in Figure 5.8, the proton conductivity of the composites decreases with the increase of deposited bilayers [48], [59]. When the number of bilayers is increased at three, the coating deposited on the surface acts as a barrier against the water absorption, limiting the passage of protons across the composite [24], [49]. In contrast, when a single bilayer is deposited, a strongly increase of the proton conductivity is observed. This is attributed to the higher amount of hydrophilic domains in the composites built-up from one bilayer, contributing to maintain an optimal water uptake increasing the continuous proton transport channels through the membrane [22]. Moreover, it was found that the sulfonation in the 15sPVA(GO/sPVA)$_1$ composite slightly enhances the proton conductivity beyond 50 ºC compared to its homologue 15PVA(GO/PVA)$_1$. Therefore, using sPVA as polymer matrix both in the substrate and the bilayers leads to an increase in the number of proton carriers (-SO$_3$H) which promote proton conduction across the membrane [60].

Comparing with the composites previously prepared by solution-casting (S-C) method (15PVA/GO and 15sPVA/GO) in Contribution I and II [56], [61], it was found that the one-bilayer LbL composites show higher proton conductivity up to 50 ºC, as shown in Table 5.4. Beyond 50 ºC, the values of proton conductivity for 15PVA(GO/PVA)$_1$ are

nearly equal to the 15PVA/GO composite (S-C method). However, the $15sPVA(GO/sPVA)_1$ composite show lower values than that obtained for the 15sPVA/GO. This is attributed to the much lower water uptake values obtained for the $15sPVA(GO/sPVA)_1$, which restrict the mobility of the proton carrier species through the membrane, resulting in a decreasing in proton conductivity.

The dependence of proton conductivity with temperature in PEMs can be taken as indicator of a particular type of conduction mechanism. Therefore, the proton conductivity data are also analyzed in terms of Arrhenius plot, log σ_{prot} versus 1/T, as shown in Figure 5.9.
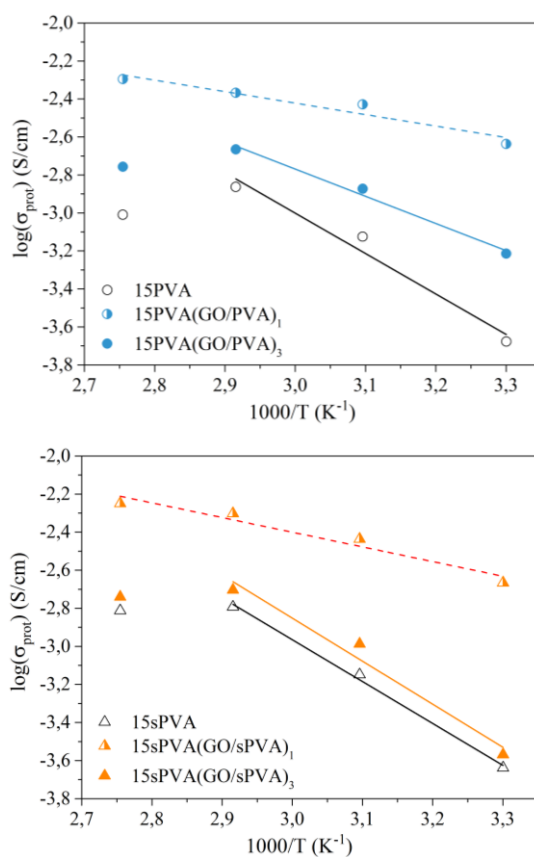
Figure 5.9. Arrhenius plots for proton conductivity (σ_{prot}) of the 15PVA(GO/PVA)$_n$ and 15sPVA(GO/sPVA)$_n$ composites and their substrates

A linear dependence of the proton conductivity with temperature is observed for both the three-bilayer composites and the substrates in the range from 30 to 70 ºC. In contrast, the composites with a single bilayer show a linear correlation in all the range of temperature. This linear dependence confirms that the proton transport is described by the Grotthus mechanism.

The proton conductivity data were fitted using the Arrhenius equation,

$$\log \sigma_{prot} = \log \sigma_0 - \frac{E_a}{RT}$$

where σ_{prot} is the proton conductivity (S/cm), σ_0 is a pre-exponential factor, E_a is the activation energy (kJ/mol), R is the universal gas constant (8.314 J/mol K), and T is the absolute temperature (K). From the slope of log σ_{prot} vs 1000/T, the E_a can be calculated, which is equivalent of the energy required for the proton transfer. The values of E_a for each composite and the substrates are listed in Table 5.5.

Table 5.5. Activation energy (E_a) values calculated for the 15PVA(GO/PVA)$_n$, 15sPVA(GO/sPVA)$_n$ composites and their respective substrates

Membrane	E_a (kJ/mol)
15PVA	40.8
15PVA(GO/PVA)$_1$	11.6
15PVA(GO/PVA)$_3$	27.2
15sPVA	42.2
15sPVA(GO/sPVA)$_1$	14.7
15sPVA(GO/sPVA)$_3$	39.4

After deposition of GO/PVA and GO/sPVA bilayers, the activation energy decreases indicating that the proton transfer becomes easier for the LbL composites [48]. Particularly, the one-bilayer composites show the lowest values of E_a, in accordance with the higher values of proton conductivity that these composites showed.

One of the requirements that a PEM must meet in order to be used in fuel cell applications is a low electrical conductivity to prevent the flow of electrons through it. Figure 5.10 compares the electrical conductivity plots of the LbL composite membranes with the substrates. All membranes show low electrical conductivity values ranged between 10^{-9} and 10^{-10} S/cm, which confirms that the prepared LbL composites are good electrical insulators.
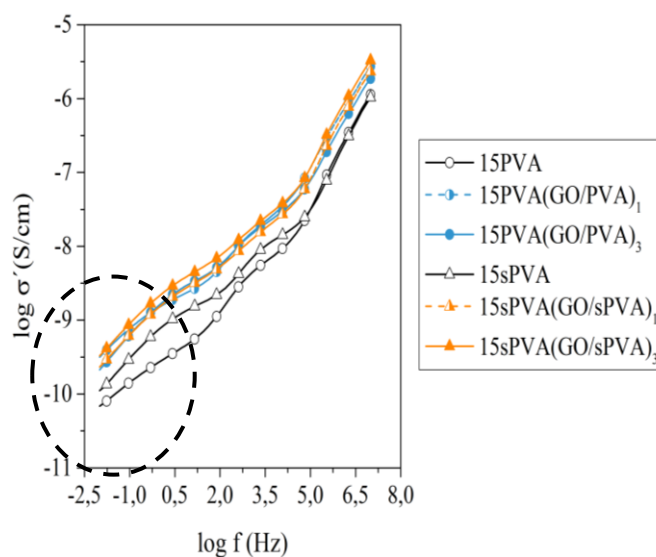
Figure 5.10. Electrical conductivity (σ_{elec}) of the 15PVA(GO/PVA)$_n$ and 15sPVA(GO/sPVA)$_n$ composites compared to their substrates

H_2-O_2 fuel cell test

The performance of the composites in a H_2-O_2 fuel cell was evaluated from the polarization curves measured at 25 ºC. The polarization curves of the 15PVA(GO/PVA)$_n$ and 15sPVA(GO/sPVA)$_n$ composites compared to their substrates are shown in Figure 5.11.
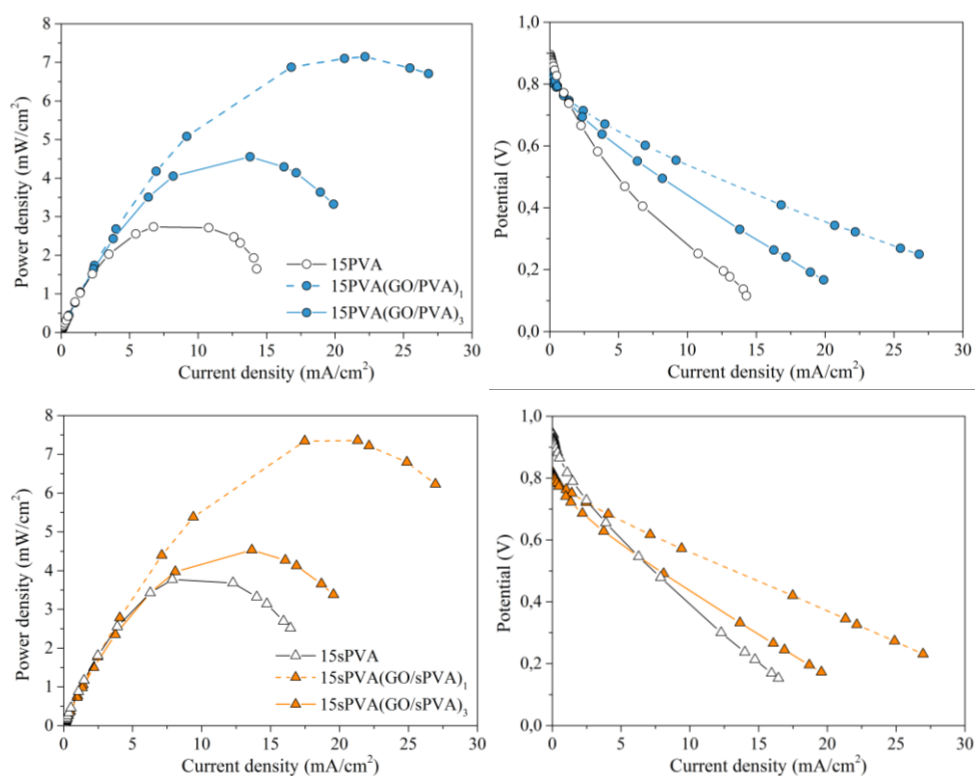
Figure 5.11. Polarization curves of the 15PVA(GO/PVA)$_n$ and 15sPVA(GO/sPVA)$_n$ composites compared to their substrates at 25 ºC

Table 5.6 summarizes the values of the maximum power density (P_{max}) obtained for the LbL composites and their substrates. The one-bilayer composites show the best performance in the fuel cell test, reaching the highest value of P_{max} the composite modified by sulfonation, 15sPVA(GO/sPVA)$_1$, in agreement with its higher proton conductivity. Nevertheless, the performance of the three-bilayer composites is low. This result can be attributed to their low water uptake. Membrane dehydration results

in an increase of the ohmic resistance in the cell, which leads to a decrease of the proton conductivity and the fuel cell performance.

In comparison with the composites prepared by solution-casting method in Contribution I and II [56], [61] (Table 5.6), the LbL composites show values of P_{max} slightly lower, despite showing higher values of proton conductivity. This effect can be attributed to the higher water uptake of the solution-casting composites. It was found a water uptake of 41 % for the 15PVA/GO composite and of 34 % for the 15sPVA/GO composite. In contrast, the $15PVA(GO/PVA)_1$ and $15sPVA(GO/sPVA)_1$ composites show a water uptake of the 35 and 24 %, respectively.

Table 5.6. Maximum power density (P_{max}) values measured at 25 ºC for the $15PVA(GO/PVA)_n$ and $15sPVA(GO/sPVA)_n$ composites compared with their substrates. The composites previously prepared by solution-casting (S-C) method are included for comparison

Membrane	P_{max} (mW/cm^2)
15PVA	2.7 ± 0.2
$15PVA(GO/PVA)_1$	7.1 ± 0.4
$15PVA(GO/PVA)_3$	4.6 ± 0.2
15PVA/GO (S-C method)	7.4 ± 0.1
15sPVA	3.7 ± 0.2
$15sPVA(GO/sPVA)_1$	7.4 ± 0.2
$15sPVA(GO/sPVA)_3$	4.5 ± 0.3
15sPVA/GO (S-C method)	8.3 ± 0.3

MeOH diffusion coefficients (D_{MeOH})

Direct Methanol Fuel Cells (DMFCs) have been proposed as alternative to H_2-O_2 fuel cells because of the simple liquid fuel handling and their improved safety. Nevertheless, DMFCs suffer a severe methanol crossover through the PEM. This methanol crossover not only wastes the fuel but also causes performance losses at the cathode due to the consumption of oxygen and catalyst poisoning [62]. Therefore, a further study of the methanol diffusion coefficients of the LbL composites was obtained in order to evaluate their feasibility as PEMs in DMFCs.

Figure 5.12 shows the rate of methanol mass loss through the $15PVA(GO/PVA)_n$ and $15sPVA(GO/sPVA)_n$ composites and their substrates as a function of time measured at 30 ℃.
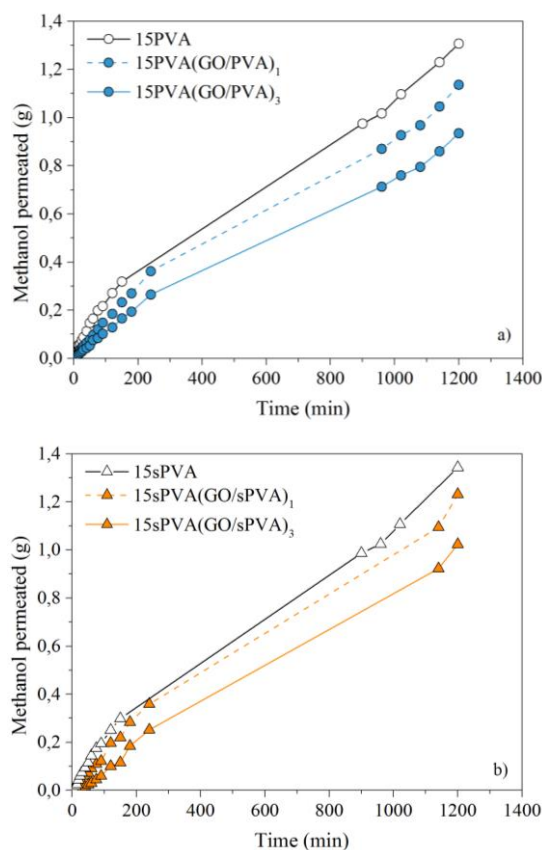
Figure 5.12. Permeation curves of the a) $15PVA(GO/PVA)_n$ and b) $15sPVA(GO/sPVA)_n$ composites compared to their substrates at 30 ℃

Table 5.7 lists the values of methanol diffusion coefficients (D_{MeOH}) of all measured membranes.

Table 5.7. Methanol diffusion coefficients (D_{MeOH}) and methanol selectivity (Φ) values of the 15PVA(GO/PVA)$_n$ and 15sPVA(GO/sPVA)$_n$ composites compared to their substrates at 30 ºC

Membrane	$D_{MeOH} \times 10^8$ (cm^2/s)	Φ (S·s·cm^{-3})
15PVA	7.00 ± 0.03	0.03×10^5
15PVA(GO/PVA)$_1$	4.26 ± 0.02	0.53×10^5
15PVA(GO/PVA)$_3$	2.62 ± 0.01	0.23×10^5
15sPVA	5.38 ± 0.02	0.04×10^5
15sPVA(GO/sPVA)$_1$	3.06 ± 0.01	0.71×10^5
15sPVA(GO/sPVA)$_3$	1.96 ± 0.01	0.15×10^5

The results show a decrease of the methanol diffusion coefficients with increasing the number of bilayers. After deposition of three bilayers, the D_{MeOH} values of the 15PVA and 15sPVA substrates decrease a 63 % and 64 %, respectively. This suggests that the deposition of GO/polymer bilayers on the substrates acts effectively as methanol barrier [48]. Moreover, under the same number of bilayers, the sulfonated composites show lower values of methanol diffusion coefficients than those prepared from PVA, in agreement with their lower values of water uptake.

The selectivity, which is defined as the ratio of proton conductivity to methanol diffusion coefficient, is often used as an indicator of the suitability of a given membrane for DMFC applications. A higher selectivity means that the membrane has high proton conductivity and a low methanol crossover, which is favorable for DMFC applications [63]. Table 5.7 also shows the methanol selectivity values calculated for the LbL composites and their substrates.

It could be expected that the methanol selectivity (Φ) of the LbL composites increased with the deposited bilayers. However, the opposite trend is observed. The three-bilayer composites, despite exhibiting lower values of D_{MeOH}, have lower methanol selectivity than the one-bilayer composites. This effect can be explain by the low proton conductivity that the 15PVA(GO/PVA)$_3$ (0.61 mS/cm) and 15sPVA(GO/sPVA)$_3$ (0.27 mS/cm) composites show at 30 ºC [49]. Therefore, it is not only important the methanol diffusion coefficient, but also the proton conductivity is a crucial factor to determine the potential of a PEM for DMFC applications.

Conclusions

A sequentially assembly of one and three GO/PVA and GO/sPVA bilayers onto the surface of 15PVA and 15sPVA substrates were carried out by LbL assembly method through the hydrogen bonding interactions between the active hydroxyl groups of the polymer matrix and the oxygen-containing functional groups of the GO. The build-up of deposited bilayers was ranged from one to three. FTIR, SEM and AFM results confirm the successful deposition of GO/PVA and GO/sPVA bilayers on the surface of the 15PVA and 15sPVA substrates, respectively. The thermal and mechanical stability of the LbL modified composites was gradually increased due to the incorporation of GO/PVA and GO/sPVA bilayers. The results show that both the proton conductivity and the performance in H_2-O_2 fuel cell of the 15PVA(GO/PVA)$_n$ and 15sPVA(GO/sPVA)$_n$ (n=1 and 3) composites, sharply depend of the sulfonation of the substrate (15sPVA) and the n-parameter related with the overall thickness of the composite. The 15PVA(GO/PVA)$_1$ composite shows a proton conductivity of 5.07 mS/cm at 90 ºC, while the 15sPVA(GO/sPVA)$_1$ composite reaches a value of 5.63 mS/cm at the same temperature. In both cases, the proton conductive mechanism follows an Arrhenius dependence in all the range of temperature, indicating that the proton transport takes place through the Grotthus mechanism. The improvement of the one-bilayer composites performance was also evidenced by H_2-O_2 fuel cell test. Finally, the methanol diffusion coefficients of the composites were measured as a preliminary study to test their potential in DMFC applications. The 15sPVA(GO/sPVA)$_3$ composite exhibited the lowest value of methanol diffusion coefficient (D_{MeOH} = 1.96 cm^2/s), but its low proton conductivity results in a low methanol selectivity. Among all the LbL composites assayed, the 15sPVA(GO/sPVA)$_1$ composite showed the best methanol selectivity (Φ = 0.71×10^5 S·s·cm^{-3}) with a reasonable D_{MeOH} of 3.06×10^{-8} cm^2/s and σ_{prot} of 2.16 mS/cm measured at 30 ºC.

References

[1] F. Barbir, *PEM Fuel Cells: Theory and Practice*, Elsevier. 2013.

[2] S. Javaid and T. Matsuura, *Polymer Membranes for Fuel Cells*. Springer, 2009.

[3] T. Higashihara, K. Matsumoto, and M. Ueda, "Sulfonated aromatic hydrocarbon polymers as proton exchange membranes for fuel cells," Polymer (Guildf)., vol. 50, no. 23, pp. 5341–5357, 2009.

[4] J. N. Solanki, P. S. Mishra, and Z. V. P. Murthy, "In situ prepared TiO_2 nanoparticles cross-linked sulfonated PVA membranes with high proton conductivity for DMFC," Quim. Nova, vol. 39, no. 6, pp. 704–711, 2016.

[5] R. Kumar, M. Mamlouk, and K. Scott, "Sulfonated polyether ether ketone-sulfonated graphene oxide composite membranes for polymer electrolyte fuel cells," RSC Adv., vol. 4, no. 2, p. 617, 2014.

[6] C.-Y. Tseng, Y.-S. Ye, K.-Y. Kao, J. Joseph, W.-C. Shen, J. Rick, and B.-J. Hwang, "Interpenetrating network-forming sulfonated poly(vinyl alcohol) proton exchange membranes for direct methanol fuel cell applications," Int. J. Hydrogen Energy, vol. 36, no. 18, pp. 11936–11945, 2011.

[7] A. Abdolmaleki, M. Zhiani, M. Maleki, S. Borandeh, and K. Firouz, "Preparation and evaluation of sulfonated polyoxadiazole membrane containing phenol moiety for PEMFC application," Polymer (Guildf)., vol. 75, pp. 17–24, 2015.

[8] R. Zeng, S. Xiao, L. Chen, and Y. Chen, "Sulfonated poly(ether sulfone ether ketone ketone)/sulfonated poly(ether sulfone) blend membranes with reduced methanol permeability," High Perform. Polym., vol. 24, no. 3, pp. 153–160, 2012.

[9] H. Beydaghi, M. Javanbakht, A. Bagheri, P. Salarizadeh, H. Ghafarian-Zahmatkesh, S. Kashefic and E. Kowsari, "Novel nanocomposite membranes based on blended sulfonated poly(ether ether ketone)/poly(vinyl alcohol) containing sulfonated graphene oxide/Fe3O4 nanosheets for DMFC applications," RSC Adv., vol. 5, no. 90, pp. 74054–74064, 2015.

[10] N. Seeponkai and J. Wootthikanokkhan, "Proton conductivity and methanol permeability of sulfonated poly(vinyl alcohol) membranes modified by using sulfoacetic acid and poly(acrylic acid)," J. Appl. Polym. Sci., vol. 105, no. 2, pp. 838–845, Jul. 2007.

[11] C. Zhang, X. Zhuang, X. Li, W. Wang, B. Cheng, W. Kang, Z. Cai, and M. Li, "Chitin nanowhisker-supported sulfonated poly(ether sulfone) proton exchange for fuel cell applications," Carbohydr. Polym., vol. 140, pp. 195–201, 2016.

[12] T. Yang, S. X. Zhang, Y. Gao, F. Cheng, J. Tang, and W. Liu, "Multilayer Membranes Based on Sulfonated Poly(Ether Ether Ketone) and Poly(Vinyl Alcohol) for Direct Methanol Membrane Fuel Cells," Open Fuel Cells J., vol. 1, no. January 2009, pp. 4–8, 2008.

[13] Y. Zhao and J. Yin, "Synthesis and properties of poly(ether ether ketone)-block-sulfonated polybutadiene copolymers for PEM applications," Eur. Polym. J., vol. 46, no. 3, pp. 592–601, 2010.

[14] H. Yao, K. Shi, N. Song, N. Zhang, P. Huo, S. Zhu, Y. Zhang, and S. Guan, "Polymer electrolyte membranes based on cross-linked highly sulfonated co-polyimides," Polym. (United Kingdom), vol. 103, pp. 171–179, 2016.

[15] M. S. Boroglu, S. U. Celik, A. Bozkurt, and I. Boz, "The synthesis and characterization of anhydrous proton conducting membranes based on sulfonated poly(vinyl alcohol) and imidazole," J. Memb. Sci., vol. 375, no. 1–2, pp. 157–164, 2011.

[16] M. Sakamoto, S. Nohara, K. Miyatake, M. Uchida, M. Watanabe, and H. Uchida, "Effects of Incorporation of SiO2 Nanoparticles into Sulfonated Polyimide Electrolyte Membranes on Fuel Cell Performance under Low Humidity Conditions," Electrochim. Acta, vol. 137, pp. 213–218, 2014.

[17] M. Yoonessi, T. D. Dang, H. Heinz, R. Wheeler, and Z. Bai, "Investigation of nanostructures and properties of sulfonated poly(arylenethioethersulfone) copolymer as proton conducting materials by small angle neutron scattering," Polymer (Guildf)., vol. 51, no. 7, pp. 1585–1592, 2010.

[18] H. Bai and W. S. W. Ho, "New sulfonated polybenzimidazole (SPBI) copolymer-based proton-exchange membranes for fuel cells," J. Taiwan Inst. Chem. Eng., vol. 40, no. 3, pp. 260–267, 2009.

[19] H. Pan, S. Chen, Y. Zhang, M. Jin, Z. Chang, and H. Pu, "Preparation and properties of the cross-linked sulfonated polyimide containing benzimidazole as electrolyte membranes in fuel cells," J. Memb. Sci., vol. 476, pp. 87–94, 2015.

[20] K. Ahn, M. Kim, K. Kim, I. Oh, H. Ju, and J. Kim, "Low methanol permeable crosslinked sulfonated poly(phenylene oxide) membranes with hollow glass microspheres for direct methanol fuel cells," Polym. (United Kingdom), vol. 56, pp. 178–188, 2015.

[21] W. Chen and B. Wunderlich, "Nanophase separation of small and large molecules," Macromol. Chem. Phys., vol. 200, no. 2, pp. 283–311, 1999.

[22] Y. Hu, X. Li, L. Yan, and B. Yue, "Improving the Overall Characteristics of Proton Exchange Membranes via Nanophase Separation Technologies: A Progress Review," Fuel Cells, no. 1, pp. 3–17, 2017.

[23] J. S. Park, S. M. Cho, W.-J. Kim, J. Park, and P. J. Yoo, "Fabrication of graphene thin films based on layer-by-layer self-assembly of functionalized graphene nanosheets.," ACS Appl. Mater. Interfaces, vol. 3, no. 2, pp. 360–368, 2011.

[24] Y. Xue and S. Chan, "Layer-by-layer self-assembly of CHI/PVS-Nafion composite membrane for reduced methanol crossover and enhanced DMFC performance," Int. J. Hydrogen Energy, vol. 40, no. 4, pp. 1877–1885, 2015.

[25] H. Zhang, H. Huang, and P. K. Shen, "Methanol-blocking Nafion composite membranes fabricated by layer-by-layer self-assembly for direct methanol fuel cells," Int. J. Hydrogen Energy, vol. 37, no. 8, pp. 6875–6879, 2012.

[26] X. Zhao, Q. Zhang, Y. Hao, Y. Li, Y. Fang, and D. Chen, "Alternate multilayer films of poly(vinyl alcohol) and exfoliated graphene oxide fabricated via a facial layer-by-layer assembly," Macromolecules, vol. 43, no. 22, pp. 9411–9416, 2010.

[27] L. Wang, Z. Wang, X. Zhang, J. Shen, L. Chi, and H. Fuchs, "A new approach for the fabrication of an alternating multilayer film of poly(4-vinylpyridine) and poly(acrylic acid) based on hydrogen bonding," Macromol. Rapid Commun., vol. 18, pp. 509–514, 1997.

[28] D. Chen, X. Wang, T. Liu, X. Wang, and J. Li, "Electrically conductive poly(vinyl alcohol) hybrid films containing graphene and layered double hydroxide fabricated via layer-by-layer self-assembly," ACS Appl. Mater. Interfaces, vol. 2, no. 7, pp. 2005–2011, 2010.

[29] M. E. Buck, J. Zhang, and D. M. Lynn, "Layer-by-layer assembly of reactive ultrathin films mediated by click-type reactions of poly(2-alkenyl azlactone)s," Adv. Mater., vol. 19, no. 22, pp. 3951–3955, 2007.

[30] G. K. Such, J. F. Quinn, A. Quinn, E. Tjipto, and F. Caruso, "Assembly of Ultrathin Polymer Multilayer Films by Click Chemistry Assembly of Ultrathin Polymer Multilayer Films by Click Chemistry," Polymer (Guildf)., vol. 128, no. 29, pp. 9318–9319, 2006.

[31] R. K. Layek and A. K. Nandi, "A review on synthesis and properties of polymer functionalized graphene," Polymer (Guildf)., vol. 54, no. 19, pp. 5087–5103, 2013.

[32] M. Yoo, M. Kim, Y. Hwang, and J. Kim, "Fabrication of highly selective PVA-g-GO/SPVA membranes via cross-linking method for direct methanol fuel cells," Ionics (Kiel)., vol. 20, no. 6, pp. 875–886, 2014.

[33] S. Yun, H. Im, Y. Heo, and J. Kim, "Crosslinked sulfonated poly(vinyl alcohol)/sulfonated multi-walled carbon nanotubes nanocomposite membranes for direct methanol fuel cells," J. Memb. Sci., vol. 380, no. 1–2, pp. 208–215, 2011.

[34] W. S. Hummers and R. E. Offeman, "Preparation of Graphitic Oxide," J. Am. Chem. Soc., vol. 80, no. 6, pp. 1339–1339, 1958.

[35] L. Shahriary and A. A. Athawale, "Graphene Oxide Synthesized by using Modified Hummers Approach," Int. J. Renew. Energy Environ. Eng., vol. 2, no. 1, pp. 58–63, 2014.

[36] B. Konkena and S. Vasudevan, "Understanding Aqueous Dispersibility of Graphene Oxide and Reduced Graphene Oxide through pKa Measurements.," J. Phys. Chem. Lett., vol. 3, no. 7, pp. 867–72, Apr. 2012.

[37] F. J. Baltá Calleja, "Microhardness relating to crystalline polymers," in Characterization of Polymers in the Solid State I: Part A: NMR and Other Spectroscopic Methods Part B: Mechanical Methods, H. H. Kaush and H. G. Zachman, Eds. Berlin, Heidelberg: Springer Berlin Heidelberg, 1985, pp. 117–148.

[38] X. Qian, N. Gu, Z. Cheng, X. Yang, E. Wang, and S. Dong, "Methods to study the ionic conductivity of polymeric electrolytes using a.c. impedance spectroscopy," J. Solid State Electrochem., vol. 6, no. 1, pp. 8–15, 2001.

[39] S. Xiao, C. Moresoli, J. Bovenkamp, and D. De Kee, "Sorption and permeation of organic environmental contaminants through PVC geomembranes," J. Appl. Polym. Sci., vol. 63, no. 9, pp. 1189–1197, 1997.

[40] H. S. Mansur, C. M. Sadahira, A. N. Souza, and A. A. P. Mansur, "FTIR spectroscopy characterization of poly (vinyl alcohol) hydrogel with different hydrolysis degree and chemically crosslinked with glutaraldehyde," Mater. Sci. Eng. C, vol. 28, no. 4, pp. 539–548, 2008.

[41] H. Hou, X. Hu, X. Liu, W. Hu, R. Meng, and L. Li, "Sulfonated graphene oxide with improved ionic performances," Ionics (Kiel)., vol. 21, no. 7, pp. 1919–1923, 2015.

[42] S. Morimune, T. Nishino, and T. Goto, "Poly(vinyl alcohol)/graphene oxide nanocomposites prepared by a simple eco-process," Polym. J., vol. 44, no. 10, pp. 1056–1063, Oct. 2012.

[43] J. M. Morancho et al., "Kinetic studies of the degradation of poly(vinyl alcohol)-based proton-conducting membranes at low temperatures," Thermochim. Acta, vol. 521, no. 1–2, pp. 139–147, 2011.

[44] C. C. Yang, W. C. Chien, and Y. J. Li, "Direct methanol fuel cell based on poly(vinyl alcohol)/titanium oxide nanotubes/poly(styrene sulfonic acid) (PVA/nt-TiO2/PSSA) composite polymer membrane," J. Power Sources, vol. 195, no. 11, pp. 3407–3415, 2010.

[45] S. Zhong, X. Cui, Y. Gao, W. Liu, and S. Dou, "Fabrication and properties of poly(vinyl alcohol)-based polymer electrolyte membranes for direct methanol fuel cell applications," Int. J. Hydrogen Energy, vol. 39, no. 31, pp. 17857–17864, 2014.

[46] A. Martínez-Felipe, C. Moliner-Estopiñán, C. T. Imrie, and A. Ribes-Greus, "Characterization of crosslinked poly(vinyl alcohol)-based membranes with different hydrolysis degrees for their use as electrolytes in direct methanol fuel cells," J. Appl. Polym. Sci., vol. 124, no. 2, pp. 1000–1011, Apr. 2012.

[47] D. S. Kim, H. B. Park, J. W. Rhim, and Y. M. Lee, "Preparation and characterization of crosslinked PVA/SiO2 hybrid membranes containing sulfonic acid groups for direct methanol fuel cell applications," J. Memb. Sci., vol. 240, no. 1–2, pp. 37–48, 2004.

[48] C. Zhao, H. Lin, Z. Cui, X. Li, H. Na, and W. Xing, "Highly conductive, methanol resistant fuel cell membranes fabricated by layer-by-layer self-assembly of inorganic heteropolyacid," J. Power Sources, vol. 194, no. 1, pp. 168–174, Oct. 2009.

[49] H. Lin, C. Zhao, W. Ma, H. Li, and H. Na, "Layer-by-layer self-assembly of in situ polymerized polypyrrole on sulfonated poly(arylene ether ketone) membrane with extremely low methanol crossover," Int. J. Hydrogen Energy, vol. 34, no. 24, pp. 9795–9801, Dec. 2009.

[50] J. Zhao, Y. Zhu, F. Pan, G. He, C. Fang, K. Cao, R. Xing, and Z. Jiang, "Fabricating graphene oxide-based ultrathin hybrid membrane for pervaporation dehydration via layer-by-layer self-assembly driven by multiple interactions," J. Memb. Sci., vol. 487, pp. 162–172, Aug. 2015.

[51] D. Yu and L. Dai, "Self-assembled graphene/carbon nanotube hybrid films for supercapacitors," J. Phys. Chem. Lett., vol. 1, no. 2, pp. 467–470, 2010.

[52] N. Wang, S. Ji, G. Zhang, J. Li, and L. Wang, "Self-assembly of graphene oxide and polyelectrolyte complex nanohybrid membranes for nanofiltration and pervaporation," Chem. Eng. J., vol. 213, pp. 318–329, 2012.

[53] X. He, L.-L. Wu, J.-J. Wang, T. Zhang, H. Sun, and N. Shuai, "Layer-by-layer assembly deposition of graphene oxide on poly(lactic acid) films to improve the barrier properties," High Perform. Polym., vol. 27, no. 3, pp. 318–325, 2015.

[54] M. L. Di Vona, Z. Ahmed, S. Bellitto, A. Lenci, E. Traversa, and S. Licoccia, "SPEEK-TiO$_2$ nanocomposite hybrid proton conductive membranes via in situ mixed sol–gel process," J. Memb. Sci., vol. 296, no. 1, pp. 156–161, 2007.

[55] M. Han, G. Zhang, M. Li, S. Wang, Y. Zhang, H. Li, C. M. Lew, and H. Na, "Considerations of the morphology in the design of proton exchange membranes: Cross-linked sulfonated poly(ether ether ketone)s using a new carboxyl-terminated benzimidazole as the cross-linker for PEMFCs," Int. J. Hydrogen Energy, vol. 36, no. 3, pp. 2197–2206, 2011.

[56] S. C. Sánchez-Ballester, A Ribes-Greus, V. Soria, G. Rydzek, K. Ariga, "Bi-sulfonation of poly(vinyl alcohol)/Graphene oxide composite membranes for Proton Exchange Membrane Fuel Cell applications. Part 2: Functional membrane properties," *In Preparation*.

[57] S. Li, S. Zhang, Q. Zhang and G. Qin, "Assembly of unbalanced charged polyampholyte onto Nafion® to produce high-performance composite membranes," Chem. Commun., no. 1, pp. 1173–1184, 2008.

[58] H. Beydaghi, M. Javanbakht, and E. Kowsari, "Preparation and physic-chemical performance study of proton exchange membranes based on phenyl sulfonated graphene oxide nanosheets decorated with iron titanate nanoparticles," Polymer (Guildf)., vol. 87, pp. 26–37, 2016.

[59] T. Lee, S. H. Min, M. Gu, Y. K. Jung, W. Lee, J. U. Lee, D. G. Seong, and B.-S. Kim, "Layer-by-Layer Assembly for Graphene-Based Multilayer Nanocomposites: Synthesis and Applications," Chem. Mater., vol. 27, no. 11, pp. 3785–3796, 2015.

[60] Y. Xiang, S. Lu, and S. P. Jiang, "Layer-by-layer self-assembly in the development of electrochemical energy conversion and storage devices from fuel cells to supercapacitors," Chem. Soc. Rev., vol. 41, no. 21, p. 7291, 2012.

[61] S. C. Sánchez-Ballester, A. Ribes-Greus, V. Soria, G. Rydzek, and K. Ariga, "Bi-sulfonation of poly(vinyl alcohol)/Graphene oxide composite membranes for Proton Exchange Membrane Fuel Cell applications. Part 1: Membrane preparation and characterization," *In Preparation*.

[62] S. Q. Song, W. J. Zhou, W. Z. Li, G. Sun, Q. Xin, S. Kontou, and P. Tsiakaras, "Direct methanol fuel cells : Methanol crossover and its influence on single DMFC performance," Ionics (Kiel)., vol. 10, no. 5, pp. 458–462, 2004.

[63] B. S. Pivovar, Y. X. Wang, and E. L. Cussler, "Pervaporation membranes in direct methanol fuel cells," J. Memb. Sci., vol. 154, no. 2, pp. 155–162, 1999.

5.3. Contribution V:

Layer-by-Layer assembly of poly(vinyl alcohol)/graphene oxide hybrid composite membranes via electrostatic interactions for direct methanol fuel cells

Layer-by-Layer assembly of poly(vinyl alcohol)/graphene oxide hybrid composite membranes via electrostatic interactions for direct methanol fuel cells

S. C. Sánchez-Ballester[a], L. Monreal[b], A. Ribes-Greus[a], V. Soria[c], G. Rydzek[d] and K. Ariga[d]

[a]Instituto de Tecnología de Materiales (ITM), Universitat Politècnica de València, Valencia, Spain
[b]Instituto Universitario de Matemática Pura y Aplicada, Universitat Politècnica de València, Valencia, Spain.
[c] ICMUV, Universitat de València, Burjassot, Valencia, Spain
[d] World Premier International (WPI) Research Center for Materials Nanoarchitectonics (MANA), National Institute for Materials Science (NIMS), Tsukuba, Japan.

Abstract

The surface of PVA-based substrate membranes, 15PVA and 15sPVA, negatively charged was modified by alternating deposition of a positively charged dispersion of graphene oxide-poly(allyl amine) hydrochloride (GO-PAH) followed by the deposition of a negatively charged solution of sulfonated polyvinyl alcohol (sPVA) via layer-by-layer (LbL) electrostatic assembly method in order to reduce the methanol crossover of the composite membranes. A set of six composites denoted as 15PVA(GO-PAH/sPVA)$_n$ and 15sPVA(GO-PAH/sPVA)$_n$, where the number of bilayer assembled (*n*) varied from 1 to 3, were prepared. FTIR, SEM and AFM analyses were carried out to confirm the successful deposition of the GO-PAH/sPVA bilayers onto the substrates surface. The thermal and mechanical properties of the LbL composites were investigated by TGA analysis and Vickers microhardness as a function of the deposited bilayers and the sulfonation of the substrate. In order to evaluate the potential of the prepared composite membranes as electrolytes for fuel cells, their proton-conducting properties were also evaluated in terms of water contact angle, water uptake, swelling ratio, proton conductivity and H_2-O_2 fuel cell test. Finally, the methanol diffusion coefficients of the LbL composites were determined as preliminary measure to assess their possible application in DMFCs. The best performance was attained for the 15PVA(GO-PAH/sPVA)$_1$ composite, showing a σ_{prot} of 8.26 mS/cm at 90 ºC and a maximum power density in a H_2-O_2 fuel cell of 12.2 mW/cm^2 with the highest value of methanol selectivity (1.38×10^5 S·s·cm^{-3}) among all the prepared LbL composites.

Keywords: poly(vinyl alcohol), graphene oxide, poly(allyl amine) hydrochloride, Layer-by-Layer assembly, electrostatic interaction, proton exchange membrane, proton conductivity

Introduction

Perfluorosulfonic acid (PFSA) polymers, such as Nafion®, are the most commonly materials used as proton exchange membranes (PEMs) in Direct Methanol Fuel Cells (DMFCs). Nafion® exhibits high thermal and mechanical properties as well as high proton conductivity when the membrane is fully hydrated [1], [2]. However, its high methanol crossover leads to a reduction of the cell voltage by the effect so-called mixed potential.

An attractive strategy to the suppress methanol crossover effect in DMFCs, is the modification of the PEM by the addition of inorganic fillers. This can drastically reduce the methanol crossover of the membranes while their proton conductivity is not greatly affected. Among the different inorganic fillers, the graphene oxide (GO) is considered an attractive filler for the preparation of hybrid organic-inorganic composite membranes since it is easy to disperse in polar polymers due to the oxygen functional groups that it contains in its structure. Moreover, its laminar structure with high surface area favors the formation of proton transport channels through the membrane and acts as a methanol-barrier reducing its drawback of crossover [3], [4].

One of the most versatile fabrication techniques for the preparation of hybrid organic-inorganic composite membranes is the Layer-by-Layer (LbL) electrostatic assembly method. The LbL assembly method consists of alternate dipping of a substrate into oppositely charged polycation and polyanion electrolyte solutions, as reported by Decher [5]. In recent years, the use of the LbL assembly method has been extensively used in the preparation of multilayered composite membranes for fuel cell applications [6], [7]. B. G. Kim et al. prepared multilayers polyelectrolyte membranes by LbL method by alternating deposition of poly(diallyl dimethyl ammonium chloride) (PDDA) and an anionic polyelectrolyte chosen from graphene oxide (GO), sulfonated GO (sGO), or sulfonated poly(phenylene oxide) (sPPO) onto a Nafion membrane, and their adaptability as membranes for DMFCs was investigated in terms of methanol permeability [8]. It was found that the deposition of tetra-layers of PDDA/GO/PDDA/sPPO and PDDA/sGO/PDDA/sPPO on Nafion film decreases the permeability of the composites membranes compared to untreated Nafion. S. P. Jiang et al. assembled effective multilayer methanol-blocking thin film on a Nafion membrane using LbL self-assembly of oppositely charged polyelectrolytes [9]. The polyelectrolytes used were poly(diallyldimethylammonium chloride) (PDDA, polycation), poly(sodium styrene sulfonate) (PSS, polyanion), and poly(1-(4-(3-carboxy-4-hydroxyphenylazo) benzene sulfonamido)-1,2-ethanediyl, sodium salt) (PAZO, polyanion). The LbL self-assembly of oppositely charged polyelectrolytes on a Nafion membrane showed a significant effect on the reduction in methanol crossover and on the enhancement of the performance of DMFCs.

The aim of this study was the preparation of PVA/GO composite membranes with low methanol permeability and high proton conductivity by the LbL electrostatic assembly method for DMFC applications. Two different substrates, 15PVA and 15sPVA, were prepared by solvent-casting method and were further crosslinked with sulfosuccinic acid (SSA) at 15 wt.% of concentration, which introduces simultaneously sulfonic acid groups to the structure in order to improve the proton conductivity of the composites. In addition, the 15sPVA substrate was also modified by intra-sulfonation of the matrix with the aim to study the effect of the matrix sulfonation on the proton conductivity properties. The composites were assembled by alternating dipping of the substrates in a solution of GO dispersed in poly(allyl amine)hydrochloride (GO-PAH) positively charged and a negatively charged solution of sPVA, obtaining the composites denoted as $15PVA(GO-PAH/sPVA)_n$ and $15sPVA(GO-PAH/sPVA)_n$. The effect of both the number of bilayers deposited and the intra-sulfonation of the polymer matrix of the substrate on the structural (FTIR), morphological (SEM, AFM), thermal (TGA) and mechanical properties (Vickers hardness) was studied. Moreover, the evaluation of the proton-conducting properties of the composites was carried out in terms of the water contact angle, water uptake (WU) and swelling ratio (SW), ion exchange capacity (IEC), proton conductivity (σ_{prot}) and H_2-O_2 fuel cell test. Finally, the methanol diffusion coefficients of the prepared LbL composites were determined as a preliminary assay to validate their potential as electrolytes in DMFCs.

Experimental

Chemicals

Graphite powder (particle size < 20 μm), sodium nitrate (NaNO$_3$, ≥ 99.0%), sodium hydride (NaH, dry 95%), 1,3-propane sultone (97%), poly(vinyl alcohol) (PVA, molecular weight 130000 g/mol degree of hydrolysis, min. 99%), poly(allylamine) hydrochloride (PAH, molecular weight 15000 g/mol), sulfosuccinic acid (SSA, 70 wt.% solution in water) and glutaraldehyde (GA, 25 wt.% solution in water) were purchased from Sigma-Aldrich. Concentrated sulfuric acid (H$_2$SO$_4$, 95%), hydrogen peroxide (H$_2$O$_2$, 30% w/w), ethanol absolute (EtOH), hydrochloric acid (HCl, 37%) and potassium permanganate (KMnO$_4$, extra pure) were purchased from Scharlab.

Synthesis of sulfonated poly(vinyl alcohol) (sPVA)

sPVA was synthesized according to the procedure previously described in Contribution I and III [10], [11]. In a first step, 10 g of commercial PVA were added in 250 mL of EtOH, followed by the slow addition of 3.8 g of NaH under constant stirring. Next, 5 g of 1,3-propane sultone were added dropwise to the mixture and stirred at 80 ℃ for 24 hours. The obtained sodium sulfonated salt was transformed to the protonated form by immersion in hydrochloric acid solution for 12 hours. The sPVA powder was filtered, washed with ethanol and finally dried for 4 hours in a vacuum oven at 50 ℃.

Synthesis of graphene oxide (GO)

GO was synthesized from graphite powder using the Modified Hummers Method (MHM) [12], [13]. Briefly, 2 g of graphite in 46 mL of concentrated H$_2$SO$_4$ were mixed with 1 g of NaNO$_3$ in an ice bath under constant stirring. After 5 minutes, 6 g of KMnO$_4$ were added gradually to the above solution while keeping the temperature below 20 ℃ to prevent overheating. The ice bath was then removed and the mixture was stirred at 35 ℃ for 30 minutes. The resulting solution was diluted by adding 92 mL of distilled water dropwise under constant stirring. Then, the temperature was increased at 98 ℃ and 280 mL of distilled water was added under vigorous stirring. After 2 hours, the suspension was filtered and treated with 30% H$_2$O$_2$ solution. The resulting GO was washed several times with HCl and EtOH until the washings reach pH 7, followed by filtration. Finally, the powder was suspended in distilled water and sonicated for 3 hours, filtered and dried in a vacuum oven for 12 hours.

Preparation of substrate membranes

Two types of crosslinked membranes, 15PVA and 15sPVA, were prepared by solution-casting method to use as substrate membranes in Electrostatic LbL assembly. First, PVA and sPVA aqueous solution (5 wt.%) were prepared by dissolving the polymer in water and refluxing at 90 °C for 6 hours. Then, the solutions were mixed with 15 wt.% of sulfosuccinic acid (SSA) and vigorously stirred at room temperature for 24 hours. The homogeneous solutions were poured onto a Teflon plate and the cast membranes were allowed to dry at room temperature. As the last step, the dried membranes were crosslinked at 110 °C for 2 hours.

Preparation of Layer-by-Layer solutions

sPVA solutions were prepared by dissolving 1 wt.% of polymer in water and refluxing at 90 °C for 6 hours. GO-PAH solution was prepared dispersing the GO (1mg/mL) by sonication in a PAH solution previously prepared at 1 wt.%. The pH of the GO-PAH and the sPVA solutions was adjusted to 5.5 in order to favors the interaction between the carboxylic acid groups of GO in deprotonated form ($-COO^-$, $pK_a = 4.3$) and the amine groups of PAH in protonated form ($-NH_3^+$, $pK_a = 8.5$) during the LbL assembly process via electrostatic interactions with sPVA ($-SO_3^-$, $pK_a = 1$) [14], [15].

Layer-by-Layer (LbL) assembly of composite membranes

Prior to the LbL assembly process, the substrate was conditioned in Mili-Q water (pH 5.5) for 15 minutes. Next, the substrate was alternately dipped in the GO-PAH solution and the sPVA solution for 10 minutes. After each dipping step, the membrane was rinsed with Mili-Q water for 5 minutes to remove weakly bonded molecules. The process was repeated to increase the number of GO-PAH/sPVA bilayers on the substrate surface. Scheme 5.2 shows schematically the one bilayer deposition process by the LbL assembly method based on electrostatic interactions. Finally, the composites were crosslinked by immersing into 3 % solution of GA for 30 minutes at room temperature in order to fix the deposited bilayers. The composites were denoted as 15PVA(GO-PAH/sPVA)$_n$ and 15sPVA(GO-PAH/sPVA)$_n$, where *n* represents the number of GO-PAH/sPVA bilayers deposited.

1 bilayer deposition process
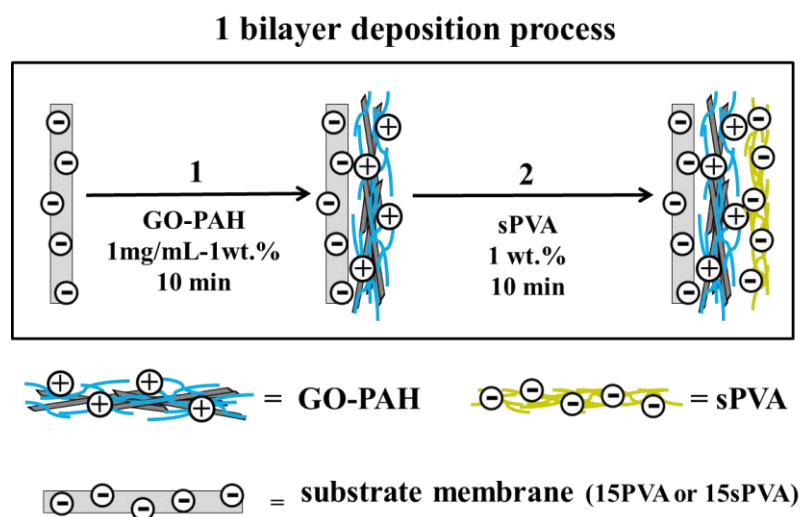
Scheme 5.2. Schematic representation of the one bilayer deposition process by LbL assembly method based on electrostatic interactions

Characterization techniques

The charge properties of the GO-PAH and sPVA solutions were measured at pH 5.5 using a *Zetasizer Nano ZS90 analyzer (Malvern Instruments)*. The pH values of individual samples were adjusted by adding HCl or NaOH.

Fourier Transform Infrared (FTIR) spectra were recorded with a *Thermo Nicolet 5700 FTIR*. The FTIR spectra were collected after 64 scans in the 4000-400 cm^{-1} region using the Attenuated Total Reflectance (ATR) mode at a resolution of 4 cm^{-1}. Backgrounds spectra were collected before each series of experiments. All the experiments were performed three times and the average was taken as a representative value.

The degradation process and thermal stability of the composites were investigated by Thermogravimetric Analysis (TGA) on a *TA Instruments TGA Q-500* analyzer. Measurements were carried out under nitrogen atmosphere at 10 ºC/min heating rate covering from 25 to 800 ºC temperature range.

The surface and cross-sectional morphology of the composites was studied using a *JEOL JSM-6300* scanning electron microscope with an acceleration voltage of 20 kV. The samples for cross-sectional analysis were prepared by immersing the films in liquid nitrogen for 10 minutes before fracture.

The morphology surface of composite membranes was also studied using an Atomic Force Microscope (AFM) *Multimode Nanoscope IVa, Digital Instrument/ Veeco* operating in tapping mode at room temperature under ambient conditions

Microhardness (MH) measurements were carried out using a Vickers indentor equipped with a *Leitz RZD-DO* microhardness tester. A load of 100 g was used, with a loading cycle of 25 s at room temperature. The hardness value was measured immediately after indentation. MH values (in MPa) were calculated according to the following relationship [16].

$$MH = 2 \sin 68° \left(\frac{P}{d^2} \right)$$

where *P* is the contact load in *newtons* (N) and *d* is the diagonal length of the projected indentation area in *millimeters* (mm). The experimental values were taken from the average of three measurements.

Water contact angle

The wettability of composites was measured according to its water contact angle. Hence, static contact angle was evaluated using a *Theta Optical Tensiometer (KSV Instruments, Ltd)* and electrooptics comprising a CCD camera connected to a computer at room temperature. The distilled water (2 µL) was dropped on the sample surface at five different sites and the average value was taken as the representative value.

Water Uptake (WU) and Swelling ratio (SW)

The absorption of water was evaluated by performing swelling tests. Rectangular specimens of 4 x 1 cm^2 were dried at 60 ºC under vacuum for 12 hours, and the weight of the dried composite was measured in a microbalance. The composites were immersed in tests tubes containing distilled water at 30 ºC. The absorption of water was measured gravimetrically at different times, taken out, wiped with tissue paper, and immediately weighted the sample on a microbalance. The samples were weighted until no further gain weight was observed, denoting that the equilibrium condition was achieved. The water uptake, WU (%), was calculated as the mass difference between the samples exposed to water (M_{eq}) and the dry sample (M_{dry}). The results were normalized respect to the mass of the dried sample by

$$WU_{eq}(\%) = \frac{M_{eq} - M_{dry}}{M_{dry}} \times 100$$

The swelling ratio (SW) was calculated from the change in length between the fully hydrated at equilibrium and dry composites, L_{eq} and L_{dry}, respectively, as follows

$$SW_{eq}(\%) = \frac{L_{eq} - L_{dry}}{L_{dry}} \times 100$$

Ion Exchange Capacity (IEC)

The IEC of each composite was determined by titration method. The pre-weighted dry sample was soaked in a 0.5 M HCl solution for 24 hours at room temperature to obtain its protonated form. The sample was washed with an excess amount of distilled water and then was immersed in a 2M NaCl solution for 24 hours at room temperature to exchange H^+ with Na^+ ions. The amount of H^+ liberated was estimated by acid-base titration against a standard 0.1 N (0.0955 ± 0.0009 N) NaOH solution with phenolphthalein as the indicator. The IEC values were calculated using the following equation:

$$IEC(mequiv/g) = \frac{N_{NaOH} \times V_{NaOH}}{W_{dry}}$$

where N_{NaOH} is the normality of the titrant in mequiv/L, V_{NaOH} is the added titrant volume in *liters* (L), and W_{dry} is the dry mass of sample in *grams* (g).

Conductivity measurements

Conductivity of the composites was measured with a *Novocontrol Broadband Dielectric Spectrometer (BDS)* in the frequency range of 10^{-1} to 10^7 Hz using an *Alpha-A Frequency Response Analyzer (Novocontrol)*.

The proton conductivity (σ_{prot}) was measured using a *BDS-1308 (Novocontrol)* liquid parallel plate sample cell. The samples were previously equilibrated with Mili-Q water to ensure fully hydrated state. The measurements were performed at 30, 50, 70 and 90 ºC. The proton conductivity (in S/cm) of the membranes was calculated using

$$\sigma_{prot} = \frac{L}{R A}$$

where *L* is the thickness of the conducting membranes in *centimeters* (cm), *A* the area of the electrode in contact with the sample in cm^2, and *R* the protonic resistance in *ohms* (Ω), taken from the Bode plot at high frequencies [17].

Electrical conductivity was measured at 30 °C using a *BDS-1200 (Novocontrol)*, parallel-plate capacitor cell with two gold-plated electrodes. The electrical conductivity was taken at low frequencies, where the measured real part of the conductivity (σ') reaches a plateau which corresponds directly to the DC conductivity (σ_0).

H$_2$-O$_2$ fuel cell test

The performance of the composites in a H$_2$-O$_2$ fuel cell was tested by measuring the polarization curves. The samples were equilibrated with Mili-Q water during 24 hours and then were sandwiched between two sheets of gas diffusion electrodes (*Fuels Cells Etc*, 4 mg/cm^2 Platinum Black). The electrochemical performances were evaluated with a single-cell fixture having an active area of 16 cm^2. The fuel cell was operated with hydrogen and oxygen at 25 °C and atmospheric pressure.

Methanol diffusion coefficients (D$_{MeOH}$)

The methanol diffusion coefficients (D$_{MeOH}$) through the composites were tested by a home-made gravimetric permeation cell. The composites were cut into disks of 15 mm in diameter. The cell was filled with methanol solution (2M) and then was quickly assembled with the sample clamped to seal the pathway of the solvent. The sealed cell was immediately put on an analytical balance in a constant temperature chamber. The weight loss, related to the methanol diffused through the membrane, was recorded as a function of time. The diffusion coefficients were obtained from the transient state, which is valid for short times, using the Rogers equation [18],

$$\ln\left(F\, t^{\frac{1}{2}}\right) = \ln\left[2c_1 \left(\frac{D}{\pi}\right)^{1/2}\right] - \frac{l^2}{4Dt}$$

where *F* is the permeation flux in g·cm^{-2}·s^{-1}, *t* is the time in *seconds* (s), c_1 is the penetrant concentration at x = 0, *l* is the thickness of the sample in *centimeters* (cm), and *D* is a constant diffusion coefficient in cm^2/s. The plot of ln(F t$^{1/2}$) vs (1/t) gives the slope (–l^2/4D) from which the value of D$_{MeOH}$ can be estimated.

Results and discussion

Charge properties

The charge properties of the GO-PAH and the sPVA solutions were analyzed by zeta potential measurements in order to evaluate the feasibility of the GO-PAH/sPVA layer-by-layer assembly at pH 5.5. The values of zeta potential show that the GO-PAH and the sPVA solutions are able to remain positively (+29.19 mV) and negatively (-6.78 mV) charged, respectively, at this pH. This ensures the stability of the GO-PAH/sPVA bilayers electrostatic assembled.

Structural characterization

FTIR analysis was carried out in order to verify the deposition of the bilayers on the surface of the substrates. Figure 5.13 compares the FTIR spectra of the 15PVA and 15sPVA substrates before and after deposition of one and three GO-PAH/sPVA bilayers with the spectrum of the GO and PAH samples.

The FTIR spectra of the unmodified 15PVA and 15sPVA substrates show four main characteristic bands. At 3400 cm^{-1} it is found the stretching vibration band of the hydroxyl groups of the polymer matrix [19]. The symmetric and asymmetric stretching bands of the methylene groups (C-H) appear at 2800 cm^{-1} and 2900 cm^{-1}, respectively. The band associated to the carbonyl groups (C=O) introduced by the SSA is observed at 1710 cm^{-1} [20]. Finally, the band at 1037 cm^{-1} may be assigned to the stretching vibration band of the sulfonic acid groups ($-SO_3H$) from the SSA and the sPVA.

The deposition of GO/sPVA bilayers does not produce substantially changes in the structure of the composites, showing the 15PVA(GO-PAH/sPVA)$_n$ and 15sPVA(GO-PAH/sPVA)$_n$ composites the same spectrum pattern than their substrates. However, slight differences that evidence the successful LbL assembly process can be found. At 3450 cm^{-1}, the hydroxyl vibration band shows a shoulder attributed to the stretching vibration of the amine groups (N-H) from the PAH. Moreover, the decrease in intensity of the carbonyl band at 1710 cm^{-1} and the appearance of a new band at 1646 cm^{-1}, combination of the vibration band of the aromatic double bonds (C=C) of GO and the scissoring vibration band of the N-H from the PAH [21], [22], confirms the deposition of the GO-PAH/sPVA bilayers onto the substrates.
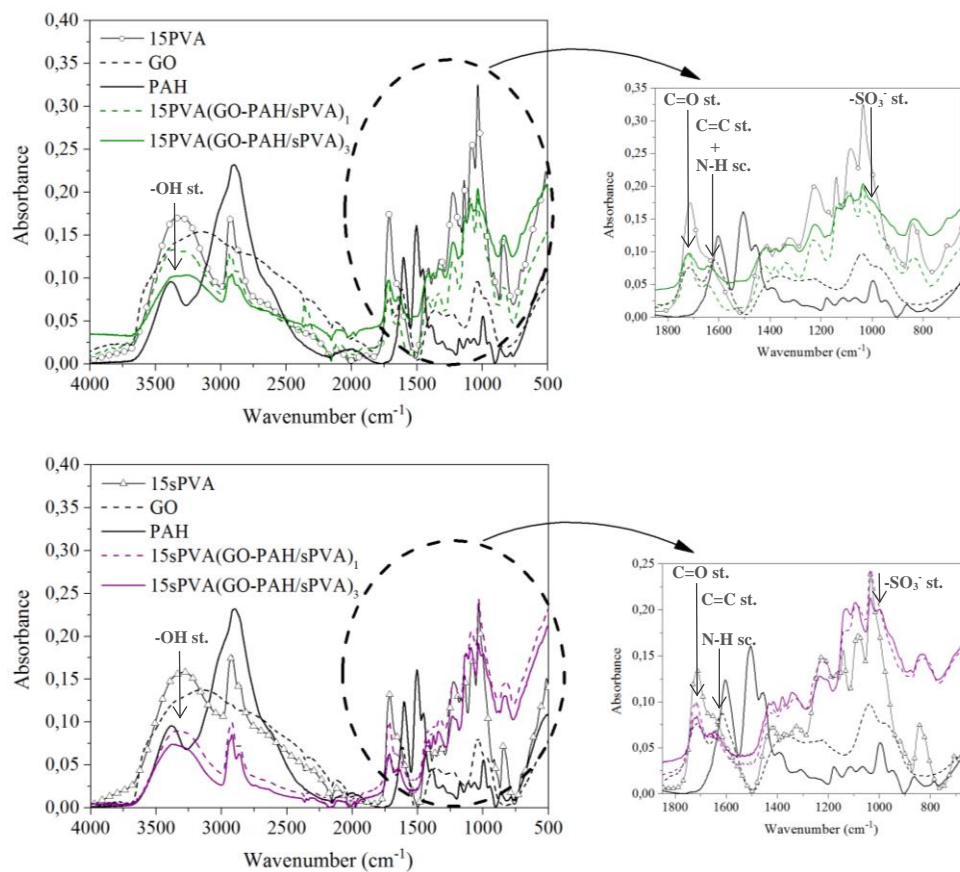
Figure 5.13. FTIR spectra of the 15PVA and 15sPVA membranes before and after deposition of one and three GO/sPVA bilayers compared to the spectrum of GO and PAH

Thermal characterization

The thermal stability of the composites was investigated by TGA. Figure 5.14 compares the thermogravimetric (TG) and the first-order derivative (DTG) curves of the 15PVA and 15sPVA substrates before and after deposition of one and three GO-PAH/sPVA bilayers.
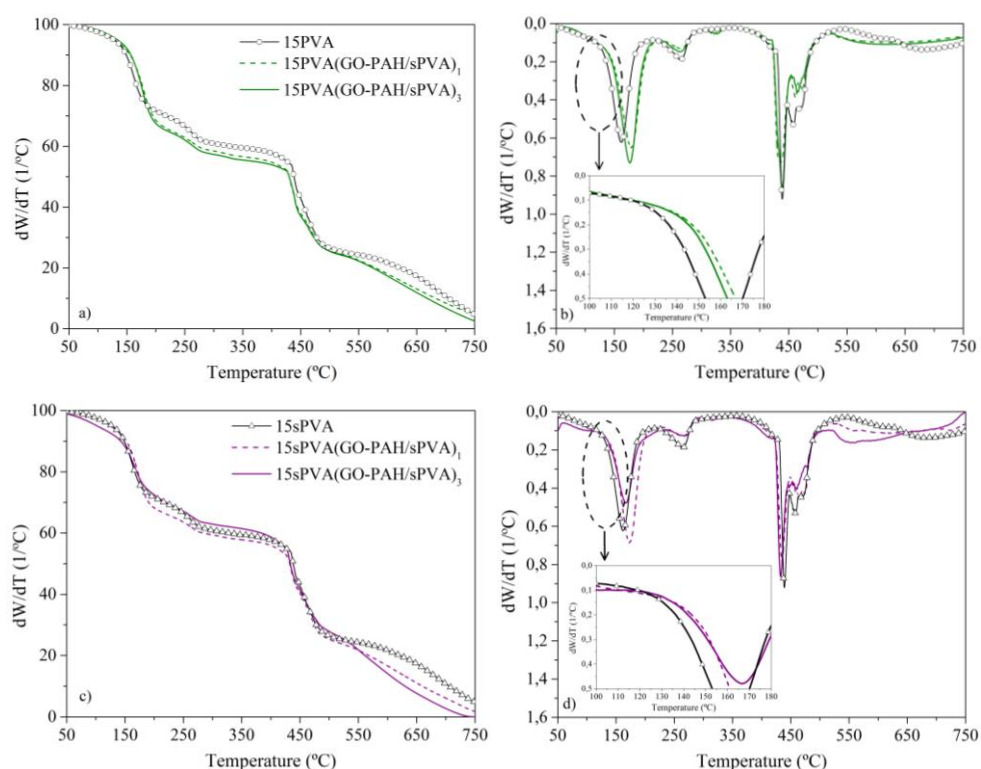
Figure 5.14. Comparison of the TG (a, c) and DTG (b, d) curves of the 15PVA and 15sPVA substrates before and after deposition of one and three GO-PAH/sPVA bilayers. The inset graph in DTG curves shows a magnification of the first decomposition stage

Both the 15PVA(GO-PAH/sPVA)$_n$ and the 15sPVA(GO-PAH/sPVA)$_n$ composites show the same three-step decomposition pattern similar than their substrates. The first decomposition stage, occurred between 50 and 200 ºC, is due to the elimination of the hydroxyl groups of the polymer matrix [11], [23]. The second stage, ranging from 200 ºC to 350 ºC, is attributed to thermal desulfonation of the sulfonic acid groups grafted

to the sPVA chains and those introduced by the SSA crosslinking agent [23]-[26]. The last decomposition stage is observed in the range from 350 to 750 ºC and is associated to the breakage and main chain scission of the polymer matrix [23], [27]. Notice that beyond 500 ºC the thermal decomposition of the formed char takes place. Table 5.8 summarizes the temperature weight losses extracted from the thermograms curves of each evaluated composite.

Table 5.8. Temperature dependent weight loss values extracted from the thermograms of the electrostatic LbL composites

Membrane	Stage I		Stage II (ºC/%)		Stage III	
	T_{peak}	ΔW	T_{peak}	ΔW	T_{peak}	ΔW
15PVA	164	28	265	11	432	32
15PVA(GO-PAH/sPVA)$_1$	179	34	265	8	437	32
15PVA(GO-PAH/sPVA)$_3$	177	35	264	8	439	31
15sPVA	162	29	264	9	439	35
15sPVA(GO-PAH/sPVA)$_1$	173	34	265	8	435	34
15sPVA(GO-PAH/sPVA)$_3$	167	29	265	8	433	35

The results show that after deposition of one bilayer the thermal properties of the 15PVA and 15sPVA substrates improves. However, the thermal stability of the composites is reduced when the deposited bilayers are increased to three. This can be attributed to the higher amount of sPVA layers deposited in the three-bilayer composites that catalyzes the elimination reactions of the hydroxyl groups decreasing the stability of the composites to thermal decomposition [23]. In particular, the 15sPVA(GO-PAH/sPVA)$_n$ composites exhibit stronger influence due to the higher amount of sulfonic acid groups in their structure.

Morphological characterization

SEM measurements were carried out in order to provide a visual evidence that the 15PVA and 15sPVA substrates were uniformly covered by the GO-PAH/sPVA bilayers during the LbL assembly process. Figure 5.15 compares the membrane surface after deposition of one and three bilayers at two different magnifications (at 200× and 1.5K× for the inset image). In the images can be clearly observed the GO nano-platelets deposited on the surface of the 15PVA and 15sPVA substrates. Moreover, the amount of the deposited GO increases with increasing the bilayers. On the other hand, the 15sPVA(GO-PAH/sPVA)$_n$ composites show a denser coverage than the 15PVA(GO-PAH/sPVA)$_n$ composites. The higher negative charge density in the 15sPVA substrate favors the electrostatic interactions between the substrate and the GO-PAH layer positively charged [28], [29].
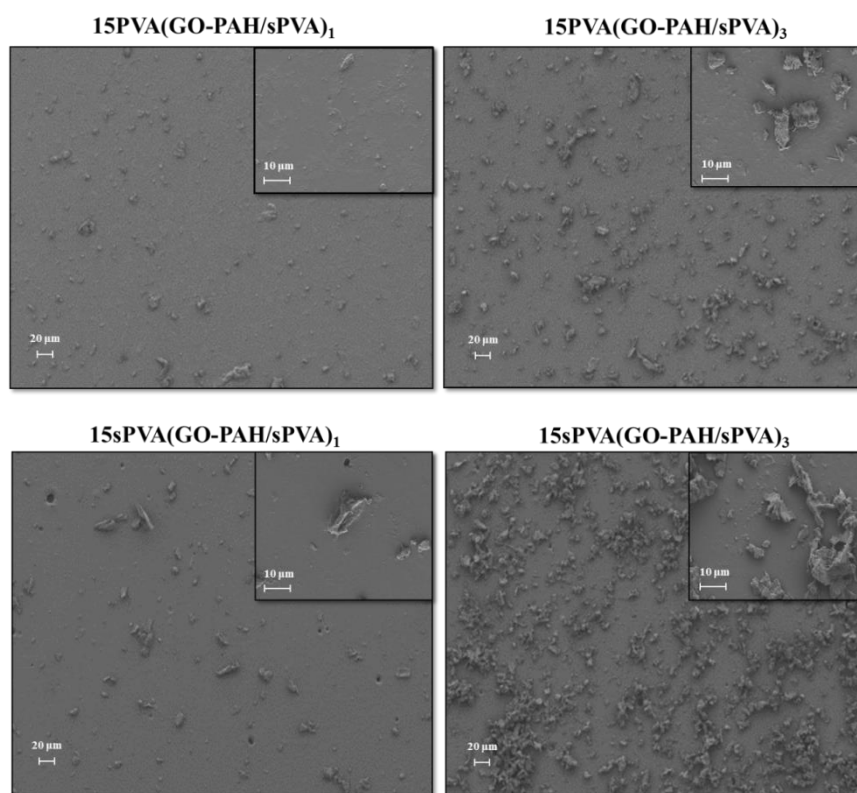
Figure 5.15. SEM images of the substrates surface after deposition of one and three GO-PAH/sPVA bilayers (magnification 200×). Inset SEM images are at 1.5K× magnification

Figure 5.16 shows the cross-section SEM images of the 15PVA(GO-PAH/sPVA)$_3$ and 15sPVA(GO-PAH/sPVA)$_3$ composites. It is clearly seen from these images that the GO-PAH/sPVA bilayers homogenously covered the surface of the 15PVA and 15sPVA substrates. In the images can be distinguish a sharp boundary between the 15PVA and 15sPVA substrates (darker color) and the lighted band assigned to the deposited GO-PAH/sPVA bilayers, evidencing the distinct morphology of both phases [30]-[32].
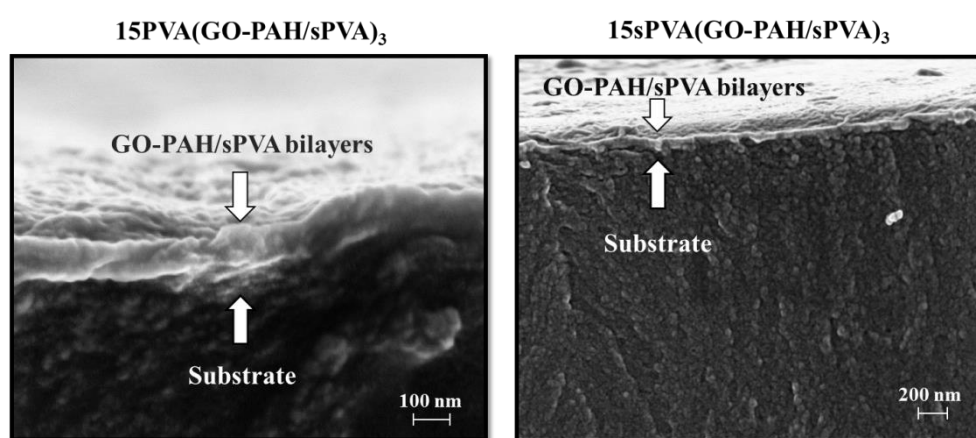
Figure 5.16. SEM images of the cross-section view of the 15PVA(GO-PAH/sPVA)$_3$ and 15sPVA(GO-PAH/sPVA)$_3$ composites

The surface morphology of the composites was further investigated by AFM. Figure 5.17 shows the tapping-mode AFM images of the 15PVA and 15sPVA substrates and their derived 15PVA(GO-PAH/sPVA)$_n$ and 15sPVA(GO-PAH/sPVA)$_n$ composites build-up from one and three bilayers. A smooth topography is observed in both substrates (Figure 5.17a, d), showing a roughness average (R_a) of about 0.5 nm. In contrast, the height profile of the composites reveals a non-uniform surface with sharp peaks attributed to the GO nano-platelets deposited on the surface [33]. Nevertheless, the peak distribution over the studied surface (5×5 μm^2) is homogeneous, indicating a good dispersion of the GO in the deposited coating [34], [35]. The one-bilayer composites show a roughness average of 2.9 and 3.1 nm (Figure 5.17b, e), whereas for the three-bilayer composites the values increase up to 8.6 and 10.9 nm (Figure 5.17c, f), respectively. The total coating thickness was about 10 nm and 30 nm after deposition of one and three bilayers.

15PVA

15sPVA

a)

Ra = 0.4 nm

d)

Ra = 0.5 nm

15PVA(GO-PAH/sPVA)₁

15sPVA(GO-PAH/sPVA)₁

b)

Ra = 2.9 nm

e)

Ra = 3.1 nm

15PVA(GO-PAH/sPVA)₃

15sPVA(GO-PAH/sPVA)₃

c)

Ra = 8.6 nm

f)

Ra = 10.9 nm
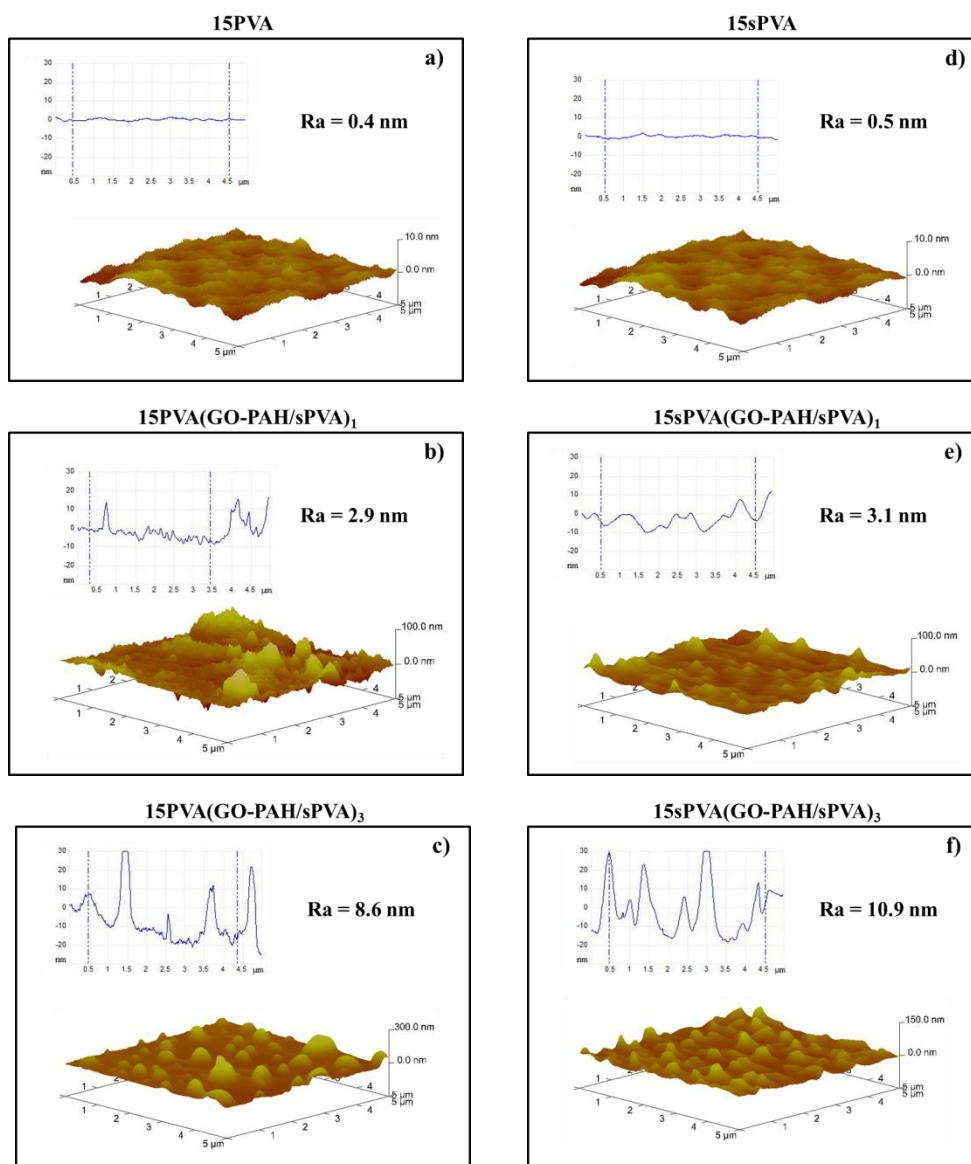
Figure 5.17. AFM images of the 15PVA and 15sPVA substrates before and after deposition of one and three GO-PAH/sPVA bilayers, respectively.

Mechanical characterization

The Vickers hardness (HV) tests were performed in order to investigate the effect of the deposition of GO-PAH/sPVA bilayers on the mechanical properties of the composites. Table 5.9 summarizes the values of HV of the $15PVA(GO-PAH/sPVA)_n$ and $15sPVA(GO-PAH/sPVA)_n$ composites and their respective substrates.

Table 5.9. Values of Vickers Hardness (HV) of the $15PVA(GO-PAH/sPVA)_n$ and $15sPVA(GO-PAH/sPVA)_n$ composites compared to their respective substrates

Membrane	HV (MPa)
15PVA	148 ± 1
$15PVA(GO-PAH/sPVA)_1$	108 ± 2
$15PVA(GO-PAH/sPVA)_3$	152 ± 4
15sPVA	153 ± 3
$15sPVA(GO-PAH/sPVA)_1$	136 ± 3
$15sPVA(GO-PAH/sPVA)_3$	203 ± 2

Both the $15PVA(GO-PAH/sPVA)_n$ and $15sPVA(GO-PAH/sPVA)_n$ composites show the same trend with increasing the number of deposited bilayers. After deposition of one bilayer, contrary to expectations, the composites show lower values of hardness than their substrates. In each deposition a layer of polymer, PAH with GO dispersed or sPVA, is assembled onto the surface of the substrate. This polymer coating shows lower resistance to plastic deformation than the substrates, resulting in a decrease of the hardness [36]. However, when three GO-PAH/sPVA bilayers are deposited the hardness of the composites strongly increases due to the high amount of GO nano-platelets deposited on the surface as well as to the increment of the coating thickness, in agreement with the results from the SEM images.

In addition, the $15sPVA(GO-PAH/sPVA)_n$ composites show higher values of HV than the $15PVA(GO-PAH/sPVA)_n$ composites. The higher amount of negatively charges on the 15sPVA substrate surface leads to increase the density of ion-pair ($SO_3^- \cdots NH_3^+$) electrostatic interactions [36], obtaining a more compact assembly with improved hardness.

Water contact angle

The wettability properties of the 15PVA and 15sPVA substrates before and after deposition of GO-PAH/sPVA bilayers were studied by contact angle measurements. Small contact angles ($< 90°$) correspond to high wettability, while large contact angles ($> 90°$) correspond to low wettability. Figure 5.18 depicts the values of water contact angle and the differences in shape of water droplets onto the surface of the composites as a function of the number of deposited bilayers and the sulfonation of the substrate, taken the substrates as reference.
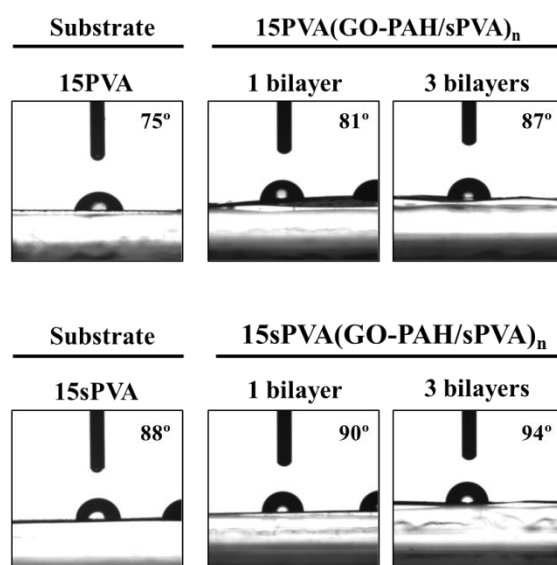
Figure 5.18. Values of water contact angle and differences in shape of water droplets onto the surface of the 15PVA and 15sPVA substrates before and after deposition of one and three GO-PAH/sPVA bilayers

As it was observed in the composite membranes assembled LbL by hydrogen-bonding interactions (Contribution IV) [37], the hydrophobicity of the membranes gradually increases with deposition of GO-PAH/sPVA bilayers. The hydrophilic groups, positively charged groups ($-NH_3^+$) of the PAH and negatively charged groups ($-COO^-$ and $-SO_3^-$) of the GO and the sPVA, are totally involved in the assembly of the LbL structure via electrostatic interactions. As a result, the hydrophobic groups are placed in the surface of the membrane increasing the water contact angle values. In addition, part of the hydroxyl groups remaining on the surface reacts with the GA during the final crosslinking process, forming new covalent bonds and so increasing the hydrophobic

domains on the membrane surface. Therefore, the results of water contact angle evidence that the studied composites have a hydrophilic-hydrophobic nano-phase separation morphology.

This behaviour is observed both the $15PVA(GO-PAH/sPVA)_n$ and $15sPVA(GO-PAH/sPVA)_n$ composites. However, the composites prepared from the 15sPVA substrate show higher values of water contact angles, which mean a surface more hydrophobic. This result might be attributed to the strong electrostatic interactions between the 15sPVA substrate and the deposited bilayers as compared to the 15PVA substrate, keeping the hydrophilic groups interacting inside of the structure.

Water Uptake (WU) and Swelling ratio (SW)

Water uptake (WU) is closely related to the proton conductivity in PEMs, since water molecules are involved in the proton transport according to the Grotthus and Vehicular mechanisms. Nevertheless, an excess of water uptake is not desirable because it leads to a low dimensional stability. Figure 5.19a shows the evolution of water uptake of the 15PVA and 15sPVA substrates as a function of the deposited GO-PAH/sPVA bilayers at 30 ºC.
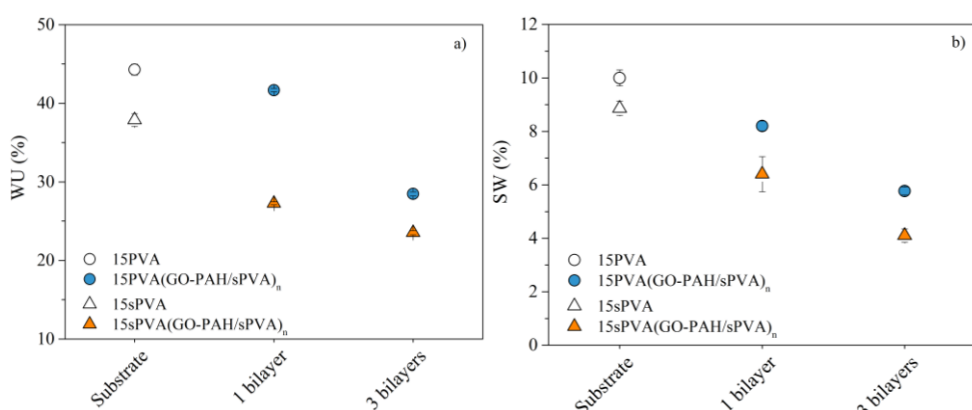
Figure 5.19. Water uptake (WU) and b) swelling ratio (SW) of the LbL composites as a function of the number of deposited GO-PAH/sPVA bilayers at 30 ºC

It can be found that the water uptake gradually decreases with increasing the deposited GO-PAH/sPVA bilayers [29], [32]. After deposition of three bilayers, the $15PVA(GO-PAH/sPVA)_3$ and $15sPVA(GO-PAH/sPVA)_3$ composites show a decrease in water uptake of 36 % and 38 %, respectively, compared to their substrates. This corroborates

the increase of the hydrophobic character of the composites by deposition of a higher amount of bilayers, in agreement with the water contact angle results. In addition, the 15sPVA substrate and their composites exhibit lower values of water uptake than that prepared from the 15PVA substrate, as was also seen for the LbL composites assembled via hydrogen bonding interactions in Contribution IV [37]. The higher hydrophobic character of the 15sPVA substrate compared to the 15PVA might lead to a decrease of the affinity of the water molecules to the membranes, decreasing their water uptake.

Swelling ratio values show a similar trend to water uptake, as shown in Figure 5.19b. For example, the swelling ratio of the 15PVA is 8.9 %, whereas, the 15sPVA(GO-PAH/sPVA)$_n$ composites show a swelling ratio of 6.1 % and 4.1 % after deposition of one and three bilayers, respectively. These results evidence an improvement of the dimensional stability of the LbL composites [32].

Ion Exchange Capacity (IEC)

The ion exchange capacity (IEC) is directly related to the proton conductivity in proton exchange membranes (PEMs) since it gives information about the number of exchangeable groups (typically sulfonic acid groups) per unit of mass. Table 5.10 summarizes the IEC values obtained for the LbL composites and their substrates.

Table 5.10. Ion exchange capacity (IEC) values of the 15PVA and 15sPVA substrates before and after deposition of one and three GO-PAH/sPVA bilayers

Membrane	IEC (mequiv/g)
15PVA	0.67 ± 0.03
15PVA(GO-PAH/sPVA)$_1$	0.90 ± 0.13
15PVA(GO-PAH/sPVA)$_3$	1.04 ± 0.16
15sPVA	0.69 ± 0.00
15sPVA(GO-PAH/sPVA)$_1$	1.10 ± 0.08
15sPVA(GO-PAH/sPVA)$_3$	1.32 ± 0.07

The IEC values of the LbL composites are higher than those obtained for the unmodified substrates, and are increased with the number of the deposited bilayers [38]. It was found that the IEC of the 15PVA and 15sPVA substrates increase a 55 % and 91 %, respectively, after deposition of three GO-PAH/sPVA bilayers. Moreover, the 15sPVA(GO-PAH/sPVA)$_n$ composites show higher values of IEC than those

prepared from the 15PVA substrate, which confirms the introduction of a greater amount of proton-exchangeable groups ($-SO_3H$ groups) by sulfonation of the substrate and deposition of sPVA layers.

Proton conductivity (σ_{prot})

Figure 5.20 shows the evolution of proton conductivity of the pre-hydrated $15PVA(GO-PAH/sPVA)_n$ and $15sPVA(GO-PAH/sPVA)_n$ composites and their substrates as a function of the temperature.
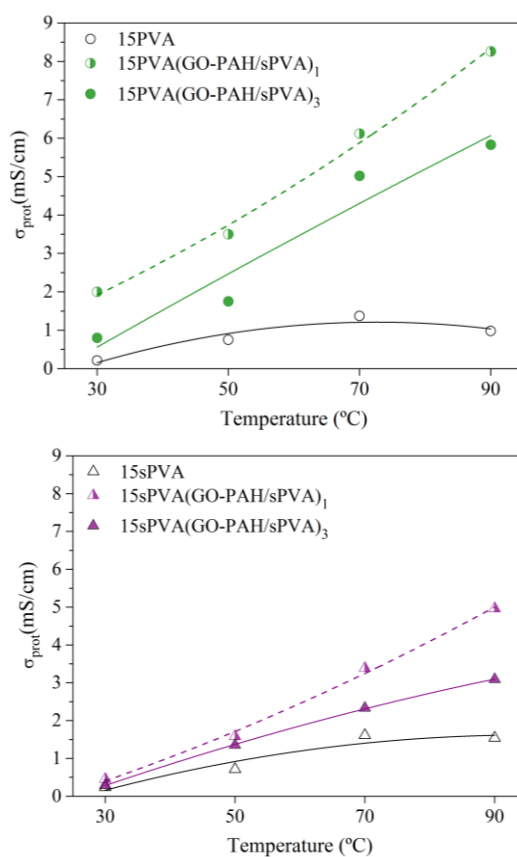

Figure 5.20. Evolution of proton conductivity (σ_{prot}) of the pre-hydrated a) 15PVA(GO-PAH/sPVA)$_n$, b) 15sPVA(GO-PAH/sPVA)$_n$ composites and their respective substrates as a function of temperature

The values of proton conductivity obtained for the pre-hydrated composites measured at 30, 50, 70 and 90 ºC are listed in Table 5.11. For comparison, the values of proton conductivity of the LbL composites assembled via hydrogen bonding interactions as well as the 15PVA/GO and 15sPVA/GO composites previously prepared by solution-casting method in Contribution II are also shown [37], [39], [40].

Table 5.11. Proton conductivity (σ_{prot}) values of the pre-hydrated electrostatic LbL composites measured as a function of temperature. The composites previously prepared by Hydrogen-bonding (H-B) LbL assembly and solution-casting (S-C) method are included for comparison

Membrane	σ_{prot} (mS/cm)			
	30 ºC	50 ºC	70 ºC	90 ºC
15PVA	0.21	0.75	1.37	0.98
15PVA(GO-PAH/sPVA)$_1$	2.00	3.50	6.12	8.26
15PVA(GO-PAH/sPVA)$_3$	0.80	1.75	5.02	5.83
15PVA(GO/PVA)$_1$ (H-B LbL)	*2.31*	*3.73*	*4.29*	*5.07*
15PVA(GO/PVA)$_3$ (H-B LbL)	*0.61*	*1.34*	*2.16*	*1.75*
15PVA/GO (S-C method)	*0.88*	*2.26*	*4.57*	*4.90*
15sPVA	0.23	0.71	1.61	1.54
15sPVA(GO-PAH/sPVA)$_1$	0.45	1.58	3.38	4.96
15sPVA(GO-PAH/sPVA)$_3$	0.29	1.35	2.33	3.09
15sPVA(GO/sPVA)$_1$ (H-B LbL)	*2.16*	*3.66*	*4.99*	*5.63*
15sPVA(GO/sPVA)$_3$ (H-B LbL)	*0.27*	*1.03*	*1.98*	*1.82*
15sPVA/GO (S-C method)	*0.97*	*2.23*	*6.16*	*6.24*

The proton conductivity of all membranes increases with the increase of temperature. Higher temperatures enhance the mobility of the polymer chains favoring the proton conduction through the membrane [41].

In general, the proton conductivity of the LbL composites is influenced by both the concentration and mobility of the proton carriers [42], in this case the sulfonic acid (-SO$_3$H) groups. After deposition of one GO-PAH/sPVA bilayer, an improvement of the proton conductivity is observed due to the increase in the number of -SO$_3$H groups introduced by the sPVA layer [28]. In contrast, when the deposited bilayers are increased to three, the proton conductivity is strongly reduced. This effect may be

explained by the formation of a thicker coating, which could reduce the mobility of the proton carriers through the composite [28].

It could be expected that the proton conductivity of the 15sPVA(GO-PAH/sGO)$_n$ composites reach higher values than that obtained for the 15PVA(GO-PAH/sPVA)$_n$ composites since the former contain higher amount of proton carriers (-SO$_3$H groups) in their substrate (15sPVA). Nevertheless, a contrary trend is observed. The proton conductivity of the 15sPVA(GO-PAH/sPVA)$_1$ composite is 3.38 mS/cm at 70 ºC, while the 15PVA(GO-PAH/sPVA)$_1$ composite shows a σ$_{prot}$ of 6.12 mS/cm under the same conditions. The high charge density of the 15sPVA substrate increase the electrostatically interactions between the substrate and the deposited bilayers, resulting in a much dense and compact coating in which the mobility of the proton carriers is restricted [43].

Comparing with the composites previously prepared by Hydrogen-bonding LbL assembly and solution-casting method [37], [39], [44], it was found a strong improvement of the proton conductivity in the 15PVA(GO-PAH/sPVA)$_n$ composites. In particular, the 15PVA(GO-PAH/sPVA)$_1$ composite shows an improvement of 63 % and 69 % compared to the 15PVA(GO/PVA)$_1$ composite (H-B method) and the 15PVA/GO composite (S-C method), respectively. However, the sulfonation of the substrate in the 15sPVA(GO-PAH/sPVA)$_n$ composites does not enhance their proton conductivity; showing higher values of proton conductivity the 15sPVA/GO composite as compared to those composites prepared by LbL assembly method.

The dependence of the proton conductivity with temperature is analyzed in terms of Arrhenius plot according to the following equation,

$$\log \sigma_{prot} = \log \sigma_0 - \frac{E_a}{RT}$$

where σ_{prot} is the proton conductivity in S/cm, σ_0 is a pre-exponential factor, E_a is the activation energy in kJ/mol, R is the universal gas constant (8.314 J/mol K), and T is the absolute temperature in Kelvin (K). The slope of log σ vs 1000/T gives the activation energy of proton conductivity, which is equivalent to the minimum energy required for the proton conduction. Figure 5.21 shows the Arrhenius plot for the pre-hydrated composites and their substrates.
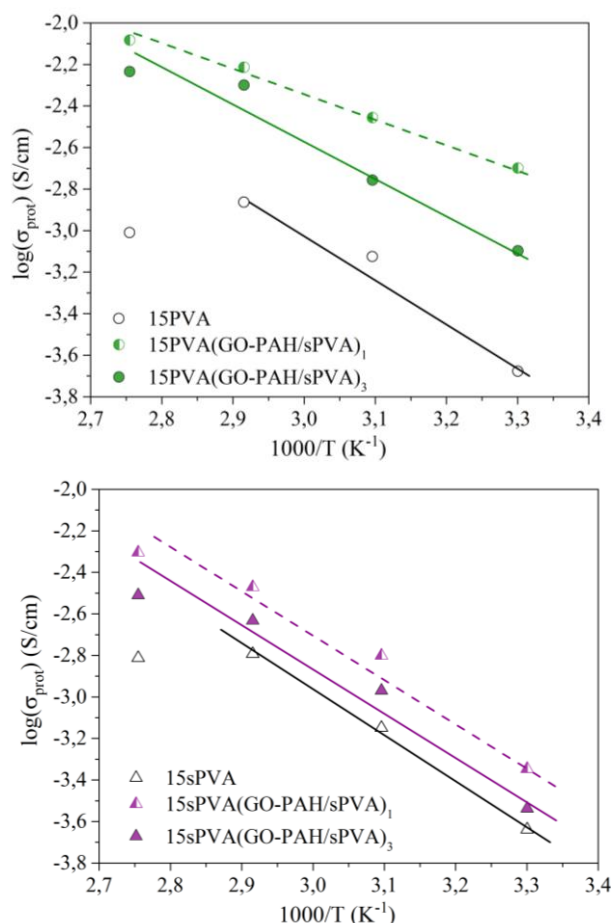
Figure 5.21. Arrhenius plots for proton conductivity (σ_{prot}) of the 15PVA(GO-PAH/sPVA)$_n$ and 15sPVA(GO-PAH/sPVA)$_n$ composites and their substrates

A linear correlation between the proton conductivity and temperature is observed for the LbL composites in all the range of temperature. However, the substrates only show linearity from 30 to 70 °C since beyond 70 °C part of the absorbed free-water evaporates decreasing their proton conductivity [39]. This linear dependence suggests that the proton conduction in the LbL composites follows an Arrhenius behaviour associated to the Grotthus mechanism [45]. The values of E_a calculated for each of the composites and their substrates are listed in Table 5.12.

Table 5.12. Activation energy (E_a) values calculated for the 15PVA(GO-PAH/sPVA)$_n$ and 15sPVA(GO-PAH/sPVA)$_n$ composites compared to their respective substrates

Membrane	E_a (kJ/mol)
15PVA	40.8
15PVA(GO-PAH/sPVA)$_1$	22.1
15PVA(GO-PAH/sPVA)$_3$	32.3
15sPVA	42.2
15sPVA(GO-PAH/sPVA)$_1$	43.7
15sPVA(GO-PAH/sPVA)$_3$	45.2

After deposition of GO-PAH/sPVA bilayers, the activation energy for the 15PVA(GO-PAH/sPVA)$_n$ composites strongly decreases. In particular, the E_a for the 15PVA(GO-PAH/sPVA)$_1$ composite is reduced almost at half (46%) compared to its substrate. This indicates that the proton transfer becomes easier after deposition of GO-PAH/sPVA bilayers in the 15PVA(GO-PAH/sPVA)$_n$ composites [32], in accordance with their higher values of proton conductivity. However, the activation energy values for 15sPVA(GO-PAH/sPVA)$_n$ composites are higher than those of their substrate. The strong electrostatic interactions between the substrate and the bilayers in these composites results in a compact coating that restricts the proton transport through it.

Moreover, low electrical conductivity is required in PEMs in order to avoid the pass of electrons through the membrane, since this will decrease the performance of the fuel cell. Figure 5.22 compares the electrical conductivity plots of the LbL composite membranes with the substrates. All composites show a low electrical conductivity of the order of 10^{-10} S/cm, confirming the electrical insulating property of the prepared electrostatic LbL composites.
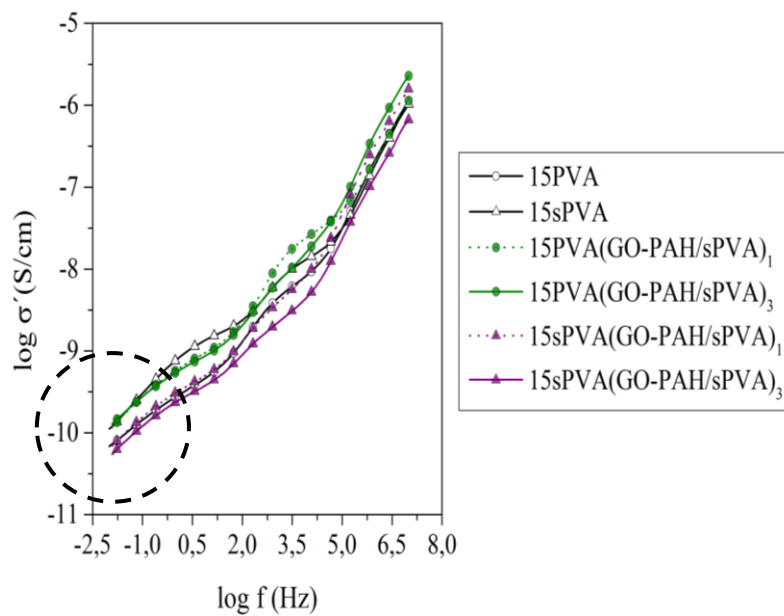
Figure 5.22. Electrical conductivity (σ_{elec}) of the 15PVA(GO-PAH/sPVA)$_n$ and 15sPVA(GO-PAH/sPVA)$_n$ composites compared to their substrates

H_2-O_2 fuel cell test

The performance of the electrostatic LbL assembled composites in a H_2-O_2 fuel cell was evaluated from the polarization curves measured at 25 ºC. The polarization curves of the 15PVA(GO-PAH/sPVA)$_n$ and 15sPVA(GO-PAH/sPVA)$_n$ composites compared to their substrates as shown in Figure 5.23.
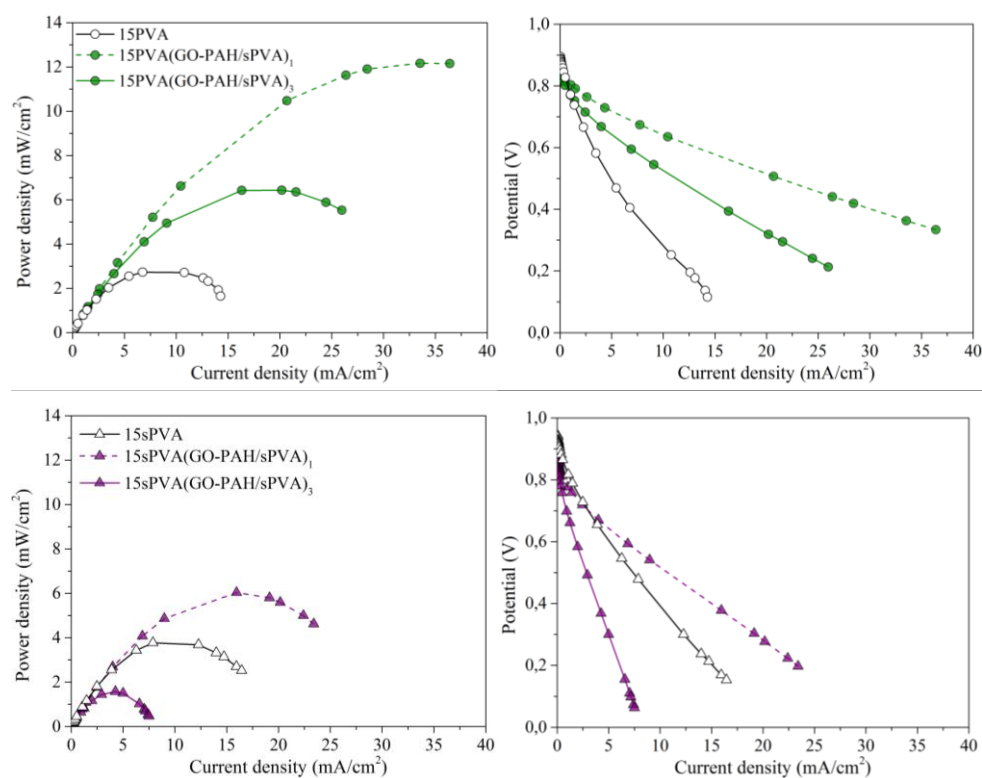
Figure 5.23. Polarization curves of the 15PVA(GO-PAH/sPVA)$_n$ and 15sPVA(GO-PAH/sPVA)$_n$ composites compared to their substrates at 25 ºC

The values of the maximum power density (P_{max}) obtained for each of the LbL composites and their substrates are summarized in Table 5.13. According to the results, the 15PVA(GO-PAH/sPVA)$_n$ composites show the best performance in the fuel cell test, particularly the 15PVA(GO-PAH/sPVA)$_1$ composite which exhibits a value of P_{max} of 12.2 mW/cm^2. This is an increase of the 352 % and 103 % compared to its substrate 15PVA and its homologue composite 15sPVA(GO-PAH/sPVA)$_1$, respectively. However, the increase of the sulfonic acid groups (-SO$_3$H) by sulfonation

of the substrate membrane in the 15sPVA(GO-PAH/sPVA)$_n$ composites sharply reduce their performance in a H$_2$-O$_2$ fuel cell. The higher density of electrostatic interactions in these composites leads to obtain a coating much more dense and compact, restricting the proton transport through the membrane and so reducing their performance in the fuel cell.

Table 5.13. Maximum power density (P$_{max}$) values measured at 25 ºC for the 15PVA(GO-PAH/sPVA)$_n$ and 15sPVA(GO-PAH/sPVA)$_n$ composites compared to their substrates. The composites previously prepared by Hydrogen-bonding (H-B) LbL assembly and solution-casting (S-C) method are included for comparison

Membrane	P$_{max}$ (mW/cm^2)
15PVA	2.7 ± 0.2
15PVA(GO-PAH/sPVA)$_1$	12.2 ± 0.1
15PVA(GO-PAH/sPVA)$_3$	6.4 ± 0.3
15PVA(GO/PVA)$_1$ (H-B LbL)	*7.1 ± 0.4*
15PVA(GO/PVA)$_3$ (H-B LbL)	*4.6 ± 0.2*
15PVA/GO (S-C method)	*7.4 ± 0.1*
15sPVA	3.7 ± 0.2
15sPVA(GO-PAH/sPVA)$_1$	6.0 ± 0.2
15sPVA(GO-PAH/sPVA)$_3$	1.6 ± 0.1
15sPVA(GO/sPVA)$_1$ (H-B LbL)	*7.4 ± 0.2*
15sPVA(GO/sPVA)$_3$ (H-B LbL)	*4.5 ± 0.3*
15sPVA/GO (S-C method)	*8.3 ± 0.3*

The electrostatic LbL composites prepared from the 15PVA substrate show values of P$_{max}$ almost twice higher than that obtained for the composites prepared by Hydrogen-bonding LbL assembly and solution-casting method prepared in Contribution IV [37] and II [39], respectively. Nevertheless, an excess of sulfonic acid groups (-SO$_3$H) in the assembled structure negatively affects to the performance of the 15sPVA(GO-PAH/sPVA)$_n$ composites in a H$_2$-O$_2$ fuel cell. This behaviour is oppositely than that observed in the Hydrogen-bonding LbL composites, in which the sulfonation of the substrate increases their performance in fuel cell. As was mentioned previously, this effect is due to the structure more compact that the 15sPVA(GO-PAH/sPVA)$_n$ composites show which restrict the mobility of protons through the membrane.

MeOH diffusion coefficients (D_{MeOH})

One of the most important problems associated to DMFCs is the methanol diffusion through the proton exchange membrane, effect so-called methanol crossover. This effect reduces drastically the performance of the fuel cell. Thus, the methanol barrier properties of the electrostatic LbL composites were also evaluated.

Figure 5.24 shows the rate of methanol mass loss through the 15PVA(GO-PAH/sPVA)$_n$ and 15sPVA(GO-PAH/sPVA)$_n$ composites and their substrates as a function of time measured at 30 ºC.
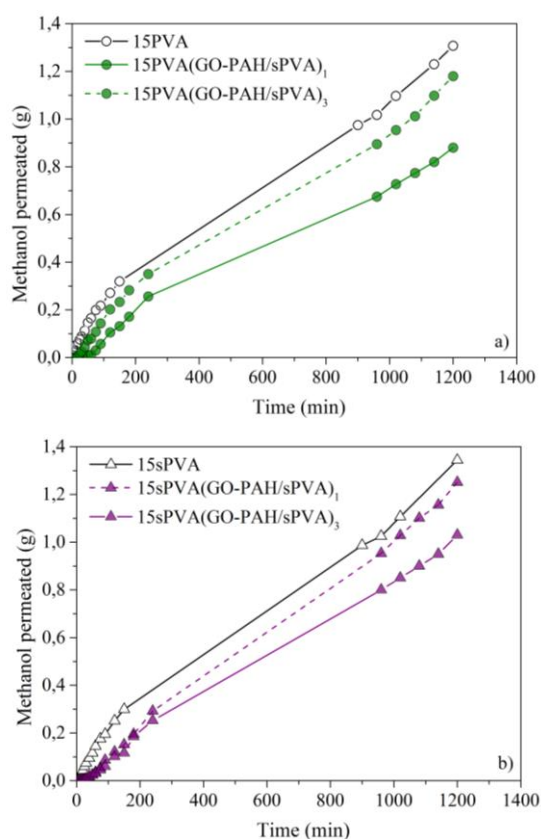

Figure 5.24. Permeation curves of the a) 15PVA(GO-PAH/sPVA)$_n$ and b) 15sPVA(GO-PAH/sPVA)$_n$ composites compared to their substrates at 30 ºC

Table 5.14 lists the values of methanol diffusion coefficients (D_{MeOH}) of all measured composites.

Table 5.14. Methanol diffusion coefficients (D_{MeOH}) and methanol selectivity (Φ) values of the 15PVA(GO-PAH/sPVA)$_n$ and 15sPVA(GO-PAH/sPVA)$_n$ composites compared to their substrates at 30 ºC. The composites previously prepared by Hydrogen-bonding (H-B) LbL assembly method are included for comparison

Membrane	$D_{MeOH} \times 10^8$ (cm^2/s)	Φ (S·s·cm^{-3})
15PVA	7.00 ± 0.03	0.03×10^5
15PVA(GO-PAH/sPVA)$_1$	1.45 ± 0.01	1.38×10^5
15PVA(GO-PAH/sPVA)$_3$	0.99 ± 0.00	0.80×10^5
15PVA(GO/PVA)$_1$ (H-B LbL)	*4.26 ± 0.02*	*0.53×10^5*
15PVA(GO/PVA)$_3$ (H-B LbL)	*2.62 ± 0.01*	*0.23×10^5*
15sPVA	5.38 ± 0.02	0.04×10^5
15sPVA(GO-PAH/sPVA)$_1$	0.71 ± 0.02	0.71×10^5
15sPVA(GO-PAH/sPVA)$_3$	0.40 ± 0.01	0.75×10^5
15sPVA(GO/sPVA)$_1$ (H-B LbL)	*3.06 ± 0.01*	*0.71×10^5*
15sPVA(GO/sPVA)$_3$ (H-B LbL)	*1.96 ± 0.01*	*0.15×10^5*

An increase of the deposited bilayers strongly reduce the methanol diffusion coefficients of the composites, showing the 15PVA(GO-PAH/PVA)$_3$ and 15sPVA(GO-PAH/sPVA)$_3$ composites a decrease of the 86 % and 93 %, respectively, compared to their substrates. This suggests that the deposition of GO-PAH/sPVA bilayers on the substrates reduces efficiently the methanol permeation in the LbL composites [32].

In addition, the methanol selectivity that is defined as the ratio of proton conductivity to methanol diffusion coefficient was also calculated, as shown in Table 5.14. High values of methanol selectivity mean that the membrane has high proton conductivity and low methanol crossover which is favorable for the application in DMFCs [46]. Among all the evaluated composites, the 15PVA(GO-PAH/sPVA)$_1$ composite shows the best methanol selectivity as a result of the combination of a high proton conductivity and a relative low methanol diffusion coefficient. Therefore, both the proton conductivity and the methanol permeability are important parameters that determine the suitability of a membrane for DMFC applications. Notice that the electrostatic LbL composites exhibit higher methanol selectivity than those prepared via hydrogen-bonding interactions.

Conclusions

LbL composites containing up to three GO-PAH/sPVA bilayers were assembled onto the 15PVA and 15sPVA substrates by alternately immersing the membrane into the GO-PAH and sPVA polyelectrolyte solutions. The GO was dispersed in a PAH solution in order to promote electrostatic interactions between the cationic character of the GO-PAH complex and the anionic component of the sPVA solution. From the FTIR, SEM and AFM analyses were confirmed that the deposition of the GO-PAH/sPVA bilayers was carried out successfully. The thermal and mechanical properties of the LbL composites were improved with increasing the number of deposited layers, which can be attributed to the higher density of electrostatic interactions between the ion-pairs $SO_3^- \cdots NH_3^+$ that stabilize the structure. Moreover, the water contact angle values evidence a hydrophilic-hydrophobic nano-phase separation morphology in the LbL composites. Among all the studied composites, the $15PVA(GO-PAH/sPVA)_1$ composite show the best performance to be use as electrolyte in DMFCs, exhibiting a proton conductivity of 8.26 mS/cm (at 90 ºC), a maximum power density of 12.2 mW/cm^2 (at 25 ºC) and a methanol selectivity of 1.38 $S \cdot s \cdot cm^{-3}$. In contrast, the multiple sulfonation in the $15sPVA(GO-PAH/sPVA)_n$ composites does not shown an enhancement of the proton-conducting properties.

Acknowledgements

References

[1] H. Pu, *Polymers for PEM Fuel Cells*. Wiley, 2014.

[2] S. Javaid and T. Matsuura, *Polymer Membranes for Fuel Cells*. Springer, 2009.

[3] K. Pourzare, Y. Mansourpanah, and S. Farhadi, "Advanced nanocomposite membranes for fuel cell applications : a comprehensive review," Biofuel Res. J., vol. 12, pp. 496–513, 2016.

[4] Z. U. Khan, A. Kausar, and H. Ullah, "A Review on Composite Papers of Graphene Oxide, Carbon Nanotube, Polymer/GO, and Polymer/CNT: Processing Strategies, Properties, and Relevance," Polym. Plast. Technol. Eng., vol. 55, no. 6, pp. 559–581, 2016.

[5] G. Decher, "Fuzzy Nanoassemblies: Toward Layered Polymeric Multicomposites," Science (80)., vol. 277, no. 5330, pp. 1232–1237, 1997.

[6] K. Ariga, Y. Yamauchi, G. Rydzek, Q. Ji, Y. Yonamine, Kevin C.-W. Wu, and J. P. Hill, "Layer-by-layer Nanoarchitectonics: Invention, Innovation, and Evolution," Chem. Lett., vol. 43, no. 1, pp. 36–68, Jan. 2014.

[7] S. Yılmaztürk, H. Deligöz, M. Yılmazoğlu, H. Damyan, F. Öksüzömer, S. Naci Koç, A. Durmuş, and M. Ali Gürkaynak, "A novel approach for highly proton conductive electrolyte membranes with improved methanol barrier properties: Layer-by-Layer assembly of salt containing polyelectrolytes," J. Memb. Sci., vol. 343, no. 1, pp. 137–146, 2009.

[8] B. G. Kim, H. Park, T. H. Han, and C. G. Cho, "LbL Assembled sPPO Composite Membrane Containing GO for DMFC Applications," Mol. Cryst. Liq. Cryst., vol. 598, no. 1, pp. 16–22, 2014.

[9] S. P. Jiang, Z. Liu, and Z. Q. Tian, "Layer-by-layer self-assembly of composite polyelectrolyte-nafion membranes for direct methanol fuel cells," Adv. Mater., vol. 18, no. 8, pp. 1068–1072, 2006.

[10] M. Yoo, M. Kim, Y. Hwang, and J. Kim, "Fabrication of highly selective PVA-g-GO/SPVA membranes via cross-linking method for direct methanol fuel cells," Ionics (Kiel)., vol. 20, no. 6, pp. 875–886, 2014.

[11] S. Yun, H. Im, Y. Heo, and J. Kim, "Crosslinked sulfonated poly(vinyl alcohol)/sulfonated multi-walled carbon nanotubes nanocomposite membranes for direct methanol fuel cells," J. Memb. Sci., vol. 380, no. 1–2, pp. 208–215, 2011.

[12] W. S. Hummers and R. E. Offeman, "Preparation of Graphitic Oxide," J. Am. Chem. Soc., vol. 80, no. 6, pp. 1339–1339, 1958.

[13] L. Shahriary and A. A. Athawale, "Graphene Oxide Synthesized by using Modified Hummers Approach," Int. J. Renew. Energy Environ. Eng., vol. 2, no. 1, pp. 58–63, 2014.

[14] S. W. Cranford, C. Ortiz, and M. J. Buehler, "Mechanomutable properties of a PAA/PAH polyelectrolyte complex: rate dependence and ionization effects on tunable adhesion strength," Soft Matter, vol. 6, no. 17, p. 4175, 2010.

[15] S. W. Cranford and M. J. Buehler, "Critical cross-linking to mechanically couple polyelectrolytes and flexible molecules," Soft Matter, vol. 9, p. 1076, 2013.

[16] F. J. Baltá Calleja, *Microhardness relating to crystalline polymers*. Springer, pp. 117–148, 2005.

[17] X. Qian, N. Gu, Z. Cheng, X. Yang, E. Wang, and S. Dong, "Methods to study the ionic conductivity of polymeric electrolytes using a.c. impedance spectroscopy," J. Solid State Electrochem., vol. 6, no. 1, pp. 8–15, 2001.

[18] S. Xiao, C. Moresoli, J. Bovenkamp, and D. De Kee, "Sorption and permeation of organic environmental contaminants through PVC geomembranes," J. Appl. Polym. Sci., vol. 63, no. 9, pp. 1189–1197, 1997.

[19] H. S. Mansur, C. M. Sadahira, A. N. Souza, and A. A. P. Mansur, "FTIR spectroscopy characterization of poly (vinyl alcohol) hydrogel with different hydrolysis degree and chemically crosslinked with glutaraldehyde," Mater. Sci. Eng. C, vol. 28, no. 4, pp. 539–548, 2008.

[20] H. Hou, X. Hu, X. Liu, W. Hu, R. Meng, and L. Li, "Sulfonated graphene oxide with improved ionic performances," Ionics (Kiel), vol. 21, no. 7, pp. 1919–1923, 2015.

[21] S. Morimune, T. Nishino, and T. Goto, "Poly(vinyl alcohol)/graphene oxide nanocomposites prepared by a simple eco-process," Polym. J., vol. 44, no. 10, pp. 1056–1063, Oct. 2012.

[22] P. Gentile, Maria E. Frongia, M. Cardellach, Cheryl A. Miller, Graham P. Stafford, Graham J. Leggett, and Paul V. Hatton, "Functionalised nanoscale coatings using layer-by-layer assembly for imparting antibacterial properties to polylactide-co-glycolide surfaces," Acta Biomater., vol. 21, no. May, pp. 35–43, 2015.

[23] J.M. Morancho, , J.M. Salla, A. Cadenato, X. Fernández-Francos, X. Ramis, P. Colomer, Y. Calventus, and R. Ruíz, "Kinetic studies of the degradation of poly(vinyl alcohol)-based proton-conducting membranes at low temperatures," Thermochim. Acta, vol. 521, no. 1–2, pp. 139–147, 2011.

[24] C. C. Yang, W. C. Chien, and Y. J. Li, "Direct methanol fuel cell based on poly(vinyl alcohol)/titanium oxide nanotubes/poly(styrene sulfonic acid) (PVA/nt-TiO2/PSSA) composite polymer membrane," J. Power Sources, vol. 195, no. 11, pp. 3407–3415, 2010.

[25] S. Zhong, X. Cui, Y. Gao, W. Liu, and S. Dou, "Fabrication and properties of poly(vinyl alcohol)-based polymer electrolyte membranes for direct methanol fuel cell applications," Int. J. Hydrogen Energy, vol. 39, no. 31, pp. 17857–17864, 2014.

[26] A. Martínez-Felipe, C. Moliner-Estopiñán, C. T. Imrie, and A. Ribes-Greus, "Characterization of crosslinked poly(vinyl alcohol)-based membranes with different hydrolysis degrees for their use as electrolytes in direct methanol fuel cells," J. Appl. Polym. Sci., vol. 124, no. 2, pp. 1000–1011, Apr. 2012.

[27] D. S. Kim, H. B. Park, J. W. Rhim, and Y. M. Lee, "Preparation and characterization of crosslinked PVA/SiO2 hybrid membranes containing sulfonic acid groups for direct methanol fuel cell applications," J. Memb. Sci., vol. 240, no. 1–2, pp. 37–48, 2004.

[28] S. Yılmaztürk, H. Deligöz, M. Yılmazoğlu, H. Damyan, F. Öksüzömer, S. Naci Koç, A. Durmuş, and M. Ali Gürkaynak, "Self-assembly of highly charged polyelectrolyte complexes with superior proton conductivity and methanol barrier properties for fuel cells," J. Power Sources, vol. 195, no. 3, pp. 703–709, Feb. 2010.

[29] H. Lin, C. Zhao, W. Ma, H. Li, and H. Na, "Layer-by-layer self-assembly of in situ polymerized polypyrrole on sulfonated poly(arylene ether ketone) membrane with extremely low methanol crossover," Int. J. Hydrogen Energy, vol. 34, no. 24, pp. 9795–9801, Dec. 2009.

[30] H. Zhang, H. Huang, and P. K. Shen, "Methanol-blocking Nafion composite membranes fabricated by layer-by-layer self-assembly for direct methanol fuel cells," Int. J. Hydrogen Energy, vol. 37, no. 8, pp. 6875–6879, 2012.

[31] L. Vinhola, T. Facci, L. G. Dias, D. C. De Azevedo, G. Borissevitch, and F. Huguenin, "Self-assembled films from chitosan and poly(vinyl sulfonic acid) on Nafion?? for direct methanol fuel cell," J. Braz. Chem. Soc., vol. 23, no. 3, pp. 531–537, 2012.

[32] C. Zhao, H. Lin, Z. Cui, X. Li, H. Na, and W. Xing, "Highly conductive, methanol resistant fuel cell membranes fabricated by layer-by-layer self-assembly of inorganic heteropolyacid," J. Power Sources, vol. 194, no. 1, pp. 168–174, Oct. 2009.

[33] X. Zhao, Q. Zhang, Y. Hao, Y. Li, Y. Fang, and D. Chen, "Alternate multilayer films of poly(vinyl alcohol) and exfoliated graphene oxide fabricated via a facial layer-by-layer assembly," Macromolecules, vol. 43, no. 22, pp. 9411–9416, 2010.

[34] N. Wang, S. Ji, G. Zhang, J. Li, and L. Wang, "Self-assembly of graphene oxide and polyelectrolyte complex nanohybrid membranes for nanofiltration and pervaporation," Chem. Eng. J., vol. 213, pp. 318–329, 2012.

[35] L. Zhao, B. Yuan, Y. Geng, C. Yu, N. H. Kim, J. H. Lee, and P. Li, "Fabrication of ultrahigh hydrogen barrier polyethyleneimine/graphene oxide films by LBL assembly fine-tuned with electric field application," Compos. Part A Appl. Sci. Manuf., vol. 78, no. August, pp. 60–69, 2015.

[36] Q. Nanoindentation, P. V Pavoor, A. Bellare, A. Strom, D. Yang, and R. E. Cohen, "Mechanical Characterization of Polyelectrolyte Multilayers Using," Film, pp. 4865–4871, 2004.

[37] S. C. Sánchez-Ballester, L. Monreal, A. Ribes-Greus, V. Soria, "Layer-by-Layer assembly of poly(vinyl alcohol)/graphene oxide hybrid composite membranes via hydrogen-bonding interactions for direct methanol fuel cells," *In Preparation*.

[38] S. Li, S. Zhang, Q. Zhang and G. Qin, "Assembly of unbalanced charged polyampholyte onto Nafion® to produce high-performance composite membranes," Chem. Commun., no. 1, pp. 1173–1184, 2008.

[39] S. C. Sánchez-Ballester, A. Ribes-Greus, V. Soria, G. Rydzek, and K. Ariga, "Bi-sulfonation of poly(vinyl alcohol)/Graphene oxide composite membranes for Proton Exchange Membrane Fuel Cell applications. Part 2: Functional membrane properties," *In Preparation*.

[40] S. C. Sánchez-Ballester, O. Santiago, T. J. Leo, E. Navarro, A. Ribes-Greus, V. Soria, G. Rydzek, and K. Ariga, "Effect of the multiple sulfonation on the proton conductivity properties of poly(vinyl alcohol)/graphene oxide composites membranes.", *In Preparation.*

[41] H. Beydaghi, M. Javanbakht, and E. Kowsari, "Preparation and physic-chemical performance study of proton exchange membranes based on phenyl sulfonated graphene oxide nanosheets decorated with iron titanate nanoparticles," Polymer (Guildf)., vol. 87, pp. 26–37, 2016.

[42] Y. Xiang, S. Lu, and S. P. Jiang, "Layer-by-layer self-assembly in the development of electrochemical energy conversion and storage devices from fuel cells to supercapacitors," Chem. Soc. Rev., vol. 41, no. 21, p. 7291, 2012.

[43] Y. Xue and S. Chan, "Layer-by-layer self-assembly of CHI/PVS-Nafion composite membrane for reduced methanol crossover and enhanced DMFC performance," Int. J. Hydrogen Energy, vol. 40, no. 4, pp. 1877–1885, 2015.

[44] S. C. Sánchez-Ballester, A. Ribes-Greus, V. Soria, G. Rydzek, and K., Ariga, "Bi-sulfonation of poly(vinyl alcohol)/Graphene oxide composite membranes for Proton Exchange Membrane Fuel Cell applications. Part 1: Membrane preparation and characterization," *In Preparation*.

[45] S. J. Huang, H. K. Lee, and W. H. Kang, "Preparation and characterization of proton conductive phosphosilicate membranes based on inorganic-organic hybrid materials," Bull. Korean Chem. Soc., vol. 26, no. 2, pp. 241–247, 2005.

[46] B. S. Pivovar, Y. X. Wang, and E. L. Cussler, "Pervaporation membranes in direct methanol fuel cells," J. Memb. Sci., vol. 154, no. 2, pp. 155–162, 1999.

Conclusions and further work

Chapter 6

6.1. Conclusions

The main goal of this PhD was the design, preparation and characterization of new nano-engineered proton exchange membranes (PEMs) based on inexpensive materials with high proton conductivity and low methanol permeability for their use as electrolytes in fuel cells, particularly in Direct Methanol Fuel Cells (DMFCs).

The main conclusions of this thesis are organized according to the different strategies that have been followed to improve the proton-conducting and methanol-barrier properties of the prepared membranes. Moreover, two different methods have been evaluated in order to find a simple and effective procedure for the preparation of PEMs: solution-casting method and Layer-by-Layer (LbL) assembly method.

SOLUTION-CASTING METHOD

Crosslinking degree (inter-sulfonation process)

- PVA-based crosslinked proton exchange membranes were prepared by solution-casting method using sulfosuccinic acid (SSA) as crosslinking agent at two different concentrations, 15 and 30 wt.% respect to the polymer, in order to ensure dimensional stability and promote proton conductivity in the membranes by introduction of inter-chain sulfonic acid groups ($-SO_3H$).

- A good dimensional stability was achieved by crosslinking the membranes with SSA at 30 wt.%. A higher concentration of crosslinking agent restrict the mobility of the polymer chains, which reducing the free volume available to accommodate water molecules in their structure.

- Both the proton-conducting properties and the performance of the crosslinked membranes in a H_2-O_2 fuel cell are strongly influenced by the crosslinking degree of membranes. The introduction of a higher concentration of active groups involved in the proton transport (sulfonic acid groups, $-SO_3H$) in the membrane with higher crosslinking degree (30PVA) resulted in strong improvement of the proton conductivity and the values of maximum power density (P_{max}) obtained in H_2-O_2 fuel cell.

Intra-sulfonation of the polymer matrix (sPVA)

- A two-step methodology in which PVA matrix was first intra-sulfonated (sulfonation degree of 0.1 %) with propane sultone and subsequently inter-sulfonated using sulfosuccinic acid (SSA) as a crosslinking agent was followed in order to enhance the proton conductivity of the studied membranes.

- The membranes became more brittle when the hydroxyl groups were replaced by sulfonic acid groups by direct sulfonation of the polymer matrix, showing a slightly decrease of their mechanical properties.

- The bi-sulfonation of the polymer matrix in the membrane crosslinked at 30 wt.% of SSA (30sPVA) sharply improved its proton-conducting properties compared to the non-modified 30PVA membrane. This improvement is attributed to the higher concentration of sulfonic acid groups in the sPVA-based membranes, which are directly involved in the proton conduction mechanism.

Addition of graphene oxide (GO)

- GO nano-platelets were successfully synthesized by the Modified Hummers Method to use them as filler in the preparation of the composite membranes.

- Hybrid organic-inorganic composite membranes based on GO (1 wt.%) were prepared by solution-casting method. The good exfoliation of the GO nano-platelets into the polymer matrix was confirmed by TEM analysis.

- An improvement of the thermal and mechanical properties of the membranes was achieved by addition of 1 wt.% of GO nano-platelets into the polymer matrix. The oxygen-containing groups of the GO favour the interfacial adhesion between the polymer matrix and the filler via hydrogen bonding interactions which stabilizes the structure of the composites.

- The experimental results showed a significant enhancement of the proton-conducting properties in the prepared GO composites. The addition of GO favours the proton mobility through the membrane by formation of well-connected proton-conducting channels, while at the same time the water uptake of the composites is reduced improving their dimensional stability and their methanol barrier properties.

- Proton conductivity in the composite membranes is strongly influenced by temperature since an increase of temperature promotes the polymer chains mobility, enhancing the proton conduction through the membrane. The dependence of the proton conductivity with temperature followed an Arrhenius behaviour suggesting that the proton conduction mainly occurs by Grotthus mechanism.

- Among all the GO composite membranes, the highest values of proton conductivity and P_{max} were reached for the 30sPVA/GO composite. Therefore, not only the proton-conducting properties of the PVA-based membranes are affected by the addition of GO, but also it is crucial an optimal concentration of sulfonic groups in their structure.

- The prepared GO composites showed comparable results to the reference Nafion 117 membrane in a H_2-O_2 fuel cell at the same operating conditions.

Sulfonation of the filler (sGO)

- The sulfonation of the GO nano-platelets (sGO) was proposed as a new strategy to improve the proton conductivity of the composite membranes. For this purpose, sGO (sulfonation degree of 10 %) was synthesized from GO via free radical addition using the aryl diazonium salt of sulfanilic acid as adduct.

- Hybrid organic-inorganic composite membranes based on sGO (1 wt.%) were prepared by solution-casting method. The exfoliation of the sGO nano-platelets into the polymer matrix was confirmed by TEM analysis.

- In general, the sulfonation of the filler (sGO) did not significantly affect to the proton conductivity of the prepared composites. Only it was possible to observe a strongly increase of the proton conductivity for the 30PVA/sGO composite in all the range of temperature.

- The dependence of the proton conductivity with temperature for the sGO composites showed the typical Vogel-Tamman-Fulcher (VTF) behaviour in the range from 50 to 90 ºC, indicating that the proton conductivity at high temperature takes place mainly via Vehicular mechanism.

- Among all the studied composites, the 30PVA/sGO composite showed the best performance, exhibiting high proton conductivity (7.38 mS/cm at 50 ºC), low methanol permeability (1.84×10^{-8} cm^2/s at 30 ºC) and high open circuit voltage (OCV) values in DMFC test (0.76 V at 50 ºC and a 2M methanol feed concentration), indicating that it is a good candidate to be used as PEM in DMFC applications.

- Nevertheless, contrary to expectations, the multiple sulfonation of the 30sPVA/sGO composite strongly decreased its proton-conducting properties.

LAYER-BY-LAYER ASSEMBLY METHOD

- The Layer-by-Layer (LbL) assembly method was employed as alternative procedure to prepare PEMs based on PVA and GO with high methanol selectivity to use as electrolytes in DMFCs.

- Membranes crosslinked at 30 wt.% of SSA (30PVA and 30sPVA) were selected in a first attempt as a substrates for the preparation of the LbL composite membranes. However, their low mechanical stability led to finally chose the 15PVA and 15sPVA membranes, with a lower crosslinking degree, for the preparation of the LbL composites.

- According to the forces responsible to keep the LbL assembled structure, two different types of composite membranes were prepared: Hydrogen-bonding and Electrostatic LbL membranes.

Hydrogen-bonding LbL composite membranes

- Hydrogen-bonding LbL composite membranes were prepared by deposition of GO/PVA and GO/sPVA bilayers onto the surface of crosslinked 15PVA and 15sPVA substrates, respectively.

- The successful deposition of the GO/PVA and GO/sPVA bilayers onto the 15PVA and 15sPVA substrates, respectively, was confirmed by FTIR, SEM and AFM analysis.

- By increasing the deposited bilayers, both the proton conductivity and the performance of the composites in a H_2-O_2 fuel cell decrease since the coating deposited on the surface of the substrates membranes acts as a barrier against the water absorption, limiting the passage of protons across the composite. Moreover, the sulfonation of the polymer matrix in the 15sPVA(GO/sPVA)$_1$ composite resulted in an increase of the number of proton carriers (-SO$_3$H groups) in the membrane improving its proton-conducting properties.

- The experimental results showed the lowest values of methanol diffusion coefficients for the three-bilayer LbL composite membranes, but their low proton conductivity resulted in low methanol selectivity. Therefore, it is not only important the methanol diffusion coefficient, but also the proton conductivity is a crucial factor to determine the potential of a PEM for DMFC applications.

- Among all the hydrogen-bonding LbL composite membranes assayed, the 15sPVA(GO/sPVA)$_1$ composite showed the best methanol selectivity ($\Phi = 0.71\times10^5$ S·s·cm^{-3}) with a reasonable D$_{MeOH}$ of 3.06×10^{-8} cm^2/s and σ_{prot} of 2.16 mS/cm measured at 30 ºC.

Electrostatic LbL composite membranes

- The electrostatic LbL composite membranes were assembled by alternating dipping of the 15PVA and 15sPVA substrates in a solution of GO dispersed in poly(allyl amine) hydrochloride (GO-PAH) positively charged and a negatively charged solution of sPVA.

- The successful deposition of the GO-PAH/sPVA bilayers onto the substrates was confirmed by FTIR, SEM and AFM analysis.

- In general, the proton-conducting properties of the electrostatic LbL composites are influenced by both the concentration and mobility of the proton carriers (-SO$_3$H

groups). After deposition of one GO-PAH/sPVA bilayer, an improvement of the proton conductivity was observed due to the increase in the number of -SO$_3$H groups introduced by the sPVA layer. However, the proton conductivity after deposition of three bilayers was strongly reduced due to the formation of a much thicker and compact coating in which the mobility of the proton carriers is restricted.

- However, **t**he multiple sulfonation of the 15sPVA(GO-PAH/sPVA)$_n$ composite did not enhance their proton-conducting properties. The higher density of electrostatic interactions in these composites leads to obtain a coating much more dense and compact, restricting the proton transport through the membrane and so reducing their proton conductivity and their performance in a fuel cell.

- The deposition of GO-PAH/sPVA bilayers on the substrates reduced efficiently the methanol permeation in the electrostatic LbL composites.

- The best performance was attained for the 15PVA(GO-PAH/sPVA)$_1$ composite, showing a σ_{prot} of 8.26 mS/cm at 90 ºC and a maximum power density in a H$_2$-O$_2$ fuel cell of 12.2 mW/cm^2 with the highest value of methanol selectivity (1.38×10^5 S·s·cm^{-3}) among all the prepared electrostatic LbL composites.

6.2. Further work

1. Membrane-Electrode Assembly (MEA) fabrication

In order to optimize the performance of the prepared PEMs in a fuel cell, the fabrication of MEAs is proposed. Further experimental works are being undertaken to suppress the delamination problems that arise in the preparation of the MEAs. The experience acquired in this thesis in the Layer-by-Layer technology can help in the design of a new route to prepare thin-film MEAs based on PVA with enhanced performance in fuel cells.

2. Biofouling problems in Microbial Fuel Cells (MFCs)

A MFC is a device which uses bacteria as bio-catalyst to oxidize organic matter and generates electricity. PEM biofouling problems can be occurred during long-term operation of the MFCs as a consequence of the direct contact of the membrane and the bacteria used. During my internship last year in the Biomaterials group of the ICTP (CSIC, Madrid), a study to develop anti-biofouling composite PEMs based on PVA and GO were initiated. The potential of GO as anti-biofouling agent due to its bacteriostatic activity had been explored. In this context, the bacteriostatic activity of the prepared 15PVA/GO composite was confirmed by the reduction in the colony count of *E. Coli* adhered onto the surface of the composite. Currently, the anti-biofouling properties of other PVA/GO composite membranes with different structures and morphologies are being studied.

3. Marine uses of fuel cells

Fuel cells have been considered as one of several alternative propulsion systems for the ships of the future. Some of the benefits that fuel cells provide to the utility industry could be also applied in the marine field. Why consider fuel cells for marine applications? This idea came from the collaboration with the electrochemical Fuel Cell group of the ETSI Navales (Polytechnic University of Madrid), where the performance tests of the prepared membranes where carried out in a single DMFC. In our meetings, the possibility to direct our efforts towards the preparation of PVA-based membranes to marine applications was contemplated. A question inevitable arises, however, what would it take in order for the fuel cell become competitive in the commercial marine industry? The major factor inhibiting fuel cell usage for marine commercial applications is high cost. In this regard the use of PVA for the preparation of electrolyte membranes is an attractive strategy for marine fuel cells, since it is one of the cheapest commercial polymers availaible actually in the market.

List of publications

Journal articles

S. C. Sánchez-Ballester, L. Monreal, A. Ribes-Greus, V. Soria, G. Rydzek and K. Ariga, *Layer-by-Layer assembly of poly(vinyl alcohol)/graphene oxide hybrid composite membranes via electrostatic interactions for direct methanol fuel cell.* (To be submitted)

S. C. Sánchez-Ballester, L. Monreal, A. Ribes-Greus, V. Soria, G. Rydzek and K. Ariga, *Layer-by-Layer assembly of poly(vinyl alcohol)/graphene oxide hybrid composite membranes via hydrogen-bonding interactions for direct methanol fuel cell.* (To be submitted)

S. C. Sánchez-Ballester, A. Ribes-Greus, V. Soria, G. Rydzek, K. Ariga, *Effect of multiple sulfonation on the proton conductivity of poly(vinyl alcohol)/graphene oxide composites membranes.* (To be submitted)

S. C. Sánchez-Ballester, A. Ribes-Greus, V. Soria, G. Rydzek, K. Ariga, *Bi-sulfonation of poly(vinyl alcohol)/graphene oxide composite membranes for Proton Exchange Membrane Fuel Cell applications. Part 2: Functional membrane properties.* (To be submitted)

S. C. Sánchez-Ballester, A. Ribes-Greus, V. Soria, G. Rydzek, K. Ariga, *Bi-sulfonation of poly(vinyl alcohol)/graphene oxide composite membranes for Proton Exchange Membrane Fuel Cell applications. Part 1: Membrane preparation and characterization.* (To be submitted)

L. Santonja-Blasco, I. Rodriguez, **S. C. Sánchez-Ballester**, JD Badia, F. Meseguer, A. Ribes-Greus, *Protection of high density polyethylene/silicon composites from UV/Vis photo-degradation*, J. Appl. Polym. Sci., 2017. DOI: 10.1002/app.45439

Research Contribution

S. C. Sánchez-Ballester, V. Soria and A. Ribes-Greus, *Sulfonated graphene oxide-poly(vinyl alcohol) composite membranes with high proton conductivity for fuel cell applications,* Fifth International Symposium Frontiers in Polymer Science, 2017, Sevilla, Spain.

S. C. Sánchez-Ballester, L. Rojo, V. Soria, A. Ribes-Greus and Julio San Román, *Design of anti-biofouling proton-conducting membranes based on poly(vinyl alcohol) and graphene oxide composites,* Fifth International Symposium Frontiers in Polymer Science, 2017, Sevilla, Spain.

S. C. Sánchez-Ballester, A. Ribes-Greus, V. Soria, G. Rydzek, K. Ariga and J. San Román, *Preparation and characterization of proton-conducting membranes based on functionalized poly(vinyl alcohol)/graphene oxide composites,* Seminario de jóvenes investigadores del CSIC, ICTP-CSIC, 2016, Madrid, Spain.

S. C. Sánchez-Ballester, V. Soria, Amparo Ribes-Greus, Gaulthier Rydzek and Katsuhiko Ariga, *Preparation of new polymeric electrolyte membranes by multiple sulfonation of PVAGO nanocomposites*, MANA-RSC symposium: Materials for Energy Generation and Storage, 2015, Tsukuba, Japan.

S. C. Sánchez-Ballester, C. Gonzalez-Guisasola, V. Soria, A. Ribes-Greus, *Estudio del efecto de la sulfonación y adición de óxido de grafeno a membranas de PVA para uso en pilas de combustible de metanol directo*, 9º Congreso Nacional Ingeniería Termodinámica, ISBN 978-84-606-8931-7, 2015, Cartagena, Spain.

S. C. Sánchez-Ballester, L. Santonja-Blasco, J.D Badia, I. Rodriguez, F. Meseguer, A. Ribes-Greus, *Evaluation of the degradation of HDPE and PP with silicon particles exposed to sunlight radiation*, 5th International Conference on Polyolefin Characterization, 2014, Valencia, Spain.

M. Bermejo, M. Schmitt, **S. C. Sánchez-Ballester**, O. Gil-Castell, R. Teruel-Juanes, M. Rosado-Gil, L. Santonja-Blasco, A. Martínez-Felipe, I. Rodriguez, F. Meseguer, A. Ribes-Greus, *Silicon colloids light/UV stabilisers of polystyrene and polypropylene*, Baltic Polymer Symposium 2013, BPS 2013, ISBN 978-609-459-227-0, Vilnius, Lithuania.

O. Gil-Castell, M. Rosado-Gil, **S. C. Sánchez-Ballester**, R.Teruel-Juanes, C. Moliner-Estopiñán, A. Martínez-Felipe, J.D. Badia, A. Ribes-Greus, *Influence of sisal fibers on thermal decomposition of poly(hydroxibutyrate-co-valerate) biocomposites*, Baltic Polymer Symposium 2013, BPS 2013, ISBN 978-609-459-227-0, Vilnius, Lithuania.

J. Alonso, C. Moran, O. Gil-Castell, **S. C. Sánchez-Ballester**, R.Teruel-Juanes, M. Rosado-Gil, J.D. Badia, A. Martínez-Felipe, A. Ribes-Greus, *Influence of maleic*

anhydride as coupling agent in PLA/sisal biocomposites under hydrothermal degrading conditions, Baltic Polymer Symposium 2013, BPS 2013, ISBN 978-609-459-227-0, Vilnius, Lithuania.

A. Martínez-Felipe, **S. C. Sánchez-Ballester**, J.D. Badía, C. Moliner-Estopiñan, M. Rosado-Gil, V. Soria, A. Ribes-Greus, *Estudio cinético de la formación de fases esmécticas en cristales líquidos poliméricos de cadena secundaria con grupos sulfónicos*, VIII Congreso Nacional de Ingeniería Termodinámica, ISBN 978-84-92681-62-4, 2013, Burgos, Spain.

S. C. Sánchez-Ballester, J.D. Badia, A. Ribes-Greus, V. Soria, *Estudio del espectro de relajaciones dinámico-mecánicas de copolímeros de metil metacrilato y metil isopropenil cetona*, XIII Congreso Nacional de Propiedades Mecánicas de Sólidos, PMS2012, ISBN 978-84-8363-897-2, 2012, Alcoy, Spain.

A. Martínez-Felipe, J.D. Badía, L. Santonja-Blasco, **S. C. Sánchez-Ballester**, R. Teruel-Juanes, C. Moliner-Estopiñán, M. Rosado-Gil, V. Sáenz de Juano, M.J. Felipe-Román, L. Monreal-Mengual, V. Soria, M.D. Ingram, C.T. Imrie, A. Ribes-Greus, *Dielectric response and conductivity of novel side-chain liquid crystal polymers containing sulfonic acid groups*, 11th European Symposium on Polymer Blends, ISBN 978-84-695-2762-7, 2012, San Sebastian, Spain.

A. Martínez-Felipe, J.D. Badia, L. Santonja-Blasco, **S. C. Sánchez-Ballester**, R. Teruel-Juanes, C. Moliner-Estopiñán, M. Rosado-Gil, V. Sáenz de Juano, M.J. Felipe-Román, L. Monreal-Mengual, V. Soria, C.T. Imrie, A. Ribes-Greus, *New LCI materials for DMFC and DEFC*, Innostock 2012, The 12th International Conference on Energy Storage, ISBN 978-84-938793-3-4, Lleida, Spain.

S. C. Sánchez-Ballester, J.D. Badia, A. Martinez-Felipe, L. Santonja-Blasco, A. Ribes-Greus, V. Soria, *Degradación Fotoquímica de Polímeros lineales: Evolución temporal de la Función de Distribución*, XXXIII Reunión Bienal de la RSEQ, 2011, Valencia, Spain.

S. C. Sánchez-Ballester, J.D. Badia, A. Martinez-Felipe, A. Ribes-Greus, V. Soria, *Changes in Molar Mass Distribution in UV-Irradiated films of Methacrylate/Methyl Isopropenyl Ketone Copolymers*, European Polymer Congress EPF 2011 and XII Congress of the Specialized Group of Polymers GEP, Granada, Spain.